Multi-component Epoxy Resin Formulation for High Temperature Applications

A thesis submitted to The University of Manchester for the degree of Doctor of Philosophy in the Faculty of Engineering and Physical Sciences.

2014

Gary Poynton

School of Materials

Table of Contents

Word Count: 48664

List of Figures

List of Tables

List of Abbreviations

AEW	Amine equivalent weight
AFM	Atomic force microscopy
BSE	Back scattered electrons
CCD	Central composite design
CMC	Ceramic matrix composite
DDM	diaminodiphenylmethane
DDS	diaminodiphenlysulphone
DGEBA	Diglycidyl ether of Bisphenol A
DGEBF	Diglycidyl ether of Bisphenol F
DGP	Dynamic gel point
DMTA	Dynamic mechanical thermal analysis
DSC	Differential scanning calorimetry
DV	Dependent variable
EEW	Epoxy equivalent weight
FED	Factorial experimental design
FTIR	Fourier transmission infra-red
LCST	Lower critical solution temperature
ILSS	Interlaminar shear strength

IR	Infra-red
IV	Independent variable
MDPA	m-phenylenediamine
MFED	Mono functional epoxy diluent
Mir	Mid infra-red
MMC	Metal matrix composite
NLR	Non linear regression
NRD	Non-reactive diluent
PEEK	Polyether ether ketone
PES	Polyethersulphone
PFED	Poly functional epoxy diluent
PMC	Polymer matrix composite
PPS	Polyphenylene sulphide
rpm	Revolutions per minute
RFI	Resin film infusion
SEM	Scanning electron microscopy
SENB	Single edge notch bending
TEM	Transmission electron microscopy
TGDDM	Tetraglycidyl-4,4'-diaminodiphenylmethane
TGPAP	Triglycidyl-p-aminophenol
$TGPAP_m$	Triglycidyl-p-aminophenol in the TGPAP/TGDDM mix

$TGPAP_t$	Triglycidyl-p-aminophenol in total
TRIR	Time-resolved infra-red
VARI	Vacuum assisted resin infusion
VARTM	Vacuum assisted resin transfer moulding

Abstract

The high functionality epoxy resins tetraglycidyl-4,4'-diaminodiphenyl-methane (TGDDM) and triglycidyl-p-aminophenol (TGPAP) are the main components in most aerospace grade epoxy resin formulations. Owing to their high reactivity and high viscosity, TGDDM and TGPAP pose difficulties when used in wet layup composite manufacturing. As such, these resins are often modified to achieve the desired performance both in the liquid and cured states.

The main objective of this thesis is to optimise a low viscosity multi-component epoxy resin formulation suitable for use as an aerospace grade composite matrix. The formulation will allow for the addition of high levels of thermoplastic to improve the fracture toughness of the resin whilst also maintaining resin processability. Through the use of thermal analytical techniques this thesis aims to study the effects of varying the TGDDM/TGPAP ratio, incorporation of a low viscosity bi-functional epoxy resin, the diglycidyl ether of bisphenol F (DGEBF) and changes to the stoichiometric ratio (r) between reactive groups of the epoxy resin and amine hardener (4,4'-diaminodiphenylsulphone, DDS) in multi-component epoxy resin formulations.

Resin formulations were optimised using factorial experimental design (FED). Results from two FED's showed curing multi-component resins at a low stoichiometric ratio significantly increased the processing window whilst also increasing the glass transition temperature (T_g) of the cured resin. No apparent benefit could be assigned to the inclusion of TGDDM owing to its poor processability and a T_g similar to TGPAP. Up to 60% DGEBF was incorporated in a multi-component resin formulation whilst still attaining a T_g greater than 220°C. Its inclusion at 60% had the additional benefit of increasing the processing window by 48 minutes over TGPAP, an increase of 62%.

Two optimised resin formulations, 100% TGPAP (100T) and a binary mix of 60% DGEBF and 40% TGPAP (60D) were taken forward to study the effects of adding a thermoplastic toughener (polyethersulphone, PES) in incremental amounts up to 50 wt%. SEM images showed all toughened 100T resins had a phase separated morphology whilst all 60D resins were homogenous. The phase separation seen in 100T did not improve the matrix fracture toughness when loaded at 10 wt% and 30 wt% PES. Only when 50 wt% PES was added did fracture toughness increase in comparison to the homogenous 60D resins.

Through factorial experimental design two epoxy resin formulations which excluded TGDDM were optimised with a low stoichiometric ratio. The optimum aerospace formulation is dependent on the desired processability and fracture toughness of the resin. High DGEBF-containing formulations give the longest processing windows whilst the 100%TGPAP formulation toughened with 50% PES has the highest fracture toughness.

Declaration

No portion of the work referred to in this thesis has been submitted in support of an application for another degree or qualification of this or any other university or other institute of learning.

Gary Poynton

Copyright Statement

Acknowledgements

I wish to express my thanks and gratitude to Dr Arthur Wilkinson for his supervision and support throughout this work.

I with to thank all the staff of NCCEF including Dr Payam Jamshidi, Dr Simon Barnes, Bill Godwin and Chris Cowan. There have been points throughout this work when I have needed your knowledge and expertise and you were always there to help. I wish to make a special thanks to Dr Alan Nesbitt who would go out of his way to help me with laboratory testing and problem solving. I thank you not only for your help in the labs but also your friendship. Thanks also to Polly Crook for her assistance with DSC and FTIR.

I wish to thank all the students in the postgraduate office of the Paper Science Building for providing a fun and enjoyable place to study. A special thank you to my colleague Jasmin Stein as without her advice, friendship and general nagging this thesis would not exist. Further thanks to Yan Liu and Ramli Bin Junid who started their PhD's by generating results I have used in this thesis. Thank you for your time and hard work.

I would also like to thank my family for their constant support, particularly my dad, Neil, who would regularly phone and check how things were going in the lab or with the write up. Thank you to my mum, Carol, for always showing an interest in my work despite not understanding what I have studied for 4 years. I would like to extend that sentiment to my girlfriend, Hannah, who when asked what I study tells people, 'he makes aeroplanes' – a joke which has continued throughout my PhD. On a serious note, I would like to thank Hannah for her constant love and support over the last 4 years. You have been the biggest welcome distraction from my work.

1. Introduction

Advanced polymer composites are a relatively new category of materials that exhibit superior specific properties in comparison to traditional engineering materials such as steel and aluminium alloys. Owing to their excellent specific properties their use has become increasingly important in applications where weight saving is a critical factor. Such industries include the automotive, marine, aerospace and sports industries to name but a few [1].

The fundamental success of composites lies in the combining of two chemically distinct materials, which when used in conjunction provides material properties far superior than either of the constituents on their own [2]. Engineering composites tend to consist of fibres and a matrix. The fibres, commonly produced from glass, carbon and aramid provide the composite with strength and stiffness whilst the matrix, commonly produced from epoxy, polyester or vinylester resins, binds the fibres together, thus keeping them in the desired location and orientation. The matrix has added benefits as it acts as a load transfer medium between an applied force and the fibres. The most widely used advanced composite material is carbon fibre reinforced epoxy resin. Carbon fibre is extensively used due to its high strength and high stiffness, even when compared to alternative fibre reinforcements. Epoxy resin is frequently used as the composite matrix. Its high stiffness combined with good processability and strong fibre adhesion make it a versatile polymer matrix.

The most common form of epoxy resin is the diglycidyl ether of bisphenol-A (DGEBA). The resin has a very low viscosity and is relatively cheap to manufacture as well as being easy to process [3]. DGEBA's primary applications are in the automotive and sporting industries owing to its commercial availability and cost. However, its applications are restricted to low temperatures owing to the low crosslink density of the bi-functional DGEBA prepolymers that leads to low glass transition temperatures (T_gs)

of the cured polymer. Materials used in the aerospace industry are subjected to high temperatures, making DGEBA an unsuitable composite matrix. As such, a high molecular weight, tetra-functional epoxy resin, tetraglycidyl-4,4'-diaminodiphenyl-methane (TGDDM) was developed. This prepolymer comprises of four long branches each terminating with an epoxy group, allowing the resin to form a highly crosslinked polymer network resulting in a high T_g. However, the liquid resin has a high viscosity, undesirable for composite manufacturing. A tri-functional epoxy resin, triglycidyl-p-aminophenol (TGPAP) was developed with a lower viscosity than TGDDM, and a higher T_g than DGEBA. Resin formulations developed for aerospace applications often include TGPAP and TGDDM, along with a hardener and other additives such as tougheners.

Hardeners are added to the epoxy prepolymers to increase the rate of polymerisation by reacting with the epoxy groups. There is a wide variety of hardeners suitable for epoxy polymerisation and the choice of hardener depends on the processing method, desired curing conditions, desired physical and chemical properties, environmental limitations and cost [4], [5]. Consideration of these factors has resulted in amines having the largest share of the epoxy hardener market [6]. A commonly used amine hardener is 4,4'-diaminodiphenylsulphone (4,4'-DDS) which is used due to its high T_g in comparison to other amines, whilst retaining a comparable tensile strength, stiffness and strain at break.

Tougheners are often added to epoxy resins due to their inherent brittleness, which leads to a low fracture resistance, an undesirable property for composite matrices. Common tougheners are liquid rubbers and engineering thermoplastics. These materials are incorporated into epoxy matrices owing to their high ductility and miscibility with epoxy resin. However, the addition of toughening agents increases the viscosity of the liquid resin leading to difficult processing. To reduce the viscosity, diluents are often incorporated into epoxy resin formulations. Diluents can either be reactive or non-reactive, however reactive diluents are often preferred as they become chemically bound into the crosslinked polymer, minimising their detrimental effects on mechanical properties [7]. The diglycidyl ether of bisphenol-F (DGEBF) is a bi-functional epoxy

resin similar in chemical structure to the more commonly-used DGEBA, however it has a much lower viscosity than DGEBA [8] whilst maintaining the same strength [9]. The addition of DGEBF in an epoxy system (with the intentions of it acting as a reactive diluent) is implied by its inclusion in the commercially available HexPly M21, an aerospace epoxy resin, which incorporates up to 30% DGEBF [10]. That said there is no available literature that reports on the effect of its inclusion in aerospace grade epoxy resin systems.

The main objective of this thesis is to optimise a low viscosity multi-component epoxy resin formulation suitable for use as an aerospace grade composite matrix. The formulation will allow for the addition of high levels of thermoplastic to improve the fracture toughness of the resin whilst also maintaining resin processability. Using two high-functionality epoxy resins, TGDDM and TGPAP, along with an epoxy-containing reactive diluent (DGEBF) and a diamine hardener (4,4'-diaminodiphenylsulphone, 4,4'-DDS) the aims of this work are to:

- Assess and understand the reaction kinetics of the three base epoxy resins cured with 4,4'-DDS using thermal analytical techniques.
- Optimise a resin formulation by varying TGDDM and TGPAP ratios, DGEBF quantity and the ratio of 4,4'-DDS hardener to epoxy resin (stoichiometry) using factorial experimental design (FED).
- Study the effects of adding a thermoplastic toughener to an optimised epoxy resin formulation.

Chapter 2 discusses literature surrounding epoxy resins (including common resins, network formation and common curing agents), diluents (including non-reactive, reactive and epoxy-containing reactive diluents), toughening of epoxy resins and several conventional composite manufacturing and curing techniques.

Chapter 3 describes the experimental equipment and methods used throughout the thesis including an overview of factorial experimental design, thermal analytical techniques

(including DSC, FTIR, rheometry and DMTA), fracture toughness testing and scanning electron microscopy. Details on sample preparation are provided where necessary.

The objectives of the thesis lead naturally to the division of the results and discussion into three parts, chapters 4, 5 and 6. Chapter 4 describes the three base epoxy resins, TGDDM, TGPAP and DGEBF mixed with 4,4'-DDS at a stoichiometric ratio of r = 1.0. The chapter compares the epoxy reactivities studied using DSC and FTIR and links the results to the resins processability, studied using rheology. A kinetics model was fitted to DSC data and isothermal viscosity plots. The gel point conversion was found through a combination of the aforementioned techniques and the glass transition temperature assessed using DMTA.

Chapter 5 describes the results from two factorial experimental designs examining the effects of varying resin quantities and stoichiometric ratio in a multi-component resin formulation. Properties studied include processability, reaction kinetics and glass transition temperature. DSC, FTIR and rheology were used for an in-depth study on the effects of stoichiometric ratio on the rate of reaction, gel point conversion and glass transition temperature.

Chapter 6 describes the addition of polyethersulphone (PES), an engineering thermoplastic, to four epoxy resins selected from the FED study in chapter 5. The effects of its addition on viscosity and processability, morphology, fracture toughness and glass transition temperature were studied.

2. Literature Review

2.1. Composites

The fundamental success of composites lies in the combining of two chemically distinct materials which when used in conjunction provides material properties far superior than either of the constituents on their own [2]. All engineering composites fall into one of three categories, polymer matrix composites (PMC), metal matrix composites (MMC) or ceramic matrix composites (CMC). All three types of composites have commercial applications, however it is PMCs that are used extensively, finding applications in the aerospace, automotive, military, marine, biomedicine and sports industries [1].

Engineering composites tend to consist of fibres and a matrix. The properties of a composite are a combination of both components, thus mechanical properties such as strength and modulus are often expressed using the rule of mixtures shown in Equation 2.1, where E_c, E_m and E_f are the moduli of the composite, matrix and fibres, respectively, and V_f and V_m the volume fractions of the fibres and the matrix.

$$E_c = E_m V_m + E_f V_f \tag{2.1}$$

The fibres provide the composite with strength and stiffness whilst the matrix binds the fibres together [11], thus keeping them in the desired location and orientation [1]. The matrix acts as a load transfer medium between any applied forces and the fibres whilst protecting the fibres from environmental damage [1]. The most common forms of reinforcement are carbon, glass and aramid fibres whereas common matrix materials include a wide range of thermosetting and thermoplastic polymers. Different industries have particular property requirements of materials, whether it is high strength, high stiffness, low cost or good processability. However, using PMCs yields one advantage

over traditional engineering materials – a low density. PMCs tend to have densities in the region of 1.35-1.85 g cm^{-3} (Table 2.1) whereas high performance metal alloys tend to have densities in the region of 2.7-8.2 g cm^{-3}. Materials with low density often exhibit poor mechanical properties however PMCs are capable of possessing mechanical properties equal to or better than lightweight alloys. Therefore, the ratio of strength to weight, or stiffness to weight (specific properties) of PMCs are far superior to those of engineering alloys.

Table 2.1 Typical mechanical properties of metals and composites (Reproduced from [2])

Material	Density (g cm^{-3})	Modulus (GPa)	Tensile Strength (MPa)	Specific Modulus (m^2 s^{-2})	Specific Strength (m^2 s^{-2})
HS Steel	7.87	207	365	26.3	46.4
6061-T6 Al Alloy	2.7	68.9	310	25.5	114.8
Nickel Alloy	8.2	207	1399	25.2	170.6
HS CF-epoxy matrix	1.55	137.8	1550	88.9	1000.0
HM CF-epoxy matrix	1.63	215	1240	131.9	760.7
AF-epoxy matrix	1.38	75.8	1378	54.9	998.6
GF-epoxy matrix	1.85	39.3	965	21.2	521.6

*HS and HM are high strength and high modulus and CF, GF and AF are carbon, glass and aramid fibres.

The use of PMCs has become increasingly important in applications where saving weight is a critical factor. The aerospace industry has seen a significant rise in the use of composites over recent years. The most significant advance was the production of the Boeing 787 'Dreamliner', manufactured with 50 weight% composite components [12] which, Boeing claims, leads to a 20% reduction in fuel consumption compared to other similar sized aircraft [12]. The majority of the composite used in the Boeing 787 is carbon fibre-reinforced epoxy matrix. Whilst there is a variety of fibres and matrix materials available for use in PMCs it is this combination that is used extensively in

aerospace applications owing to the superior properties and processability compared to the alternative materials [13]–[15]. Carbon fibre is the world's leading fibre reinforcement due to its low weight, high strength, high stiffness and high fatigue resistance [16], as well as low coefficient of thermal expansion and high thermal conductivity [1]. However, the use of carbon fibre is generally restricted to high specification applications owing to its relatively high manufacturing costs.

PMC matrices can be either thermoplastic or thermoset depending on the processing method and desired mechanical properties. Thermoplastics exist as an arrangement of individual molecules with no chemical bonding between them [17], only relatively weak van der Waals forces or hydrogen bonding. These interactions can be broken on the application of heat, allowing the material to flow. Once cooled, the interactions reform creating a solid structure [17]. Typical examples of commonly used thermoplastics in PMCs include; commodity materials such as polypropylene; engineering polymers such as polyesters, polycarbonates and polyamides; and high performance materials such as polyether ether ketone (PEEK), polyphenylene sulphide (PPS) and polysulphones. The use of thermoplastics as matrices in PMCs has several advantages over thermosets, including higher toughness, low moisture absorbance, reformability and easier recyclability [17]. However, whilst some thermoplastics have properties suitable for aerospace applications there remain issues with the processing for composite manufacturing, as they often require high processing temperatures (260-420°C) [17].

Thermosetting plastics are defined by the linking of low molecular weight monomers or oligomers by covalent bonding to form a rigid three dimensional polymer network [4]. Unlike thermoplastics, the polymerisation of a thermosetting polymer results in a permanently bonded structure that cannot be reversed. The most common thermosets used as composite matrices are polyurethanes, unsaturated polyester resins, vinylester resins and epoxy resins [18].

2.2. Epoxy Resin

Epoxy resins are prepolymers containing at least two highly-strained epoxy groups (or oxiranes) [18]. An epoxy group is a cyclic ether containing two carbon atoms and one oxygen atom (Figure 2.1). Whilst the epoxy ring can exist within the body of a molecule, they are more commonly a terminal group [5], [19] and can be attached to a large variety of aliphatic or aromatic organic molecules [18]. Due to the highly strained nature of the ring, the epoxy group is more reactive than other ethers making it attractive for polymerisation processing. Polymers produced using epoxy resin prepolymers (which are also known as epoxy resins) typically exhibit a wide range of desirable properties including high stiffness, mechanical strength, good adhesion, thermal stability, chemical resistance and good processability [4], [20]. They also have low shrinkage during polymerisation (cure), which is a significant advantage over alternative thermosets such as polyester resins [4]. Consequently epoxy resins find applications in protective coatings, encapsulations, adhesives, and structural composites [21]–[24].

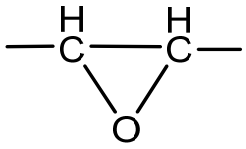

Figure 2.1 Chemical structure of the epoxy ring.

2.2.1. Common Epoxy Resins

2.2.1.1. Diglycidyl Ether of Bisphenol A (DGEBA)

Epoxy resins exist in a variety of forms, with different numbers of epoxy groups attached to various chemical structures. The most commonly used epoxy resins are based on the diglycidyl ether of bisphenol A (DGEBA) (Figure 2.2), which is produced by the condensation of epichlorohydrin with bisphenol A in the presence of sodium hydroxide [8], [25]. The molecular weight of DGEBA can vary depending on the feed ratio of epichlorohydrin to Bisphenol A, where an increase in the ratio results in a decrease in molecular weight [4]. The molecular weight of DGEBA is dependent on the

number of repeat units, n. A value of less than 2.5 is required for room temperature liquid resins but can increase up to 18 for high melting temperature resins [4].

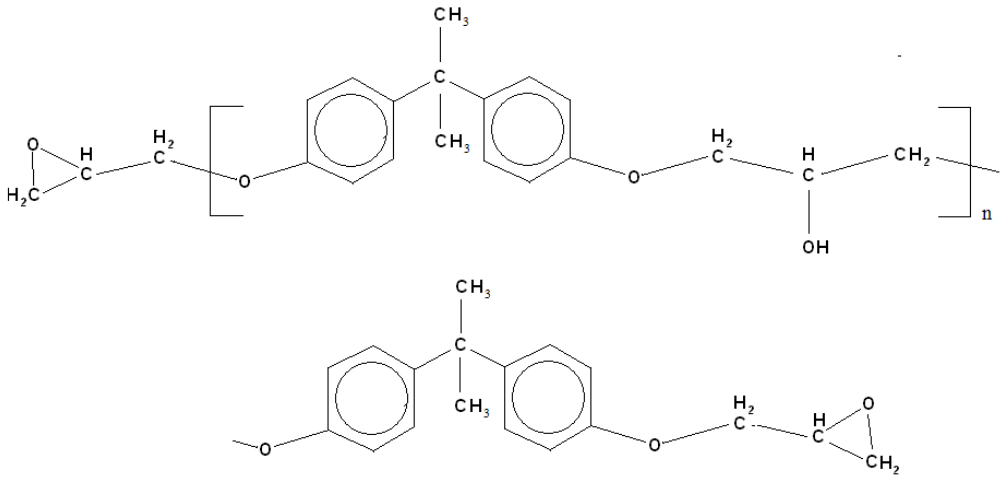

Figure 2.2 Chemical structure of diglycidyl ether of bisphenol A (DGEBA) prepolymers (n = 0 for pure DGEBA).

The majority of research concerned with epoxy resins is conducted on DGEBA prepolymers owing to attractive properties such as good fluidity, low shrinkage during cure and ease of processing [3]. The properties and commercial availability of DGEBA are appealing to a wide range of composite-using industries such as sport and automotive. However, DGEBA-based polymers tend to have relatively low glass transition temperatures (T_g). The T_g of a polymer refers to the temperature at which it changes from a rigid glassy solid into a flexible rubber [2]. The T_g of a thermoset is directly related to the crosslink density; that is the molecular distance between the covalent bonds formed during polymerisation. As DGEBA is a linear prepolymer the crosslink density is relatively low, although its exact value is dependent on the number of repeat units/DGEBA molecule (n), the hardener used and the quantity of hardener used for polymerisation (a hardener is a co-reagent used to polymerise epoxy resins).

2.2.1.2. High Functionality Epoxy Resins

Epoxy prepolymers with more than 2 epoxy groups per molecule (functionality) cure to produce highly crosslinked polymers, with higher T_gs. Whilst there is some research into the use of hyper-branched epoxy resins [26], [27] it is much more common for epoxy resins with a functionality of three or four to be used as matrices in composites requiring a high T_g.

Tetraglycidyl-4,4'-diaminodiphenylmethane (TGDDM) (Figure 2.3) is the most widely used resin used in formulating epoxy systems to be used in high temperature applications, such as the aerospace industry [28]–[30]. The prepolymer contains four epoxy groups located at the ends of four chains attached to an aromatic backbone. The aromatic backbone provides thermal stability [4] whilst the high functionality of the prepolymer leads to the development of a highly crosslinked polymer network that imparts excellent strength, rigidity and a high T_g to the cured resin [29].

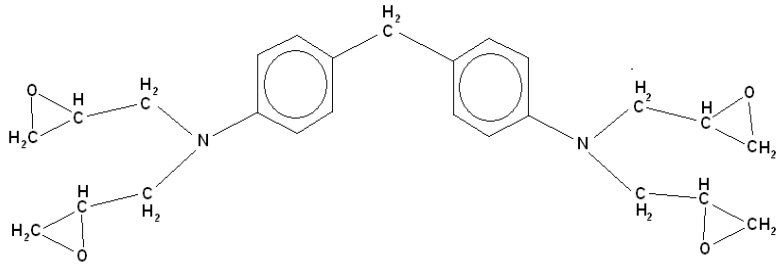

Figure 2.3 Chemical structure of tetraglycidyl-4,4'- diaminodiphenyl methane (TGDDM).

An attributing factor to the commercial success of TGDDM lies in the relatively low costs of the raw materials [31]. TGDDM is synthesised in several steps by reacting 4,4'-diaminodiphenylmethane (DDM) with a slight excess of epichlorohydrin, which is subsequently reacted with sodium hydroxide to yield epoxy groups [32]. Obtaining pure TGDDM on a commercial scale is almost impossible owing to the multistep technique used to synthesise the prepolymer. As a result, commercial TGDDM resins such as Huntsman's Araldite MY720 and MY721 contain a variety of impurities. St John et al. [32] found, using high performance liquid chromatography (HPLC), that the purest form of TGDDM contained 93% TGDDM monomer whereas MY720 and MY721

contained only 63% and 79% TGDDM monomer respectively. Both commercial resins contained significant levels of high molecular weight oligomers that also lead to increased viscosity. Thoseby et al. [31] found MY720 to have a viscosity at 50°C of 120 Pa s, whereas pure TGDDM had a viscosity at 50°C of 11 Pa s. Owing to the high viscosity of commercial grades of TGDDM, along with the brittleness of the cured resin, low viscosity diluents and toughening agents are often added. Furthermore, it is often necessary to add the hardener/toughener to TGDDM using a solvent [31], which often leads to a reduction in mechanical properties due to residual solvent the cured polymer.

Triglycidyl-p-aminophenol (TGPAP) (Figure 2.4) is a tri-functional epoxy resin and is therefore capable of forming a highly crosslinked network, with a T_g similar to TGDDM. Mallick [1] published T_g values for TGDDM and TGPAP cured with 4,4'-diaminodiphenyl sulphone (DDS) of 262°C and 261°C respectively. However, TGPAP has a much lower viscosity than TGDDM, making it a more attractive resin for composite manufacturing as solvent is not necessarily required for the mixing of hardeners and toughenes into the prepolymer.

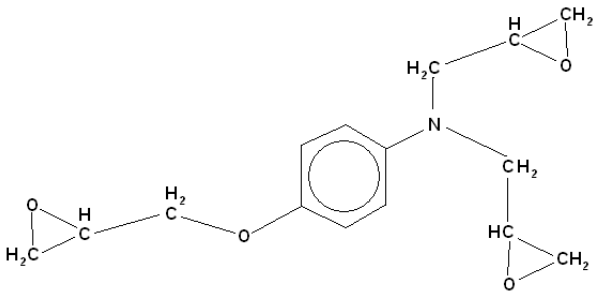

Figure 2.4 Chemical structure of triglycidyl-p-aminophenol (TGPAP).

2.2.2. Curing Agents

There are numerous combinations of curing agents (or hardeners) available to cure epoxy resins [22], [25]. There are two types of hardener; co-reactive and catalytic [4]. A catalytic curing agent acts as an initiator for homo-polymerisation whereas a co-reactive hardener acts as a co-monomer in the polymerisation. Catalytic curing agents initiate chain growth polymerisation and as such can lead to premature chain transfer and termination leading to low values of the average degree of polymerisation of primary chains [33] which in turn leads to poor mechanical properties. Consequently, co-reactive hardeners find wider application with epoxy systems.

There is a wide variety of co-reactive hardeners, and the choice of hardener depends on the processing method, desired curing conditions, desired physical and chemical properties, environmental limitations and cost [4], [5]. Due to a combination of these factors amines have the largest share of the epoxy hardener market [6].

2.2.2.1. Amines

Amines are organic compounds, classified according to the number of amine groups in the molecule as either a mono-, di-, tri-, or polyamine [5]. They can be further categorised as aromatic (containing stable cyclic bonds) or aliphatic (non-aromatic carbon bonds). Both types have been used extensively in epoxy resin systems, although the differences in chemical structure of these two types of amine result in different properties in cured epoxy resins.

The reaction between primary amines and epoxy resins is that between each hydrogen atom attached to nitrogen atoms within the amine and a carbon atom in the epoxy ring. This results in the formation of strong covalent bonds. Each amino-hydrogen can react with an epoxy group. Therefore, a diamine hardener has an amine-functionality of four which can lead to the development of a highly crosslinked polymer. Figure 2.5 shows the possible reaction mechanisms of a bi-functional epoxy resin with an amine hardener [34]–[37]. The reaction between higher functionality epoxy resins and amines is somewhat more complicated owing to the close proximity of the epoxy groups in these

molecules, as reported by Matejka and Dusek who stated that at least 12 reactions are required to describe the mechanisms between said epoxy resins and primary amines [38].

In Figure 2.5, the first reaction (i) is between an epoxy group and a primary amine, leading to the production of a secondary amine and a hydroxyl group. The secondary amine can then react to form a tertiary amine (ii) which remains a part of the cured polymer network. It is the formation of tertiary amines that leads to branching and crosslinking in systems with bi-functional epoxy prepolymers (such as DGEBA), as primary amine addition would only result in linear polymerisation [39]. The third reaction, etherification, involves epoxy and hydroxyl groups and occurs predominantly at high temperatures (>150°C).

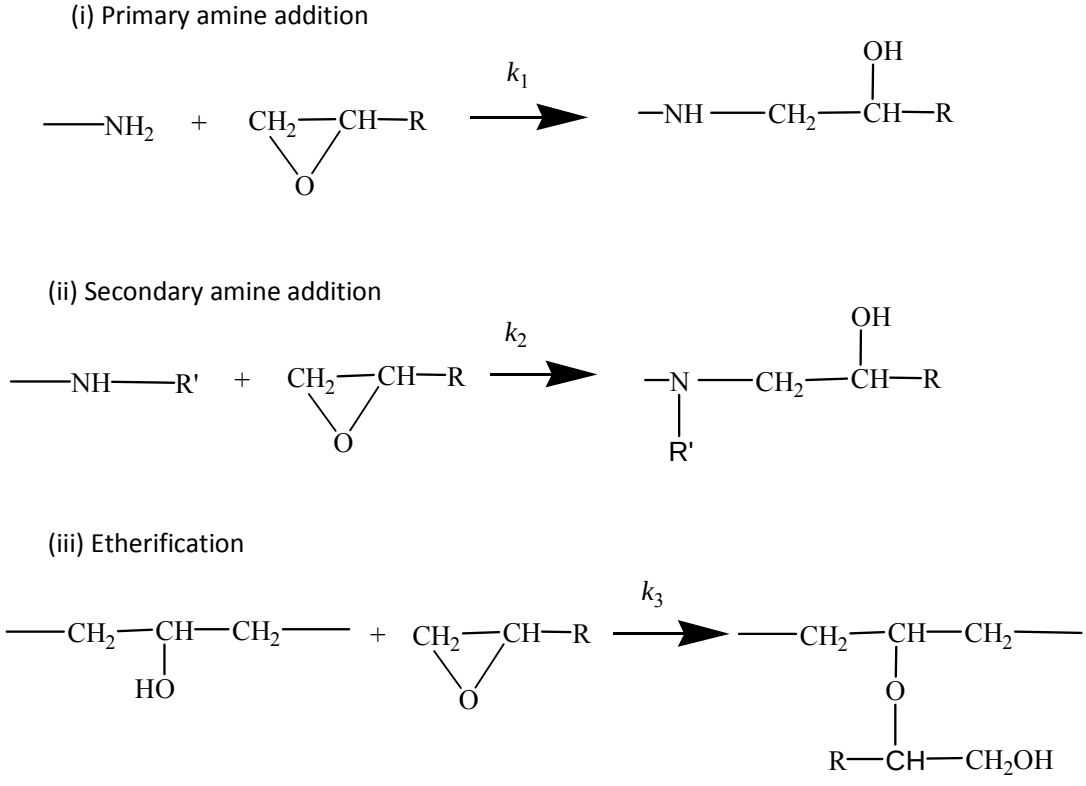

Figure 2.5 Reaction mechanisms during epoxy-amine polymerisation, where k_1, k_2 and k_3 are the reaction constants associated with primary amine addition, secondary amine addition and etherification respectively.

This reaction is more common when using high functionality epoxy resins such as TGPAP and TGDDM owing to the close proximity of their epoxy groups. As such, intramolecular etherification is more common in these systems [40], increasing the crosslink density and therefore the T_g. However, the extent to which etherification occurs can be reduced by using stoichiometric ratios (r) close to r = 1.0, that is equal molar quantities of amine hydrogens to epoxy groups, as all the epoxy groups are involved in amine addition [36].

2.2.2.2. Aliphatic Amines

Aliphatic amines were among the earliest materials to gain acceptance as curing agents for epoxy resins [5], [41]. Poly-functional primary aliphatic amines provide a fast cure rate [41] which, along with wide availability, accounts for their preferential use in high-performance room temperature curing epoxy coatings and adhesives [20], [42]. They can also provide similar properties to resins cured with aromatic amines at room temperature and when used in the correct stoichiometric proportions [5]. However, in practice the production of such a resin is difficult to achieve, owing to their high volatility [20], and it is more common for aliphatic amine cured epoxy resins to have inferior properties to those cured with an aromatic amine.

2.2.2.3. Aromatic Amines

Aromatic amines contain both a stable phenyl group and at least one nitrogen atom. Compared to aliphatic-hardened resins as they tend to give a noticeably higher T_g, with values of heat distortion temperature (an industrial measure of T_g) usually 40-60^oC higher than a fully cured aliphatic cured resin [41]. The rate of reaction is also lower in aromatic systems and, unlike aliphatic amine cured resins, elevated temperatures are required for cure. Consequently, aromatic amines are commonly utilised in curing epoxy resins for high temperature applications such as the aerospace industry. Examples of aromatic amines used commercially include m-phenylenediamine (MDPA), 4,4'-diaminodiphenylmethane (DDM), 3,3'-diaaminodiphenyl sulphone (DDS) and 4,4'-DDS.

a) b)

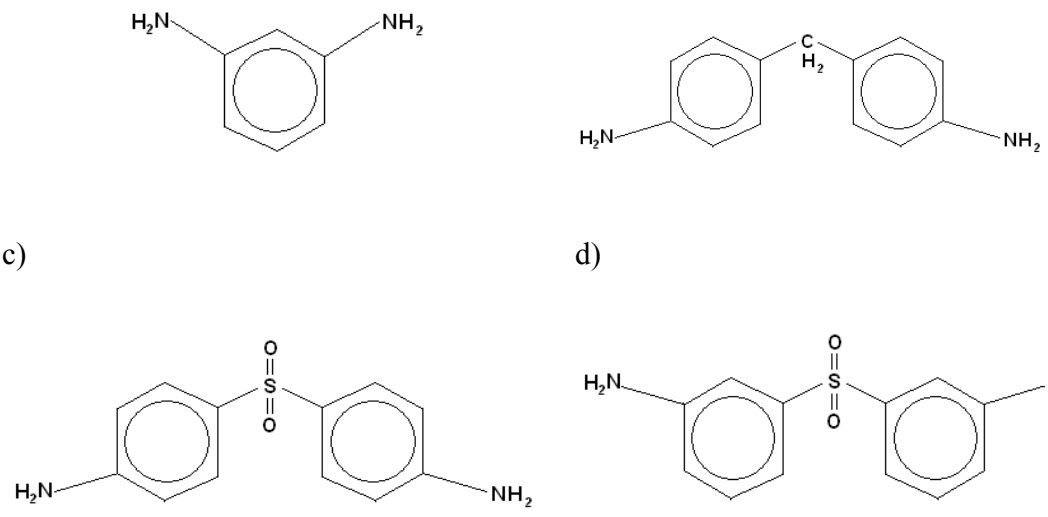

Figure 2.6. Common aromatic amine hardeners, (a) m-phenylenediamine (MDPA), (b) 4,4'-diaminodiphenyl methane (DDM), (c) 4,4'-diaminodiphenyl sulphone (4,4'-DDS) (d) 3,3'-diaminodiphenyl sulphone (3,3'-DDS).

Of the aforementioned hardeners, 4,4'-DDS (Figure 2.6c) gives the highest HDT and glass transition temperature when reacted with DGEBA [5]. The tensile strength, stiffness and strain at break of DGEBA-4,4'-DDS are also comparable to DGEBA cured with alternative hardeners. 4,4'-DDS is also the least reactive of the aromatic diamines in Figure 2.6 [4]. For this reason 4,4'-DDS is often used as a hardener for high performance epoxy resins in aerospace applications, and a significant amount of research has been conducted using it with epoxy resins [28, 43-49]. [43]–[49]

2.2.3. Network Formation

Network formation of epoxy resins occurs by step-growth polymerisation. Step-growth polymers are produced by the reactions of the monomer functional groups in a stepwise progression from dimers, trimers, etc, to eventually form high molecular weight polymers [50]. Each independent step causes the disappearance of two co-reacting sites and creates a new covalent bond between the pair of functional groups [33] (as shown previously in Figure 2.5). Bi-functional reactants (such as DGEBA) form networks

with greater molecular weight between junction points (i.e. a lower degree of crosslinking) whereas higher functionality prepolymers (such as TGDDM and TGPAP) lead to higher degrees of crosslinking. Higher crosslink densities typically result in stiffer materials with higher glass transition temperatures. The glass transition temperature (T_g) of a polymer refers to the temperature at which it changes from a rigid glassy solid into a flexible rubber [2]. The change is a result of supplying sufficient thermal energy to induce chain segmental rotation about single bonds [51] resulting in the crosslinks no longer being locked in position. The T_g of a thermoset is directly related to the overall conversion, stiffness of the crosslinked chains and the free volume entrapped in the network [52]. Thus, for polymers with high crosslink densities, high chain stiffness and little free volume entrapment, high energies are required in order to induce segmental motions.

2.2.3.1. Transformations during Epoxy Network Formation

During cure, the degree of polymerisation of thermosetting monomers increases with time. As the degree of cure progresses, thermosets experience two notable transformation steps, gelation and vitrification. Gelation takes place during the formation of the polymer network and corresponds to the generation of a macromolecular structure (a gel molecule) that percolates the whole system [33]. The point in time that this occurs is the gel point (or gel time). Prior to gelation, the fraction of solvent-soluble molecules (the sol fraction) equals one. Once gelation occurs the sol fraction decreases as the gel fraction increases, and it continues increasing until the system is fully cured, resulting in a zero sol fraction (and a gel fraction of 1.0). However, a second transformation called vitrification can significantly reduce the rate of reaction and ultimately stop it before the sol fraction is zero.

Vitrification occurs when the liquid reacting mixture is transformed into the glassy state as a result of the increase in molecular weight [53]. Once vitrified, the T_g of the system is equal to (or has increased just beyond) the temperature at which the material is being cured [33]. In other words if a system is exposed to a temperature higher than its current T_g (and is currently not fully reacted) it will devitrify and further reactions will take place until its T_g is equal to or greater than that of the temperature it is exposed to. This

is a transformation from a liquid-like or rubber-like material to a glassy material (for an ungelled and gelled system, respectively). Figure 2.7 is a time/temperature/ transformation diagram for a typical thermosetting system [54]. The shaded area represents vitrification whilst the clear area represents pre-vitrification, where the system is either liquid or a gel. At temperatures below gel T_g and above T_{g0} the system is limited to the extent to which it can react (or cure), resulting in vitrification whilst the system has not formed a gel. Applying temperatures greater than the gel T_g will see the system experience both transformations; the first being from a sol to a gel and the second being from a gel to a vitrified system.

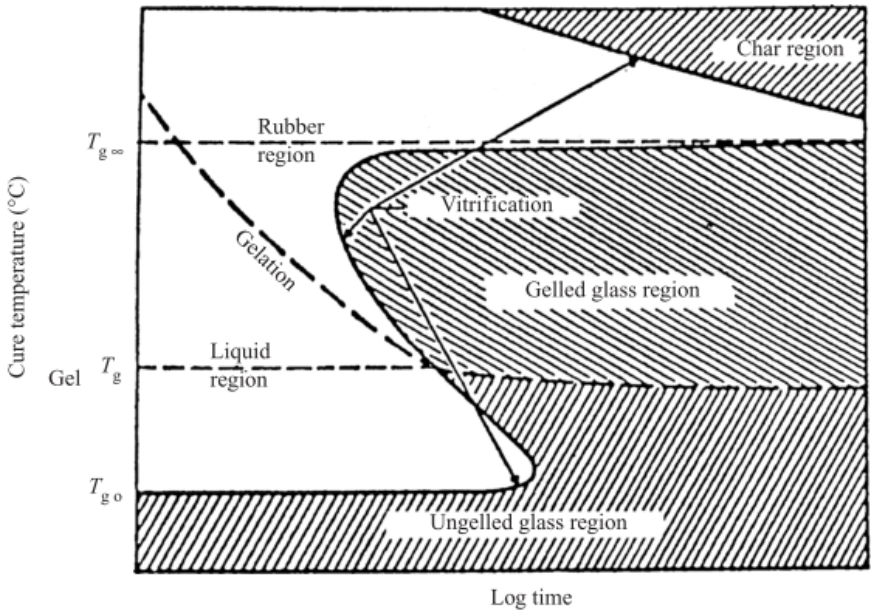

Figure 2.7 Time/Temperature/Transformation (TTT) diagram for a thermosetting polymer [55]**.**

Once vitrified, the system continues to react albeit at a slower rate than in a previtrified state [56]. This is due to the change from the reaction being a kinetic controlled parameter to becoming diffusion-controlled [57]. Therefore once vitrified the T_g of the system can continue to increase beyond that of the curing temperature. Examples of this can be found in literature where epoxy resins are cured at temperatures less than 200°C and yet exhibit a T_g of the order of 260°C [58].

2.2.3.2. Effects of Increasing Molecular Weight and Crosslinking

Miller and Macosko [59], [60] developed a series of equations for the molecular weight and post gel properties for the formation of non-linear step-growth polymer networks. Figure 2.8 shows the changes during network formation of a stoichiometric mix of a tetra-functional and bi-functional reactive species as the extent of reaction proceeds (equivalent to DGEBA cured with a diamines). In Figure 2.8, the sol fraction (W_s) = 1 until the gel conversion, α_{GP}, as the system is completely soluble until gelation occurs. Flory [61] defined the theoretical gel point conversion using the functionality of the reactive monomers and the stoichiometric ratio between them by:

$$\alpha_{GP} = \sqrt{\frac{1}{r(f_E - 1)(f_A - 1)}} \tag{2.2}$$

Where α_{GP} = conversion at the gel point, f_E = functionality of the epoxy resin, f_A = functionality of the hardener and r = ratio of reactive species (stoichiometric ratio) and can be expressed as:

$$r = \frac{[AEW]}{[EEW]} \tag{2.3}$$

Where EEW = epoxy equivalent weight and AEW = amine equivalent weight.

Therefore, for a reaction between two prepolymers, one with a functionality of four and the other of two (an RA_4 + RB_2 reaction), as shown in Figure 2.8, the gel point conversion is 58%, assuming an equal number of reactive groups present. At conversions below 58%, the weight-average degree of polymerisation, $\overline{X}_{w,}$ is finite, however as the conversion progresses it increases at an exponential rate until at the gel point conversion it becomes infinite. Once a gel macromolecule of infinite molecular mass is formed, further polymerisation will occur by the addition of the smaller molecules in the sol fraction to the gel molecule. This is seen in Figure 2.8 as both a reduction in W_s and as a gradual increase in the fractional conversion of tri-functional crosslinks (C_c'(3)).

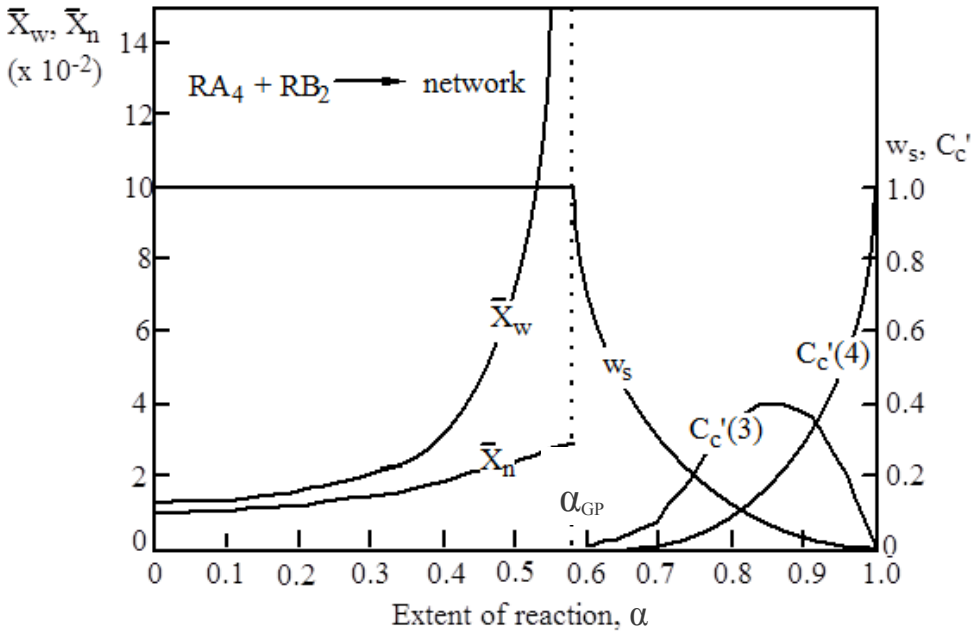

Figure 2.8 The development of number- and weight-average degrees of polymerisation ($\bar{X}_n$ and $\bar{X}_w$) and changes in fractional conversion of tri (C_c'(3)) and tetra (C_c'(4)) functional crosslinks for an $RA_4 + RB_2$ polymerisation ([59]).

Figure 2.8 also demonstrates how the rate of formation of tetra-functional crosslinks is directly related to the increase in the formation of tri-functional crosslinks. Tetra-functional crosslinking (C_c'(4)) can only develop once tri-functional crosslinks exist. This results in a reduction in tri-functional crosslinks towards a fully cured system as the fraction of tetra-functional crosslinks approaches 1.

Whilst it is only required for a thermoset to be vitrified in order to behave as a rigid, glassy material, increasing the molecular weight (by further post-gel reaction) so to maximise the T_g is important to develop the materials properties at higher temperatures. Thermosets with T_g values significantly below their maximum-obtainable T_g, T_g^∞, can contain unreacted molecules which can lead to a reduction in some mechanical properties.

Attaining values of T_g in a thermosetting system which are close to T_g^∞ often requires exposure to high temperatures for an extended period of time. This is because as the gel

fraction increases (and particularly if the system vitrifies) reactions become diffusion-controlled resulting in a slower rate of reaction (very much slower if vitrification occurs). However, this post-gel reaction is very important, as even a relatively small change in the degree of post-gel conversion can cause large variations in the T_g. Barton [62] examined the extent of curing on T_g for a bi-functional epoxy with a tetra-functional amine hardener (DGEBA/DDM). He found that the final 10% of conversion corresponded to an increase in T_g of 70 °C.

The vast majority of research concerning the curing of epoxy resins indirectly supports Barton's work, as cure cycles tend to adopt a multi-step temperature curing approach. Alternatively some researchers use a 'post-cure' [20], [22], [49], [56], [63]–[65], whereby samples are exposed to a higher temperature in order to develop the crosslinked network and T_g by increasing post-gel reaction. For systems involving highly crosslinking epoxy resins, such as those used in aerospace composites, the materials are typically required to be exposed to temperatures in the range of 180-200°C to generate between 90-100% of cure [47], [66]–[68].

2.2.3.3. The Influence of Stoichiometric Ratio on Crosslinking

The rate of polymerisation, or cure, is dependent on the stoichiometric ratio, r, between the two reacting co-monomers. The stoichiometry of a system is the ratio between the numbers of reactive groups in the hardener to that of epoxy groups in the resin and is expressed in Equation 2.3 (p 43). The epoxy equivalent weight (EEW) is calculated based on the average molecular mass divided by the number of epoxy groups per molecule. The amine equivalent weight (AEW) is calculated based on the average molecular mass divided by the number of active amino-hydrogens per molecule; thus for DDS there are four active amino-hydrogens and the molecular mass is 248, meaning the AEW is 68.

Optimisation of stoichiometry between epoxy and curing agent has been well documented [58], [69]–[72], with the majority of research focused on the stoichiometry between amine and epoxy reaction for DDS and DGEBA systems. Meyer et al. studied the effects of altering the stoichiometric ratio over the range of r = 0.8–1.2 for a

DGEBA/DDS system [58]. They discovered that a stoichiometric ratio of r = 1.0 produces a cured polymer with the highest T_g and that an epoxy-rich ratio resulted in the lowest T_g. Excess amine also led to lower T_g due to the formation of rings consisting of partially reacted diamine molecules and epoxy chains [73] which increase the free volume of the system.

These results are in agreement with Boye et al. who looked at stoichiometric variations of DGEBA reacted with DDM hardener [72]. Both Boye et al. and Meyer et al. attributed the differences in T_g with stoichiometry to be as a direct result of differences in molecular weight between crosslinks, whereby higher T_g resins have a smaller distance between crosslinks. The molecular weight between crosslinks (M_c) (g mol^{-1}) was calculated using Nielsen's equation [52] (Equation 2.4) where E_r = rubbery state modulus (GPa), ρ = network density (g cm^{-3}), T = temperature (K) and R = the gas constant (J K^{-1} mol^{-1}).

$$E_r = \frac{3\rho RT}{M_c} \qquad (2.4)$$

The equation relates the average molecular weight between crosslinks to the rubbery state storage modulus found using DMTA. Whilst the popular bi-functional epoxy DGEBA has been widely studied concerning stoichiometric ratio, little work exists on the stoichiometric optimisation of higher functionality epoxy resins. A paper by Guerrero et al. [70] studied the effects of varying the stoichiometric ratio between TGDDM and an anhydride curing agent. It was reported that the optimum T_g was at a stoichiometric ratio of between r = 0.8-0.9. As with the DGEBA based systems, the measured distance between crosslinks was lower for resins cured within this stoichiometric range. The paper goes on to show superior mechanical properties for mixtures slightly in excess of epoxy, assuming the improvements were due to an increase in etherification reactions between epoxy groups and hydroxyls, which resulted in an increase in crosslink density. This is supported by Nikolic et al. who studied network formation of epoxy resins using FTIR. They reported that etherification

reactions are insignificant during network formation for stoichiometric or amine rich systems and only become significant in epoxy rich systems [74].

2.2.4. Reaction Kinetics

The rate of polymerisation is an important property for an epoxy resin system as it has a direct influence on the resin gel time. The reactivity of the resin is dependent on the accessibility of the epoxy group and the electronic nature of the epoxy oxygen [5], that is, electron-attracting substituent groups present in the epoxy prepolymer increase the rate of reaction with nucleophilic curing agents such as amines [5]. Using near infra red FTIR Liu et al. [75] studied the reaction kinetics of DGEBA, TGPAP and TGDDM with several curing agents and found the reactivity of the epoxy groups was in the order DGEBA > TGPAP > TGDDM. This showed the reactivity of the epoxy groups was dependent on the steric effect, or 'bulkiness' of the prepolymer, whereby increasing the prepolymer bulkiness reduces the reactivity of the epoxy groups.

In addition, the accessibility of the co-reacting groups and electron-attracting substituent groups present in the hardener also affects the reactivity of the resin system. For example, the SO_2 group bonded to the central carbon atom in DDS (Figure 2.6, p 40) reduces the reactivity of the amino-hydrogens compared to the central methyl group in DDM. This is because SO_2 is a high electron-attracting group which decreases the basicity of the diamine [36].

The mechanisms of the curing reaction of thermosetting resins follow one of two general kinetic models, the nth-order and autocatalytic models [76]. The reaction rate following nth-order kinetics can be expressed as:

$$\mathrm{d}\frac{\mathrm{d}\alpha}{\mathrm{dt}} = \mathrm{k}(\mathrm{T})(1-\alpha)^{\mathrm{n}} \qquad (2.5)$$

Where dα = change in conversion, dt = change in time, k(T) = the rate constant, which is a function of temperature and n = the order of reaction.

The rate of reaction following autocatalytic kinetics can be expressed as:

$$\frac{d\alpha}{dt} = k'\alpha^m(1-\alpha)^n \qquad (2.6)$$

Where k' = kinetic rate constant and m and n = orders of reaction.

However, Equation 2.6 does not take into account an autocatalytic reaction where the initial rate of reaction is not equal to zero. Kamal [77] modified Equation 2.6 to give:

$$\frac{d\alpha}{dt} = (k_1 + k_2\alpha^m)(1-\alpha)^n \qquad (2.7)$$

Where k_1 and k_2 = the rate constants for the non-catalysed and auto-catalysed reactions respectively.

Reaction kinetics of epoxy resins have been widely studied using a variety of techniques, the most popular being differential scanning calorimetry (DSC) [23], [78]–[80] and Fourier transform infra-red (FTIR) spectroscopy [81], [82]. Kamal's autocatalytic model has been widely used to study the isothermal reaction kinetics of epoxy resins using DSC [76], [79], [83], [84]. As a technique for characterising epoxy polymerisation, DSC relies on the assumption that the heat of reaction is linearly proportional to the extent of reaction. By assuming this, one can plot the rate of reaction as a function of conversion, to which Kamal's autocatalytic model can be fitted using either linear or non-linear regression analysis. Many workers proposed different fixed values of the reaction orders m and n [79], with most choosing m = 1 and n = 1 or 2 [40], [85], [86]. However, others have shown these values vary depending on the cure temperature [76], [87], suggesting that fixing the reaction orders may result in skewed results for the rates of reaction found by non-linear regression.

There are two limitations to Kamal's autocatalytic model. Firstly, the model assumes that the thermoset reacts through to completion i.e. all epoxy groups are consumed. Whilst this is certainly possible at elevated temperatures, when curing epoxy resin with

aromatic hardeners (such as DDS and DDM) at low temperatures, the polymer is likely to vitrify before being fully cured, resulting in a partially cured network. Owing to the onset of vitrification, the rate of reaction decreases rapidly, as shown in Figure 2.9.

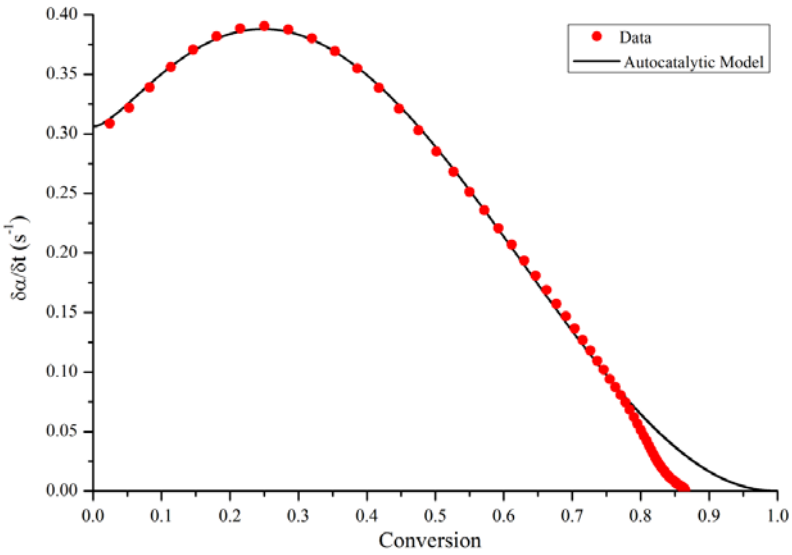

Figure 2.9 An example of Kamal's autocatalytic model fitted to a rate of reaction curve. The graph is taken from work in this thesis.

Kamal's model does not consider vitrification and therefore deviates at high degrees of conversion. Attempts have been to consider vitrification in fitting an empirical model. Chern and Poehlein [88] added an additional term to Kamal's model, taking into account the critical conversion at vitrification and the diffusion coefficient. The model showed a good fit with the rate of reaction once vitrified, however this amendment to the autocatalytic model is not widely considered, as most researchers are concerned with the rate of reaction prior to gelation.

Secondly, the model assumes that only two types of reaction occur, catalysed and non-catalysed reactions. Whilst this is true, there are two types of catalysed reaction, epoxy-amine reactions and epoxy-hydroxyl reactions via etherification. The hydroxyl reacts with the epoxy group to form an ether link, and in doing so produces another hydroxyl group. Therefore, the single rate constant for catalysed reactions in Kamal's model may

be misleading, as etherification and amine addition have different reactivities depending on the reaction temperature.

2.3. Diluents

Diluents in this context are free flowing liquids used to reduce the viscosity of a resin system [4], the benefits of which are to improve penetration in casting [13] and allow for the incorporation of other materials such as fillers and toughеners [89]. Additional benefits to their inclusion within a resin system may include an extended pot life, reduction or increase in exotherm, alterations to electrical properties or chemical resistance [5] as well as modification of the adhesive performance and the mechanical properties such as brittleness, flexibility and tensile and shear strength [90]. There are three types of diluents; non-reactive diluents, epoxy-containing reactive diluents, and reactive diluents containing other functional groups [5], [91].

2.3.1. Non-reactive Diluents

Non-reactive diluents (NRDs) are primarily used in epoxy systems as a means of controlling the viscosity. Incorporation of small quantities can lead to a significant reduction in viscosity, which will enhance processability. Common NRDs are based on dibutyl phthalate and styrene [5]. However owing to the nature of the non-reactive chemicals used, they are not covalently bonded within the epoxy network [89] and as such can lead to a dramatic decrease in the mechanical properties and chemical resistance. That said, there are suggestions within the literature that the inclusion of NRDs can have a positive effect on the epoxy resins properties. It has been reported that using small amounts of 4,4-dimethyl-5-hydroxy-methylmetadioxane improved the tensile strength of DGEBA based systems [5], whilst the inclusion of poly(methyl acetal) improved the adhesive strength. These are very specific cases and it is more common for their influence on properties (other than viscosity) to be negative.

2.3.2. Reactive Diluents

Reactive diluents are preferred in resin chemistry as they provide two functions; firstly, they become chemically bound in the crosslinked system, thus minimising effects on mechanical properties [7], and secondly they reduce resin viscosity [4]. Typical reactive diluents are low molecular weight compounds containing multiple reactive functionalities [92]. However, their use with high functionality epoxy resins results in a reduction in the overall functionality, which in turn leads to a decrease in the crosslink density [89], and consequently a reduction in the T_g. Therefore, whilst any low molecular weight reactive compound can be considered for use as a reactive diluent, the aim should be to include a material that will optimise the diluting effect whilst minimising the adverse effects on the properties of the cured resin. Reactive diluents are subcategorised into epoxy containing and non-epoxy containing reactive diluents.

2.3.2.1. Non-Epoxy Reactive Diluents

Non-epoxy containing reactive diluents are a broad group of diluents as any chemical which can react with any species in an epoxy system whilst simultaneously reducing the viscosity is considered. That said, this group of diluents is a lot less widely used in comparison to the epoxy containing diluents [89]. Materials that fall into this group can be further categorised into the following:

- Materials that are low viscosity curing agents – an example of which would be tertiary amines. They can easily be blended into primary amines and therefore act as a diluent in a resin system.
- Materials that may react with curing agents rather than epoxy groups.
- Materials that are not curing agents but will react with non-epoxy functional groups that may be present [5]. Examples of these materials are short chained polyols that contain more than one hydroxyl group. This makes them highly reactive; however, they have a low molecular mass that reduces the viscosity of the system. Despite their high reactivity it is suggested that they are capable of increasingly pot life and wetting capability of an epoxy resin [93] whilst also improving the fracture toughness of an

epoxy resin [94]. Other compounds containing active hydrogens such as phenols may be considered reactive diluents.

2.3.2.2. Epoxy Reactive Diluents

There are two sub-categories of diluents containing epoxy groups, molecules with a single epoxy group (mono-functional) and molecules with multiple epoxy groups (poly-functional). Mono-functional epoxy-containing diluents (MFEDs) such as phenyl glycidyl ether and butyl glycidyl ether (Figure 2.10), are regarded as 'chain stoppers' [13] owing to the fact that once reacted with an amine hydrogen growth of the polymer chain is terminated. This in turn leads to a lower crosslink density and thus reduced high temperature properties [7]. As with both the other types of diluent, increasing the concentration of MFEDs reduces the mechanical properties of the resin system. That said, slight increases in flexural strength, impact resistance and electrical properties have been observed below the heat distortion temperature with the inclusion of a MFED [13]. Therefore, mono-epoxy resins are added primarily to reduce viscosity [4] and are generally restricted to low temperature applications.

The use of poly-functional epoxy-containing reactive diluents (PFEDs) can be highly beneficial to an epoxy resin system and can result in the mechanical properties of the resin being maintained at elevated temperatures whilst serving the primary function of reducing the viscosity of the system in the liquid state. This is due to the high functionality of the diluents that allow a high crosslink density to be maintained. In some cases, it is possible to increase the overall functionality of a system whilst using a reactive diluent [5].

In these cases, high concentrations of diluent may be required to achieve the desired resin viscosity. The concentration of diluent required is also related to its epoxy equivalent weight. That is, the longer the molecular chains are, the larger the molecular mass is per epoxy group in the diluent, thus reducing its effectiveness as a diluent. The rate of reaction can also be affected by the PFED depending on the resin system and the curing agent. Diluents containing glycidyl ether groups are quite reactive with amines, whereas diluents containing internal epoxy groups or ring-situated epoxy groups are

more reactive towards anhydrides and acids [80]. It is common for amine curing agents to be used with glycidyl ether containing diluents.

a)

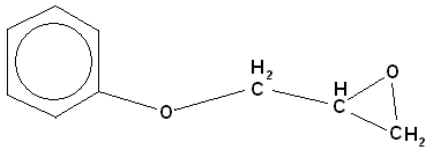

b)

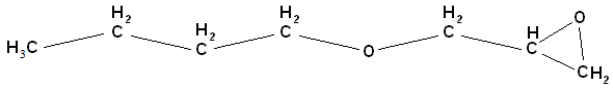

Figure 2.10 Mono-functional epoxy-containing reactive diluents: (a) Phenyl glycidyl ether and (b) 1-butyl glycidyl ether.

2.3.2.2.1. Diglycidyl Ether of Bisphenol F (DGEBF)

As mentioned earlier, bisphenol A (BPA) is widely used in the production of a bi-functional epoxy resin, the diglycidylether of bisphenol A (DGEBA). Bisphenol F (BPF) (Figure 2.11) is a chemical similar to BPA in structure; but is less sterically hindered due to the replacement of two methyl groups with hydrogen atoms bonded to the central carbon atom. As with BPA, BPF can also be reacted with NaOH to produce a bi-functional epoxy resin called the diglycidyl ether of bisphenol F (DGEBF) (Figure 2.12). DGEBF based epoxy resins have much lower viscosities for the same value of 'n' than their corresponding bisphenol A resins [8] whilst maintaining the same strength in cured resins [9]. The viscosities are typically 2-4 Pa s for DGEBF systems compared to 10-14 Pa s for those based on DGEBA based [8]. However, in 2000 it was reported that DGEBA cost 2.2 $/kg whereas DGEBF cost 4.4 $/kg [95], restricting its applications despite its desirable properties.

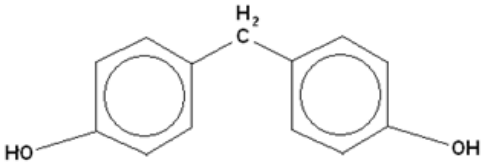

Figure 2.11 Chemical structure of bisphenol F (BPF).

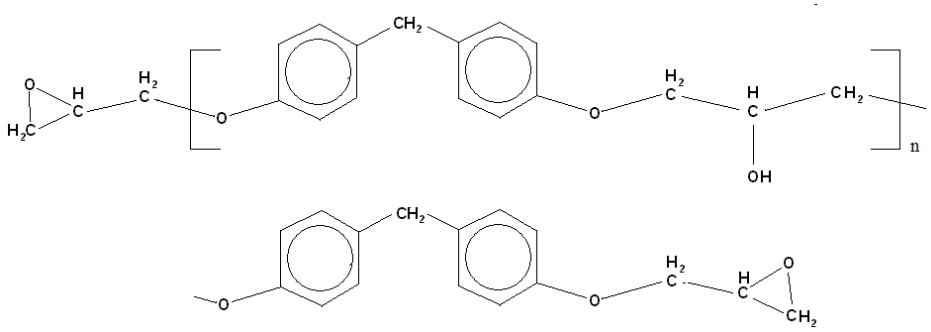

Figure 2.12 Chemical structure of diglycidyl ether of bisphenol F (DGEBF).

The addition of DGEBF in an epoxy system with the intentions of it acting as a reactive diluent is implied by its inclusion in the commercially available HexPly M21, an aerospace grade epoxy resin, which incorporates up to 30% DGEBF [10]. That said, there is no literature available that reports on the effects of its inclusion in high functionality epoxy resin systems. The only available literature involving the use of DGEBF is in an epoxy blend, usually with a tri-functional epoxy or DGEBA [84], [96]–[99], and is concerned with using the resin as a solvent for the addition of various other chemicals. Therefore, the effects of DGEBF on the properties of highly crosslinked TGDDM and TGPAP epoxy resins are not published.

2.4. Toughening

Epoxy resins have a wealth of desirable properties including high stiffness, mechanical strength, adhesive properties, thermal stability, chemical resistance, good room temperature handling and versatile processability [4], [20]. However they have a major flaw in that they are inherently brittle [43], [100]. Composites used in structural applications require matrices with high fracture resistance [66], and therefore epoxy

resins are rarely used as the sole material in these composite matrices. A common technique of improving the toughness of epoxy resins is to add a second phase. There is significant literature regarding the addition of a second phase to epoxy resins. The most common tougheners are liquid rubbers such as carboxyl-terminated copolymer of butadiene and acrylonitrile (CTBN) [22], [65], [101]–[104] and engineering thermoplastics such as polysulphone (PSF) [105]–[107], polyetherimide (PEI) [64], [68], [108], [109] and polyethersulphone (PES) [110]–[114]. These materials have been incorporated into the polymer matrix owing to their high ductility and miscibility with uncured epoxy resins. However, whilst the inclusion of rubber as a second phase increases the polymer's toughness, it also significantly reduces the stiffness. With this in mind, the quantity to which rubber can be included in an epoxy matrix is severely limited. Alternatively, the addition of engineering thermoplastics to epoxy resins gains similar fracture resistance to the addition of rubber, but does so with little to no compromise in stiffness of the cured resin [66], making them more favourable tougheners. Furthermore, the glass transition temperature of engineering thermoplastics is significantly higher than rubber, making their inclusion as a toughener more viable in matrices required for use at high temperatures.

Varley et al. proposed several criteria for the optimum thermoplastic toughener [43], which are as follows:

- Good thermal stability and soluble in uncured epoxy resins.
- Phase separation from the epoxy during cure to form a co-continuous or phase inverted morphology (more on this in the next section).
- Presence of reactive end groups in order to bond with the epoxy matrix.
- Has a greater effect with highly crosslinked epoxy systems.
- Higher molecular weight thermoplastics increase toughness more.
- The epoxy must be cured to completion to minimise unreacted functional groups.

An in depth understanding of all the criteria mentioned above is beyond the scope of this literature review. However, the most important factor in maximising the toughening effect of thermoplastic modifiers is in attaining a phase separated morphology.

2.4.1. Reaction Induced Phase Separation

Reaction induced phase separation refers to the change in morphology of a polymer blend from a miscible blend to one where the individual polymeric components separate from each other owing to the increase in molecular weight during cure of a thermosetting phase. Phase separation is determined by a combination of thermodynamic and kinetic factors. Thermodynamic analysis enables one to determine regions in conversion-composition coordinates where the system remains stable, or is metastable or unstable [115], whilst kinetic analysis is concerned with the time frame over which phase separation can occur.

2.4.1.1. Thermodynamics of Phase Separation

The stability of a system is governed by the free energy of mixing, ΔG_m, where ΔH_m = the enthalpy of mixing, T = temperature and ΔS_m = the entropy of mixing.

$$\Delta G_m = \Delta H_m - T\Delta S_m \tag{2.8}$$

For a system to be miscible, ΔG_m must be negative and satisfy the additional requirement:

$$\left[\frac{d^2\Delta G_m}{d\phi^2}\right]_{T,P} > 0 \tag{2.9}$$

Where ϕ = volume fraction.

Therefore, for phase separation to occur in an originally miscible blend ΔG_m must increase beyond zero. This can be achieved by a reduction in the entropic contribution to the free energy of mixing. The simplest model examining ΔS_m, which introduces the most important element needed for polymer blends, is that developed by Flory [116]

and Huggins [117] originally for the treatment of polymer solutions. The Flory-Huggins expression for the entropy of mixing can be extended to the mixing of a polymer-polymer blend. The ΔS_m associated with mixing n_1 moles of thermoset with n_2 moles of thermoplastic is expressed as:

$$\Delta S_m = -R\left(n_1 \ln \phi_1 + n_2 \ln \phi_2\right) \tag{2.10}$$

Where R = the gas constant, and ϕ_i is the volume fraction of component i in the mixture.

Equation 2.10 can be transformed in to a volumetric based equation as follows:

$$\Delta S = \frac{\Delta S_m}{V} = -R\left(\frac{n_1 \ln \phi_1}{V_1} + \frac{\ln \phi_2}{V_2}\right) \tag{2.11}$$

Where V_i = molar volume of component in the mixture and V = total volume of the system = $n_1V_1 + n_2V_2$

While V_2 (thermoplastic toughener) remains constant during the polymerisation of the epoxy, V_1 increases with chemical conversion (α), following a particular law that depends on the functionalities of the reactants. As the molar volume, V_i, is related to molecular weight and density ($V_i = M_i/\rho_i$), then V_1 increases as the reaction proceeds, (the epoxy molecular weight M_1 increases). For this reason, phase separation is the result of a decrease in the entropic contribution to the free energy of mixing during polymerisation. Thus, as the polymer molecular weight increases, the entropic stabilisation of the blend decreases, and phase separation becomes more likely. It is only when $\Delta G_m > 0$ that phase separation is possible. This demonstrates that phase separation is driven by an increase in chemical conversion.

2.4.2. The Interaction Parameter

The Flory Huggins interaction parameter, χ_{12} can affect the degree of phase separation between two polymers and contains both enthalpic and entropic contributions (Equation 2.12).

$$\chi_{12} = \chi_{\Delta S} + \frac{V_r(\delta_1 - \delta_2)^2}{RT} \tag{2.12}$$

Where $\chi_{\Delta S}$ = the entropy change on demixing, V_r= the reference volume and can be taken as the molar volume of the starting monomer or as the molar volume of the repeat unit of the modifier, δ_1 and δ_2 = solubility parameter of polymer 1 and 2 respectively, R = gas constant and T = temperature.

For polymer blends, the entropy change on demixing is assumed negligible, thus Equation 2.12 can be rewritten as:

$$\chi_{12} = \frac{V_r(\delta_1 - \delta_2)^2}{RT} \tag{2.13}$$

The solubility parameter of a material, as used in the calculating the interaction parameter, can be calculated using Fedors' method [118], where Δe_i and Δv_i are the additive atomic and group contributions for the energy of vaporisation and molar volume respectively. The Δe_i and Δv_i terms for each functional group are found in the reference tables prepared by Fedors [118]. Systems with similar solubility parameters are more likely to be miscible.

$$\delta = \left(\frac{\sum \Delta e_i}{\sum \Delta v_i} \right)^{0.5} \tag{2.14}$$

2.4.3. Morphology

An understanding of the morphology of modified epoxy systems is important in gaining the optimum properties from a multi-phase resin. Figure 2.13 shows the varying morphologies that can be obtained when a thermoplastic is dispersed in an epoxy resin. Phase separation can lead to one of three morphologies; particulate, co-continuous or phase inverted. When the system is not phase separated is it homogeneous.

The morphology can often be seen using scanning electron microscopy (SEM) although dynamic mechanical thermal analysis (DMTA) can often indicate whether phase separation exists within a polymer blend. A single-phase material will exhibit a single peak in the DMTA tan delta curve, whereas a multi-phase system exhibiting phase separation will often exhibit twin peaks – one attributed to the T_g of each phase present. For blends that are phase separated but have similar T_g values a single peak may only be distinguished.

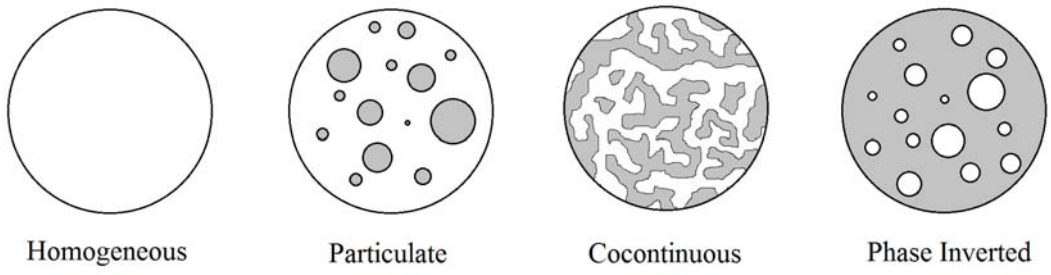

Figure 2.13 Variations of morphology seen in a phase separated polymer blend (Redrawn from [119]**).**

Developing a phase separated morphology leads to improved fracture toughness over a homogeneous morphology. In order to initiate phase separation, the Gibbs free energy is required to be positive. For an initially miscible blend, this is achieved by increasing the molecular weight of the epoxy resin during polymerisation to reduce the entropy of mixing. Graphically this is represented using phase diagrams (Figure 2.14). The three phases on the diagram, stable, metastable and unstable, can be used to represent the morphology of the final polymer blend.

In the stable region, the system is miscible and therefore homogenous because $\Delta G_m<0$. With an increase in chemical conversion, the system moves from the stable region into the metastable or unstable region. In the metastable region phase separation is possible through nucleation and growth [115] which results in a particulate morphology, whereas phase separation in the unstable region occurs via spinodal decomposition. For a blend within the unstable region the final morphology is dependent upon the kinetics of the system as is depicted in Figure 2.15. Initial decomposition results in a co-continuous morphology, however with time the distribution of the second phase alters in favour of becoming a particulate morphology. Diffusion of the second phase is severely restricted by gelation [120] and the morphology of the cured polymer is fixed once the T_g exceeds the curing temperature [28] i.e. once vitrified.

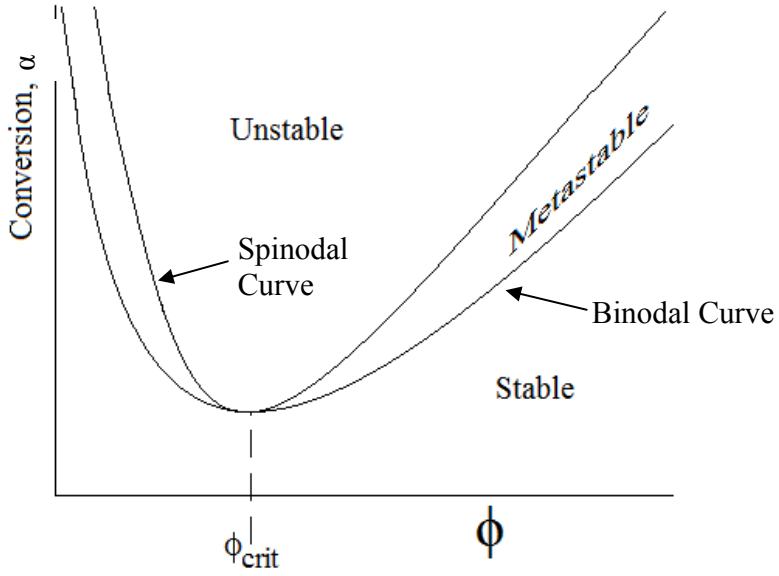

Figure 2.14 Phase Diagram for a polymer blend showing binodal and spinodal curves as a function of degree of conversion (reproduced from [28]**).**

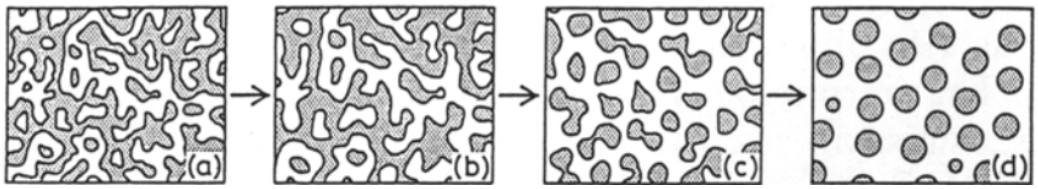

Figure 2.15 Schematic representation of the change in phase separation with time for a binary mixture undergoing spinodal decomposition [112]**. (a) shows the formation of a bi-continuous structure, (b) is a similar structure to (a) with longer periodic distance, (c) phase connectivity becomes a fragmented structure and (d) fragmented structure develops into spherical domains.**

There is ample literature discussing the benefits of phase separation between epoxy and thermoplastics [28], [43], [49], [66], [111] with the majority of research supporting the idea that generation of a co-continuous morphology leads to optimum mechanical properties [114], [121] and that this is typically achieved with the addition of between 20-30% thermoplastic [66].

However, controlling the morphology is not as simple as adding a precise amount of thermoplastic. Other variables can drastically affect the morphology by either altering the kinetic of thermodynamic properties. These variables include curing temperature [110], type of curing agent [111], molecular weight of the epoxy [49], [106] and molecular weight of the thermoplastic [49]. Research papers often examine one or two of these variables and their effects on phase separation. Irrespective of the factor being studied the effects on the thermodynamics of the system are often graphically represented using the critical solution temperature or cloud point. This temperature is the point at which a polymer blend is no longer miscible. Blends of epoxy and polyethersulphone (PES), a common toughener in epoxy resins, exhibit a lower critical solution temperature (LCST) whereby they become increasingly immiscible with an increase in temperature. This effect can be seen in Figure 2.16 [115] which demonstrates that an increase in temperature results in a reduced LCST for a binary mixture. Consequently, as temperature increases the degree of epoxy conversion required for the system to enter in to the unstable phase region (above the LCST) reduces.

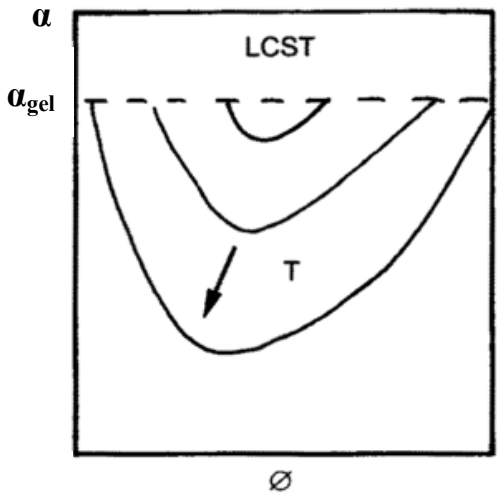

Figure 2.16 The degree of conversion (α) against second-phase content (Ø) showing the effect of temperature on the lower critical solution temperature of a polymer blend [115]**.**

The effect of temperature on phase separation was observed by Mimura et al. [110] who studied the curing of a bi-functional epoxy resin (commercial known as YX4000) containing PES. They observed using SEM imaging that phase separation occured when the system was cured at 180°C, but that a homoegeneous morphology was observed when cured at 140°C. These results imply that the LCST of the resin system studied is between 140-180°C, as at 140°C the polymer gelled before it could move in to the unstable region of the phase diagram.

In resin systems exhibiting LCST behaviour, raising the molar mass of the resin by chemical reaction has a similar effect to increasing the temperature of the mixture (whilst keeping the molar masses constant): both types of change establish conditions under which phase separation can take place [49]. This is shown schematically in Figure 2.17 [115]. Increasing chemical conversion increases the molecular weight of the epoxy resin which reduces the free entropy of mixing and thus drives phase separation.

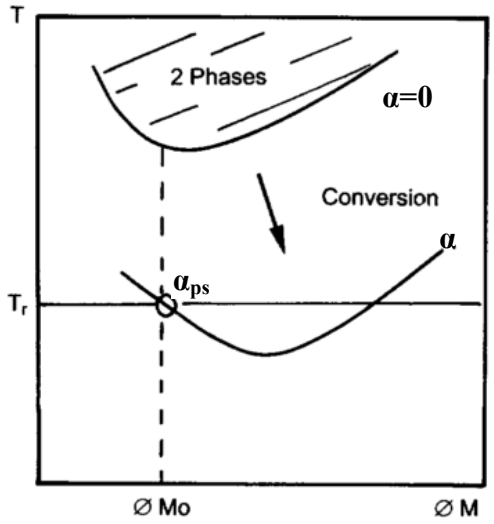

Figure 2.17 Effect of chemical conversion (α) on the temperature (T) required for phase separation (ps) to occur in a binary component mixture, where T_r = reaction temperature and ØM = volume fraction of the thermoplastic phase [115]**.**

The same trend can be observed with monomers of different molecular weights. Bucknall et al. [49] calculated LCST curves for three DGEBA prepolymers of different molecular weight from cloud-point curves. They observed that an increase in the molecular weight by 31 g mol^{-1} reduced the LCST by ~20°C, with a further increase in molecular weight of 100 g mol^{-1} reducing it by an additional 40°C. Therefore using a high molecular weight monomer of the same resin type is favourable towards the thermodynamics of phase separation. That said, it is at the same time detrimental to the kinetics of phase separation as the addition of a higher molecular weight modifier leads to a higher viscosity, which in turn slows the diffusion of phase separation. Therefore the final morphology is the result of the competition between the increase in molecular weight increase of the epoxy driving phase separation, and the increasing viscosity of the system which slows it [28], [110].

2.4.4. Polyethersulphone (PES)

One of the most suitable thermoplastics for incorporation within an epoxy network is polyethersulphone (PES). This is primarily due to its high thermal stability and easy processability in melt or solution processes [122]. Studies have investigated the disparity of the modified end groups attached to PES [112], [123], differences in molecular weight of the PES [49] and the weight content of PES within the epoxy system [112], [113], [124]. The effect of the toughener also varies dependent on the curing agent used within the epoxy system [125] and indeed the type of epoxy resin used. Whilst there is a significant amount of literature regarding PES mixed with various epoxy resins, particular attention will be paid to the morphology obtained when mixed with various epoxy resins and the resultant fracture behaviour.

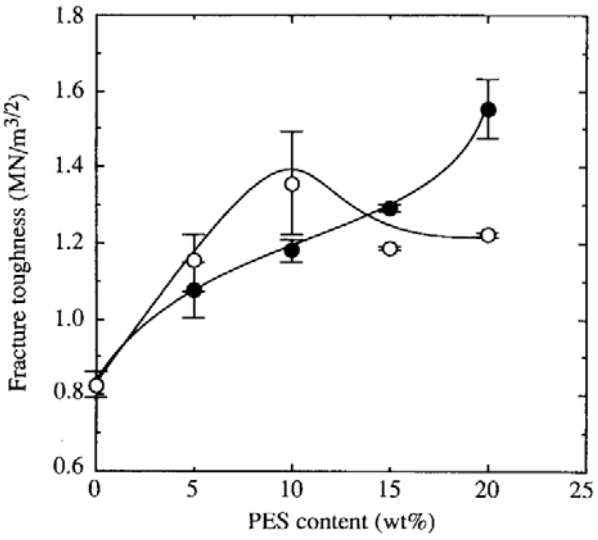

Figure 2.18 The K_{1C} fracture toughness of a DGEBA/ epoxy resin cured with a phenol novolak type resin (PSM4261) loaded with PES up to 20 wt%. ○data points = 140°C cured systems with a homogenous morphology and ● = 180°C cured systems with a heterogeneous morphology [110]**.**

As mentioned earlier in the review, Mimura et al. [110] studied the incorporation of PES into DGEBA and demonstrated that a heterogeneous morphology was achieved when the system was cured at 180°C using a phenol novolak type resin (PSM4261) as a curing agent but was homogeneous when cured at 140°C. The fracture toughness values

associated with these morphologies are shown in Figure 2.18 for PES contents ranging from 0-20 wt%.

A significant increase in the K_{1C} fracture toughness up to 20 wt% PES resulted when the system had a heterogeneous morphology; with the 20 wt%-containing system having a K_{1C} value twice that of the untoughened resin. Their findings for the homogenous morphology systems were somewhat unexpected as a 'peak in toughness' was found at the inclusion of 10 wt%. They claimed this was due to the formation of 'very fine domains' of PES which were observed using TEM. These domains were not found for the 20 wt%-containing system. Whilst these domains do exists the researchers failed to draw attention to the large error bars associated with the 10 wt% K_{1C} value. As such, it may be suggested that a lower value at 10 wt% is more fitting with the rest of the data, and that it may be more likely that at 10 wt% the fracture toughness reaches a plateau instead of peaking as shown in Figure 2.18.

The inclusion of PES into tetraglycidyl-4,4'-diaminodiphenyl methane (TGDDM) and triglycidyl-p-aminophenol (TGPAP) show different results regarding phase separation. Bucknall et al. [124] studied phase separation and its effect on the fracture toughness of PES-toughened epoxy blends of TGDDM and TGPAP at resin ratios of 100:0, 80:20, 50:50, 20:80 and 0:100 respectively. They reported that for all epoxy blends (cured with DDS) it was only the 100 wt% TGPAP system where phase separation was observed for all PES loading levels. Above 20 wt% TGDDM in the epoxy mix there was no phase separation visible by SEM. They suggested that this could be due to reactions occurring between TGDDM and the hydroxyl groups attached to the PES as the block copolymer formed would be detrimental to the thermodynamics of phase separation.

Fernandez et al. [126] studied the inclusion of PES into TGDDM using another aromatic amine hardener, DDM. They manufactured carbon fibre reinforced composites using resin systems containing up to 15 wt% PES. Mode I fracture toughness testing revealed no effect of PES inclusion on the fracture toughness, despite observing a shoulder on the DMTA tan δ peak; indicative of phase separation. This was attributed primarily to a nanoscale level of phase separation seen by atomic force microscopy

(AFM), although SEM images of the resins showed no visible morphology.. Other studies have examined the toughening of TGDDM with PES using anhydride curing agents and have successfully achieved a heterogeneous morphology [123], [127]. Oyanguren et al. [128] found that the inclusion of 15 wt% PES resulted in an increase in fracture toughness by ~300% compared to the untoughened resin.

Mackinnon et al. [121] studied TGPAP and PES cured with DDS and showed that up to 20 wt% PES incorporation resulted in a particulate morphology, 20-30 wt% resulted in a co-continuous morphology and above 40 wt% resulted in a phase-inverted morphology, whereby the PES formed a continuous phase with a discontinuous epoxy phase. They also reported a dramatic increase in the fracture toughness when the system contained more than 20 wt% PES; correlating with the change in morphology.

2.5. Composite Manufacturing

2.5.1. Prepreg

The term 'prepreg' is a common abbreviation for pre-impregnated reinforcement and usually consists of thin sheets of uni- or multi-directional fibres coated with an exact proportion of resin which has been partially cured [129]. In theory, a prepreg provides the user with a single, easy-to-handle material that can be used immediately for the layup of components, allowing for ease of layup and curing and thus maximising efficiency and consistency [130].

A major drawback when using prepreg is the requirements of additional pressure intermittently during layup and during cure, both of which increase layup and curing time. The additional pressure applied during cure is required to minimise void content in the final component. Prepreg laminates are prone to high void contents as there is minimal resin flow between fibre layers, thus it is essential to maximise contact between the fabric layers. The most common method for applying additional pressure during cure is by using an autoclave, however this curing technique is time consuming and expensive making it commercially unfavourable.

2.5.2. Vacuum Assisted Resin Infusion

Vacuum assisted resin infusion techniques have become increasingly popular for the manufacturing of advanced composites owing to their low cost tooling, scalability to large structures [131] and the requirement of no additional pressure (other than vacuum induced) during cure [132]. The literature addresses these techniques by several acronyms including vacuum assisted resin infusion moulding (VARIM), Vacuum Assisted Resin Infusion (VARI) and, the most common, vacuum assisted resin transfer moulding (VARTM) [131] to name but a few. The aforementioned techniques are derived from the principle of using a vacuum pressure to impregnate a dry fabric preform with liquid resin (see Figure 2.19). The dry preform is placed on the mould followed by a resin distribution fabric (usually a nylon based mesh) before a plastic vacuum bag is taped on top, completely enclosing the preform. For a simple component, there is one inlet and one outlet port, however for components that are more complex, several inlets and outlets may be required. The inlet goes directly in to a reservoir of liquid resin and the outlet to the vacuum line (via a resin trap). Resin begins to flow through the preform once the vacuum line is opened. When the resin has flowed completely through the preform and in to the outlet piping the vacuum line is turned off and the tool is placed in an oven for curing. The ultimate goal of resin infusion is to fill any spaces between the fibre mats, fibre tows and individual fibres with resin [133]. Ideally, infusion of the preform with liquid resin would be done as quickly as possible in order to minimise production time and thus manufacturing costs [134]. However, as the architecture of the preform becomes more complex the ability to wet out the entire preform becomes increasingly difficult [133]. With this in mind, it is now becoming common to model the flow through the preform using computer software in order to obtain information regarding infiltration time, tool plate temperature, resin composition and resin inlet and vacuum outlet positioning.

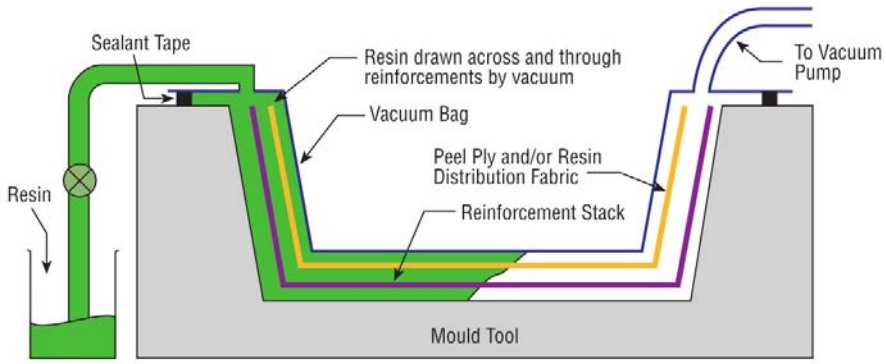

Figure 2.19 Schematic of the vacuum assisted resin transfer moulding (VARTM) process [11]**.**

Owing to the aerospace industry continuing to reduce manufacturing costs, the use of infusion techniques has received considerable interest. Whilst cost is always a factor, other benefits of using wet layup techniques include placement of fibres at the desired orientation and through thickness reinforcements in order to mitigate out of plane loads [135]. However, the use of infusion techniques for aerospace applications is somewhat difficult, as the industry tends to use matrices with toughening additives that lead to high resin viscosities. Gotch [136] suggested that the ideal resin viscosity for a vacuum injection system is 1-200 mPa s, whilst Campbell [2] suggests that the upper limit for resin infusion is 500 mPa s. Based on this, resins formulated for infusion are developed at a compromise between the mechanical properties of the cured composite and the flow of the liquid resin.

2.5.3. Resin Film Infusion (RFI)

Resin film infusion (RFI) is a composite manufacturing technique developed by NASA and the Long Beach division of McDonnell-Douglas (now Boeing) in the 1980s [137]. At the time, toughened resin systems began to show promise for improving the damage tolerance of composites, however their high costs detracted from their applications. As such alternative toughening mechanisms were investigated, with the most applicable being through-thickness stitching [138]. However using this method of toughening ruled-out the use of prepreg, the preferred fabrication technique. In addition, the use of conventional prepreg resins in an infusion technique such as resin transfer moulding

(RTM) was deemed impossible as the minimum viscosity of these resins is too high, thus the preform could not be successfully infused [137]. Thus a new innovative processing technique was developed – resin film infusion.

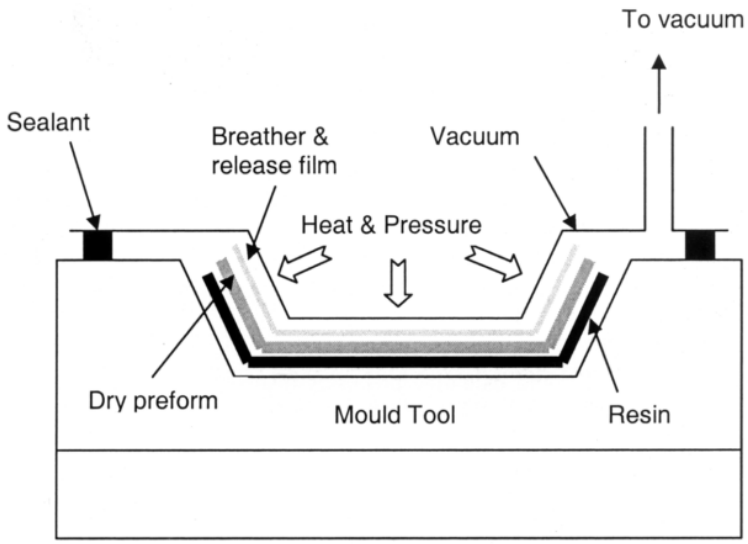

Figure 2.20 Schematic of Resin Film Infusion (RFI) [139]**.**

In recent years, RFI has gained popularity for manufacturing low-cost advanced composite structures with high mechanical performance for aerospace, automotive, military, and civil applications [140], [141]. The principles behind the technique are very similar to alternative infusion techniques, whereby liquid resin impregnates a dry preform before being fully cured. The difference with RFI (Figure 2.20) is that instead of drawing the resin through the preform via an external source (as with VARTM) the resin is included within the lay-up as a thin film. When heat is applied along with a vacuum, the resin is drawn through the preform towards the vacuum outlet.

The advantage of RFI is that only a relatively short flow distance has to be achieved which leads to both improved mould-filling time [142] and eliminates the need for a low viscosity resin system [143]. Thus, high molecular weight resins can be used to manufacture composites with mechanical properties comparable to prepregs [144]. Furthermore the technique, unlike VARTM, does not require careful and time

consuming consideration over identifying the optimum location for inlet and outlet ports [144].

The technique has the additional benefit of being less labour intensive in comparison to prepreg as just one thickness of material is laid up in to the mould before infusion [144]. RFI can also be favoured over prepreg owing to the ease with which complex shapes can be manufactured [142] along with reductions in manufacturing costs. In 1999 Qi et al. [145] reported on the efficiency of using RFI in comparison to prepreg to manufacture three aircraft components. They suggested that financial savings of between 10-18% could be made depending on the component. Whilst the technique seems to have many advantages, there are aspects that require attention. As RFI is essentially a wet layup, considerations need to be made in terms of resin viscosity and curing kinetics, as insufficient flow will lead to either dry areas of fibre or a high resin volume content – neither of which are desirable. Therefore, the most important processing parameter is temperature as it influences both of these variables. The relationship between viscosity and curing kinetics is somewhat undesirable as lower viscosities can be achieved with higher heating rates; however the time to gel reduces significantly [146]. Ideally, the viscosity should remain at a minimum value for a long period of time to maximise flow [143], though this is often difficult to achieve. Thus, a compromise between the rate of cure and viscosity must be agreed up on to optimise processing conditions.

2.5.4. Voids

There are clear benefits to the use of composites instead of traditional engineering materials such as metals. However, manufacturing composite components to a sufficiently high standard is difficult as the inclusion of entrapped gases within the final composite component in the form of voids is unavoidable [147]. Voids may be formed due to entrapment of air during resin formulation, entrapped volatiles during curing, moisture absorption during material storage and processing, inadequate temperature and/or pressure and loss of vacuum in the vacuum bag during cure [148]. Voids can act as nucleation sites for crack growth and therefore they tend to have detrimental effects

on the mechanical properties of a composite. Such properties include interlaminar shear strength, compressive strength and modulus and bending properties [149]. Chambers et al. [150] also reported that increasing void content reduces both flexural strength and fatigue performance by acting on both the initiation and propagation stages of failure. The extent to which their inclusion affects these properties has been widely documented. Costa et al. [148] reported that an increase in the void content for a carbon/epoxy laminate from 0.55-5.6% resulted in a decrease in the interlaminar shear strength (ILSS) by about 34%, and Jeong [151] reported that an increase in void content from 0-12% in an epoxy/woven carbon fabric prepreg laminate resulted in a decrease in ILSS of 30%. Judd and Wright suggested that irrespective of the fibre and resin type the ILSS decreased by ~7% for every 1% increase in void content up to 4% [152].

Owing to the effects of void content on mechanical properties it follows that minimising void content in final composite parts Manufacturing composites with little to no void content is achieved by a variety of techniques; the most common involve degassing of resins prior to manufacturing, applying an external pressure to the composite part and applying a vacuum [153]. Methods by which void content is determined are divided in to two groups; destructive and non-destructive. Non-destructive techniques such as ultrasonic c-scan inspection are used in the aerospace industry to inspect structural quality [147], [148], [154] whilst destructive techniques, such as acid digestion, can be used to generate quantitative values for void contents and this technique is widely utilised within the literature [143], [147], [148], [155], [156]. However, destructive techniques come under some criticism as they only examine a small area of a laminate, meaning their results may not represent the whole material.

2.6. Curing Methods

2.6.1. Autoclave Curing

The most common technique for manufacturing high performance aerospace composites is autoclave curing [157]. The technique can be viewed as a pressurised oven, whereby preforms are vacuum bagged and cured under a relatively high pressure of 4 to 7 bar at

temperatures of 120 to 180ºC (typical conditions for epoxy prepregs) [158]. The purpose of using such high pressures is to provide ply compaction, remove any excess resin (to increase the fibre volume fraction) and to suppress void formation [157], thus creating a better quality composite. With the optimisation of pressure and temperature it is possible to achieve void contents <1% [149], [159], [160]. The technique has the additional benefit of being applicable for the moulding and curing of prepreg or for use in conjunction with resin infusion techniques.

However, whilst autoclave curing provides high quality composites, industries are keen to move away from the technique owing to the costs and extended processing times associated with it. Autoclaves are usually pressurised with inert gases such as nitrogen in order to minimise the risk of fire within the autoclave during cure [157]. Whilst this is a necessity there are high costs associated with extensive use of pressurised gas. A further cost is associated with the curing time as autoclaves are only capable of heating at 2–3°C min^{-1} [156] which results in an extensive cure cycle, usually lasting several hours. A third consideration is the large capital cost of the equipment as, due to the pressures involved, expensive cylindrical pressure vessels are required [158].

2.6.2. Out-of-Autoclave Curing

The benefits of out-of-autoclave curing technologies include reductions in cure cycle times along with reduced overall costs (including purchase, operational and tooling costs) [143]. Some of the curing techniques that have been studied include oven curing [161] electron beam curing [97] microwave curing [162]–[165] and Quickstep curing [15], [156], [158], [166], [167]. Quickstep curing is a very promising out-of-autoclave curing technique, with reports claiming a reduction in the cure cycle of up to 90% [166] and a void content ranging from 6.0-0.5% depending on the cure cycle used [167]. A significant challenge for the industry remains the use of oven curing to produce high specification composite components. Whilst there are ‘out-of-autoclave’ grade prepregs commercially available, the lack of external pressure during cure limits the minimum achievable void content to 2%, therefore restricting their applications [161].

3. Experimental

3.1. Materials

Three epoxy resins were used in this work along with a diamine hardener and a high molecular weight thermoplastic. Details of each material are given in Table 3.1 and their chemical structures are displayed in Figure 3.1.

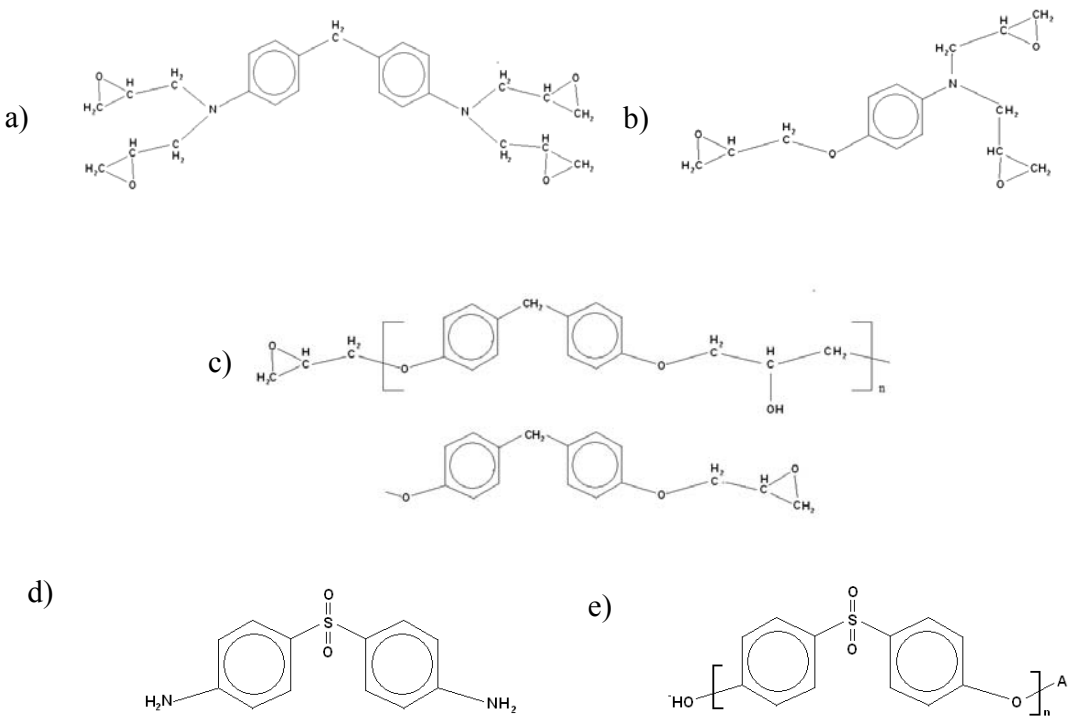

Figure 3.1 Chemical structure of (a) Tetraglycidyl-4,4'-diaminophenylmethane (TGDDM) (b) Triglycidyl-p-aminophenol (TGPAP) (c) Diglycidyl ether of Bisphenol F (DGEBF) (d) 4,4'-Diaminodiphenyl sulphone (DDS) (e) Polyethersulphone (PES).

Table 3.1 Chemicals used in Composite Matrices.

Name	Commercial Name	Abbrev.	Equivalent Weight (g eq^{-1})	Density (g cm^{-3})	Supplier
Tetraglycidyl-4,4'-diaminodiphenylmethane	Araldite MY 721	TGDDM	114	1.15	Huntsman
Triglycidyl-p-aminophenol	Araldite MY 0510	TGPAP	96	1.22	Huntsman
Diglycidyl ether of Bisphenol F	Araldite GY 285	DGEBF	164	1.19	Sigma Aldrich
4,4'-Diaminodiphenyl sulphone	Aradur 976-2	DDS	62.08	1.36	Huntsman
Polyethersulphone	Virantage VW-10200RP	PES	46500 g mol^{-1}*	1.35	Solvay Advanced Polymers

*number average molecular weight

TGPAP was supplied as a light yellow, low viscosity liquid. TGDDM was supplied as an orange, high viscosity liquid. The epoxy equivalent weights (EEW) of each resin were obtained from Huntsman and were based on the batch number of the material. No information was available regarding the exact EEW for the batch of DGEBF, therefore the range of EEW quoted from the data sheet is provided in Table 3.1. Based on the information an EEW of 164 g eq^{-1} was used for calculations.

Both the DDS hardener and polyethersulphone (PES) thermoplastic were supplied as fine white powders. The thermoplastic has a number average molecular mass of 46500 g mol^{-1} and was functionalised with hydroxyl (-OH) end groups to improve the material's dissolution.

3.2. Factorial Experimental Design

Factorial experimental design (FED) is a technique for maximising experimental efficiency. From the generation of only a few experimental results an FED can predict the relationship between the variables being investigated and subsequently estimated values, through statistical analysis, for the DV in regions that were untested. In a conventional experimental technique, whereby in each experiment the value of one of the IVs is slightly altered, the researcher would have to conduct tens if not hundreds of individual experiments. An FED will not only allow the experimenter to gain the same quantitative information about their experimental space but it will also highlight any interactions that exist between two or more variables [169]. Furthermore, through repetition of only parts of a design, the experimental error associated with the FED can be measured efficiently. A software package, Design Expert 7, was used to construct the FED and analyse the responses gained. The methods the software utilises in the construction and analysis are discussed below.

3.2.1. Regression Analysis

The following description of regression analysis is taken from Montgomery [169]. Further detail can be found in Chapter 5 of his book. Regression analysis is a group of statistic techniques for modelling and analysing the relationship between a DV and one or more IVs. By altering one of the IVs and maintaining the others constant, an understanding of its effect on the DV can be measured. This is the basis for standard experimental technique. However, when two or more of the IVs are altered an estimation of the value of the DV is required. The method by which this estimation is achieved is called the regressive function. The regressive function also determines which of the IVs has the greatest effect on the DV [169].

The explanation of regression analysis will be conducted using a simple two-factor factorial experiment as an example. The relationship between the IVs, or regressors, is modelled based on the nature of their response. The simplest model is linear and takes the form of:

$$Y = \beta_0 + \beta_1 X_1 + \beta_2 X_2 + \varepsilon \tag{3.1}$$

Where β_0 = the intercept of the plane, β_1 and β_2 = partial regression coefficients, X = the independent variables (IVs), Y = the dependent variable (DV) and ε = random error term.

A partial regression coefficient measures the expected change in Y per unit change in variable X_1, when X_2 is held constant and vice versa. More complex models include the two-factor interaction (2FI) model and quadratic model; the equations of which are shown in Equations 3.2 and 3.3 respectively.

$$Y = \beta_0 + \beta_1 X_1 + \beta_2 X_2 + \beta_{12} X_1 X_2 + \varepsilon \tag{3.2}$$

$$Y = \beta_0 + \beta_1 X_1 + \beta_2 X_2 + \beta_{12} X_1 X_2 + \beta_{11} X_1^2 + \beta_{22} X_2^2 + \varepsilon \tag{3.3}$$

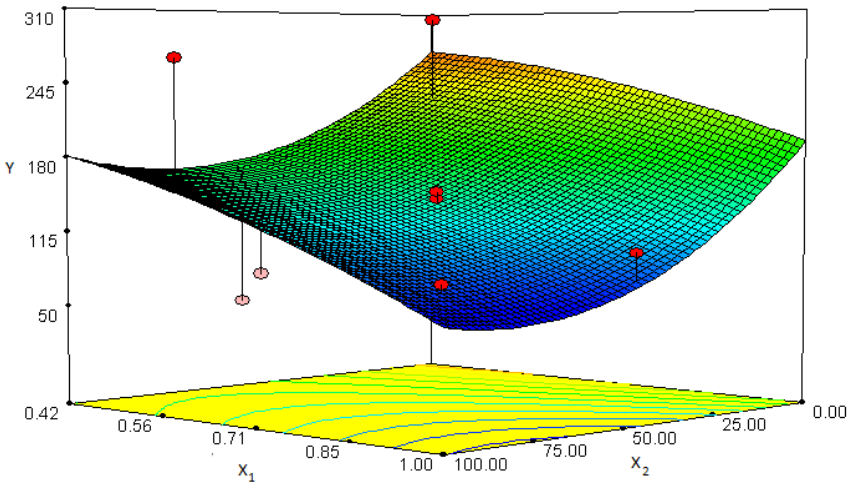

Figure 3.2 An example of a response surface plot, showing the variation of dependent variable (Y) with the independent variables X_1 and X_2.

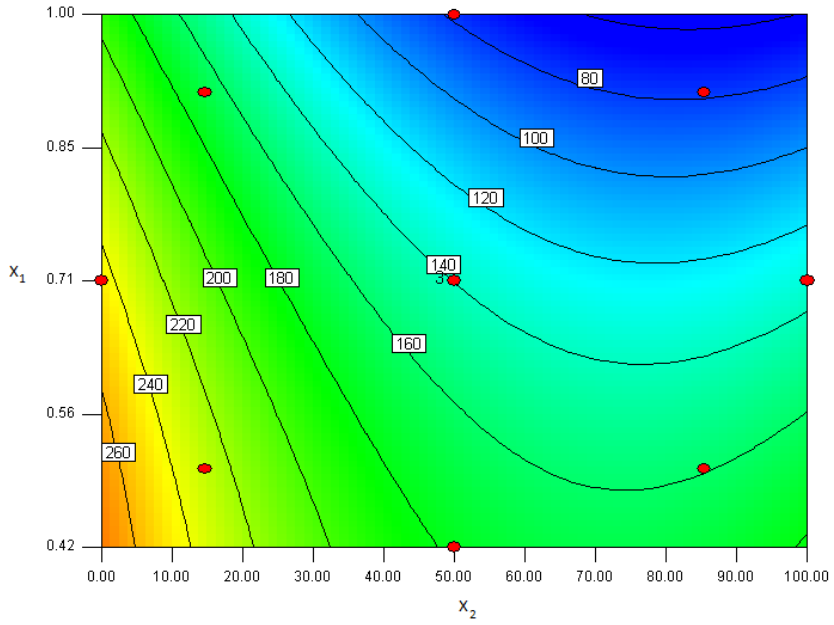

Figure 3.3 An example of a contour plot, showing the variations in the contour values of the dependent variable with the independent variables X_1 and X_2. Values given for X_1, X_2 and the dependent variable are arbitrary.

The 2FI model allows the effect of changing a control to vary with the setting of another control, whilst the quadratic model allows for curvature in the effect of a control on a response [170]. 2FI models are more complicated than linear and the

quadratic models are more complicated than 2FI. As such, data generated for the FED is required to be more statistically significant for increasing complexity of the model chosen to analyse the response. Whichever model is chosen the visual interaction between independent variables is displayed in a three-dimensional space and is known as a response surface plot (Figure 3.2). For simplicity, however, the response surface is usually converted to a two dimensional image displaying the contours of the dependent variable, Y (Figure 3.3).Based on the results from a plot the experimenter can choose to either develop a further FED or remain content with the results of the original plot and select the optimum region from the variables assessed. By developing a further FED the experimenter can focus on a specific area of the original plot in order to minimise error. Additionally they could move the experimental space to look at the effects of changing the IV's beyond the limits set in the original FED. This may be the best option if the DV results were not optimised.

3.2.2. Choosing the Correct Type of FED

The basis of an FED is a full factorial experimental design, which is an experiment whose design consists of two or more factors where each factor can only be measured to discrete possible values [169]. The drawback to using a full FED comes when the number of variables begins to increase, as doing so increases the possible number of combinations of variables leading to high numbers of experiments. In these cases it is more common to initially use a fractional FED whereby some (usually more than half) of the possible combinations are omitted from the experimental work. The combinations omitted are those that usually show little statistical significance.

For the work undertaken in this thesis, the variables are continuous rather than discrete and as such a more complicated method of design is required. A two level FED will assume the relationship between the IVs to be linear within the experimental space. If one is to assume a non-linear response for any of the DVs being measured then a quadratic model needs to be considered. As non-linear effects are likely between the variables studied within the current work, the most suitable type of FED to use was a central composite design (CCD). This method utilises the FED approach to obtaining results by combining a two level design with axial points lying outside the experimental space as seen in Figure 3.4. The eight corners of a cube represent the

corners of the experimental space and the basic axial points represent outlying 'star points'. The corners of the experimental space are often coded as the +1 and –1 values and the star points are coded as the +S and –S values. A CCD also has a centre point which lies at the median of all values for all variables being studied (coded as 0, 0, 0). It is common that this point is replicated within the design in order to improve the accuracy of the FED in determining standard error.

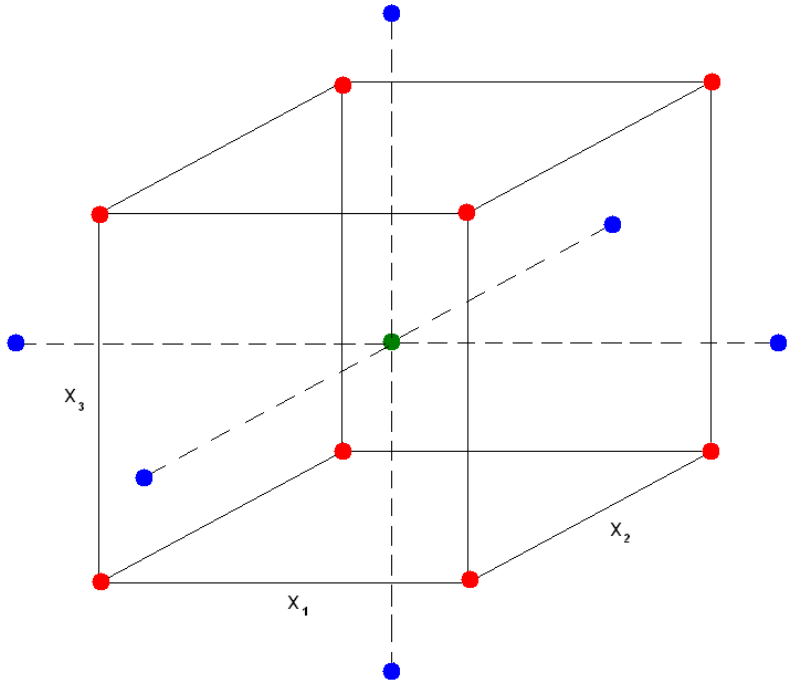

Figure 3.4 Schematic of a 3-variable central composite design (CCD) plot.

3.2.3. Construction of an Experimental Space

Once the number of variables for the CCD has been determined; the limits for each variable need to be set. Computer software Design Expert 7 allows the user to either set the axial (+S and –S) values or the corners of the experimental space (+1 and –1 values). By completing one set of values the software automatically populates the other. Once the limits have been confirmed the user must decide upon the number of repeats for the centre point. The software will then automatically generate a table of all the practical experiments that need completing. The number of 'runs' in the table will depend on the number of variables being studied in the CCD and the number of

centre-point repeats chosen by the user. The number of runs generated in this study for a 2 and 3 factor CCD, with each factor having 2 levels is explained below:

2 Factor: 2^2 (corner points) + 4 (axial points) + 3 (replicated centre point) = 11 runs

3 Factor: 2^3 (corner points) + 6 (axial points) + 6 (replicated centre point) = 20 runs

The runs are assembled by the software in a random order to eliminate any potential bias.

3.3. Calculations for Mixing

A variable from an FED in this study is the weight percent of TGPAP in the TGDDM/TGPAP mix. shows the amounts of TGPAP and TGDDM 'in the mix' of these two resins. However, a second IV is the DGEBF weight percent, given as a weight percentage of the overall resin mix. Therefore, a conversion of the TGPAP to TGDDM ratio is required, as it no longer represented 100% of the resin formulation. Equation 3.4 was used to calculate the change in weight percent of the TGPAP with the addition of DGEBF, where Wt% = weight percent, $TGPAP_t$ = the total amount of TGPAP and $TGPAP_m$ = the amount of TGPAP in the TGPAP/TGDDM mix. Table 3.2 Typical values generated by the FED software (Design Expert 7) for two variables, TGPAP in the TGPAP/TGDDM mix and DGEBF level.

Table 3.2 Typical values generated by the FED software for two variables, TGDDM and TGPAP in the TGPAP/TGDDM mix and DGEBF level.

Material	Weight %
TGPAP in mix	35
TGDDM in mix	65
DGEBF	20

$$Wt\%_{TGPAP_t} = (100 - Wt\%_{DGEBF}) \times \left(\frac{Wt\%_{TGPAP_m}}{100} \right) \qquad (3.4)$$

Using the values from Table 3.2, the actual weight percentages of each of the three resins in a multi-component resin are shown in Table 3.3**.**

Table 3.3 Modified weight percentages of each resin in a three-component epoxy resin formulation.

Material	Weight %
TGPAP	28
TGDDM	52
DGEBF	20

Once the correct weight ratios of all three resins were determined for each run of the FED the concentration of epoxy groups was calculated using Equation 3.5. This value was then used to calculate the concentration of amine groups required to achieve the stoichiometric ratio, r, (Equation 3.6) which in turn was used to calculate the weight of DDS hardener in the formulation (Equation 3.7), where [ ] donates concentration, Wt% is weight percent, EEW is epoxy equivalent weight, r is stoichiometry and AEW is amine equivalent weight.

$$[\mathrm{EPOXY}] = \left(\frac{\mathrm{Wt\%_{DGEBF}}}{\mathrm{EEW_{DGEBF}}}\right) + \left(\frac{\mathrm{Wt\%_{TGPAP}}}{\mathrm{EEW_{TGPAP}}}\right) + \left(\frac{\mathrm{Wt\%_{TGDDM}}}{\mathrm{EEW_{TGDDM}}}\right) \tag{3.5}$$

$$[\mathrm{AMINE}] = \mathrm{r} \times [\mathrm{EPOXY}] \tag{3.6}$$

$$\mathrm{Wt_{DDS}} = [\mathrm{AMINE}] \times \mathrm{AEW_{DDS}} \tag{3.7}$$

Table 3.4 An example of the final weight ratios of resins and hardener in 100 g multi-component resin formulation where r = 0.92.

r	DGEBF (g)	TGPAP (g)	TGDDM (g)	[Epoxy]	[Amine]	DDS (g)
0.92	20	28	52	0.87	0.8	50

3.4. Prepolymer Mixing

3.4.1. Pre Mixing Preparation

To achieve efficient mixing the viscosity of all three resins was required to be sufficiently low for ease of use. TGDDM is a high viscosity epoxy resin and as such requires heating in an oven at 80°C to lower the viscosity. TGPAP is a low viscosity liquid and as such, no preheating was required. DGEBF was supplied as a crystalline solid with a melting temperature of 40°C and therefore was heated at 80°C and allowed to melt. DDS hardener is supplied as a fine white powder. Before being added to the resin prepolymer blend the DDS was weighed out in disposable plastic containers in order to allow for accurate addition.

3.4.2. Mixing

Once of a suitable viscosity, TGDDM was weighed accurately in to a glass jar, which also acted as the vessel for resin mixing. All weighing was carried out on electronic scales to ±0.1 g. DGEBF and TGPAP were subsequently weighed into the same jar. The jar was transferred to a silicone oil bath (Figure 3.5) where it was held in place using a lab clamp and was preheated to 130°C. The temperature of the oil was maintained using a hotplate and measured using a thermometer placed in the oil. Once the jar of resin was added the temperature was allowed to equilibrate. The DDS hardener was then poured into the resin from the disposable container through a funnel.

An overhead stirrer with a twin bladed shaft was then lowered into the prepolymer blend so that the blade sat just below the surface. The shaft was not located in the direct centre of the jar. Instead, it was offset from the centre in order to create a narrow gap between the blades and side of the jar. The aim of this was to breakup of any agglomerates of DDS powder that may form. To disperse the DDS hardener the shaft was initially rotated at a speed of 500 rpm for 1 minute. Once the hardener was incorporated, the speed was increased to 1000 rpm and the mix was then left for a further 14 minutes (making a total mixing time of 15 minutes) for complete dissolution of the DDS.

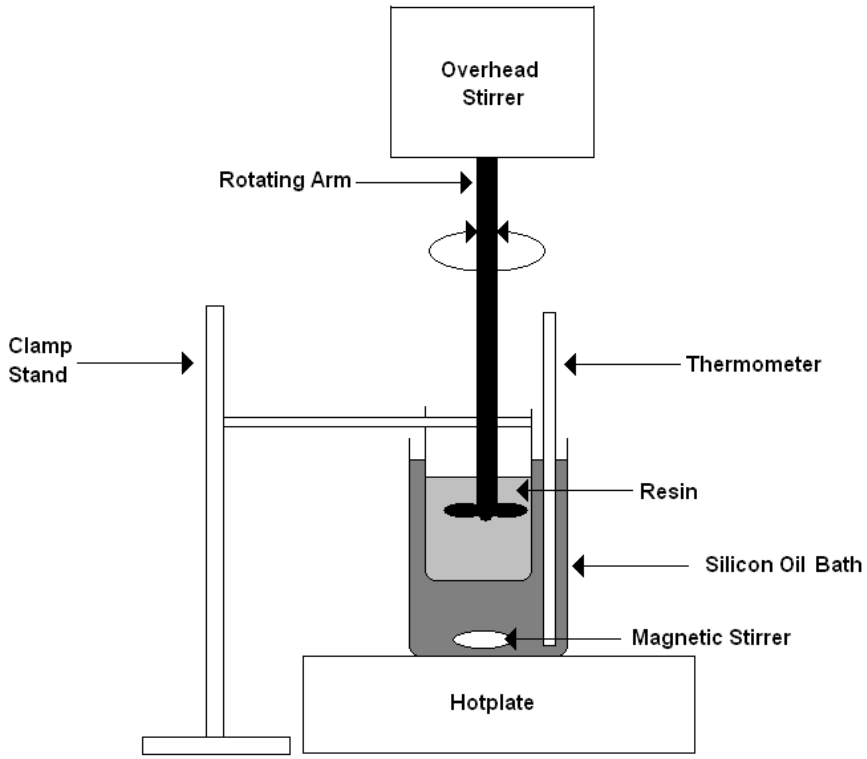

Figure 3.5 Set up for resin mixing.

3.4.2.1. *Mixing with a Thermoplastic Toughener*

In the formulations containing PES, the thermoplastic was added after mixing the resins but prior to the hardener. Like the hardener, it was added via a small funnel and in 10 wt% increments. Each increment was allowed to dissolve before more PES was added. The majority of the literature concerned with the mixing of epoxy and PES used solvent mixing techniques [49], [64], [113], [171], [172]; the sole advantage of which being a reduced viscosity which aids the dissolution of the thermoplastic. Although adding the thermoplastic to an epoxy prepolymer is made easier by the use of a solvent it does pose problems. The evaporation and degassing of the solvent prior to the use of the resin in a composite is time consuming. Furthermore, any residual solvent can have negative effects on the properties of the final resin thus making the process less commercially attractive and less environmentally friendly. In this research no solvents were used in favour of a melt mixing technique, which relies on mixing with a rotating blade in a heated environment. In fact, dissolution of PES was not

difficult at any loading level, possibly because of the –OH end groups attached to the PES, which aided its dissolution.

3.4.3. Storage

Once mixed the blend was poured on to a sheet of release film and a second sheet of film was placed on top, sandwiching the resin before storing in a freezer at -20°C. This technique allows a small sample of frozen resin to be removed and tested whilst the bulk of the resin remains frozen in storage.

3.5. Differential Scanning Calorimetry (DSC)

Differential scanning calorimetry (DSC) is a thermal analysis technique used in this study to obtain the enthalpy of reaction, dH, the degree of conversion, α, and isothermal reaction kinetics of epoxy resins. There are two types of DSC, heat flux and power-compensated. Heat flux DSC measures the change in temperature of the sample with respect to a reference sample whereas with the power compensated DSC the heat generated or absorbed is compensated by electrically heating the appropriate furnace [173]. In this study a heat flux DSC was used, therefore focus is directed towards this technique.

3.5.1. Heat Flux DSC

A schematic of the heat flux DSC technique is shown in Figure 3.6. A sample and a reference sample share the same heat source and two thermocouples monitor the change in temperature of each sample. The two thermocouples will read the same temperature until a heat change occurs in the sample. The main heat change in epoxy resins is due to an exothermic polymerisation reaction induced by an increase in temperature of the furnace. The change in heat capacity is digitally recorded as a change in power per unit weight, commonly W g^{-1}.

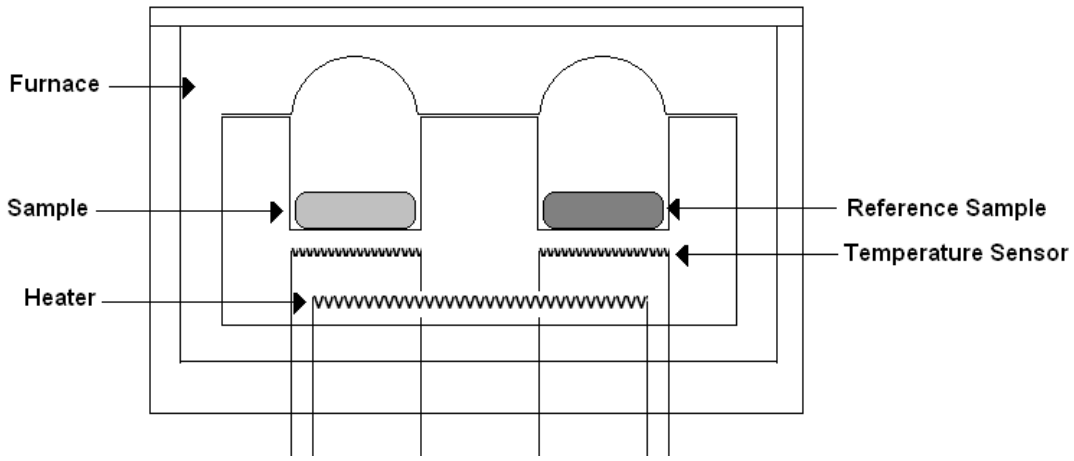

Figure 3.6 Experimental set up for heat flux DSC.

3.5.2. Total Enthalpy of Reaction

Determining the degree of conversion as a function of time and temperature provides information on the reactivity of an epoxy resin, which in turn can assist in the development of a suitable cure cycle. Raising the temperature of an epoxy resin in the presence of a diamine hardener leads to the conversion of primary amines to secondary amines and secondary amines to tertiary amines as they react with the epoxy groups. Quenching the reaction at a given time, t, allows for the degree of conversion at t to be calculated by subjecting the resin to a temperature sweep using DSC. As the resin has already been subjected to a certain amount of heat, the resin is partially cured. Therefore, the measured value for dH represents the residual heat of reaction for unreacted epoxy groups dH_r. As such, it should be smaller than the total enthalpy of reaction, dH_t. Once values for the total enthalpy and residual enthalpy of reaction are known the degree of conversion at time t can be calculated using Equation 3.8.

$$\alpha = \frac{\left(dH_0 - dH_r\right)}{dH_t} \equiv 1 - \left(\frac{dH_r}{dH_t}\right) \tag{3.8}$$

3.5.2.1. Experimental Procedure

2-6 mg samples of resin were placed in aluminium pans using a glass pipette. The pans were then weighed to 0.0001g before aluminium lids were crimped on, sealing the resin inside. The sample was placed in the DSC furnace and a reference sample (an empty aluminium pan) placed in the adjacent furnace.

The dH was measured by ramping the temperature of the furnace from 30°C to 320°C at 10°C min^{-1} in a nitrogen atmosphere. Before testing was conducted the machine was calibrated for the aforementioned ramp rate using zinc and indium standards. A baseline calibration was also obtained by subjecting an empty aluminium pan to the temperature cycle. Both calibrations were applied to every sample tested.

The temperature ramp was then started and the change in heat flow recorded. A typical graph of the change in heat flow of an epoxy resin is displayed in Figure 3.7. The change in heat flow is expressed as a peak. Integrating the area gives dH for the system. Values quoted in this thesis are from a minimum of three repeats and errors quoted are standard deviations.

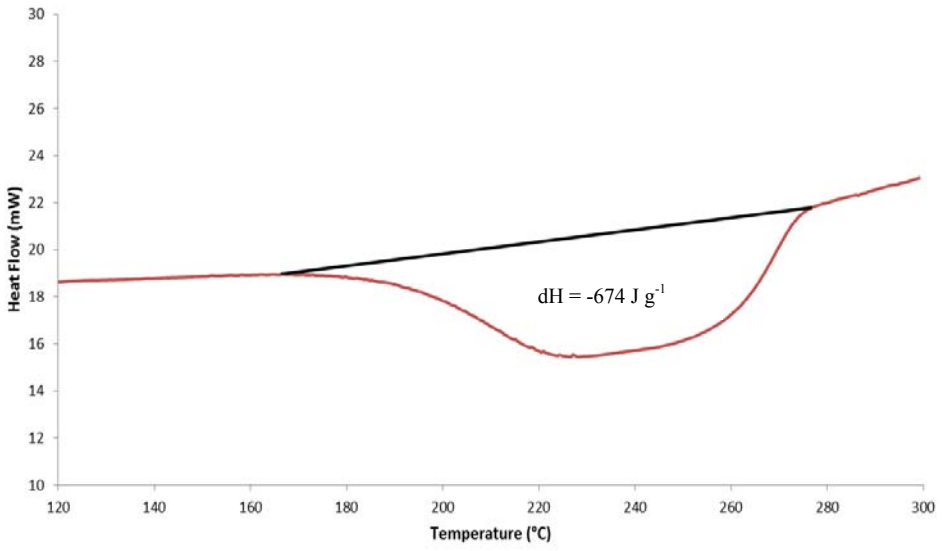

Figure 3.7 Typical DSC trace for an epoxy-amine mix ramped up to 300°C.

3.5.3. Isothermal DSC Curing and Kinetics

Integrating the area under the isothermal heat flow curve gives the rate of reaction, dα/dt at any point during the curing of a resin for that temperature. Furthermore, by isothermally curing a resin until it vitrifies one can measure the enthalpy of reaction at vitrification, from which the degree of conversion at vitrification can be calculated by subtracting the measured dH from dH_t.

The rate of reaction curves for each resin can be used to model kinetic parameters. In this thesis Kamal's autocatalytic equation (Equation 2.7) was used to model the reaction kinetics for resins cured isothermally in this work. k_1 was graphically determined as the rate of reaction at t=0. All other variables where calculated with non-linear regression analysis using the Solver function available in Microsoft Excel. The rate constants k_1 and k_2 are dependent on temperature and follow Arrhenius' law (Equation 3.9), where i = 1 or 2, A = the pre exponential factor, E_a = the activation energy (kJ mol^{-1}), R = the real gas constant (J K^{-1} mol^{-1}). and T = temperature (K).

$$\frac{d\alpha}{dt} = \left(k_1 + k_2\alpha^m\right)(1-\alpha)^n \tag{2.7}$$

Where k_1 and k_2 = the rate constants for the non-catalysed and auto-catalysed reactions respectively.

$$k_i = A.\exp\left(\frac{-E_{a_i}}{RT}\right) \tag{3.9}$$

Taking the natural logarithm of both sides generates a linear equation:

$$\ln k_i = \ln A - \frac{E_{a_i}}{RT} \equiv -\frac{E_{a_i}}{R}\frac{1}{T} + \ln A \tag{3.10}$$

Plotting ln k_1 and ln k_2 against 1/T generates lines of gradient $-E_a/R$ and intercept of ln A. As five isothermal temperatures were used a line of best fit was taken through

the points for each resin, from which the activation energies were calculated by dividing the line gradient by –R.

3.5.3.1. Experimental Procedure

Isothermal DSC was conducted at five temperatures, 160, 170, 180, 190 and 200°C. Before a sample was placed in the furnace the curing temperature was set. Samples were cured in the DSC furnace until the baseline reached a plateau, signifying the sample had vitrified.

The sample was then cooled at 50°C min^{-1} to -20°C before being subjected to a temperature ramp up to 320°C at 10°C min^{-1} to find the residual enthalpy of reaction. Typical isothermal DSC traces for an epoxy resin curing at 160°C and 200°C are shown in Figure 3.8.

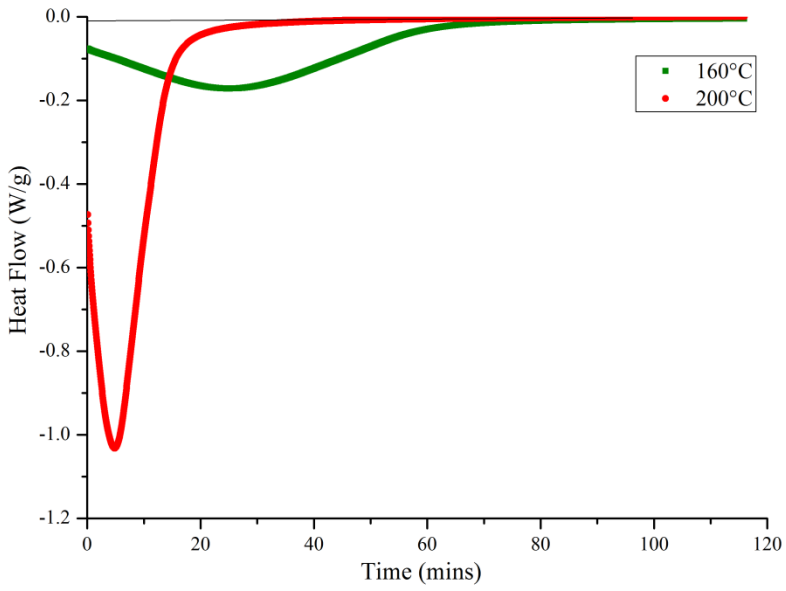

Figure 3.8 An example of two isothermal DSC traces of an epoxy resin reacting with an amine hardener at 160°C and 200°C.

3.6. Fourier Transform Infrared (FTIR) Spectroscopy

FTIR spectroscopy is an analytical technique used for characterising the chemical bonds that exist within a given material. FTIR works by splitting an infrared beam in to two beams, one of a fixed length and one of a variable length (Figure 3.9). The length of the variable beam is controlled by mirror B. By varying the distance between the path lengths, a sequence of constructive and destructive interferences occur which in turn induces variation in the intensities of the beam [174]. Practically, this allows for the characterisation of a material with unknown quantities of specific chemical bonds. Different chemical bonds absorb IR of different wavelengths irrespective of the environment. They are graphically represented as peaks in absorbance at the corresponding wavelength.

IR radiation lies between the visible and microwave regions of the electromagnetic spectrum and exists with wavenumbers between 200-14290 cm^{-1}. There are three sub categories to the infrared region, near IR, mid IR and far IR, however in this study only the mid infra IR region (650-4000 cm^{-1}) was used.

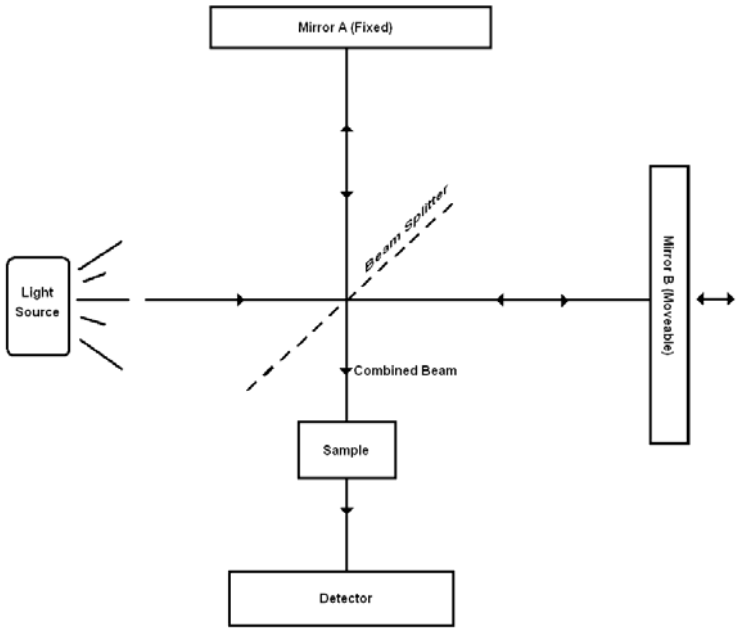

Figure 3.9 **A diagram of a Fourier transform infrared spectrometer.**

3.6.1. Time Resolved Infrared Spectroscopy (TRIR)

TRIR was used to characterise the changes in the absorbances of epoxy and amine groups during the cure cycle. A thin sample of each resin studied was sandwiched between two blocks of polished sodium chloride and placed into a heating cell attached to a Eurotherm 847 Automatic Temperature Control. The samples of TGPAP, TGDDM and DGEBF studied at a stoichiometric ratio of r = 1.0 with DDS were cured isothermally at 130°C for five hours, whereas the resins of varying stoichiometric ratio were cured following the cycle used within our research group of 3 hours at 130°C, 2 hours at 165°C and 2 hours at 200°C. Spectra were taken throughout the entire cure cycle. Each set of spectra were normalised to the 1590 cm^{-1} peak attributed to phenyl groups which is known not to be involved in epoxy-amine reactions. Absorbency peak heights were measured for the peaks given in Table 3.5. All TRIR spectra were analysed using Omnic 7.2 software.

Table 3.5 Functional groups and the FTIR peaks assigned to them.

Functional Group	Peak Range (cm^{-1})	References
Phenyl (Reference Peak)	1593	[78]
Epoxy	907-915	[82], [175]
Primary Amine	1618-1628	[82]
Hydroxyl	3450-3640	[82], [176]

3.7. Rheometry

Rheometry is an experimental technique used to characterise rheological behaviour. Rheology is defined as the study of fluid behaviour during induced deformation [177]. Figure 3.10 shows a simple diagram illustrating shearing of a Newtonian fluid. Two parallel plates of surface area, a, are separated by a distance, d. The space between the plates is filled with fluid. In the diagram, the upper plate moves with a velocity, ν. The force per unit area, F/a, required to induce a motion in the x direction is known as the shear stress, τ, and is proportional to the rate of shear deformation, $d\gamma/dt$, or velocity

gradient, v/d. The rate of shear deformation is denoted by $\dot{\gamma}$ and is equal to the rate of change in the shear strain of the fluid, γ, with respect to time, $d\gamma/dt$.

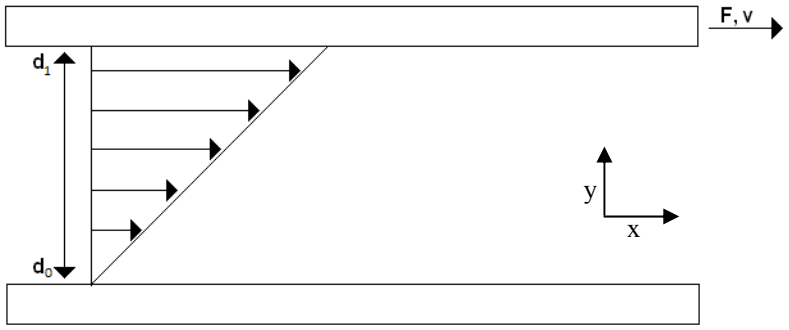

Figure 3.10 Model illustrating shearing of a Newtonian fluid.

The shearing action creates a stress profile across the gap, which in turn creates a velocity profile whereby the fluid velocity varies from a minimum at d_0 to a maximum at d_1. The relationship between shear stress and rate of shear is expressed by Newton's law of viscosity (Equation 3.11).

$$\tau = \eta \frac{d\gamma}{dt} \tag{3.11}$$

Where η = the coefficient of shear viscosity of a fluid (Pa s).

The shear strain rate is derived from the definition of the strain experienced by the fluid:

$$\dot{\gamma} = \frac{d\gamma}{dt} \tag{3.12}$$

Thus, the shear at a given point is equal to the velocity gradient at that point.

$$\frac{d\gamma}{dt} = \frac{d\left(\frac{dx}{dt}\right)}{dt} \equiv \frac{d\left(\frac{dx}{dt}\right)}{dy}$$

$$\therefore \frac{d\gamma}{dt} = \frac{dv_x}{dy} \tag{3.13}$$

Where dv_x = the change in velocity in the x direction.

In summary the lengths of the arrows in Figure 3.10 represent the change in velocity of the material for the given point along d. Materials where this is true are known as Newtonian fluids, however the majority of polymers, including epoxy resins, exhibit non-Newtonian behaviour. This means that the shear stress and shear strain rate are not related linearly.

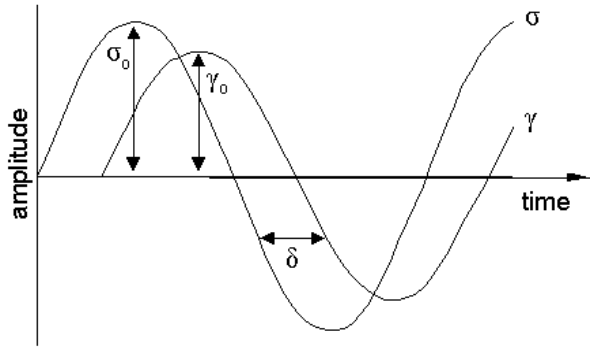

Figure 3.11 Phase lag between an applied oscillatory stress and a measured strain.

Polymers, such as curing and cured epoxy resin exhibit viscoelastic behaviour, whereby they have both characteristics of solid and liquid materials.. Viscoelastic materials consist of both viscous and elastic behaviour, thus the phase lag between an applied oscillatory stress and the measured strain is between 0-90° (Figure 3.11).The applied stress, τ, and the resultant strain, γ, are given by Equations 3.14 and 3.15).

$$\tau = \tau_0 \sin(t\omega + \delta) \tag{3.14}$$

$$\gamma = \gamma_0 \sin(t\omega) \tag{3.15}$$

Where ω = frequency of strain oscillation, δ = phase lag between stress and strain, and t = time.

The relationship between shear stress and strain can be expressed mathematically as the shear modulus, which in turn is resolved into the storage modulus (elastic response) and loss modulus (viscous response) [178]. The storage modulus, G', and loss modulus, G'', are expressed as:

$$G' = \frac{\tau_0}{\gamma_0}\cos\delta \tag{3.16}$$

$$G'' = \frac{\tau_0}{\gamma_0}\sin\delta \tag{3.17}$$

The ratio between the two moduli is used to determine the phase angle or tan δ:

$$\tan\delta = \frac{G''}{G'} \tag{3.18}$$

The point that tan δ = 1 as a result of the loss and storage moduli intersecting is often regarded as the sol/gel transition point or 'gel point' for short [179]. Thus, it is at this point that a resin ceases to flow. For this reason the time at which the G'/G'' crossover occurs is often regarded as the 'processing window' for a thermosetting resin. However, in accordance with ASTM D 4473-95a [180] the dynamic gel point, DGP, is the time at which the complex viscosity of a resin exceeds 100 Pa s. It is thought that above the DGP the resin flow would be insufficient for composite manufacturing. With this in mind both the DGP and G'/G'' crossover measurements were recorded for materials undergoing rheological study.

The complex viscosity is the summation of both the real and imaginary parts of viscosity associated with the loss and storage moduli. It is a frequency dependent viscosity function and is determined during forced oscillation of shear stress. Thus, the complex viscosity, η^*, is derived as:

$$\eta^* = \eta' + i\eta''$$

$$\eta' = \frac{G'}{\omega} \qquad (3.19)$$

$$\eta'' = \frac{G''}{\omega}$$

Where η' = dynamic viscosity or in phase viscosity, η'' = imaginary or out of phase viscosity, $i = \sqrt{-1}$ and ω = 2πf, where f = frequency of oscillation.

3.7.1. Experimental Procedure

In this work dynamic shear rheometry was conducted on a Haake MARS (modular advanced rheometer system). Disposable parallel plates of 35mm diameter were attached to a transducer on the top and a static pole on the bottom (Figure 3.12). The furnace was closed around the two parallel plates and they were heated to 80°C. Note that the temperature was measured using a thermocouple located in the centre of the static pole; thus, the measured temperature was that of the air and not the resin sample.

Once the furnace air temperature was 80 ± 5°C, resin was either poured or placed on to the bottom plate (depending on whether liquid or frozen) and the plates closed to a gap of 0.5 mm. Any excess resin was removed using a piece of tissue before the furnace doors were closed. The sample was heated to 80°C ± 0.5°C. Ideally, an isothermal cure profile at 130°C would be recorded. However it was found that owing to differences in sample loading time, the time taken for the furnace temperature to increase back to 130°C differed. As such the temperature began with a dwell at 80°C before ramping to 130°C at 10°C min^{-1}. Once the experiment had begun the transducer oscillated at a frequency of 1 Hz with a control stress of 2.0 Pa. The experiment continued until the material had passed through the G'/G'' crossover. Values quoted in this thesis are from a minimum of three repeats and errors quoted are standard deviations.

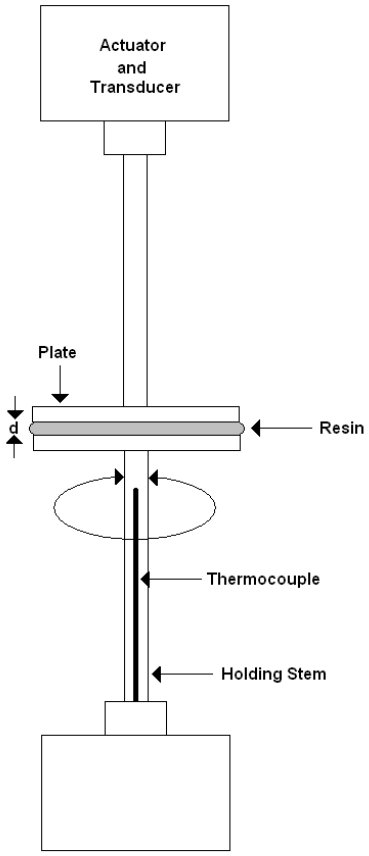

Figure 3.12 Schematic diagram of an oscillating shear rheometer.

3.8. Dynamic Mechanical Thermal Analysis (DMTA)

DMTA is a characterisation technique used to determine the viscoelastic properties of a solid material; namely the storage and loss moduli. In perfectly elastic materials there is no phase lag between an applied stress and the measured strain whereas in perfectly viscous materials there is a 90° phase lag. Like most polymers, epoxy resins are neither perfectly elastic nor perfectly viscous. When cured they are viscoelastic materials and as such have a phase lag between 0 and 90°. The stress and strain applied to a material undergoing DMTA is measured using the same equations stated in the rheology section of this chapter (section 3.7), from which the loss and storage moduli can be calculated.

DMTA was used to measure moduli as a function of temperature with the aim of identifying the glass transition temperature, T_g. The T_g is defined as the reversible transition of an amorphous polymer from a rigid glass to a flexible rubber-like state [1]. DMTA results show the temperature at which this change in behaviour occurs as a rapid decrease in the measured storage modulus and an increase in the loss modulus. As discussed in section 3.7 tan δ is the ratio between the loss and storage. Typically T_g can be easily defined using the tan δ curve as it exhibits a sharp peak, as shown in Figure 3.13. This peak is widely regarded as the T_g, however, from an engineering viewpoint the T_g is often defined at the point that the material stops behaving like a glass, and tends towards a rubber-like state i.e. the onset of the drop in storage modulus of the material. It is at this point that the mechanical properties of the material will begin to decrease, and in terms of aerospace applications, knowing this temperature is of more value. However, finding the onset can be subjective as drawing two accurate tangents on the storage modulus-temperature curve can often be difficult (see Figure 3.13). With this in mind, both values will be reported in this work.

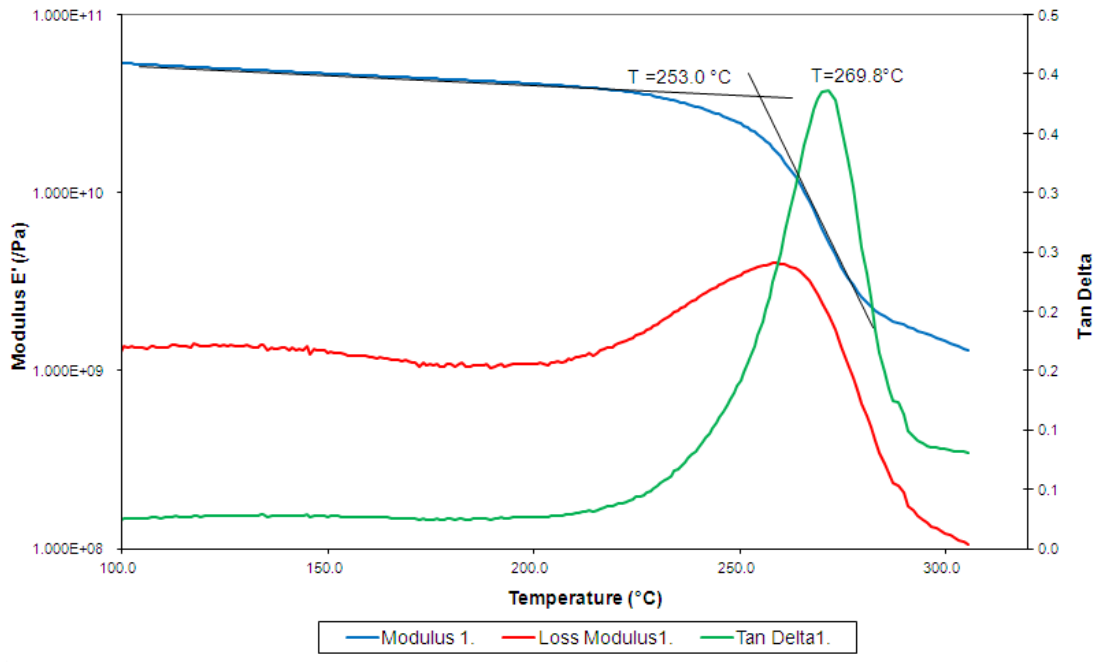

Figure 3.13 Typical DMTA trace for a highly crosslinked epoxy resin taken from this work.

Dimensions for specimens were as follows:

Length: 40 mm
Width: 9.5-10.5 mm
Thickness: 2.5-3.5 mm

DMTA was conducted on a Perkin Elmer DMA 8000 in dual cantilever mode The stress was applied at a frequency of 1 Hz and specimens were heated from 50°C to 300°C at 5°C min^{-1}. A minimum of three specimens were tested for each material. No errors are provided for any of the data presented for DMTA results in this thesis on account of the high level of accuracy associated with this technique.

3.9. Fracture Toughness

Fracture toughness testing of the cured resins was conducted in accordance with ASTM D 5045-99 [181]. The critical-stress-intensity factor (fracture toughness), K_{1C}, and the critical strain energy release rate at fracture initiation (fracture energy), G_{1C}, were determined. The fracture toughness characterises the resistance of a material to fracture in the presence of a sharp crack under severe tensile constraint, such that the state of stress near the crack front approaches plane strain conditions and the crack-tip plastic region is small compared with the crack size and specimen dimensions in the constraint direction [181].

3.9.1. Sample Preparation

Resins to be tested were first mixed, degassed until no entrapped air remained and cured following the cure cycle developed within our research group. Samples were then cut following the size criteria in Equation 3.20 and Figure 3.14, where B = thickness, W= width of sample ≡ 2B, a = crack length, σ_y = the yield stress of the material for the temperature and loading rate of the test and K_Q = the conditional K_{1C} value ≡ 0.7 times the compressive yield stress.

$$B, a, (W - a) > 2.5\left(\frac{K_q}{\sigma_y}\right)^2 \tag{3.20}$$

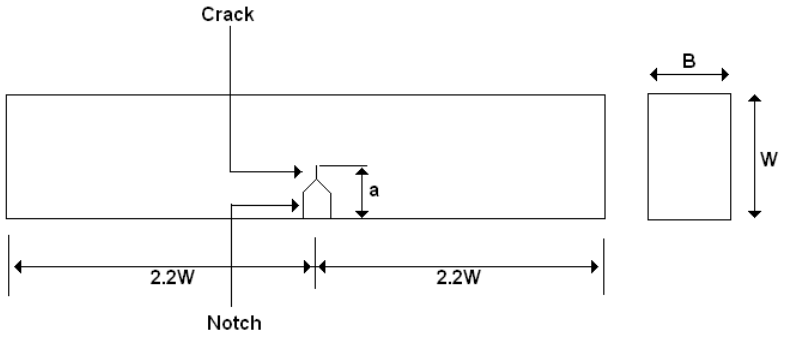

Figure 3.14 A schematic of a specimen used for polymer fracture toughness testing.

Based on these criteria samples of dimensions 44 × 10 × 5 mm were used. The width and thickness of the samples were measured at three points along each dimension and recorded. The average of the three measurements did not exceed ± 0.1% of the ideal dimensions. Once cut, samples were ground and polished.

$$0.45 \leq \frac{a}{W} \leq 0.55 \tag{3.21}$$

Based on Equation 3.21, 4.5 mm ≤ a ≤ 5.5 mm. Therefore a notch of depth 4.0 mm was cut in each sample exactly half way along the length. A crack was then initiated by inserting a fresh razor blade in to the notch and gentle tapping with a jeweller's hammer. Owing to the aforementioned grinding and polishing of each sample the initiation of a crack was easily visible. The difference between the shortest and longest lengths of the crack should not exceed 10%. Controlling the crack formation is difficult and therefore any samples which did not meet this criterion were discarded from the experiment.

The ASTM standard suggests a minimum of three replicate tests for each material being tested. However, consultation of the literature reveals that the standard deviation for fracture toughness testing can be somewhat high [101], [110], [182]. Based on this

information a minimum of five specimens were used in this study for each material. Errors quoted are standard deviations.

3.9.2. Experimental Procedure

Testing was conducted on an Instron 4411 bench top with a 500 N load cell in single-edge-notch bending (SENB) mode (Figure 3.15). Specimens were placed on rollers 40 mm apart, perpendicular to a 7.0 mm diameter loading nose with the load nose sitting directly above the crack. A crosshead rate of 10 mm min^{-1} was used and all specimens were tested at 23°C. An example of data obtained is displayed in Figure 3.16.

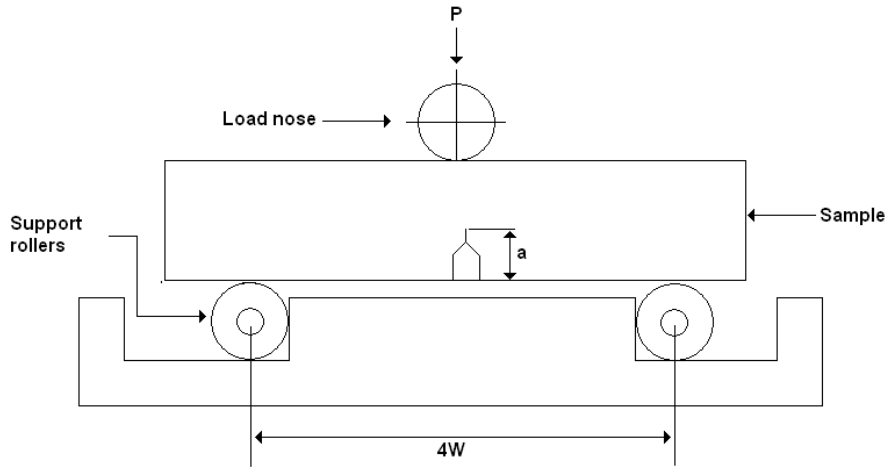

Figure 3.15 Experimental set up for polymer fracture toughness testing.

The crack length was then measured using callipers under an optical microscope. The average of three points (centre crack length and lengths at both of the specimen's edges) was taken as the crack length.

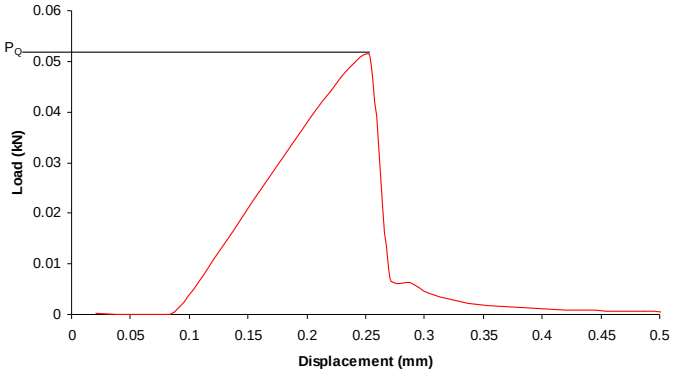

Figure 3.16 Typical load/displacement curve from an untoughened epoxy resin fracture toughness specimen.

3.9.3. Calculations

3.9.3.1. K_{1C}

The ASTM standard requires a compliance test to be undertaken for each material whereby if the maximum load at failure falls within a 5° angle of the tangent to the loading curve, then P_{max} is used to calculate K_Q. As all the materials tested failed by brittle fracture this requirement was met, therefore K_Q is equal to K_{1C} and was calculated from Equation 3.22 and Equation 3.23, where $K_Q = K_{1C,}$ P_Q = maximum load, B = sample thickness, W = sample width and x = W/a, where a = crack length.

$$K_Q = \left(\frac{P_Q}{BW^{\frac{1}{2}}} \right) f(x) \tag{3.22}$$

$$f(x) = 6x^{\frac{1}{2}} \left[\frac{1.99 - x(1-x)(2.15 - 3.93x + 2.7x^2)}{(1+2x)(1-x)^{\frac{3}{2}}} \right] \tag{3.23}$$

3.9.3.2. G_{1C}

G_{1C} is the critical strain energy release rate at fracture initiation. It is based on the specimen dimensions, crack length and energy absorbed by the specimen before failure (Equation 3.24). Where U = area under the compliance curve at maximum load, B = thickness, W = width and Φ = energy calibration factor.

$$G_Q = \frac{U}{BW\Phi} \tag{3.24}$$

Both U and Φ are calculated using Equations 3.25 and 3.26 respectively, where P_Q = maximum load from K_{1C} calculation, U_Q is the displacement at P_Q and U_i is the intersect of the tangent with P=0, A is a factor based on x and dA/dx is the differentiation of A.

$$U = P_Q\left[U_Q - U_i\right] \tag{3.25}$$

$$\Phi = \frac{A + 18.64}{\frac{dA}{dx}} \tag{3.26}$$

Where A is calculated from Equation 3.27.

$$A = \left[\frac{16x^2}{(1-x)^2}\right]\left[\frac{8.9 - 33.717x + 79.616x^2}{-112.952x^3 + 84.815x^4 - 25.672x^5}\right] \tag{3.27}$$

3.10. SEM

Scanning electron microscopy (SEM) has been widely used for viewing the morphology of polymer blends [22], [45], [110], [111], [183], [184]. The technique is favoured owing to its higher resolution and larger depth of field in comparison to optical microscopy. Sample preparation is also relatively simple [185]. The technique rasters a beam of electrons over the surface of a material and uses any radiation from the specimen to form an image [186]. The quality of the image depends on the interaction at the surface, the detector and the signal processing used.

The most common image signal techniques are backscattered electrons (BSE) and secondary electrons. BSE imaging involves using a high energy beam that penetrates up to 1 μm into the surface of the specimen. As such BSE leave the surface from a wide area, resulting in poor resolution [185]. Secondary electrons are emitted with low energy and as such only interact with the top few nanometres of the specimen. This results in a high resolution image and as such was used in this work.

3.10.1. Sample Preparation

The vast majority of SEM analyses of epoxy resins blended with thermoplastics have etched the fracture surface of the materials using a solvent; most commonly dichloromethane [49], [109], [110]. However reports examining the toughening of epoxy with a functionalised PES (such as the functional -OH groups present in the PES used in this study) used an acid etching technique [113], [114]. Whilst no direct reference was made to the bonding between the toughener and the thermoset it is inferred by the need to use acid etching instead of solvent etching. To successfully etch the polymers a combination of sulphuric and phosphoric acid is required as discussed below.

SEM was conducted on unmodified and toughened specimens of cured epoxy resin. The specimens had been previously tested for fracture toughness, and the fracture surfaces from these specimens were observed. They were etched in a 1% solution of potassium permanganate in a 5:2:2 volume mixture of concentrated sulphuric acid: phosphoric acid: distilled water. For each specimen this equated to volumes of 25:10:10 ml respectively with a potassium permanganate content of 0.45g. The mixture was placed into a glass container and was stirred using a magnetic stirrer at room temperature. Each specimen was etched individually for 20 minutes in a fresh solution. Once etched, the samples were sequentially washed in aqueous sulphuric acid, hydrogen peroxide, water and acetone and then dried for 2 hours at 80°C.

Specimens were fixed to aluminium stubs with conductive carbon paper, sputter coated with carbon and then their edges painted with conductive silver paint before testing. Images were taken on a Phillips XL30 FEG SEM operated at 8 kV.

4. Characterisation of Two Component Epoxy Resin Systems

The names, abbreviations, nominal functionalities and epoxy equivalent weights (EEW) of the prepolymers used in this study are presented in Table 4.1 and their chemical structures in Figure 4.1. The nominal functionality of the three prepolymers refers to the number of epoxy groups per monomer. The molecular weight of a prepolymer divided by its functionality gives the nominal EEW. Resin manufacturers provide the measured EEW, which, for all three prepolymers, is higher than the nominal EEW. In commercial resins such as the MY721 and MY0510 used in this study (referred to henceforth as TGDDM and TGPAP respectively), there exist some impurities which affect the EEW. St John et al. [32] studied different grades of TGDDM-based prepolymers using liquid chromatography. They reported that the purist form of the resin, TGDDM, contained 93% TGDDM monomers whereas the commercially used MY721 only contained 79% TGDDM monomers. The fact that the measured EEW of the TGDDM used in this study is larger than the nominal EEW suggests there are high molecular weight impurities present in the resin, which is in agreement with the results presented by St John. For stoichiometric calculations, the measured EEW is used for all prepolymers and for functionality-based calculations, the nominal functionalities are used.

4,4'-Diaminodiphenyl sulphone (DDS) (Figure 4.1d), a diamine hardener, was mixed with each of the resins at a stoichiometric ratio of r = 1.0; meaning these formulations contained equal numbers of available epoxy groups and primary amine-hydrogens. Whilst this may not yield the optimum properties for each of the resin systems, by fixing the stoichiometric ratio comparisons can be made between the thermal characteristics of the three epoxy resins.

Table 4.1 The names, abbreviations and nominal functionalities of epoxy resins and hardener used in this study.

Chemical Name	Abbreviation	Nominal Functionality	Nominal Epoxy Equivalent Weight (g eq^{-1})	Measured Epoxy Equivalent Weight (g eq^{-1})*
Tetraglycidyl-4,4'-diaminophenylmethane	TGDDM	4	105.5	114
Triglycidyl-p-aminophenol	TGPAP	3	92.3	96
Diglycidyl ether of Bisphenol F	DGEBF	2	157	164
4,4'-Diaminodiphenyl sulphone	DDS	4	62**	62.08**

* Data supplied by chemical manufacturers.

** Values are for the amine-hydrogen equivalent weight.

a)

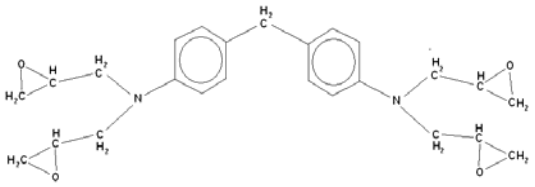

b)

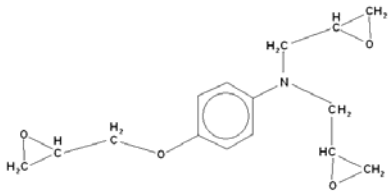

c)

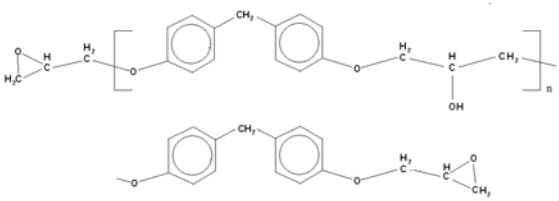

d)

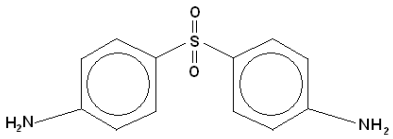

Figure 4.1 (a) Tetraglycidyl-4,4'-diaminophenylmethane (TGDDM) (b) Triglycidyl-p-aminophenol (TGPAP) (c) Diglycidyl ether of Bisphenol F (DGEBF) (d) 4,4'-Diaminodiphenyl sulphone (DDS).

4.1. Differential Scanning Calorimetry (DSC)

4.1.1. Enthalpy of Reaction and Rate of Reaction

Differential scanning calorimetry (DSC) was used to measure the total enthalpy of reaction, dH_t, and the enthalpy of reaction at a given isothermal temperature for the three epoxy resins. Specimens were subjected to a temperature ramp at 10°C min^{-1} up to 320°C, from which dH_t was measured by integrating the area under the curve. The enthalpy of reaction associated with those areas along with the enthalpy per mole of epoxy is shown in Table 4.2.

Table 4.2 Total enthalpy of reaction from dynamic DSC runs at 10°C min^{-1} for base resins at a stoichiometric ratio of r = 1.0.

Resin	Enthalpy of Reaction dH_t (J g^{-1})	Total Enthalpy per Mole (kJ mol^{-1})
TGDDM	598 ± 12	105 ± 3
TGPAP	607 ± 14	96 ± 2
DGEBF	334 ± 9	76 ± 2

The enthalpy of reaction for TGPAP was 607 ± 14 J g^{-1}, in agreement with Man [78] who reported an enthalpy of reaction of 611 ± 12 J g^{-1} for the same system. Gupta et al. [187] reported dH_t for a TGDDM-DDS resin to be 646 J g^{-1} although the stoichiometric ratio was r <1.0. Mijovic et al. [188] reported dH_t for a TGDDM-DDS resin to be 581 J g^{-1} at a stoichiometric ratio of r = 1.0; supporting the value shown in Table 4.2. No values could be found in the literature for the mixture of DGEBF with DDS but reference can be made to the chemically similar DGEBA. Tripathi [48] found DGEBA-DDS to have a dH_t of 355 J g^{-1} whereas Grillet et al. [36] reported the enthalpy of reaction for DGEBA-DDS as 386 J g^{-1}. The value for DGEBF-DDS measured in this study is in agreement with the reported values for the chemically similar DGEBA-DDS system.

The enthalpy per mole of epoxy was calculated through multiplication of dH_t by (EEW + AEW). The values for the three resins range from 105 kJ mol^{-1} for TGDDM

to 76 kJ mol^{-1} for DGEBF. The values for TGDDM and TGPAP are in relatively good agreement with reported values in the literature, which range from 90-110 kJ mol^{-1} [36], [189]–[191]. The enthalpy per mole of epoxy for DGEBF is significantly lower than the reported values in literature for the chemically similar DGEBA. However, in unpublished work by Man [119] the enthalpy per mole of epoxy in DGEBA-DDS was reported as 81 kJ mol^{-1}, similar to the value obtained in this study for DGEBF-DDS.

Specimens of each resin system were cured for two hours at five different isothermal temperatures; 200, 190, 180, 170 and 160°C. They were then quenched to -20°C before being subjected to a temperature ramp up to 320°C at 10°C min^{-1} to measure the residual cure. The area associated with the heat of reaction at each isothermal temperature was used in conjunction with the residual cure to measure the degree of conversion using Equation 3.8 (p 85).

Figure 4.2 shows for each resin, plots of conversion versus time for the five isothermal cure temperatures. A summary of the final degree of conversion with temperature is shown in Figure 4.3. For all three resins, reducing the isothermal cure temperature reduces the overall degree of conversion. This trend is most pronounced in TGDDM, which shows a reduction in the total degree of cure from 96% at 200°C to 79% at 160°C. The effect of temperature on the total degree of conversion is due to vitrification. Vitrification marks the transition from a rubber to a gelled glass [36] and occurs once the T_g of the reactive system reaches the isothermal curing temperature [33]. Once vitrified, molecular segmental mobility is substantially reduced which leads to a reduction in the polymerisation kinetics [192]. That said, vitrification does not stop the reaction progressing as reactions become diffusion controlled [34], [36], [192].

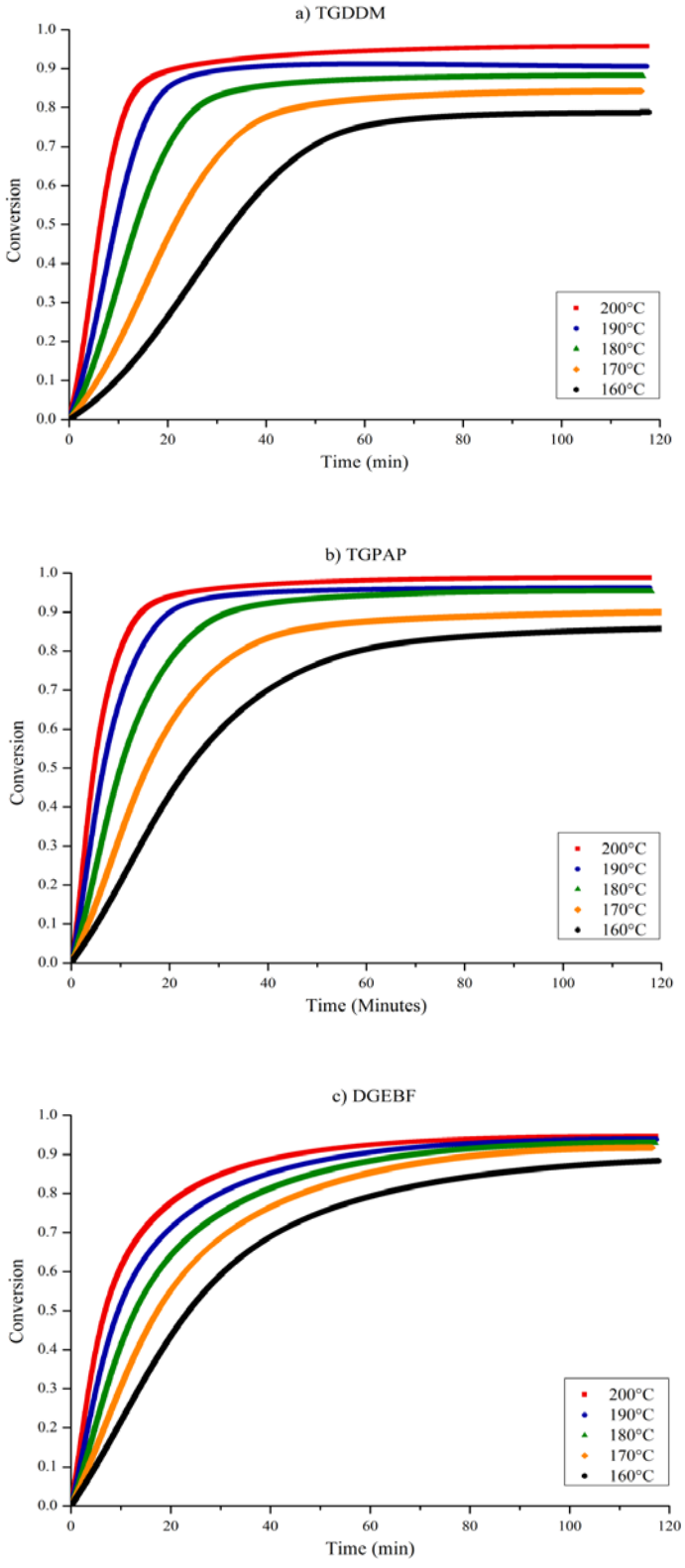

Figure 4.2 Conversion as a function of time at various temperatures for (a) TGDDM (b) TGPAP and (c) DGEBF cured with 4,4'-DDS at a stoichiometric ratio of r = 1.0.

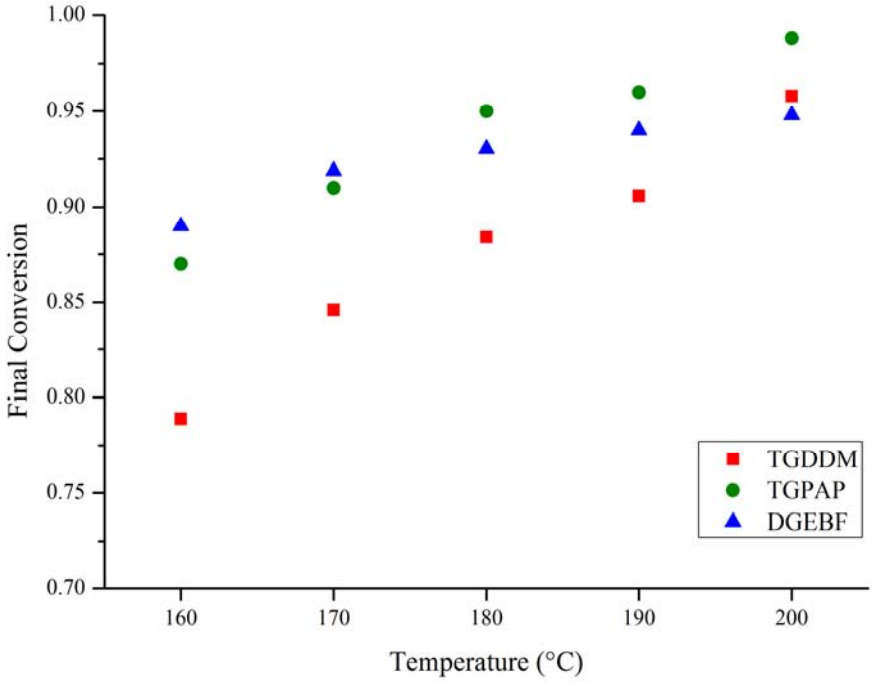

Figure 4.3 Final degree of conversion for TGDDM, TGPAP and DGEBF epoxy resins cured with 4,4'-DDS at a stoichiometric ratio of r = 1.0 as a function of isothermal cure temperature.

The onset of vitrification for TGDDM and TGPAP can clearly be seen in Figure 4.2a and 4.2b, especially at higher temperatures, as a sharp reduction in the increase in conversion with time. After this point the conversion plots plateau, however as reactions can still occur once vitrified the degree of conversion continues to increase very slowly with time. The onset of vitrification is not clear for DGEBF as seen in Figure 4.2c. Like TGDDM and TGPAP, the degree of conversion tends towards a plateau with time however; it does so at a more gradual rate. This would indicate that the resin may not have vitrified at any isothermal curing temperature and that the reduction in the rate of conversion is due to depletion in the number of available reaction sites remaining in the resin.

Figure 4.4 shows the change in T_g for the three resins as a function of isothermal curing temperature. For the purpose of this study the T_g was measured as the onset of residual cure from the DSC temperature ramp curves following isothermal curing. A residual cure can only be measured once the polymer has devitrified, and for devitrification to occur the polymer must have passed through its T_g hence justifying the use of the onset to measure T_g.

DGEBF is shown to have a T_g ~30°C below the isothermal curing temperature for all temperatures, indicating the resin is not vitrified at any curing temperature. This is supported by Ratna et al. [193] who found a DGEBA-diethyltoluene diamine (DETDA) system did not vitrify at 140°C. Furthermore, Gillham et al. [55] showed that vitrification is not necessarily observed in epoxy systems because it is dependent on the cure temperature and reaction kinetics. TGDDM and TGPAP however have T_g values significantly above the isothermal cure temperature for all temperatures, indicating they are vitrified after two hours at each temperature.

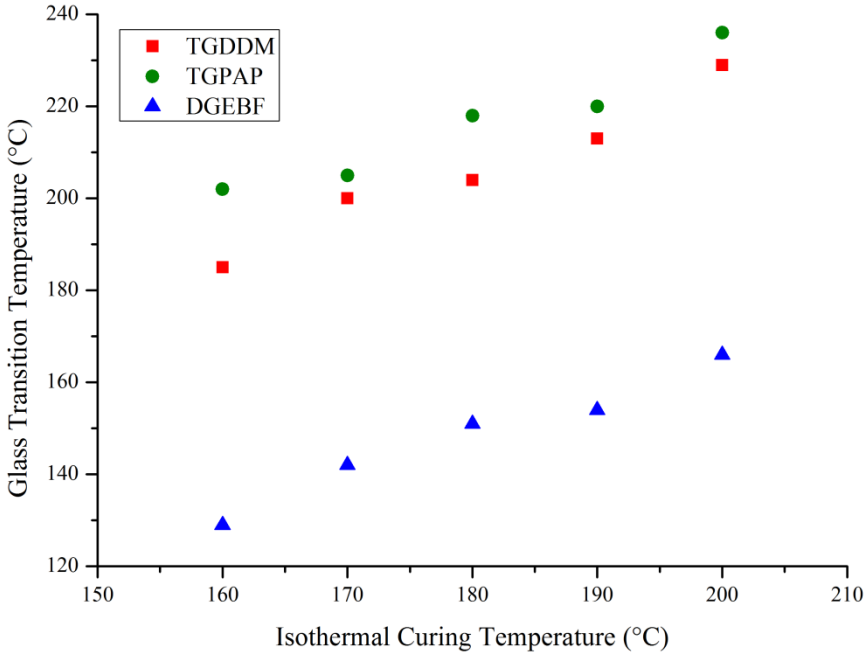

Figure 4.4 The glass transition temperature for DGEBF, TGPAP and TGDDM cured with 4,4'-DDS at a stoichiometric ratio of r = 1.0 after two hours at five isothermal curing temperatures ranging from 160-200°C.

The trapezium rule was used to integrate the conversion versus time data yielding the rate of reaction, $d\alpha/dt$ (s^{-1}). Figure 4.5 shows the change in rate of reaction with respect to time for each of the epoxy resins at the five isothermal cure temperatures used. The most notable observation from each of the three graphs is the change in peak height and peak time with respect to temperature, whereby reducing the temperature results in a lower peak rate of reaction and movement to a point later in time.

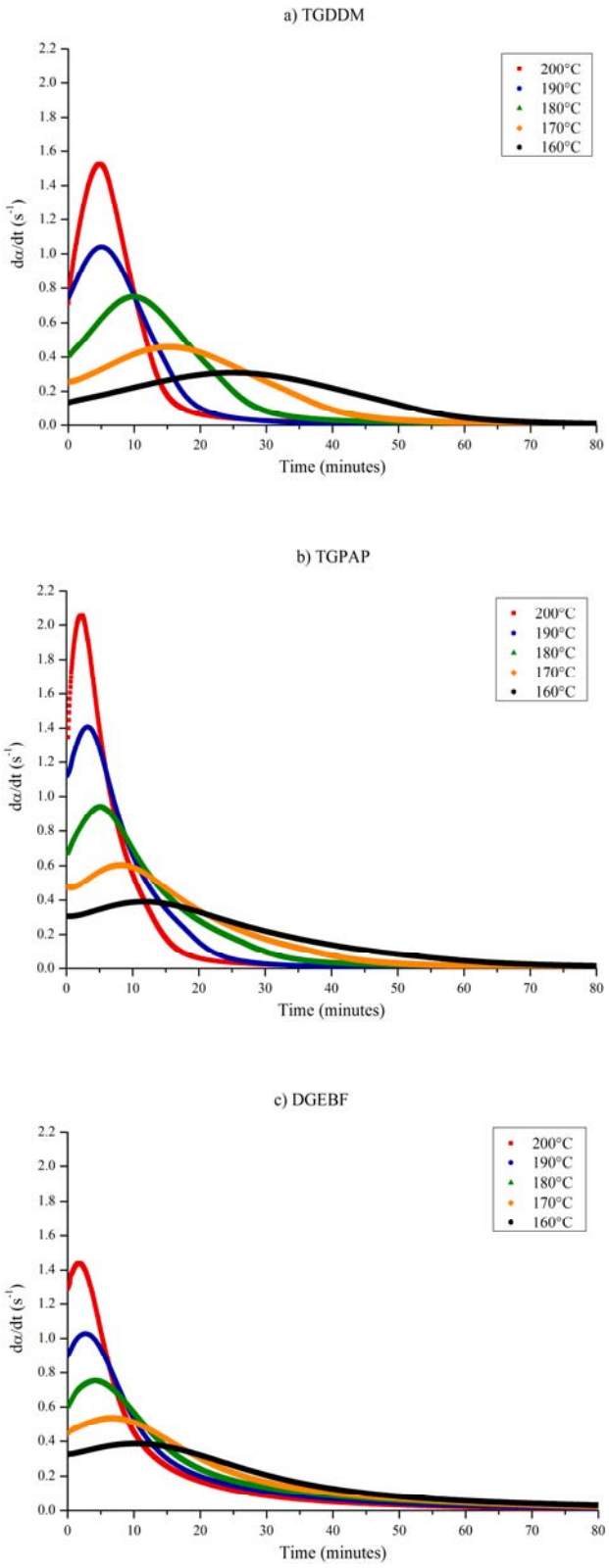

Figure 4.5 Variations in rate of reaction at different temperatures for (a) TGDDM (b) TGPAP and (c) DGEBF cured with 4,4'-DDS at a stoichiometric ratio of r = 1.0.

Owing to the Arrhenius behaviour exhibited by epoxy-amine systems [22], [84] these trends are to be expected. Plots show these two trends better (Figure 4.6 and Figure 4.7). In Figure 4.6 it can be seen that the peak heights of all three resins are similar at 160°C.

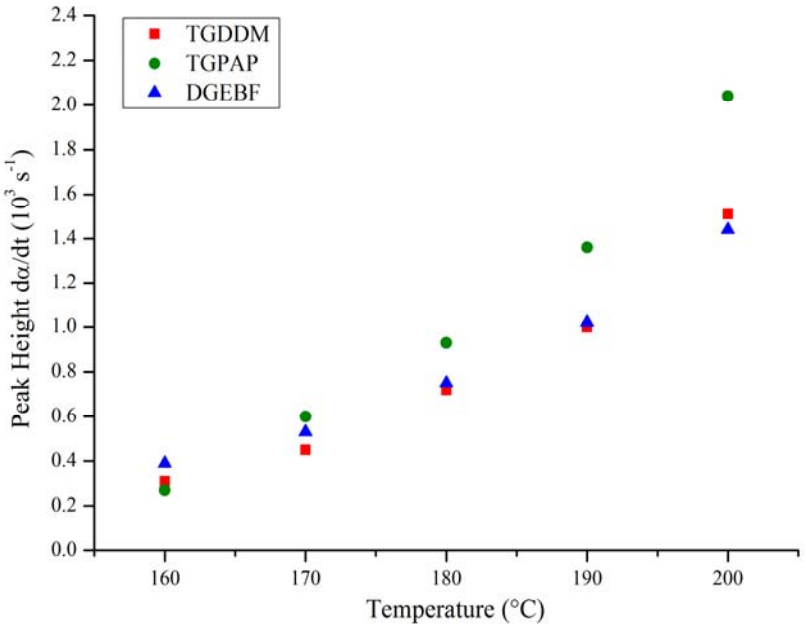

Figure 4.6 Variations in the height of peak reaction for TGDDM, TGPAP and DGEBF cured with 4,4'-DDS at a stoichiometric ratio of r = 1.0 with temperature.

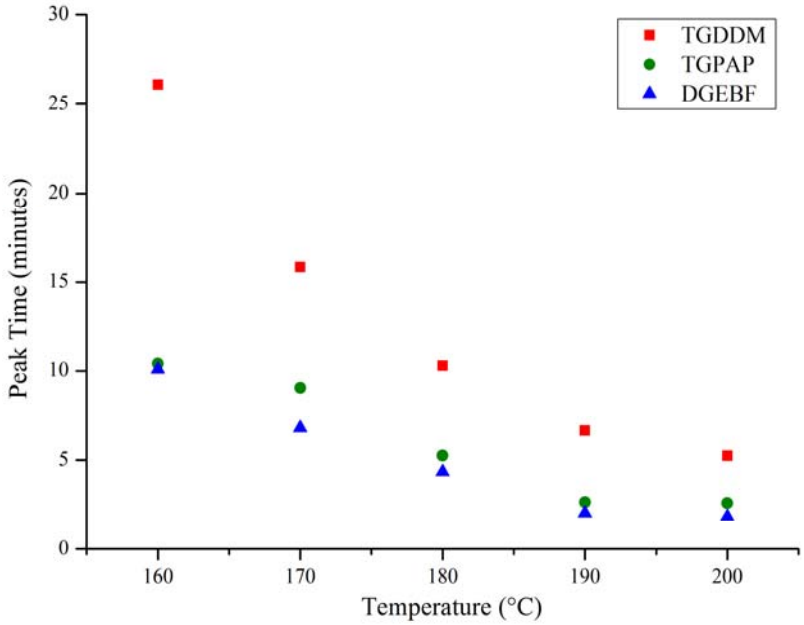

Figure 4.7 Variations in the time of peak reaction for TGDDM, TGPAP and DGEBF cured with 4,4'-DDS at a stoichiometric ratio of r = 1.0 with temperature.

As the curing temperature increases, the peak heights of TGDDM and DGEBF remain similar to one another whereas TGPAP exhibits a much more rapid increase. This would suggest the catalytic effect of hydroxyl groups in TGPAP (produced through epoxy-amine reactions) has a greater effect on the rate of reaction compared to the other two resins.

Figure 4.7 shows that TGPAP and DGEBF have similar peak reaction times whereas TGDDM is much slower to reach the peak of reaction at all curing temperatures. The epoxy groups in TGDDM are less reactive with amines that the epoxy groups of TGPAP and DGEBF

4.1.2. Autocatalytic Model and Activation Energies

For all three systems, the peak of reaction occurs at some point beyond the start of reaction; therefore simple n^{th}-order kinetics are not valid [76], [194]. Instead, the materials react following autocatalytic kinetics. This has been well documented for the reaction between epoxy groups and primary amines [76], [79], [83], [195]–[197] which react to produce a secondary amine and a hydroxyl group (see Figure 4.8).

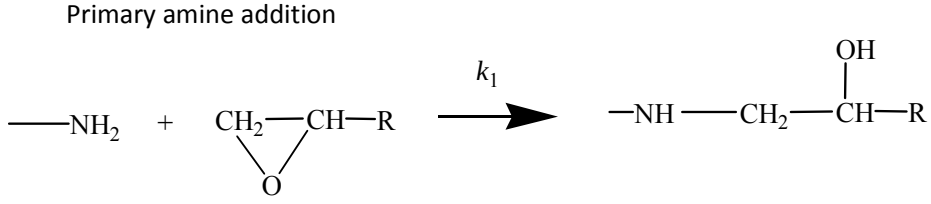

Figure 4.8 The reaction between an epoxy group and primary amine group to produce a secondary amine and hydroxyl group.

Whilst secondary amines can further react with epoxy groups to produce tertiary amines, hydroxyl groups catalyse the reaction through the formation of a trimolecular complex, which facilitates the nucleophilic attack of amine groups [33], [74]. As hydroxyl groups are continuously produced through epoxy-amine reactions (and go on to catalyse further reactions) the kinetics are said to be autocatalytic [33]. This results in an increase in the rate of reaction beyond t=0. The adopted model following autocatalytic behaviour was proposed by Kamal [77] (Equation 2.7, p 48).

The kinetic rate constant k_1 is associated with non-catalytic reactions between epoxy groups and amine groups along with the catalytic reaction due to the existence of catalysts in the initial formulation. k_2 is the kinetic rate constant associated with the autocatalytic effect of the hydroxyl groups generated from the initial epoxy group reactions [196]. Fitting this model to the rate of reaction requires the use of non-linear regression, which in this study was conducted using the 'Solver' function available in Microsoft Excel. The technique used followed a paper published by Brown [198] which provides a step-by-step guide to the use of Solver. There is a wealth of literature that use non-linear regression to fit Kamal's autocatalytic model. Some authors choose to impose restrictions on the variables such as fixing the orders of reaction (m and n) at 1, thus giving an overall order of reaction of 2 [40]. In this study however, m and n had no imposed restrictions. The only variable to be fixed was k_1 which was estimated as the initial rate of reaction; a technique adopted by other researchers [76], [196].

Figure 4.9 shows the various data and autocatalytic model fits for the rate of reaction of the three epoxy resins as a function of conversion. At all five temperatures the model exhibits a good fit for the majority of the curves, with a deviation towards high degrees of conversion (see Figure 4.10). A similar observation has been reported by several researchers [20], [45], [76], all of which suggest that the deviation is caused by vitrification, whereby chemical conversion is no longer governed by kinetic parameters but instead by diffusion mechanisms [22]. As mentioned earlier (and seen in Figure 4.2) a reduction in the cure temperature leads to a reduction in the overall degree of conversion, owing to the onset of vitrification. The autocatalytic model does not take in to account vitrification; hence, the deviation at high degrees of conversion, a trend that becomes increasingly prevalent as the cure temperature reduces.

Values for the kinetic rate constants were obtained for all three resin systems across five temperatures as shown in Tables 4.3-4.5 (p 117). For the three resin systems both k_1 and k_2 increase with curing temperature. Additionally k_2 is larger than k_1 at all temperatures and for all resins, indicating that the autocatalysed reactions are more significant in increasing the rate of reaction. TGDDM has lower k_1 values for all temperatures compared to both TGPAP and DGEBF.

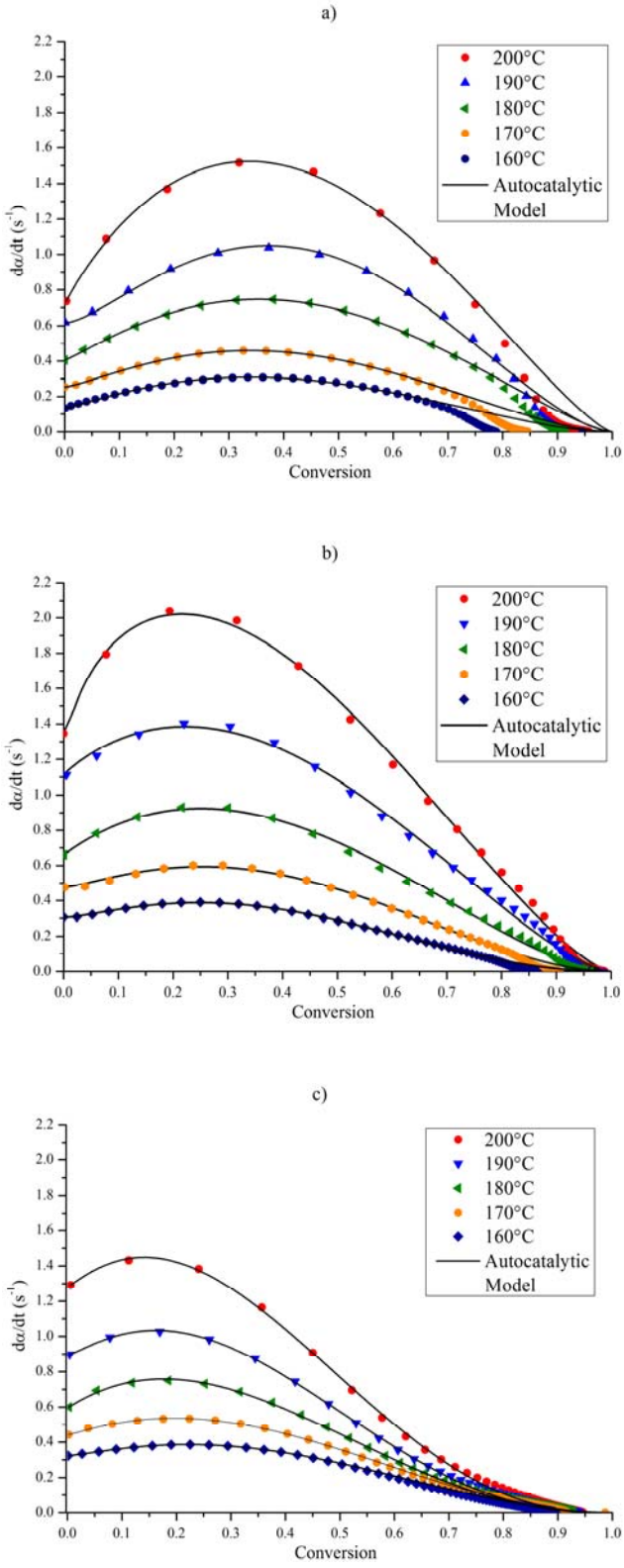

Figure 4.9 Plots of the rate of reaction and autocatalytic curves as a function of conversion for (a) TGDDM, (b) TGPAP and (c) DGEBF cured with DDS at a stoichiometric ratio of r = 1.0 at five isothermal temperatures from 160°C to 200°C.

This shows that initial epoxy conversion is slower in TGDDM, whilst the epoxy conversion in TGPAP and DGEBF are similar at lower curing temperatures and begin to deviate at higher temperatures, with k_1 for TGPAP increasing at a faster rate.

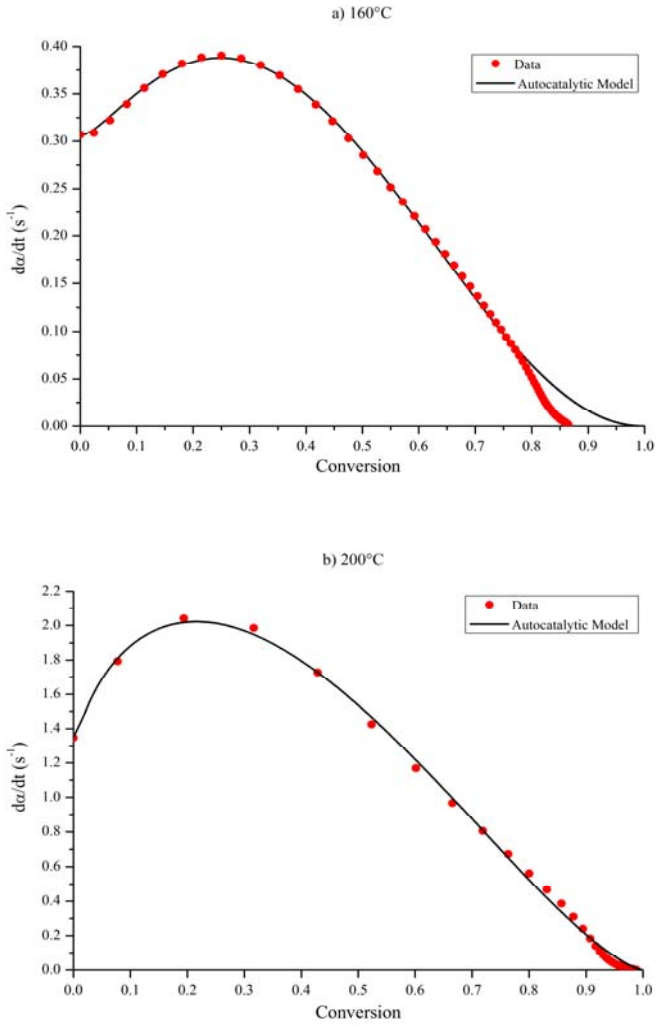

Figure 4.10 Plots of the data and autocatalytic model for the rate of reaction as a function of conversion for TGPAP cured with DDS at a stoichiometric ratio of r = 1.0 at (a) 160°C and (b) 200°C.

k_1/k_2 is the ratio of reaction rate coefficients and highlights the substitution effect. It has been widely documented that secondary amines have a negative substitution effect towards reactions with epoxy groups compared with primary amines [32]. It is regarded that a k_1/k_2 ratio of 0.5 means no substitution effect is occurring. Primary amines have two active hydrogens compared to only one active hydrogen on secondary amines, therefore primary amines have twice the probability of reacting [32]. The k_1/k_2 ratios for TGDDM and DGEBF range between 0.08-0.13 and

0.16-0.19, respectively, with change in curing temperature. The narrowness of the ranges suggest temperature has little effect on the relative reactivity of secondary amines, which is in good agreement with the results reported by Liu [75]. The ratios for TGPAP do not follow the same pattern. At 160°C the k_1/k_2 ratio lies (as expected) between the values found for TGDDM and DGEBF with a value of 0.13, however as the temperature increases so does the ratio, with a ratio of 0.33 at 200°C. This increase suggests that as the temperature increases so does the reactivity of the secondary amines, most likely induced through an increase in the catalytic effect of the hydroxyl groups with temperature.

Tables 4.3-4.5 also show the orders of reaction, m and n, for the three systems. For TGPAP both m and n decrease with an increase in temperature and therefore the total order of reaction, m + n, also decreases with temperature. This suggests that the concentration of reactive species present becomes increasingly insignificant as curing temperature increases; i.e. the rate of reaction would proceed at a similar rate at higher temperatures, regardless of the stoichiometric ratio between epoxy and amine groups.

This trend was not observed for TGDDM and DGEBF. The m and n values for TGDDM show no obvious trend, with values both increasing and decreasing slightly as temperature increases. The range over which the values alter however is minimal with m ranging from 1.1-1.34 and n ranging from 1.42-1.80. These values could be used to support the work by several authors whereby the orders of reaction were fixed at 1 or 2 [40], [63], [79]. As the total order of reaction is consistently in the range 2.8-3.0 for TGDDM (barring the potentially anomalous result of 2.52 obtained at 180°C) one can assume that the concentration of reactive species has the same effect on the rate of reaction, independent of curing temperature.

The rate constants k_1 and k_2 are dependent on temperature and follow Arrhenius' law (Equations 3. 9 and 3.10, p 87). Plotting the natural logarithms of k_1 and k_2 against 1/T creates lines of gradient $-E_a/R$ and intercept of ln A. Figures 4.11 and 4.12 show these plots for all three systems. A line of best fit was taken through the five points for each resin, from which the activation energies were calculated by dividing the line gradient by –R.

Table 4.3 Kinetic parameters and activation energies for TGDDM cured with DDS at a stoichiometric ratio of r = 1.0.

TGDDM								
Isothermal Temperature (°C)	k_1 (s^{-1})	k_2 (s^{-1})	m	n	m + n	k_1/k_2	E_{a1} (kJ mol^{-1})	E_{a2} (kJ mol^{-1})
160	0.13	1.68	1.12	1.73	2.85	0.08		
170	0.25	2.55	1.21	1.73	2.94	0.10		
180	0.41	3.10	1.10	1.42	2.52	0.13	75	73
190	0.62	6.17	1.34	1.64	2.98	0.10		
200	0.77	9.44	1.20	1.80	3.00	0.08		

Table 4.4 Kinetic parameters and activation energies for TGPAP cured with DDS at a stoichiometric ratio of r = 1.0.

TGPAP								
Isothermal Temperature (°C)	k_1 (s^{-1})	k_2 (s^{-1})	m	n	m + n	k_1/k_2	E_{a1} (kJ mol^{-1})	E_{a2} (kJ mol^{-1})
160	0.31	2.31	1.24	2.15	3.39	0.13		
170	0.48	2.84	1.19	1.89	3.08	0.17		
180	0.66	3.30	0.99	1.66	2.65	0.20	68	28
190	1.11	3.88	0.96	1.52	2.48	0.29		
200	1.48	4.48	0.74	1.43	2.17	0.33		

Table 4.5 Kinetic parameters and activation energies for DGEBF cured with DDS at a stoichiometric ratio of r = 1.0.

DGEBF								
Isothermal Temperature (°C)	k_1 (s^{-1})	k_2 (s^{-1})	m	n	m + n	k_1/k_2	E_{a1} (kJ mol^{-1})	E_{a2} (kJ mol^{-1})
160	0.32	1.82	1.16	2.02	3.18	0.18		
170	0.44	2.38	1.07	2.13	3.20	0.18		
180	0.60	3.55	1.01	2.40	3.41	0.17	59	58
190	0.90	5.62	1.11	2.61	3.72	0.16		
200	1.28	6.59	1.05	2.54	3.59	0.19		

The activation energies obtained from the gradients are given in Tables 4.3-4.5. E_{a1} is the activation energy for the epoxy-primary amine reaction and E_{a2} is for the epoxy-secondary amine reaction. It can be seen from the three tables that TGDDM has the highest activation energies for both E_{a1} and E_{a2} with values of 75 kJ mol^{-1} and 73 kJ mol^{-1} respectively. Liu et al. [75] reported on the activation energies of the reaction of TGDDM with various hardeners using mid infra-red FTIR.

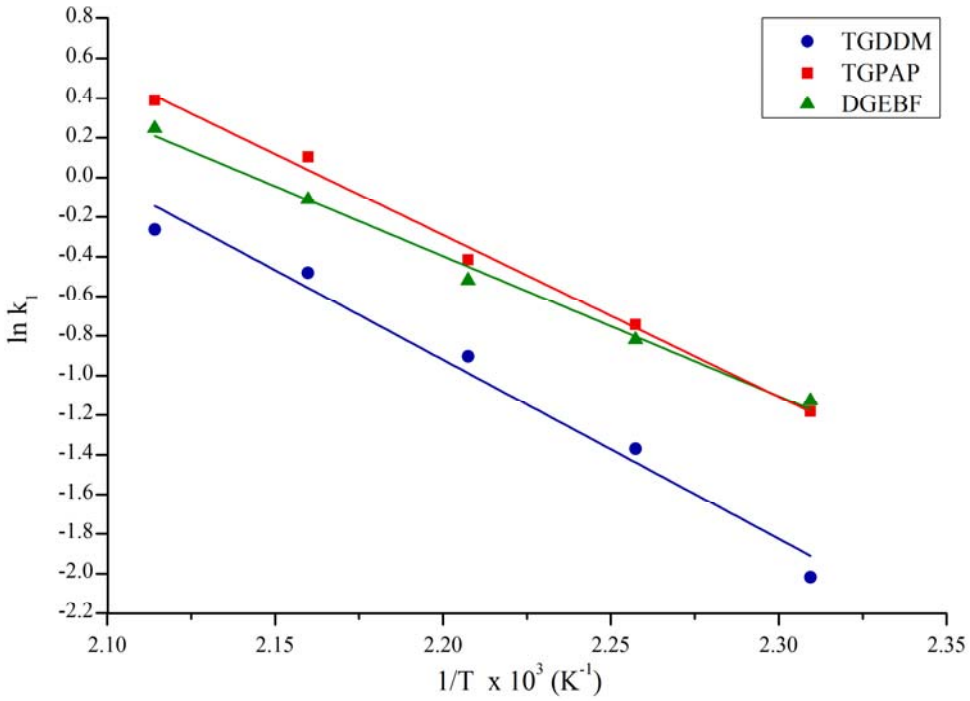

Figure 4.11 A plot of ln k_1 as a function of 1/Temperature for TGDDM, TGPAP and DGEBF cured with DDS at a stoichiometric ratio of r = 1.0.

When mixed at a stoichiometric ratio of r = 1.0 Liu found TGDDM and DDS to have activation energies of E_{a1} = 76 ± 8 and E_{a2} = 82 ± 8 kJ mol^{-1}. These values are in reasonable agreement with the values in Table 4.3, as are the results published by Lo et al. [172] who reported values of 78.3 ± 5.1 kJ mol^{-1} and 60.3 ± 5.4 kJ mol^{-1} for E_{a1} and E_{a2} respectively for TGDDM mixed with DDS at r = 1.0. Nae [199] however determined the activation energy for TGDDM and DDS to be 110.3 kJ mol^{-1}, although they did use the results from temperature-ramped DSC experiments to generate their finding, suggesting that using an alternative technique to measure enthalpy of reaction significantly affects the calculated activation energy.

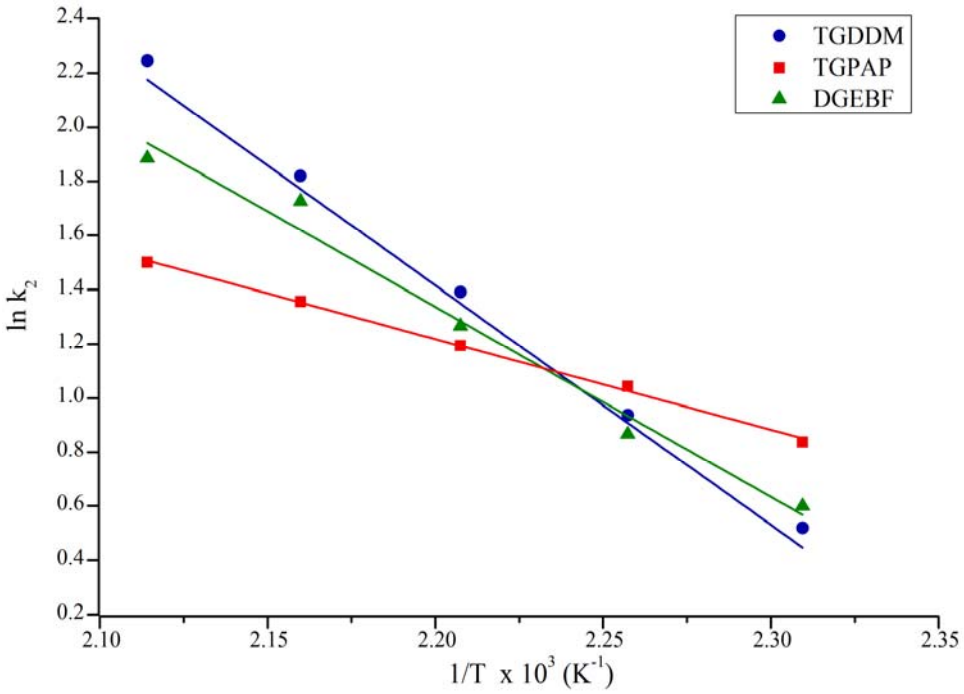

Figure 4.12 A plot of ln k_2 as a function of 1/Temperature for TGDDM, TGPAP and DGEBF cured with DDS at a stoichiometric ratio of r = 1.0.

In this study, DGEBF was found to have the lowest E_{a1} value of 59 kJ mol^{-1} (with an almost identical E_{a2} value). Liu reported the activation energies for DGEBA reacting with DDS to be E_{a1} = 62 ± 1 kJ mol^{-1} and E_{a2} = 65 ± 1 kJ mol^{-1}. As one may expect for two chemically similar materials, the activation energies reported for DGEBA do not vary significantly from those reported in Table 4.5 for DGEBF. It is noteworthy that as with TGDDM, the two activation energies for DGEBF are the same. Further agreement between these values was found in work by Karayannidou et al. [79] who reported that the two activation energies were similar for DGEBA when cured with a cyclo-diamine at r = 1.0. This is supported by Lee et al. [196] who studied DGEBA mixed with 4,4'-methylene dianiline, and reported activation energies of E_{a1} = 49 kJ mol^{-1} and E_{a2} = 46 kJ mol^{-1}.

TGDDM has significantly higher E_a values than those of DGEBF. Possible reasons for this are the higher viscosity of TGDDM (see Figure 4.18, p 130), steric hindrance [200] and the influence of chemical groups adjacent to the epoxy ring [201], [202]. It has been found that electron-withdrawing groups adjacent to the epoxy ring often enhance the reactivity of the epoxy resin to nucleophilic reagents such as amines,

while retarding its reactivity toward electrophilic reagents such as hydroxyl groups [201], [202]. Considering each pair of epoxy groups in TGDDM is attached via a tertiary amine it follows that the electron-withdrawing effects of the tertiary amine are not as strong as the ether linkage attaching the epoxy groups in DGEBF; consequently, the TGDDM epoxy groups are less reactive than those of DGEBF.

In this study TGPAP was found to have activation energy values of E_{a1} = 68 kJ mol^{-1} and E_{a2} = 28 kJ mol^{-1}. The value for E_{a1} is comparable to literature as Liu [75] reported activation energies of $E_{a1} = 65 \pm 3$ and $E_{a2} = 70 \pm 3$ kJ mol^{-1} for TGPAP and DDS. The E_{a1} value for TGPAP lies between that of TGDDM (75 kJ mol^{-1}) and DGEBF (59 kJ mol^{-1}). This value is not surprising considering the chemical groups adjacent to the epoxy rings in TGPAP. Two of the epoxy groups in TGPAP are joined via a tertiary amine as with TGDDM, and one via an ether link as with DGEBF (see Figure 3.1, p 73 for chemical structures). As previously stated, neighbouring chemical groups significantly affect the reactivity of an epoxy group, hence it follows that E_{a1} for TGPAP lies between that of TGDDM and DGEBF.

E_{a2} for TGPAP is somewhat lower than what one would have predicted based on the results obtained for E_{a2} in DGEBF and TGDDM and indeed lower than reported by Liu [75]. However the E_{a2} value is in agreement with the trend found by Carrasco et al. [203] who reported E_{a1} and E_{a2} values for TGPAP reacting with DDS of 89 kJ mol^{-1} and 34 kJ mol^{-1} respectively. Similar trends were reported by Bonnaud et al. [40] who found activation energies of 104 kJ mol^{-1} and 78 kJ mol^{-1} for TGPAP with DDS. These values are much higher than both those of Liu and those in Table 4.4; however, this is potentially due to the reaction orders, m and n, being fixed in their study at 1 and 2 respectively.

None of the aforementioned authors discussed the difference between the two TGPAP activation energies. A potential explanation is the catalytic effect caused by hydroxyl groups from primary amine addition [33], [74] and the catalytic effect of tertiary amines present in the TGPAP backbone [4]. TGDDM has two tertiary amines in the prepolymer backbone however, their catalytic potential is restricted due to steric hindrance owing to the bulky molecular structure of the TGDDM prepolymer [204].

Both of these catalysts promote alternative reactions to amine addition; namely etherification, the reaction between epoxy and hydroxyl groups. Etherification has been found to be more favourable at higher temperatures [205], [206], with the use of diglycidylaniline (DGA)-derived epoxy resins [40] (such as TGDDM and TGPAP) and at the later stages of conversion [56], i.e. when the likelihood of forming bonds with residual amines is small. That said, when combining the use of DGA-derived epoxy resins with high curing temperatures, etherification has been found to not only compete with epoxy-amine reactions but to be more favourable. The value of 28 kJ mol^{-1} found for TGPAP E_{a2} in this study would suggest that etherification is more likely in TGPAP compared with TGDDM and DGEBF, which had E_{a2} values similar to E_{a1}.

4.2. Fourier Transform Infra-red (FTIR) Spectroscopy

Fourier transform infra-red (FTIR) spectroscopy was used to study the chemical changes due to reaction. A series of spectra were obtained from the mid infra-red (mir) range between 750 cm^{-1} and 4000 cm^{-1} as a function of time at 130°C in order to mimic the initial temperature used in the cure cycle used within this study. The changes in peak areas of the epoxy and primary amine peaks were measured throughout the cure and normalised to the 1593 cm^{-1} peak attributed to phenyl groups; a chemical group known not to take part in the epoxy-amine reaction. The peaks attributed to these chemical groups were taken from values reported in the literature [79], [82], [175] and are shown in Table 3.5. The peaks have a range of wavelengths assigned to them as some peaks broaden with time whilst others are material dependent. Peak areas for the hydroxyl and secondary amine groups should be measured to develop a more extensive understanding of the kinetics of reaction however these peaks overlap in mir-FTIR spectra, making quantification of the peaks difficult [82], [207]. In future studies near infra-red FTIR should be used where possible as amine and hydroxyl peaks are more easily distinguished [207].

Table 3.5 Functional groups of epoxy resins and amine hardeners and their FTIR peak assignments.

Functional Group	Peak Range (cm^{-1})	References
Phenyl (Reference Peak)	1593	[78]
Epoxy	907-915	[82], [175]
Primary Amine	1618-1628	[82]
Hydroxyl	3450-3640	[82], [176]

Figure 4.13 shows the intensity of the 907 cm^{-1} peak in TGDDM and TGPAP and the intensity of the 911 cm^{-1} peak in DGEBF (peaks attributed to epoxy groups) changing with time at 130°C. It can be seen that the peak heights reduce with time, indicating epoxy groups are being consumed by reaction with DDS. It is noticeable from Figure 4.13 that the rate of epoxy consumption differs between the three resins. Figure 4.14 shows the intenisty of the 1628 cm^{-1} peaks (attirubted to primary amine groups) changing with time at 130°C. As with the epoxy peaks, the primary amine peaks reduce with time indicating amine groups are being consumed. Figure 4.15 shows the intensity of the 3450-3640 cm^{-1} band (attributed to hydroxyl groups) with time for all three resins. Hydroxyl groups are a byproduct formed from the reaction of epoxy and amine groups. The incrase in hydroxyl group concentration for all three resins confirms that the depletion in both amine and epoxy groups is due to epoxy-amine reactions.

It is noteworthy from Figure 4.13 and Figure 4.14 that the rate of epoxy and primary amine depletion differs between the resins. To quantify and compare the changes in epoxy and primary amine groups present within the resins, time-resolved FTIR is required. For time-resolved analysis, the peak areas of epoxy and primary amine peaks were normalised to the 1593 cm^{-1} peak attributed to the phenyl absorption; a chemical group known not to be involved in the reaction. The depletion of epoxy and primary amine groups was estimated as a function of time using Equation 4.3.

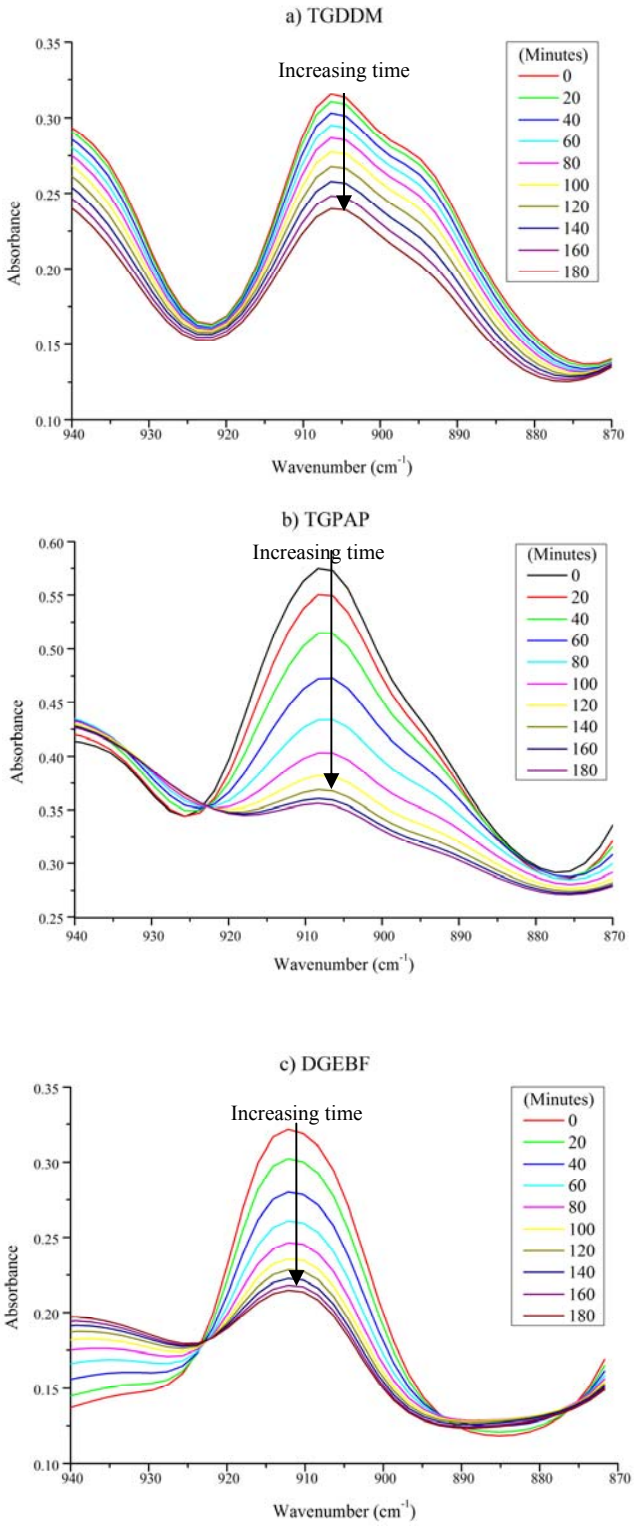

Figure 4.13 Change in the FTIR spectra of the epoxy group absorbance at a) 907 cm^{-1} for TGDDM, b) 907 cm^{-1} for TGPAP and c) 911 cm^{-1} for DGEBF cured with DDS at a stoichiometric ratio of r = 1.0 at 130°C from 0-180 minutes.

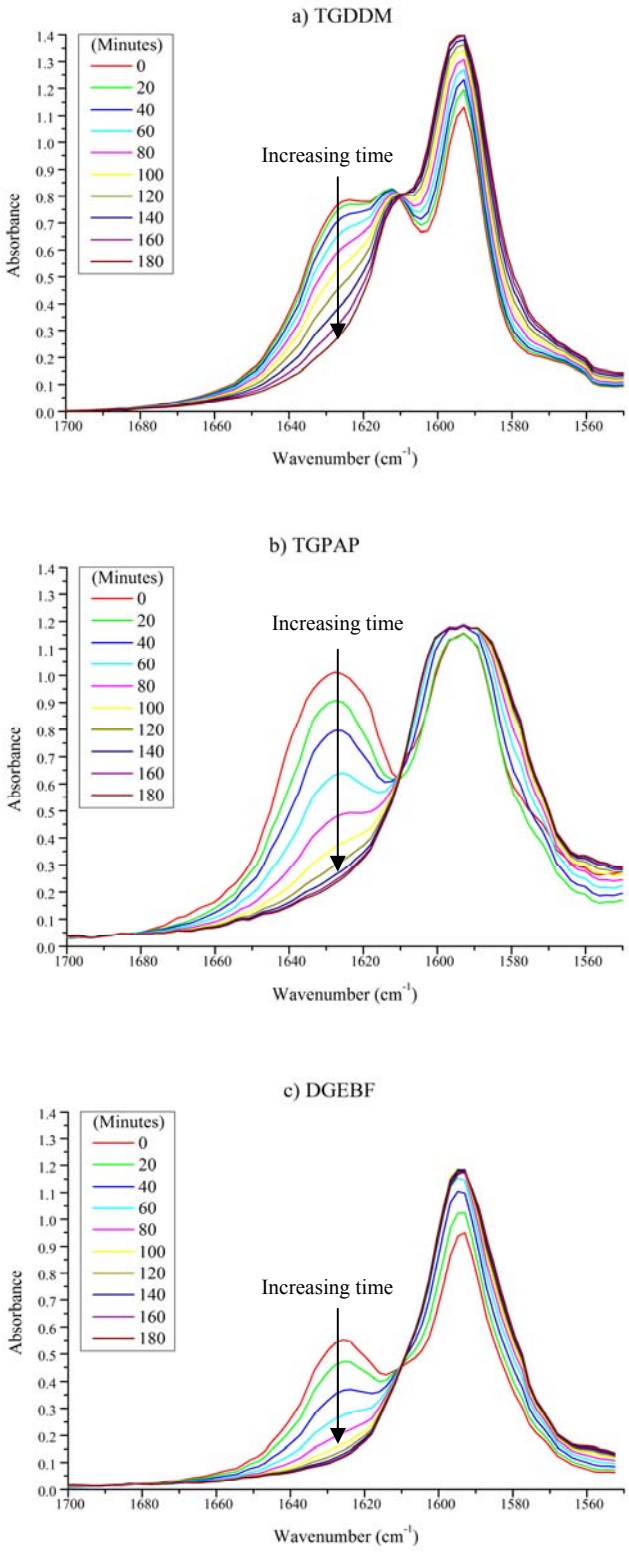

Figure 4.14 Change in the FTIR spectra of the primary amine absorbance at 1628 cm^{-1} for a) TGDDM, b) TGPAP and c) DGEBF cured with DDS at a stoichiometric ratio of r = 1.0 at 130°C from 0-180 minutes.

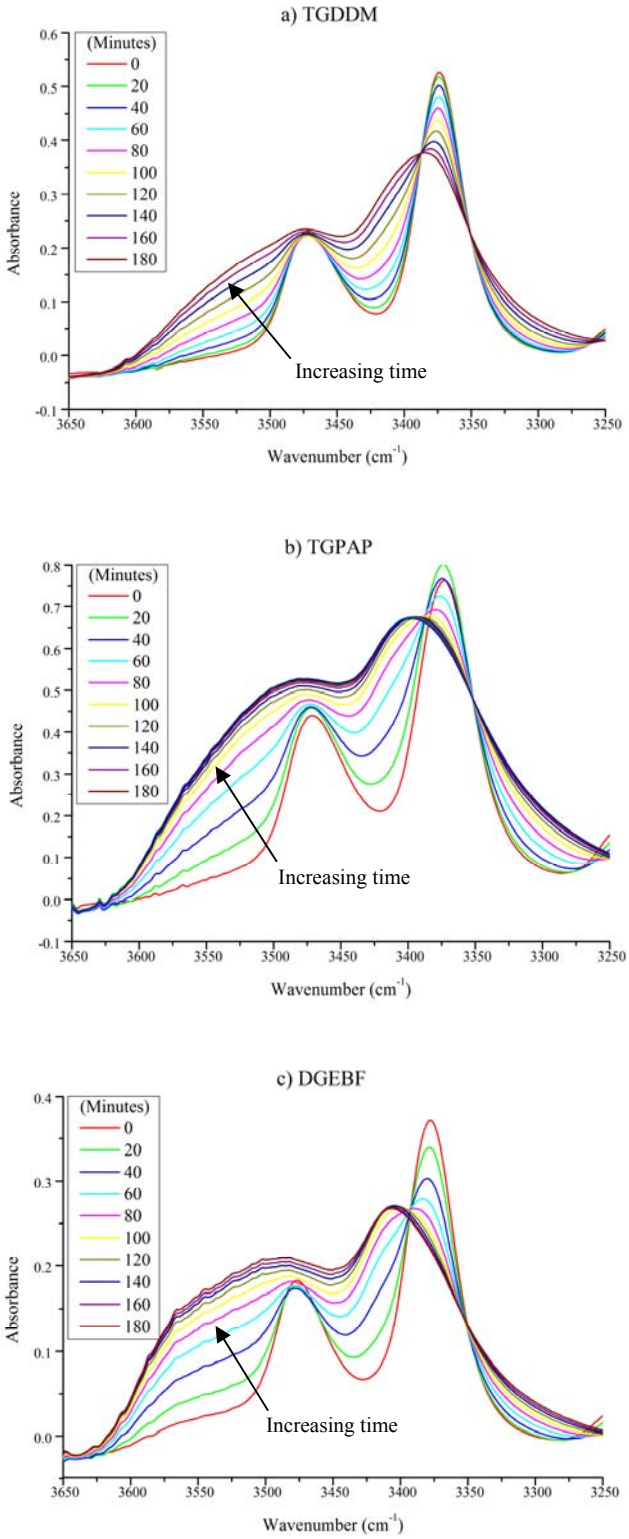

Figure 4.15 Change in FTIR spectra of the hydroxyl group absorbance at 3516 cm^{-1} for a) TGDDM, b) TGPAP and c) DGEBF cured with DDS at a stoichiometric ratio of r = 1.0 at 130°C from 0-180 minutes.

$$\{E\}_t = \frac{\left(\frac{a_{907}}{a_{1593}}\right)_t}{\left(\frac{a_{907}}{a_{1593}}\right)_0} \times 100 \qquad (4.3)$$

Where $\{E\}_t$ = fraction of residual epoxy groups, a = area; at a given time, t, during the reaction and at the start of reaction (t=0). 907 and 1593 correspond to the wavelengths (cm^{-1}) of the peaks assigned to the epoxy and normalising phenyl groups respectively.

The calculated residual epoxy groups as a function of time at 130°C are shown in Figure 4.16. The figure shows that the rate of epoxy consumption is much slower in TGDDM from t=0 compared to both TGPAP and DGEBF, which initially have a similar rate of conversion. This is in agreement with the rate of reactions calculated from DSC data for TGDDM shown in Table 4.3 (p 117) which shows the rate of reaction regarding non-catalysed epoxy conversion (k_1) is much lower at all temperatures for TGDDM than either TGPAP or DGEBF.

Similarly, Table 4.4 and Table 4.5 (p 117) show that k_1 for TGPAP and DGEBF become increasingly similar at lower temperatures. It is therefore not surprising that the rates of epoxy conversion measured using FTIR are very similar for both resins at the initial stages of cure. However, as the cure progresses, the rate of conversion decreases in DGEBF whereas epoxy depletion in TGPAP continues until <1% of epoxy groups remain. After five hours at 130°C, the residual epoxy percentages for TGDDM, TGPAP and DGEBF are 25%, <1% and 15%, respectively. The differences between these values can in part be attributed to vitrification. As shown in Figure 4.3 (p 108) TGDDM is less cured at each isothermal curing temperature, indicating the resin vitrifies at a lower degree of epoxy conversion. This is in good agreement with the FTIR results for epoxy conversion, which show that after five hours at 130°C there is significantly more unreacted epoxy groups remaining in TGDDM compared to TGPAP and DGEBF.

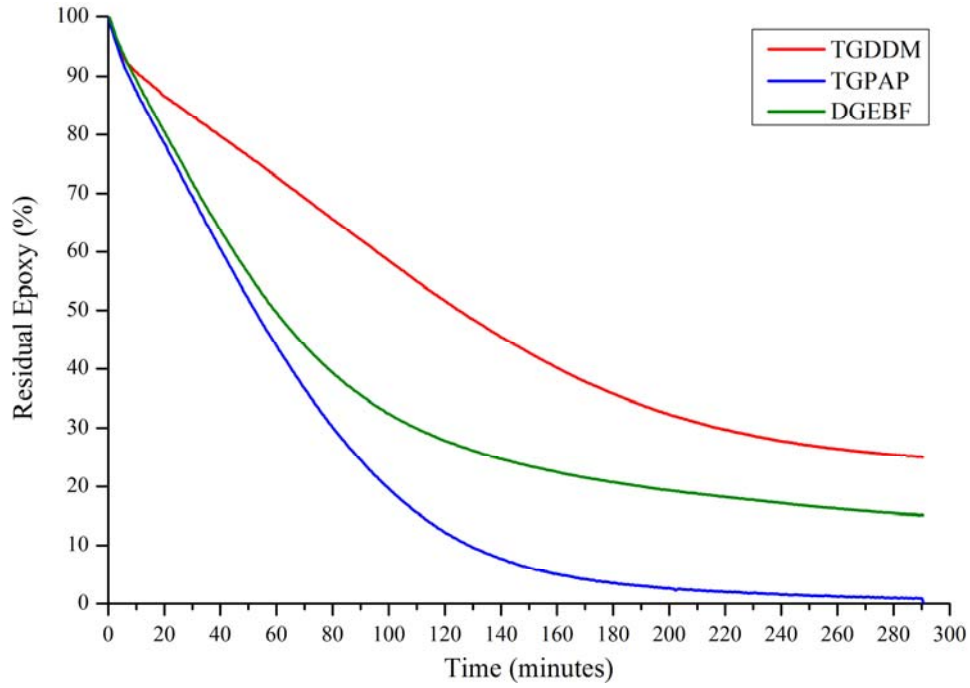

Figure 4.16 Time resolved FTIR of the residual epoxy group concentration as a function of time at 130°C for TGDDM, TGPAP and DGEBF cured with DDS at a stoichiometric ratio of r = 1.0.

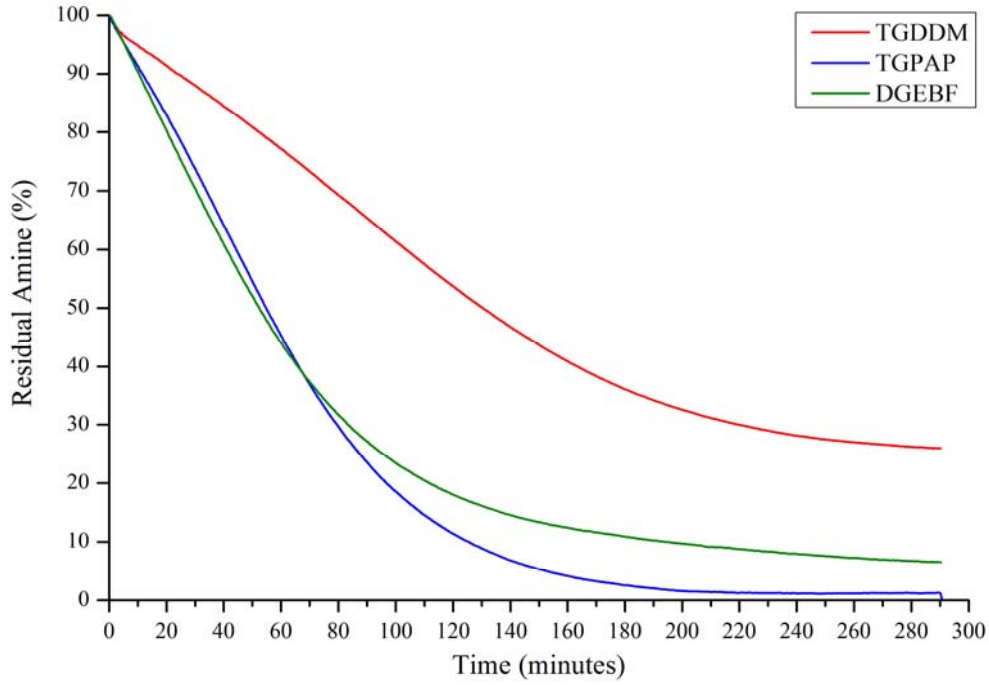

Figure 4.17 Time resolved FTIR of the residual primary amine concentration as a function of time at 130°C for TGDDM, TGPAP and DGEBF cured with DDS at a stoichiometric ratio of r = 1.0.

Comparison between the residual primary amine percentage as a function of time (Figure 4.17) and the residual epoxy percentage as a function of time (Figure 4.16) shows that the two graphs follow the same pattern for all three resins, whereby both the primary amine and epoxy curves both deplete at the same rate. As all three resins were cured at a stoichiometric ratio of r = 1.0 it follows that the primary amine concentration should be reduced twice as quickly as the epoxy concentration. Owing to the overlapping peak of the secondary amine with hydroxyl groups, it is difficult to quantify their production through this reaction, however it is apparent that the peak does not increase in height at any point for all three resins, suggesting the use of mir-FTIR is insensitive to their production by primary amine addition.

Additionally, the fact that the primary amine percentage depletes at the same rate as the epoxy percentage suggests that primary amine addition does not lead to a recognisable change in the mid-infra-red absorption of the remaining nitrogen-hydrogen bonds. As such, the evidence in this thesis suggests the primary amine peak measured using mid infra-red FTIR is more likely a measure of the total residual amines. Unfortunately, no literature was found to support this case.

Figure 4.16 shows that after 5 hours at 130°C there are significantly more unreacted epoxy groups in DGEBF than TGPAP. DSC results indicate that as the curing temperature reduces the degree of epoxy conversion in DGEBF becomes higher than both TGDDM and TGPAP (Figure 4.3 p 108), thus differing from the FTIR results (albeit different temperatures were used for the DSC study). This may be explained by the use of the 907 cm^{-1} peak as the 'epoxy' peak, as was done so in this study. Meyer et al. [58] used the same peak to monitor the change in epoxy groups at different stoichiometric ratios of DGEBA and DDS. They found that even with an amine rich stoichiometry there remained ~7.5% unreacted epoxies. Mijovic et al. [208] suggested that there is an overlap of the 907 cm^{-1} peak with a non-reactive species whose residual absorption at the end of reaction is mistakenly interpreted as residual epoxy groups.

4.3. Rheology

The success of manufacturing composites using liquid resins is dependent on the resin viscosity [209] and the time available until the resin ceases to flow, often referred to as the 'processing window' (PW). The PW may be defined by the time to gelation for a thermosetting system or by a rise in viscosity sufficient to prevent flow. The ability to control this property is vital in composite manufacturing. If the resin solidifies too quickly it is possible that it will not have flowed through the dry fabric preform and wetted out the fibre bundles. This may lead to dry spots in the cured composite if macroflow between the fibre bundles is incomplete, or poor interfacial properties rendering the composite significantly weakened if microflow within the fibre bundles is significantly reduced [209]. The viscosity of the resin system is also important. If the viscosity is too high, the resin will fail to flow when placed under vacuum. If too low it is possible for the liquid to 'racetrack' [210], whereby instead of flowing through the preform it moves rapidly along the flow-supporting materials present in the vacuum bag (such as Nylon mesh) towards the vacuum outlet, bypassing the preform.

4.3.1. Viscosity as a Function of Temperature

Figure 4.18 shows the change in viscosity with temperature for TGDDM, TGPAP and DGEBF without the addition of hardener. It should be noted that for both TGPAP and DGEBF a 15 point moving average was used to smooth the data, as at T>100°C the viscosity became too low for the rheometer to measure accurately. It can be seen from the figure that TGDDM has the highest viscosity over the full temperature range, which is roughly two orders of magnitude higher than TGPAP and DGEBF at 40°C. TGPAP has the lowest viscosity although with an increase in temperature the viscosity of TGPAP and DGEBF become very similar, with both reaching a plateau at ~0.01 Pa s.

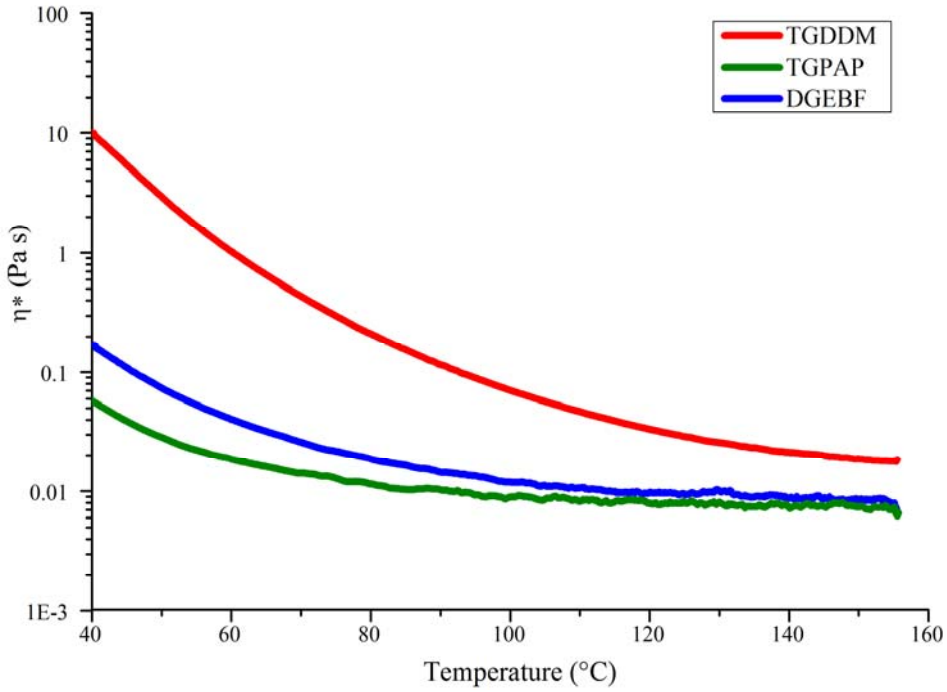

Figure 4.18 Viscosity as a function of temperature for TGDDM, TGPAP and DGEBF prepolymers without the addition of a hardener.

4.3.2. Apparent Gel Point and Processing Window

To develop a more accurate understanding of resin processability it is necessary to know the gel time; i.e. the time (at a given temperature) at which the resin will no longer flow. An apparent gel time can be attributed to the crossover point of the storage modulus (G') and the loss modulus (G''), measured using oscillatory rheometry [53], [211]. Gelation is an important transition in thermosets used in composite manufacturing as it defines the period within which the resin remains as a liquid and therefore potentially processable.

Figure 4.19 shows the two dynamic moduli and complex viscosity for DGEBF as a function of time at 130°C. It can be seen that the G' and G'' cross at ~98 minutes therefore indicating the period after which the resin no longer flows. Alternatively, a common concept in polymer processing is that of a 'no-flow' condition, i.e. the viscosity has risen to a level that there is no significant flow. It is reported in ASTM D 4473-95 that the dynamic gel time occurs once the complex viscosity reaches 100 Pa s [180]. Thus, from this point forward the 100 Pa s window will be

termed the processing window (PW). From Figure 4.19 it can be seen the PW of DGEBF is ~89 minutes, some 9 minutes less than the G'/G'' crossover.

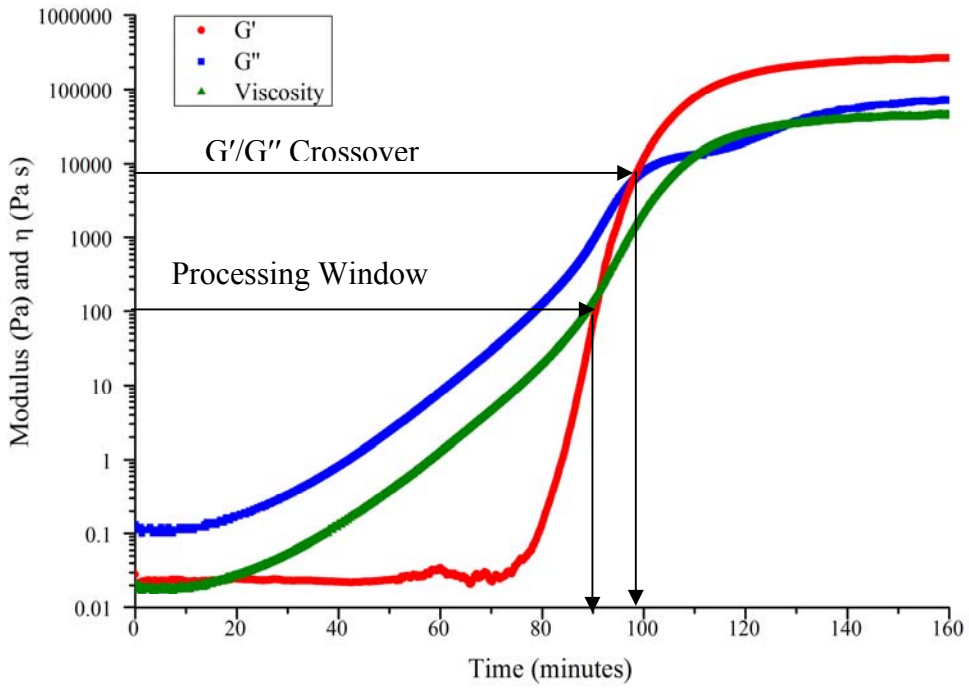

Figure 4.19 G'/G'' crossover and 100 Pa s processing window for DGEBF cured with DDS at r = 1.0 and a curing temperature of 130°C.

Figure 4.20 shows complex viscosity profiles for TGDDM, TGPAP and DGEBF and the values for the PW and G'/G'' crossover times are shown in Table 4.6. As expected based on Figure 4.18 the initial viscosities of TGPAP and DGEBF are very similar when curing isothermally and that of TGDDM is higher. Within 10 minutes of cure the viscosities of TGPAP and DGEBF alter, with that of TGPAP increasing at a much faster rate.

After 20 minutes, the viscosity of TGPAP is greater than TGDDM. The PW's for the three resins increase in the order DGEBF > TGDDM > TGPAP and have values of 89, 61 and 49 minutes respectively. Ratna et al. [193] studied TGPAP DGEBA and TGDDM cured with diethyltoluene diamine and found the same trend for the gel times of the three resins; whereby despite TGPAP having lower nominal functionality the resin gels quicker than TGDDM.

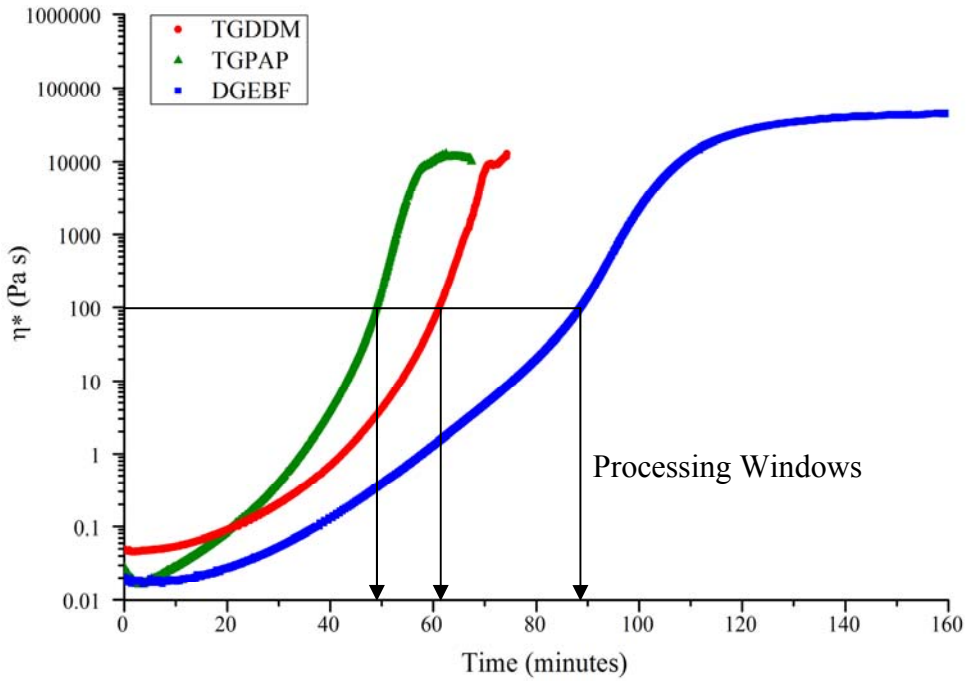

Figure 4.20 Viscosity profiles for curing of the base resins at 130°C, with DDS at a stoichiometric ratio of r = 1.0.

The rate at which the viscosity increases is dependent on the rate of increase in the weight average molecular weight, which in turn is dependent on two variables: the prepolymer functionality and the rate of reaction. A higher functionality leads to a lower degree of reaction required to form a polymer network of infinite weight average molecular weight.

Table 4.6 Apparent gel times and processing windows at 130°C for TGDDM, TGPAP and DGEBF cured at a stoichiometric ratio of r = 1.0.

Resin	Gel time (minutes)	
	G'/G" Crossover	Processing Window (100 Pa s)
TGDDM	69 ± 2	61 ± 2
TGPAP	54 ± 2	49 ± 2
DGEBF	99 ± 3	89 ± 3

This would imply that TGDDM should gel the quickest of the three resins, assuming equal reactivity of the epoxy groups; however experimentally this was found not to be the case. The reasons for this are concerned with the rate of reaction, which for TGDDM was found to be slower than both DGEBF and TGPAP (see sections 4.1.2 and 4.2 for DSC and FTIR analysis). Owing to this, TGDDM gels more slowly than TGPAP indicating that in this case the effects of the differing rates of reaction are more significant than the differences in nominal functionality of the prepolymers (i.e. 3 for TGPAP and 4 for TGDDM).

The same effect is not seen for DGEBF which has a much faster rate of reaction and lower activation energies compared to TGDDM (as shown in section 4.1.2) and yet the gel time is significantly longer. DGEBF is a bi-functional prepolymer, and as such, network formation with DDS proceeds by a $RA_2 + RB_4$ reaction. In other words, only one of the reactants present in the mix contributes to the formation of a three-dimensional polymer network, in this case the DDS hardener. Owing to this, the crosslinking potential is significantly reduced compared to both TGPAP and TGDDM, ultimately leading to a slower increase in average molecular weight. This in turn leads to a higher gel conversion and in this case a longer gel time.

4.3.3. Conversion at the Gel Point

The theoretical conversion at the gel point for a thermosetting polymer can be calculated from the stoichiometric ratio and the number of reactive groups present per monomer of each reactive species, as shown in Equation 2.2 (p 43) In this study the nominal epoxy functionalities of DGEBF, TGPAP and TGDDM were 2, 3 and 4 respectively and the amine-hydrogen functionality of DDS was 4. The theoretical gel point epoxy conversions along with the calculated conversion from DSC and FTIR data (based on the G'/G'' crossover from rheology) are presented in Table 4.7.

To determine the conversion at the gel point using DSC, samples were cured at 130°C in the DSC up to the apparent gel time of each system (determined from rheology) before being cooled at 50°C min^{-1} to -20°C to quench the curing process. The samples were then heated to 320°C at 10°C min^{-1} to find the residual enthalpy of reaction, which was used in conjunction with the total enthalpies of reaction to calculate the

degree of conversion at the apparent gel point. The gel points determined from the G'/G'' crossovers were also used to find the degree of epoxy conversion from the time resolved FTIR results. The conversions corresponding to the gel times were read from the residual epoxy concentration graph shown in Figure 4.16 (p 127).

Table 4.7 Degree of epoxy conversion at the G'/G'' crossover for TGDDM, TGPAP and DGEBF (reacted with DDS at r = 1.0): theoretical values using the Flory equation and measured values from DSC (three repeats per resin) and FTIR.

Resin	Conversion at Gel Point		
	Theoretical	Measured (DSC)	Measured (FTIR)
TGDDM	0.33	0.24 ± 0.03	0.31
TGPAP	0.41	0.17 ± 0.03	0.51
DGEBF	0.58	0.64 ± 0.01	0.67

The values in Table 4.7 show FTIR results for the gel point conversion of TGPAP and TGDDM are somewhat different in relation to the theoretical values. The value of TGDDM is 0.31, only 0.02 below the theoretical value and therefore in good agreement. The conversion for TGPAP however was found to be 0.51, some 0.10 higher than the theoretical value. Bonnaud et al. [40] reported the gel point conversion for TGPAP cured with a diamine hardener as 0.60, some 0.29 higher than the theoretical value. They attributed the significant difference to the different reactivities of the epoxy groups in TGPAP and to side reactions, such as ring formation, which do not contribute to the formation of a three dimensional polymer network at the gel point. Similarly, DGEBF was found to have a measured gel point conversion some 10-16% higher than the theoretical value. Min et al. [39] reported a gel point conversion of 0.65 for DGEBA and DDS using FTIR; in good agreement with the DSC and FTIR conversions of 0.64 and 0.67 found for DGEBF in this study.

TGPAP and TGDDM were found to have DSC-measured conversions lower than the theoretical conversions. These differences can be explained through a fundamental inaccuracy in the principle behind using DSC to determine the degree of conversion.

As stated by Lachenall et al. [212] the use of DSC in determining degree of conversion relies on the assumption that the heat of reaction is directly proportional to the extent of reaction. DSC-measured conversions significantly below the theoretical values suggest the measured residual enthalpy of reaction is higher than what one would expect. This could be due to the fast heating rate used to find the residual enthalpy of reaction, which may favour alternative reactions to amine addition, namely etherification. If the reaction chemistry alters between an isothermal dwell and a ramp cure then it is difficult to relate the two measured enthalpies of reaction during the different curing stages, leading to a misrepresentation for the degree of epoxy conversion at any given point. This is discussed in more detail in section 5.2.1.1 (p 154) where more evidence is provided for the misrepresentation of epoxy resin conversion when using DSC.

4.3.4. Viscosity Modelling

In light of the possible inaccuracies regarding gel point determination using DSC, the theoretical gel conversions were used for rheological modelling. Equation 4.5 shows an expression relating viscosity and conversion of a thermosetting polymer up to the gel point, where η_0 = initial viscosity, α = degree of conversion, α_{GP} = degree of conversion at the gel point and B and C are fitting parameters. This equation, or variations of it, have been widely utilised for viscosity modelling of epoxy resins [87], [214]–[216]. Complex viscosities are presented in Figure 4.21 for TGDDM, TGPAP and DGEBF along with the models that were fit using the Solver function available in Microsoft Excel.

$$\eta = \eta_0 \left[\frac{\alpha_{GP}}{\alpha_{GP} - \alpha} \right]^{B+C\alpha} \tag{4.5}$$

The model fits for TGDDM and TGPAP are relatively good agreement with the data; however, the model shows a poor fit for DGEBF. Observation of all three model fits suggests that the model is tailored for the viscosity to increases towards infinity as the resin gels; a characteristic which is applicable to TGDDM and TGPAP, as shown from the experimental data of the two resins (Figure 4.21a and b). However, the increase in

viscosity around the gel point for DGEBF is more gradual (Figure 4.21c), something the model seemingly cannot adapt to.

Fitting parameters B and C are presented in Table 4.8. It can be seen that as the functionality of the resin reduces, parameter B increases and parameter C decreases. The values of the fitting parameters were plotted against the resins nominal functionality and linear lines of best fit were taken through the three points. The lines of best fit for fitting parameters B and C had coefficients of determination of $R^2 = 0.95$ and $R^2 = 1.0$ respectively, and were considered a good fit.

Table 4.8 Minimum viscosity and fitting parameters for rheological modelling of TGDDM, TGPAP and DGEBF reacted with DDS at a stoichiometric ratio of r = 1.0.

Resin	Nominal Functionality	Minimum Viscosity (Pa s)	Fitting Parameters	
			B	C
TGDDM	4	0.046	2.92	0.17
TGPAP	3	0.016	5.63	-6.15
DGEBF	2	0.017	10.55	-13.57

The fitting parameters can be estimated from these equations for any multi-component system containing the three resins used in this study, assuming the same stoichiometric ratio with DDS and the same curing temperature is used. Similarly, the theoretical degree of conversion along with minimum viscosity can also be calculated. Knowledge of these variables potentially allows for the construction of a viscosity versus time plot at 130°C for any combination of TGDDM, TGPAP and DGEBF at a stoichiometric ratio of r = 1.0.

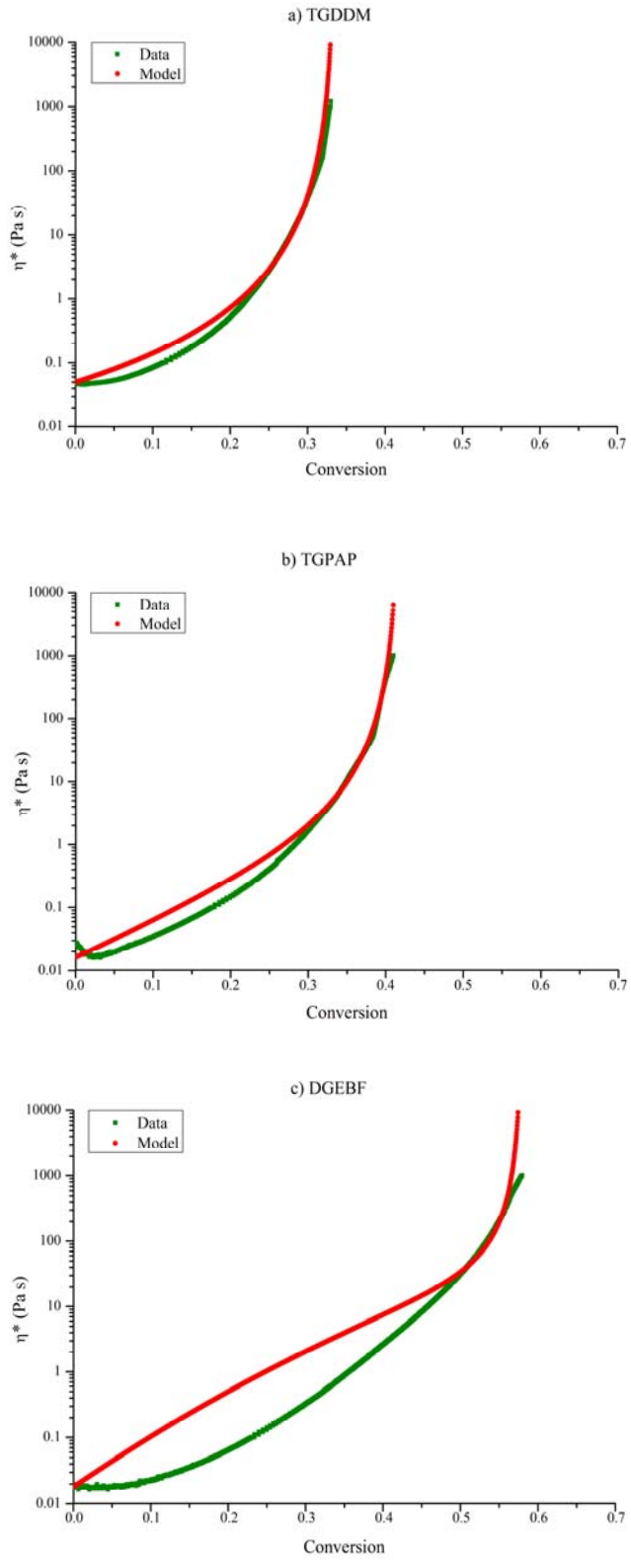

Figure 4.21 Complex viscosity and a model fit (Equation 4.5) for (a) TGDDM, (b) TGPAP and (c) DGEBF cured isothermally at 130°C with DDS at a stoichiometric ratio of r = 1.0.

4.4. Glass Transition Temperature

The glass transition temperature (T_g) is one of the most important properties of an epoxy resin as it defines the maximum operating temperature of the material. Optimising the T_g is achieved by increasing the crosslink density; most easily done by increasing the degree of reactive group conversion [217]. The T_g is attributed to the energy required for segmental mobility. Increasing the crosslink density hinders segmental mobility, which in turn means more energy is required for the polymer to pass through the glass transition. All three prepolymers were cured with DDS at r = 1.0 following a cycle developed within our group. The cycle involved 3 hours at 130°C, 2 hours at 165°C and 2 hours at 200°C. The resins were then post cured for a further 5 hours at 200°C. During a temperature ramp from 30-320°C at 10°C min^{-1} DSC showed no visible deflection in the baselines for all three resins, indicating that the resins were fully cured. DMTA was used to measure the T_g of the three cured resins and the results are shown in Figures 4.22 and 4.23. Figure 4.22 shows the change in storage modulus of the resins as a function of temperature. The graph shows that TGDDM has the highest modulus regardless of temperature whereas DGEBF has the lowest. This can be attributed to the crosslink density, as an increase in crosslink density results in a stiffer polymer. The onset of the drop in storage modulus can be used to indicate the maximum operating temperature of a polymer, which from an engineering perspective, is the point at which the mechanical properties begin to decline.

In materials science, the most common indicator of T_g from DMTA data is the peak in tan δ i.e. the ratio between the storage and loss moduli (G'/G''). Figure 4.23 shows the tan δ data for each of the three resins. From this figure, peaks in the tan δ were measured and the data is shown in Table 4.9. It can be seen that there is a strong relationship between the nominal functionality of the epoxy prepolymers and their T_g. Increasing the epoxy functionality from 2 in DGEBF to 4 in TGDDM results in an increase in the T_g of 77°C. This increase in T_g can be attributed to an increase in the crosslink density which occurs owing to the increase in functionality of the epoxy prepolymer.

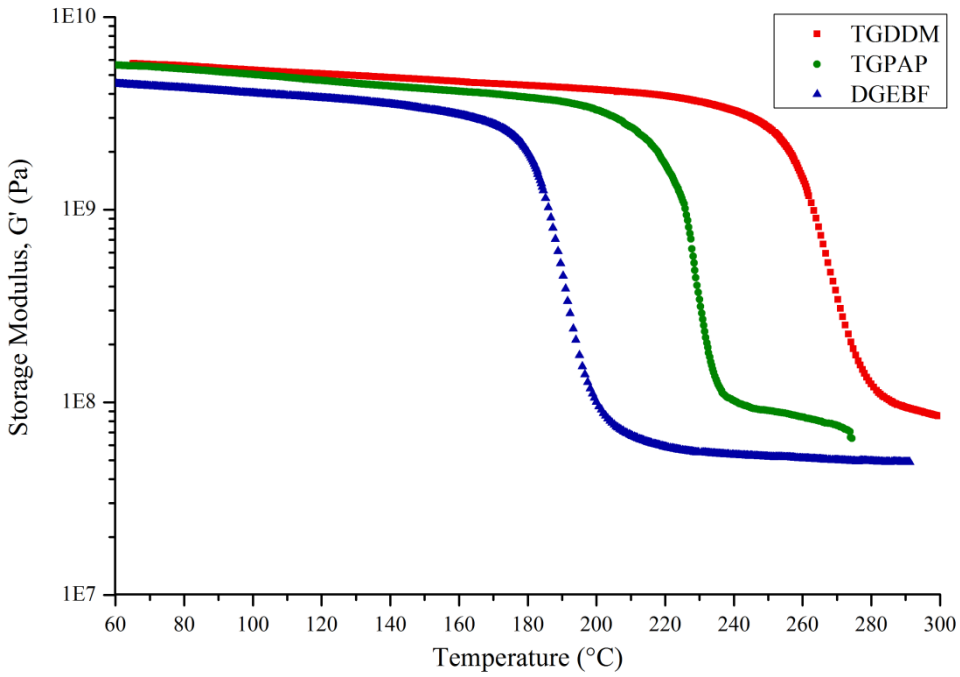

Figure 4.22 DMTA storage moduli plots of TGDDM, TGPAP and DGEBF when fully cured with DDS at a stoichiometric ratio of r = 1.0.

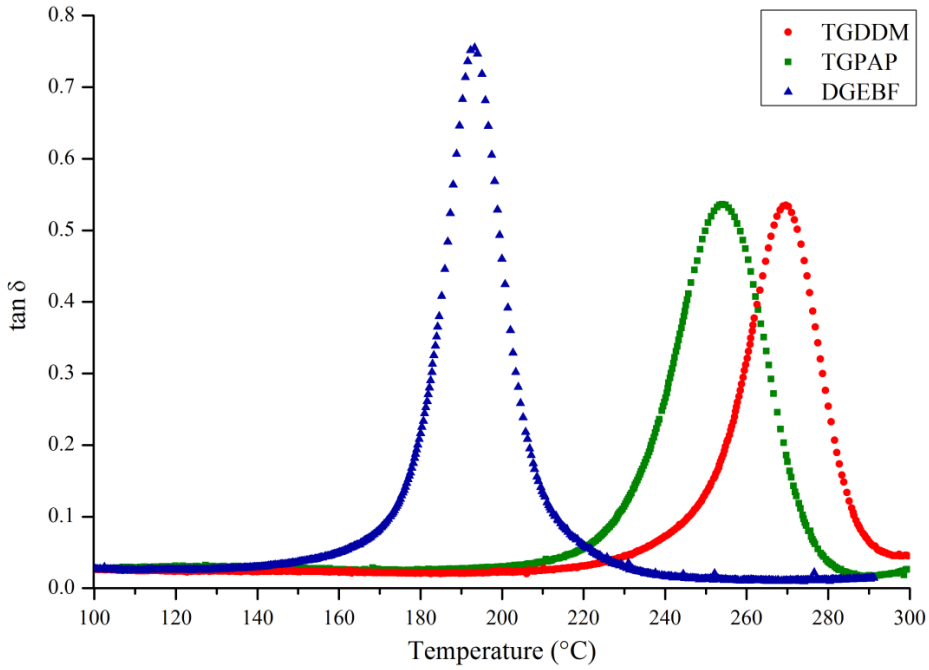

Figure 4.23 **DMTA tan δ plots of TGDDM, TGPAP and DGEBF when fully cured with DDS at a stoichiometric ratio of r = 1.0.**

Table 4.9 The glass transition temperatures of TGDDM, TGPAP and DGEBF when fully cured with DDS at a stoichiometric ratio of r = 1.0.

Resin	Glass Transition Temperature (°C)	
	G' Onset	Peak in tan δ
TGDDM	255	270
TGPAP	236	254
DGEBF	181	193

Though the resin systems used in this study were cured using a stoichiometry of r = 1.0 it should be noted that the majority of literature concerning the curing of TGPAP and TGDDM with amine hardeners report the use of stoichiometric ratios of r <1.0 with the majority ranging between $0.70 \leq r \leq 0.90$. Hourston et al. [68] using DMTA measured the T_g of various compositions of binary mixtures involving TGPAP, TGDDM and DGEBA all cured with 3-3'-DDS at a stoichiometric ratio of r = 0.8. Their results for TGPAP and TGDDM were 240°C and 190°C respectively. Direct comparison cannot be made to the values of Hourston owing to the different stoichiometric ratio used however; their results do suggest that the crosslink density of the resins cured in this study were far greater, especially for the TGDDM system.

This difference may be attributed to the stoichiometric ratio however it could also be due to the degree of conversion. Hourston et al. [68] reported using a 190°C post cure, however a researcher within our group studied an epoxy system containing 67% TGDDM and 33% TGPAP and showed that to generate the maximum degree of conversion (and thus obtain the maximum T_g of the system - T_g^{∞}) a post cure temperature of 200°C was required. Temperatures below this resulted in vitrification of the system before it was fully reacted. Whilst Hourston et al. post cured their samples for 10 hours at 190°C they did not report on any residual cure measurements. The large discrepancy between the T_g values in Hourston's study and those reported in this work, particularly for TGDDM, suggest that their systems were not fully cured. Alternatively Varley et al. [205] reported that TGPAP mixed with 4,4'-DDS at a stoichiometric ratio of r = 0.90 had a T_g of 260°C measured using DMTA; in good

agreement with the value of 254°C determined in this study. They post cured the resin for 2 hours at 205°C and using DSC found that the resin was fully cured. The author also suggests that stoichiometric ratios <1.0 may be beneficial when curing TGPAP. This is investigated further in chapter 5.

The DGEBF system was found to have a T_g of 193°C. Comparisons between this value and the literature cannot be directly made owing to the lack of studies concerning the use of DGEBF with DDS. Comparisons have to be made with DDS and DGEBA, a resin chemically similar to DGEBF. The most notable difference between the two bi-functional resins is the substitution of the hydrogens attached to the central carbon atom of the DGEBF by methyl groups, which will increase steric hindrance and increase the T_g (as discussed in chapter 2). It is also common for DGEBA prepolymers to have a higher molecular weight and thus the molecular distance between epoxy groups is usually greater. Theoretically this would lead to a lower crosslink density and therefore a lower T_g. Reported T_g values for DGEBA systems vary significantly with stoichiometry, however T_g^{∞} has been reported to range from 190°C to 234°C when cured with DDS at a stoichiometric ratio or r = 1.0 [39], [58]. The measured T_g for DGEBF in this study is within this range.

5. Multi-component Epoxy Resin Fomulation

5.1. A Formulation Study of a Multi-component Epoxy Resin System Using Factorial Experimental Design

This chapter is concerned with the resultant properties from mixing the three epoxy prepolymers used in chapter 4. They were Tetraglycidyl-4,4'-diaminophenylmethane (TGDDM), Triglycidyl-p-aminophenol (TGPAP) and Diglycidyl ether of bisphenol F (DGEBF). The resins were cured with a diamine hardener, 4,4'-diaminodiphenyl sulphone (DDS) and the quantity of DDS mixed with the resins (stoichiometric ratio) was also studied. The ranges over which each of the variables was studied were predetermined and are given in Table 5.1.

Table 5.1 The limits for the factorial experimental design variables examining TGDDM level in a TGDDM/TGPAP mix, DGEBF content and epoxy/amine stoichiometric ratio.

Material	Limits
TGDDM in TGDDM/TGPAP Mix	25-75 wt%
DGEBF	0–25 wt%
Stoichiometric Ratio (r)	0.6–1.0

Factorial experimental design (FED) is a technique for maximising experimental efficiency when investigating the effects of 2 or more independent variables (IV) on a dependent variable (DV) within a predefined experimental space [169]. Owing to the three variables studied, a three level central composite design was constructed using the limits shown in Table 5.1. These limits are graphically represented in Figure 5.1. Each of the nodes in Figure 5.1 represents a resin formulation at defined levels of the

three variables that is required to be mixed and tested. For each of the nodes one sample was mixed, except the central green node of which there were six samples (known as the centre-point repeats). The computer software, Design Expert 7, uses the centre-point repeats to determine the experimental error. The blue nodes represent the star-points. These resin mixes define the limits for the experimental space and are referred to in code terms as the +S and –S values. The red nodes are the +1 and –1 values. Results from the FED will be depicted using two-dimensional contour plots, which allows for comparisons between two variables whilst the third variable is fixed. Quantities of the resin-containing variables are given as weight percent and from this point forward will be referred to as a percentage.

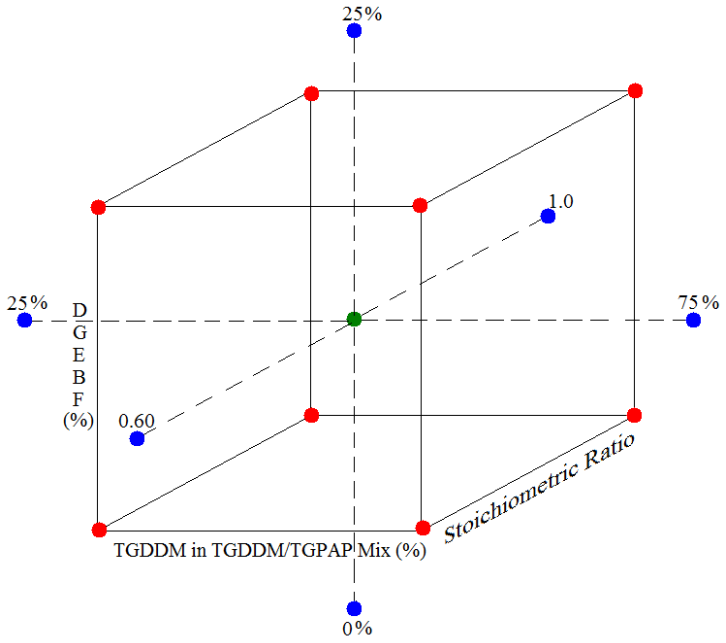

Figure 5.1 A schematic of the variables used in the central composite design FED model.

5.1.1.Rheology

5.1.1.1. Room Temperature Viscosity

The effects of the IV's on the viscosity of the resin system were studied at room temperature (~23°C). Figure 5.2 shows contour plots for the change in room temperature viscosity at three distinct DGEBF levels of 5%, 12.5% and 20%. These levels correspond to the +1, 0 and -1 planes in the 'DGEBF' axis. Figure 5.2a shows the effects of TGDDM in the TGDDM/TGPAP mix and stoichiometric ratio with the

addition of only a small amount of DGEBF (5%). This figure aptly highlights the error associated with the generation of contour plots from the FED data, particularly regions of the plot that fall outside the +1 and -1 coded values. As can be seen in the lower left corner of the plot the viscosity is projected to decrease until 0 Pa s. Clearly this is not possible and consequently one must take due care when relying on the exact values projected by the FED model.

It can be seen from Figure 5.2 that the variable with the greatest effect on the viscosity is the TGDDM content. The model predicts that varying the TGDDM content from 25-75% at r = 1.0 leads to an increase in room temperature viscosity from <50 Pa s to ~900 Pa s. The same trend is observed at all stoichiometric ratios albeit the range of viscosities is much smaller as the stoichiometry reduces, with the maximum viscosity at r = 0.6 being ~250 Pa s. This significant decrease from ~900 to ~250 Pa s with a reduction from r = 1.0 to 0.6 is attributable to the quantity of DDS being added. DDS is supplied as a fine powder and as such, its addition to the resin inevitably increases the viscosity. This effect is not as prevalent at lower TGDDM levels. As discussed in chapter 4 the viscosity of TGPAP used in this study is akin to that of DGEBF; both of which are significantly lower than TGDDM. Owing to which, the addition of higher quantities of DDS powder has a smaller effect on the overall viscosity of systems high in TGPAP and DGEBF.

The room temperature viscosity contour plots seen above can be used as a guideline of the effects of varying a resin formulation on the processability. Whilst resin flow in composite manufacturing often occurs at temperatures greater than room temperature (and therefore the viscosity reduces) one can assume that higher quantities of TGDDM in a resin system would lead to a higher viscosity, and thus more difficult infusion, as seen for the neat resins in Figure 4.18 (p 130).

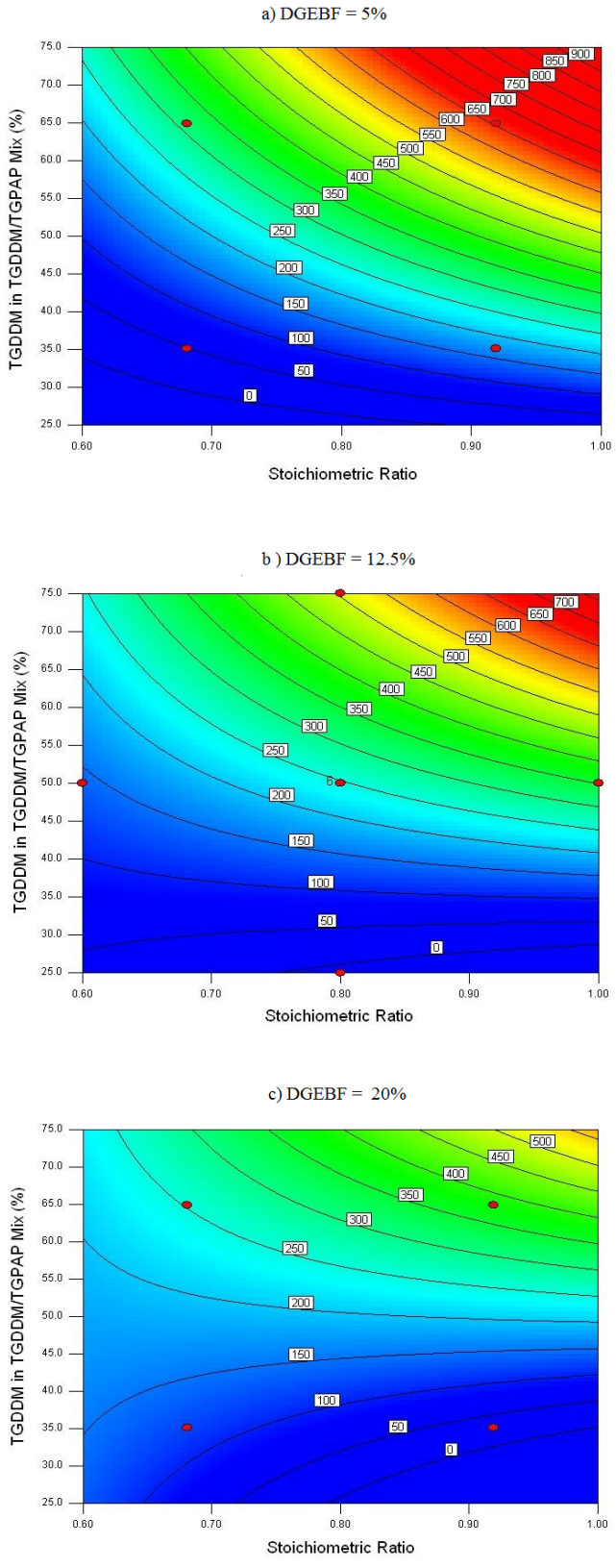

Figure 5.2 FED contour plots for the room temperature viscosity (Pa s) at DGEBF levels of (a) 5%, (b) 12.5% and (c) 20% for a multi-component epoxy resin system. The red nodes represent real data points.

Though difficulties may not arise in processing of the untoughened resins one must consider that it is common for toughening agents to be incorporated in to an epoxy system [66], [218]. Toughening agents such as engineering thermoplastics inevitably raise the viscosity of the system [210]. Thus, the optimum untoughened resin formulation in this situation is one with minimum viscosity in order to give maximum control over the viscosity once a toughening agent is incorporated.

The addition of DGEBF (as seen in Figure 5.2b and 5.2c) results in a reduction in the viscosity for formulations containing high quantities of TGDDM. However, as the TGDDM level decreases (and consequently TGPAP increases) the viscosity effects of DGEBF decrease. This is comparable through the bottom right hand corners of each of the three contour plots, which show little change in the viscosity with increasing DGEBF levels. By increasing the DGEBF level, one reduces both the TGPAP and TGDDM level in the overall resin system. The viscosities of DGEBF and TGPAP are similar, therefore a formulation which is high in TGPAP and low in TGDDM will see little change in viscosity with the addition of DGEBF, as the viscosity of the resin being added (DGEBF) is similar to that of which it is replacing (TGPAP rich TGDDM/TGPAP mix).

5.1.1.2. Processing Window

From chapter 4 it can be recalled that the PW's for the three base resins were in the following order: DGEBF > TGDDM > TGPAP, with times of 89, 61 and 49 minutes respectively. Comparison between the results obtained in the FED and those presented for the PW's of the base resins in chapter 4 are limited owing to the different stoichiometric ratios studied in the FED; however one sample from the FED had a stoichiometric ratio of r = 1.0. This sample will be referred to as S1.0 and contained the following quantities of each variable:

TGDDM in TGDDM/TGPAP Mix: 50%

DGEBF: 12.5%

Stoichiometric Ratio: 1.0

Although these values tell us the ratio of each variable, the first variable is a combination of two distinct resins whereas the DGEBF level is a percentage of the overall resin mix. With this in mind, the actual amounts of each resin in the multi-component system are as follows:

$$\text{TGDDM in overall mix} = (100\text{-}12.5) \times 0.5 = 43.75\%$$
$$\text{TGPAP in overall mix} = (100\text{-}12.5) \times 0.5 = 43.75\%$$
$$\text{DGEBF} = 12.5\%$$

Theoretically a simple rule of mixture between the PW's of the base resins can estimate the PW for S1.0, thus the PW for S1.0 should be as follows:

$$(0.4375 \times 61) + (0.4375 \times 49) + (0.125 \times 91) = 59.5 \text{ minutes}$$

The experimental PW for S1.0 was 62 ± 2 minutes averaged over three experimental runs. Although the theoretical value falls outside one standard deviation of the average it is only 3 minutes from the measured PW and is consequently considered to be in good agreement with the rule of mixtures prediction. Therefore, a rule of mixtures can be used for estimating the PW of a multi-component system based on the PW's of the individual components, assuming the same stoichiometric ratio is used.

Figure 5.3 shows three contour plots of DGEBF content against the stoichiometric ratio at +1, 0 and -1 values for the TGDDM content in the TGDDM/TGPAP mix. The contour plots show that the stoichiometric ratio has a much greater effect on the PW in comparison to the DGEBF content, although the DGEBF content becomes more effective at low stoichiometric ratios and low TGDDM contents.

A reduction in the stoichiometric ratio from r = 1.0 to r = 0.6 results in an increase in the PW of ~50 to 70 minutes depending on TGDDM content. This equates to an increase in resin flow time between 48% and 58%. Based on the results the optimum resin formulation for composite manufacturing would be one containing a low stoichiometric ratio. Although the PW's for the high stoichiometric systems would be sufficient for good resin flow to in composite manufacturing, with the inclusion of a

toughener the viscosity is certain to increase [93], resulting in a reduced flow rate and therefore requiring more time to optimise fibre wetting.

The inclusion of DGEBF is most pronounced at low TGGDM levels (Figure 5.3a) and at low stoichiometric ratios whereby its addition up to 25% increases the PW by over 15 minutes. However, from the same plot it can be seen that an increase in stoichiometry negates the effects of DGEBF. This is somewhat surprising considering the differences between the PW's of the base resins at r = 1.0 reported in chapter 4, as DGEBF was found to have the longest PW. The lack of change with its inclusion at high stoichiometries can be attributed the reaction kinetics of the base resins, in particular activation energies. Tables 4.3-4.5 (p 117) show that the non-catalysed activation energy (E_{a1}) of DGEBF was lower than TGDDM and TGPAP; meaning the epoxy groups are more reactive towards amines. Despite this, the PW of DBEBF is longer. DGEBF is bi-functional and as such, network formation with DDS proceeds by a $RA_2 + RB_4$ reaction. In other words, only one of the reactants present in the mix contributes to the formation of a three-dimensional polymer network, in this case the DDS hardener. Owing to this, the crosslinking potential of DGEBF is lower than both TGPAP and TGDDM, ultimately leading to a slower increase in average molecular weight. Based on its inclusion up to 25% having minimal effect on the PW, it can be suggested that there is equilibrium between the rate at which the average molecular mass increases (which in turn increases the PW) and the rate of reaction that reduces the PW.

This theory is supported by the contours in Figure 5.3c, as at high stoichiometric ratios the inclusion of DGEBF actually reduces the PW, the opposite of what would be expected based on the results from the base resin rheology. This suggests that owing to the small quantity of DGEBF added, its detrimental effects towards increasing molecular weight are unbalanced with its ability to lower the average activation energy that increase the rate of polymerisation, resulting in faster gelation.

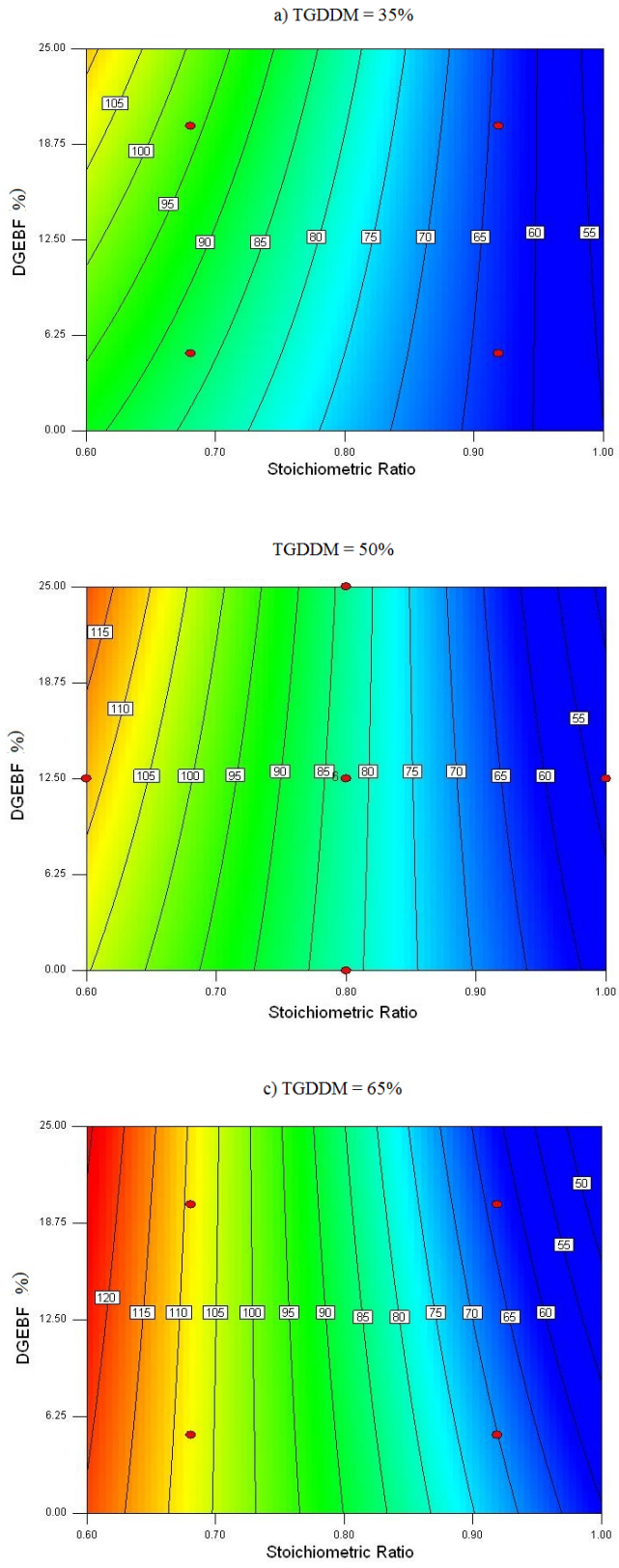

Figure 5.3 FED contour plots for the processing windows at 130°C for the (a) -1, (b) 0 and (c) +1 planes in the 'TGDDM in TGDDM/TGPAP mix' axis. These planes correspond to TGDDM quantities in the total formulation of 35%, 50% and 65% respectively.

The opposite trend was found at low stoichiometric ratios. At low TGDDM levels (Figure 5.3a) and at r = 0.6, the inclusion of DGEBF increases the PW by ~15 minutes, however the same DGEBF inclusion at high TGDDM levels (Figure 5.3c) only results in a ~5 minute increase. This trend reflects the results from the base resins, and suggests that the reduced crosslinking potential of DGEBF has a greater effect on the increase in PW compared to the activation energy associated with the epoxy groups attached to it; most likely due to the lack of crosslinking opportunities owing to the reduced DDS content.

5.1.2. Glass Transition Temperature

The glass transition temperature (T_g) of resin formulations from the FED were measured using DMTA. Details of the testing conditions were given in chapter 3 (p 95) and the curing conditions on p 90. Once cured the resins were subsequently post cured for a further eight hours at 200°C in order to fully cure the network. Maximising the degree of conversion is essential for optimising the T_g, as was found by Barton [217] who reported a 70°C increase in T_g for the final 10% of conversion in a DGEBA/DDM system. Once post cured, dynamic DSC runs of the resins revealed no measureable residual cure thus, the resins were deemed fully cured. Thus the T_g measurements reported in this section are for T_g^∞ (the maximum possible T_g for a given resin formulation).

As with the rheology results presented earlier, comparison between the T_g results obtained in the FED and those presented for the T_gs of the base resins in chapter 4 are limited owing to the different stoichiometric ratios studied in the FED. However, one sample had the same stoichiometric ratio, sample S1.0. From the FED model, S1.0 has a T_g of 255°C.

The T_gs reported for TGDDM, TGPAP and DGEBF in chapter 4 are 270°C, 254°C and 193°C respectively. Through a simple rule of mixtures, the estimated T_g of S1.0 is as follows:

$$(0.4375 \times 270.0) + (0.4375 \times 254.1) + (0.125 \times 193.0) = 253°C$$

The theoretical T_g for S1.0 of 253°C is in good agreement with the experimental value of 255°C, showing a rule of mixtures can be used to estimate the T_g for a given mixture of the three resins, assuming that the same stoichiometric ratio is used.

The contour plots for the change in T_g with respect to the three variables being studied are shown in Figure 5.4. In Figure 5.4 the stoichiometric ratio, r, is fixed at three values; 0.92, 0.8 and 0.68. These values correspond to the +1, 0 and -1 planes of the FED cube in the 'stoichiometric ratio' axis. Figure 5.4a shows the effects of TGGDM and DGEBF levels at r = 0.92. As this stoichiometric ratio is close to r = 1.0 it is not surprising that the T_g contour lines follow what one would expect based on the values from the base resins. It can be seen that with increased TGDDM levels the T_g of the system increases up to a maximum of 270°C. DGEBF has the expected effect of reducing the T_g of the system. Its inclusion from 0-25% reduces the T_g by ~20°C at high TGDDM levels and ~15°C at high TGPAP levels. As discussed in chapter 4 the lower T_g associated with DGEBF-containing systems can be attributed to the significantly lower crosslink density; a property which itself is attributable to DGEBF containing only two epoxy groups per monomer. Consequently, the crosslinking potential of each monomer is reduced compared to TGPAP and TGDDM, which have higher functionalities.

Figure 5.4b and 5.4c shows the change in T_g at stoichiometric ratios of r = 0.8 and r = 0.68 respectively. The contour plots show the same trends for both stoichiometries as was observed with the +1 plot shown in Figure 5.4a. One notable difference between the three plots is the change in maximum and minimum T_gs. For any given epoxy formulation the T_g increases with a reduction in stoichiometry.

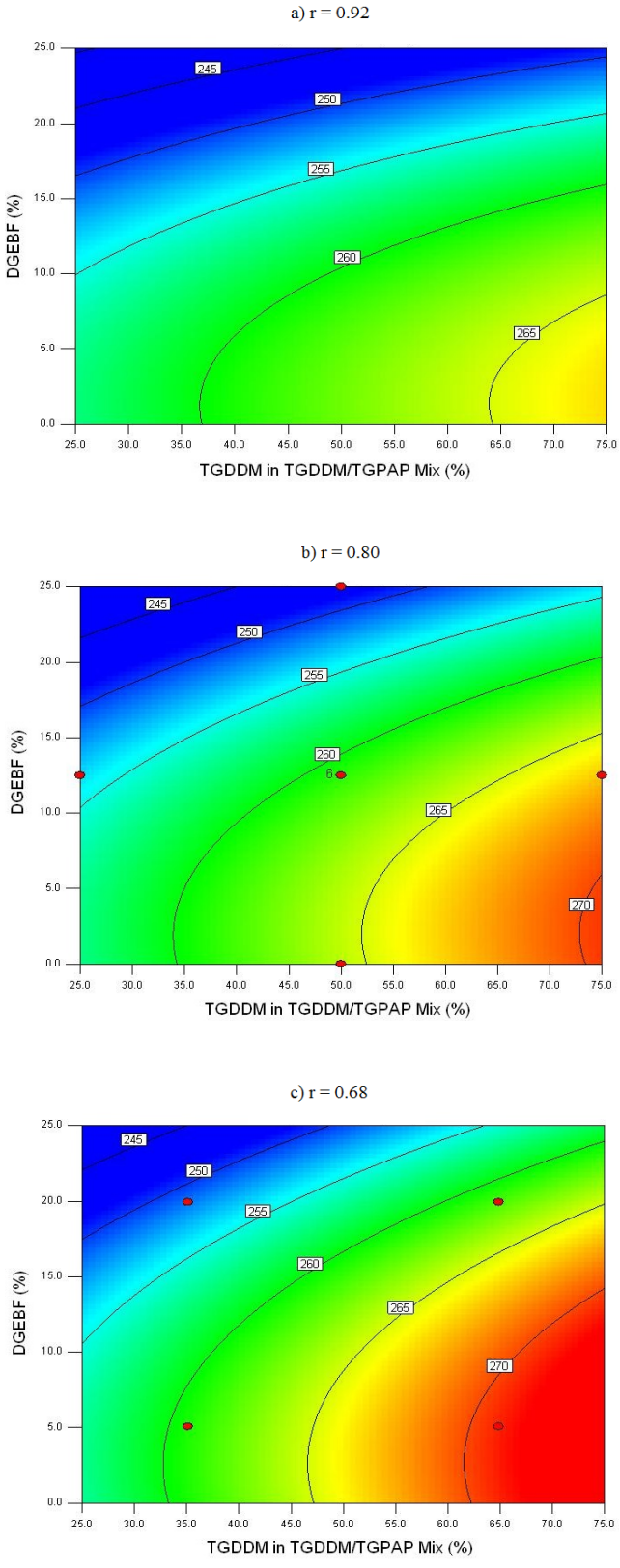

Figure 5.4 FED contour plots for the change in T_g^{∞} at three stoichiometric ratios of (a) r = 0.92, (b) r = 0.8 and (c) r = 0.68. The stoichiometric ratios correspond to the -1, 0 and +1 planes in the FED.

Although the maximum contour line is at 270°C for all stoichiometries it shifts to higher DGEBF and TGPAP levels as the stoichiometry reduces. The minimum T_g contour line also increases with a reduction in stoichiometric ratio. When r = 0.92 the minimum T_g is 250°C however when the stoichiometry reduces to r = 0.68 the T_g increases by 10°C. The value of T_g is directly related to the crosslink density of the cured polymer; with higher T_gs being attributed to higher crosslink densities [217]. Therefore, it follows that a reduction in stoichiometric ratio results in an increase in crosslink density. An in depth analysis of the effects of stoichiometric ratio are given in section 5.2.4 (p 174).

5.1.3. Conclusions

Analysis of the contour plots obtained from the FED for the glass transition temperature, room temperature viscosity and processing window allow for several initial conclusions to be drawn regarding optimising the resin formulation of a multi-component epoxy resin blended system i.e. to accommodate a toughening agent whilst maintaining a suitable viscosity, PW and T_g. From a processing standpoint the inclusion of DGEBF is not as beneficial as reducing the stoichiometric ratio. With a reduction in r the PW increases; a property that is highly beneficial for composite manufacturing techniques such as resin infusion. Higher viscosities are unfavourable for composite manufacturing and as such minimising the quantity of TGDDM in the system is an important parameter to consider. Further consideration must be made to the properties of the final cured resin, in particular the T_g. As discussed earlier in this chapter the T_g of TGDDM rich systems was found to be ~10°C higher than those rich in TGPAP. Whilst a higher T_g allows for a higher maximum operating temperature a difference of 10°C is a small advantage. Furthermore, the processability of TGDDM is a major factor that may deter its use in further experimental work. The inclusion of DGEBF had the expected effect of reducing the T_g, although over the range studied in this FED the T_g only dropped by ~20°C. Both of these trends were irrespective of stoichiometry and indeed the T_gs of the system increased as the stoichiometry was reduced.

Based on the findings presented above one can conclude that further research is required into the effects of stoichiometric ratio, especially regarding its effect on the

T_g and PW. Furthermore, additional work is required to determine the effects of DGEBF on a multi-component system over a wider range, as the range from 0–25% used in this FED was too narrow for its effects to be fully understood.

5.2. The Effects of Stoichiometric Ratio: An In-depth Analysis

The stoichiometric ratio refers to the ratio between reactive groups present within a mixture. For epoxy-amine systems, such as those studied in this work, the stoichiometric ratio is the concentration of primary amine-hydrogens divided by the concentration of epoxy groups. Thus, at a stoichiometric ratio of r = 1.0 there are equal numbers of epoxy and primary amine groups present within the initial mixture. In this section the stoichiometric ratio is studied over three values, r = 1.0, 0.8 and 0.6. The three resin systems used in this section reflect the +S, -S and 0 points in the 'stoichiometric ratio' axis from the FED studied in the previous section and details of the multi-component resin formulation used (named MC) can be seen in Table 5.2.

Table 5.2 Multi-component resin (MC) composition used in a stoichiometric ratio study.

Variable	Quantity
TGDDM in TGDDM/TGPAP Mix	50%
TGPAP in TGDDM/TGPAP Mix	50%
DGEBF in Multi-component Resin	12.5%
TGDDM in Multi-component Resin	43.75%
TGPAP in Multi-component Resin	43.75%

5.2.1. Differential Scanning Calorimetry (DSC)

5.2.1.1. Enthalpy of Reaction

Table 5.3 displays the total enthalpy of reaction for the multi-component (MC) system at r = 1.0, 0.8 and 0.6. It can be seen that with a reduction in stoichiometry dH_t increases. The same trend was found by Akay et al. [113] who reported enthalpies of reaction for TGPAP-DDS systems isothermally cured at 200°C of 555 J g^{-1}, 637 J g^{-1} and 685 J g^{-1} for stoichiometric ratios of r = 1.3, 1.05 and 0.8 respectively. A reduction

in stoichiometry leads to a change in the ratio of each reaction mechanism (primary amine, secondary amine and etherification) occurring, where etherification becomes more dominant as the stoichiometry reduces. From the dH_t results it could be interpreted that the enthalpy of reaction associated with etherification is higher compared to primary and secondary amine addition because of the increase in dH_t. However, Table 5.3 also reports that the total enthalpy per mole remains constant as the stoichiometry reduces, varying between 101-106 kJ mol^{-1}. This suggests similar enthalpies of reaction for each reaction mechanism. Therefore when coupled with the dH_t results, it can be concluded that the number of reactions occurring per unit weight increases as the stoichiometry reduces.

Table 5.3 The total enthalpy of reaction for a multi-component system (MC) at three stoichiometric ratios; r = 1, r = 0.8 and r = 0.6.

Stoichiometric Ratio	Enthalpy of Reaction dH_t (J g^{-1})	Total Enthalpy per mole (kJ mol^{-1})
1.0	600 ± 21	105 ± 4
0.8	643 ± 22	104 ± 4
0.6	678 ± 39	101 ± 6

Table 5.4 shows the enthalpy of reaction for the three base resins as a function of stoichiometry. It should be noted that the enthalpy of reaction values for the resins shown in Table 5.4 were found on a different DSC machine to the work done elsewhere in this thesis, hence slightly different values are shown for the base resins at r = 1.0 to those reported in chapter 4. The values of dH_t for TGDDM and TGPAP increase with a decrease in stoichiometric ratio. It is well documented that DGA derived epoxy resins such as TGDDM and TGPAP are more likely to form ether links on account of the close proximity of epoxy groups within the resin [40]. These results are in agreement with those reported in Table 5.3 for the MC resin system. In contrast, dH_t for DGEBF decreases as the stoichiometric ratio decreases. DGEBF, similar in structure to DGEBA, is known not to react via etherification to the same extent as TGDDM and TGPAP. Therefore, it is likely that with a reduction in stoichiometry there are unreacted epoxy groups remaining in the cured DGEBF polymer.

Table 5.4 The total enthalpy of reaction for TGDDM, TGPAP and DGEBF at stoichiometric ratios varying from 0.6-1.0.

Stoichiometric Ratio	Enthalpy of Reaction dH_t (J g^{-1})		
	TGDDM	TGPAP	DGEBF
1.0	529 ± 33	572 ± 11	286 ± 7
0.9	563 ± 13	608 ± 6	-
0.8	600 ± 15	620 ± 13	240 ± 5
0.7	652 ± 35	646 ± 21	-
0.6	658 ± 36	657 ± 7	191 ± 5

5.2.1.2. Isothermal DSC

The degree of conversion for all three systems across the five temperatures is shown in Figure 5.5. As with the base resins discussed in chapter 4, an increase in curing temperature results in an increase in the degree of conversion for all stoichiometric ratios. A detailed explanation of this can be found in section 4 (p 105). It is also noteworthy that for each isothermal temperature there is little difference in the degree of conversion with respect to the stoichiometric ratio. This would suggest than in a system where r <1.0, etherification results in epoxy conversion to a similar extent as amine addition would in a system where r = 1.0 i.e. the resin vitrifies at a similar degree of epoxy conversion regardless of stoichiometry.

Figure 5.6 shows that altering the stoichiometric ratio affects the peak heights of reaction at each isothermal temperature, whereby increasing the stoichiometry increases the peak height of reaction at all temperatures. An increase in stoichiometry means an increase in the concentration of amine groups present in the mix. Owing to this, the number of epoxy-amine reactions occurring at any given moment is higher with a higher stoichiometry, the result of which is a higher peak height of reaction. Figure 5.6 also shows that increasing the temperature has a greater effect on the peak height of reaction with an increase in stoichiometry, highlighting the catalytic effect of temperature on the rate of reaction.

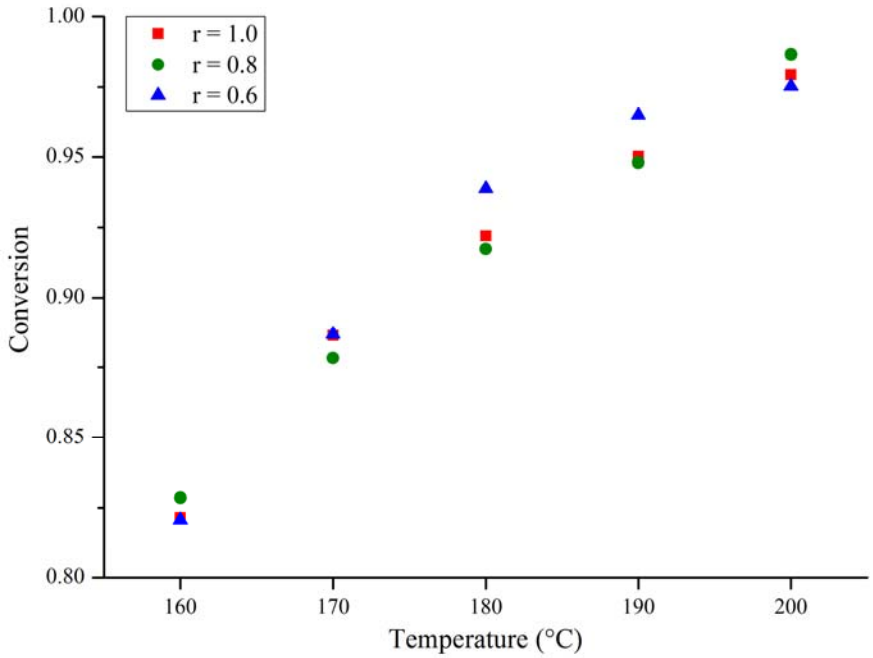

Figure 5.5 Degree of conversion from isothermal curing of the multi-component epoxy resins, MC, at temperatures from 160-200°C and at stoichiometric ratios of r = 1.0, 0.8 and 0.6.

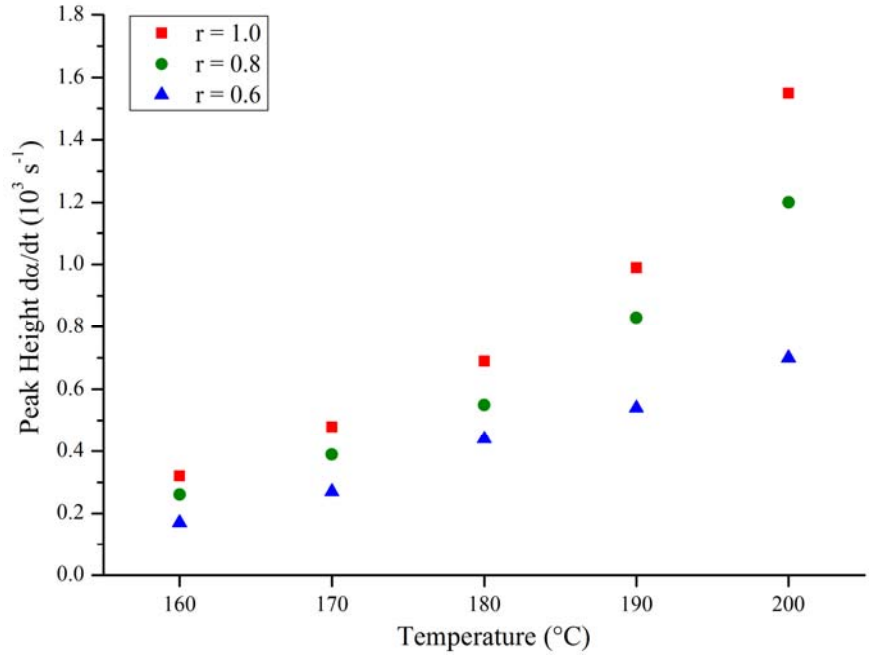

Figure 5.6 Peak heights from isothermal curing of the multi-component epoxy resin, MC, at temperatures from 160-200 °C and at stoichiometric ratios of r = 1.0, 0.8 and 0.6.

Figure 5.7 displays the peak times of reaction with respect to temperature and stoichiometric ratio. For all stoichiometries, an increase in curing temperature results in a decrease in the peak time of reaction. Owing to the Arrhenius behaviour exhibited

by epoxy-amine systems [22], [84] this trend is to be expected. It can be seen from the figure that at curing temperatures of 160°C and 170°C the stoichiometry of the system dictates the peak time of reaction, with an increase in stoichiometry reducing the peak time. At curing temperature >180°C the peak times become increasingly similar to the point where there is no measureable difference between them. The similarity between the peak times can be attributed to effect of thermal catalysis, whereby an increase in temperature supersedes the autocatalytic effect of the hydroxyl groups [197] resulting in similar rates of reaction.

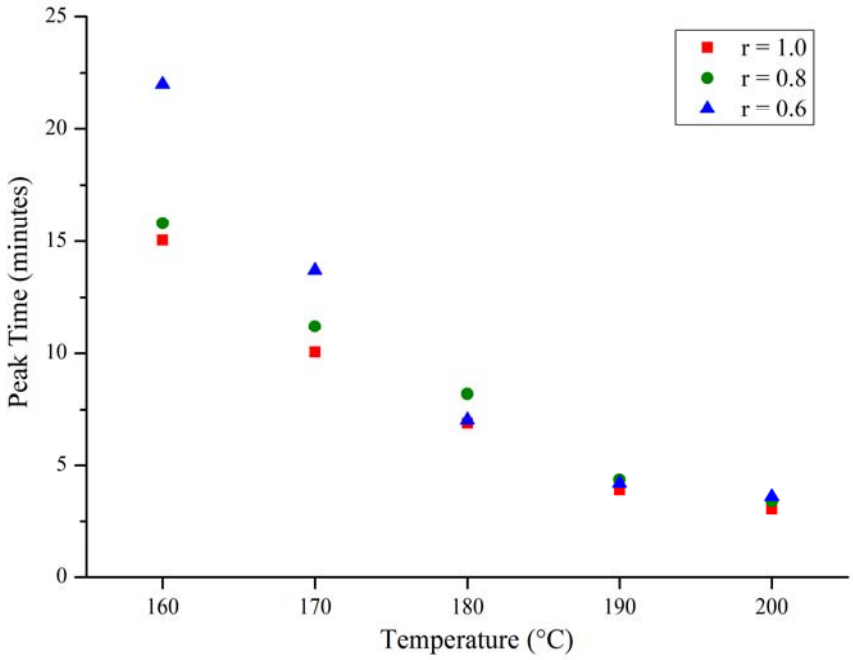

Figure 5.7 Peak times from isothermal curing of the multi-component resin, MC, at temperatures from 160-200 °C and at stoichiometric ratios of r = 1.0, 0.8 and 0.6.

5.2.1.3. Autocatalytic Model and Activation Energies

Figure 5.8 shows the rate of reaction with respect to degree of conversion for stoichiometric ratios of r = 1.0, 0.8 and 0.6 at 190°C. The curves depicted in this figure follow the autocatalytic model [77] (as was found by other researchers investigating epoxy-amine reactions [76], [79], [83], [195]–[197]) whereby the peak rate of reaction occurs at a degree of conversion, $\alpha > 0$. At a high degree of conversion (~0.85) the curves deviate from the linear decrease in rate of reaction. As discussed in many papers and in chapter 4 of this study, the decrease in rate of reaction is attributed to the

onset of vitrification [35], [76], [205]; a transformation seen in epoxy resin polymerisation not accounted for in Kamal's autocatalytic model. Figure 5.8b and Figure 5.8c are taken from r = 0.8 and r = 0.6 at 190°C respectively.

Initial observations suggest that the curve follows the same trend as r = 1.0; however on closer inspection both curves exhibit a deflection from the expected linear decrease in rate of reaction after the peak of reaction at ~0.50 conversion. Whilst this deflection may not be as obvious in the r = 0.8 system, the r = 0.6 system shows it clearly. The same deviation was observed for all temperatures and as with the 190°C examples shown, was more prevalent when r = 0.6.

The autocatalytic model proposed by Kamal was fitted to all the DSC data. Whilst the model exhibited an excellent fit with all r = 1.0 samples, when r < 1.0 a poor fit was found as seen in Figure 5.9. This can be attributed to the deflection at ~0.5 conversion as mentioned earlier. The best-fit model calculated through non-linear regression (NLR) takes into account all data points within its range and values them equally. As the deflection occurs at ~0.5 conversion there is a high proportion of data points within the NLR range that occur after this point. As such the model alters the equation variables to maximise the fit for the whole range, in doing so compromising the fit in the pre-gel portion of the curve (see Figure 5.9). This leads to an inaccurate representation of the rate of reaction during the initial cure.

Based on the results from the model shown in Figure 5.9 it was decided that the Kamal model is only accurate for systems with a high stoichiometric ratio. For comparison between the stoichiometric ratios used the model was fit to the curves using only data points prior to the aforementioned deflection, as shown in Figure 5.10. The figure shows that the model has excellent fit with the data points up to the deflection, beyond which it predicts a significantly lower rate of reaction.

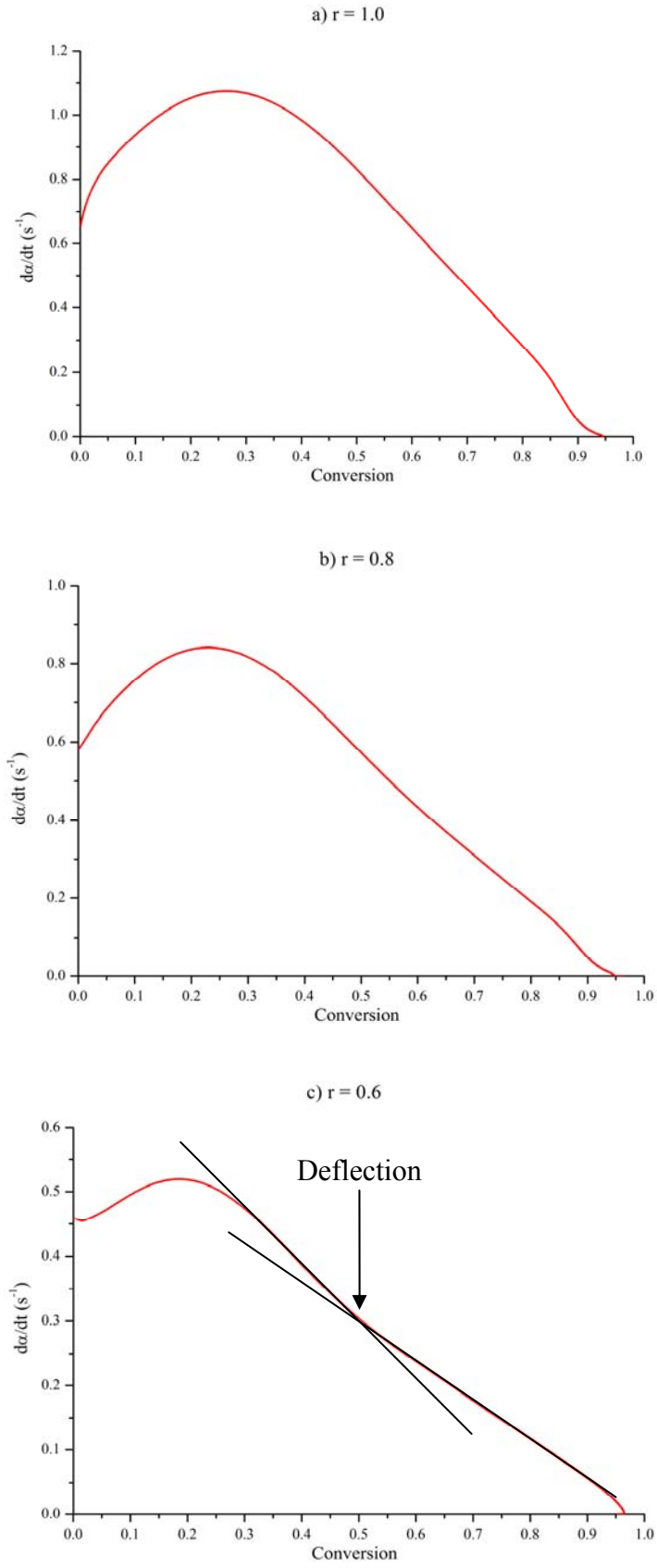

Figure 5.8 Rate of reaction with respect to degree of conversion at 190°C for the multi-component resin, MC, at stoichiometric ratios of (a) r = 1.0, (b) r = 0.8 and (c) r = 0.6.

That said the model curve is more typical of the autocatalytic reaction curves found in chapter 4 and indeed throughout literature. Based on this observation the autocatalytic model was fit using NLR up to the deflection for all r = 0.8 and r = 0.6 curves.

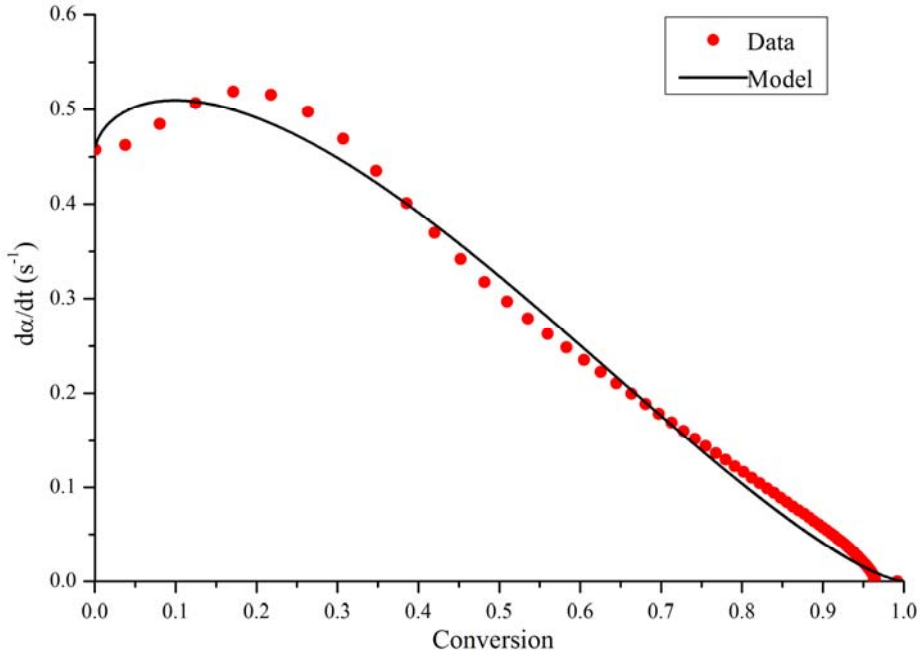

Figure 5.9 An attempt to fit the autocatalytic model to data points of the multi-component resin, MC, at a stoichiometric ratio of r = 0.6 and at a temperature of 190°C.

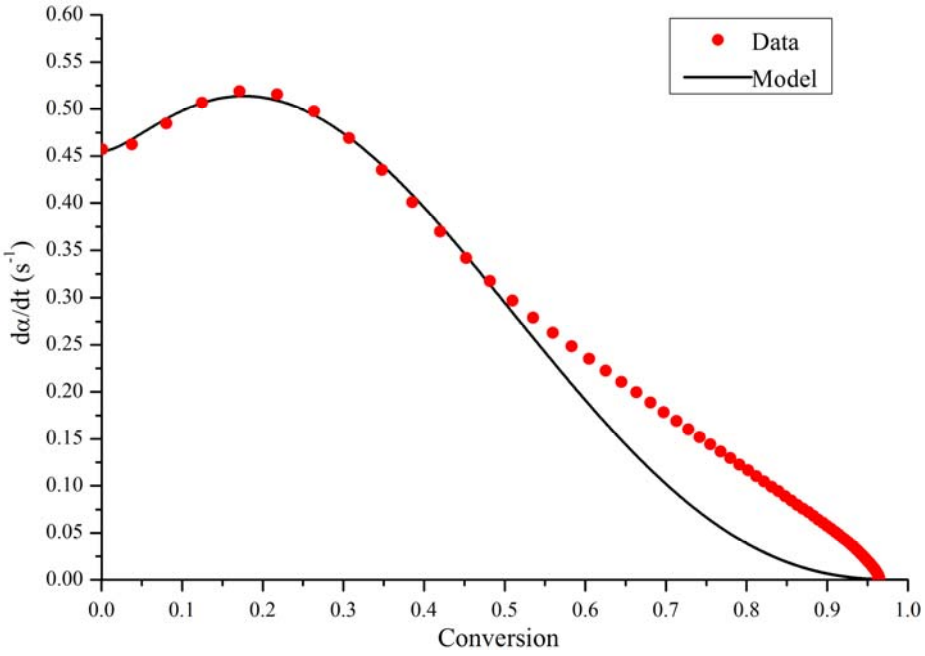

Figure 5.10 The autocatalytic model fit to the multi-component resin, MC, at a stoichiometric ratio of r = 0.6 and at a temperature of 190°C up to the deviation at ~0.50 conversion.

Values for the kinetic rate constants were obtained for all three resin systems across five temperatures and the results can be seen in Tables 5.5-5.7. For all three stoichiometries the k_1 and k_2 values increase with an increase in temperature indicating the rate of reaction with respect to both the catalyst and non-catalysed reactions increase with temperature. It can also be seen that the k_1 values increase for each isothermal temperature with an increase in stoichiometric ratio. This is to be expected as k_1 is the rate of reaction with respect to non-catalysed amine addition; a reaction which is more likely with a higher concentration of primary amines. However, the same is not found for the k_2 values that show no apparent trend with stoichiometric ratio.

Theoretically, as the stoichiometry reduces, one would expect k_2 to decrease at the same rate as k_1. The rate of reaction with respect to the hydroxyl-catalysed reactions (k_2) is directly proportional to the amount of hydroxyl groups available to act as catalysts, which in turn is dependent on the degree of epoxy conversion. The values for k_2 shown in Tables 5.5-5.7 show no apparent trend with stoichiometry. Values from r = 1.0 to r = 0.8 increase at each isothermal temperature, however when the stoichiometry is reduced further to r = 0.6 there is no apparent trend with the values at low temperatures remaining similar to those found for r = 0.8. At high temperatures when r = 0.6 k_2 is not as high as for r = 0.8 and is more akin to the values for r = 1.0. The most likely explanation for this lack of trend can be attributed to the poor fit between Kamal's autocatalytic model and the rate of reaction curves for stoichiometries where r < 1.0. As such, the results presented in Tables 5.4-5.6 for k_2 are somewhat unreliable. For a more accurate representation, a more sophisticated model should be fit to the rate of reaction curves.

k_1/k_2 is the ratio of reaction rate coefficients and highlights the substitution effect. It has been widely documented that secondary amines have a negative substitution effect on account of steric hindrance towards reactions with epoxy compared with primary amines [32], [219]. A k_1/k_2 ratio of 0.5 means no substitution effects occurring, as primary amines have two hydrogens compared to one hydrogen on secondary amines thus twice the probability of reacting [32].

Table 5.5 Kinetic parameters and activation energies for a multi-component resin formulation where r = 1.0.

r = 1.0								
Isothermal Temperature (°C)	k_1 (s^{-1})	k_2 (s^{-1})	m	n	m + n	k_1/k_2	E_{a1} (kJ mol^{-1})	E_{a2} (kJ mol^{-1})
160	0.22	1.79	1.18	2.05	3.23	0.12	67	32
170	0.31	2.20	1.04	1.81	2.85	0.14		
180	0.45	2.67	0.94	1.70	2.64	0.17		
190	0.66	3.27	0.85	1.57	2.42	0.20		
200	1.08	3.84	0.83	1.45	2.28	0.28		

Table 5.6 Kinetic parameters and activation energies for a multi-component resin formulation where r = 0.8.

r = 0.8								
Isothermal Temperature (°C)	k_1 (s^{-1})	k_2 (s^{-1})	m	n	m + n	k_1/k_2	E_{a1} (kJ mol^{-1})	E_{a2} (kJ mol^{-1})
160	0.19	2.16	1.24	2.68	3.92	0.09	64	32
170	0.27	2.58	1.19	2.44	3.63	0.10		
180	0.39	3.16	1.15	2.19	3.34	0.12		
190	0.58	3.73	1.01	2.07	3.08	0.16		
200	0.84	4.63	0.94	2.00	2.94	0.18		

Table 5.7 Kinetic parameters and activation energies for a multi-component resin formulation where r = 0.6.

r = 0.6								
Isothermal Temperature (°C)	k_1 (s^{-1})	k_2 (s^{-1})	m	n	m + n	k_1/k_2	E_{a1} (kJ mol^{-1})	E_{a2} (kJ mol^{-1})
160	0.13	2.15	1.36	3.52	4.88	0.06	65	25
170	0.22	2.60	1.30	3.06	4.36	0.08		
180	0.34	3.02	1.19	2.95	4.14	0.11		
190	0.46	3.48	1.23	2.72	3.95	0.13		
200	0.58	3.88	1.01	3.03	4.04	0.15		

The results in Tables 5.5-5.7 show a strong negative substitution effect for all stoichiometric ratios, as was found for the base resins in chapter 4 (p 117). Additionally, as the stoichiometry reduces k_1/k_2 also reduces for all isothermal temperatures, indicating an increase in the substitution effect. It is also noteworthy that unlike reports by some authors [75] there is a significant change in substitution effect with temperature. This effect is seen for all stoichiometric ratios. As the curing temperature increases the substitution effect reduces, indicating an increase in reactivity of epoxies towards secondary amines. Furthermore, this trend is more pronounced as the stoichiometry increases; most likely due to the catalytic effect of hydroxyl groups generated through primary amine addition.

The activation energies (E_as) for the three resins (Tables 5.5-5.7) were calculated from the gradient of a plot of ln $k_{1 \text{ or } 2}$ against 1/T as seen in Figure 5.11. Information on this method of calculating activation energies is detailed in section 4 (p 112). Figure 5.11 shows all data points are in relatively good agreement with their respective line of best fit. As such, the gradients of the lines and therefore the activation energies calculated are accurate in accordance with the model used to determine the k_1 and k_2 values. The activation energies (E_as) for the three systems are reported in Tables 5.5-5.7. The E_{a1} values for r = 1.0, 0.8 and 0.6 are 67, 64 and 65 kJ mol^{-1} respectively. The close agreement and lack of any trend between the values suggests there is little or no difference in the energy required for epoxy-primary amine reactions with stoichiometry.

The E_{a2} values for the three systems are 32, 32 and 25 kJ mol^{-1} respectively. As with k_2 values for r = 0.6, the E_{a2} is noticeably different to the other two stoichiometric systems. The activation energy required for the catalysed reactions should remain constant regardless of stoichiometry, as was found with E_{a1}. As such the much lower E_{a2} value for r = 0.6 can be attributed to the lack of fit between the autocatalytic model proposed by Kamal and the rate of reactions recorded for the system.

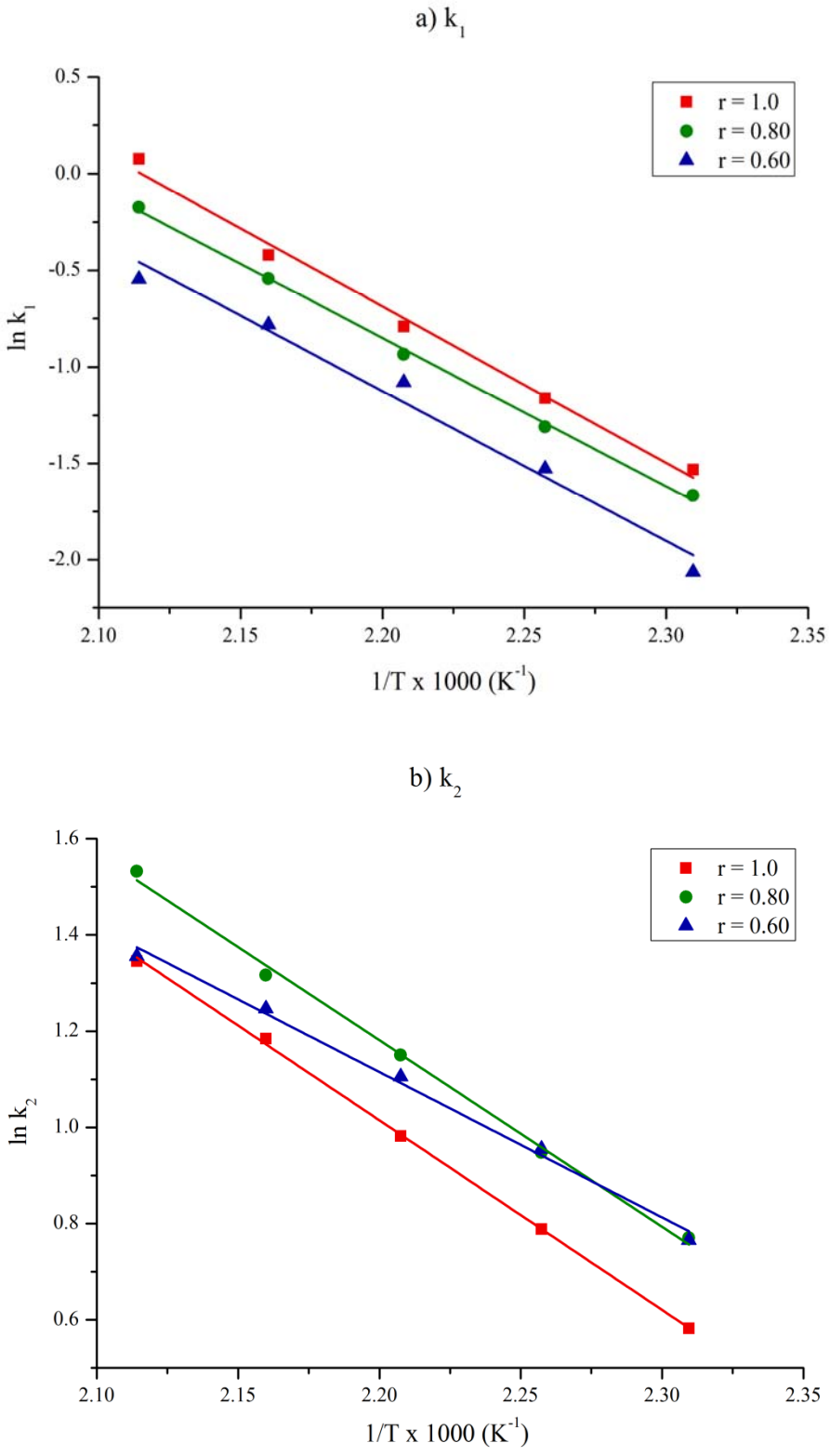

Figure 5.11 Rate constants, (a) ln k_1 and (b) ln k_2, as a function of 1/Temperature for a multi-component resin (MC) at stoichiometric ratios of r = 1.0, 0.8 and 0.6.

The E_a values for the multi-component system containing the three base resins at the same stoichiometric ratio (r = 1.0) can be compared to a theoretical value based on a rule of mixtures of the E_a values from the base resins. Using a rule of mixtures for r = 1.0 E_{a1} and E_{a2} would be 70 kJ mol^{-1} and 51 kJ mol^{-1} respectively. The measured value of 68 kJ mol^{-1} for E_{a1} is in relatively good agreement however, the value for E_{a2} was measured significantly lower and was more akin to the base resin TGPAP. In chapter 4 it was found that E_{a1} and E_{a2} were similar in both TGDDM and DGEBF (Tables 4.3-4.5, p 117) however, E_{a2} for TGPAP was significantly lower than E_{a1}, with values of 28 kJ mol^{-1} and 68 kJ mol^{-1} respectively. The fact that E_{a2} is significantly lower than E_{a1} for all stoichiometries suggests the inclusion of TGPAP is important in lowering Ea_2 beyond the rule of mixtures prediction. Whilst this could be due to the hydroxyl groups in TGPAP having a greater catalytic potential, further explanation could be derived from the catalytic effect of tertiary amines present in the TGPAP backbone [4]. TGDDM has two tertiary amines in the prepolymers backbone however their catalytic potential is restricted due to steric hindrance owing to the 'bulky molecular structure' of the TGDDM prepolymers [204]. The tertiary amine in the TGPAP backbone is more accessible and is known to catalyse epoxy-amine reactions.

5.2.2. Fourier Transmission Infra-red (FTIR) Spectroscopy

The changes in peak areas of the epoxy (907 cm^{-1}) and primary amine (1620 cm^{-1}) peaks were measured throughout the cure and normalised to the 1593 cm^{-1} peak attributed to phenyl groups; a chemical group known not to take part in the epoxy-amine reaction. See section 4.2 (p 121) for more details.

Figure 5.12 shows the residual epoxy groups as a function of time for the multi-component (MC) epoxy resins. It can be seen that there is a clear trend between the stoichiometric ratio and rate of epoxy consumption; where the epoxy percentage in r = 1.0 depletes the fastest. At the end of the initial dwell (180 minutes at 130°C) there is a clear difference between the degrees of epoxy conversion, with the residual epoxy percentages being 22%, 31% and 40% for r = 1.0, 0.8 and 0.6 respectively. This indicates that the stoichiometric ratio is significant in determining the rate of epoxy conversion. It is also noteworthy that as the cure progresses at 130°C the rate of conversion in all three systems slows as the polymers tend towards vitrification.

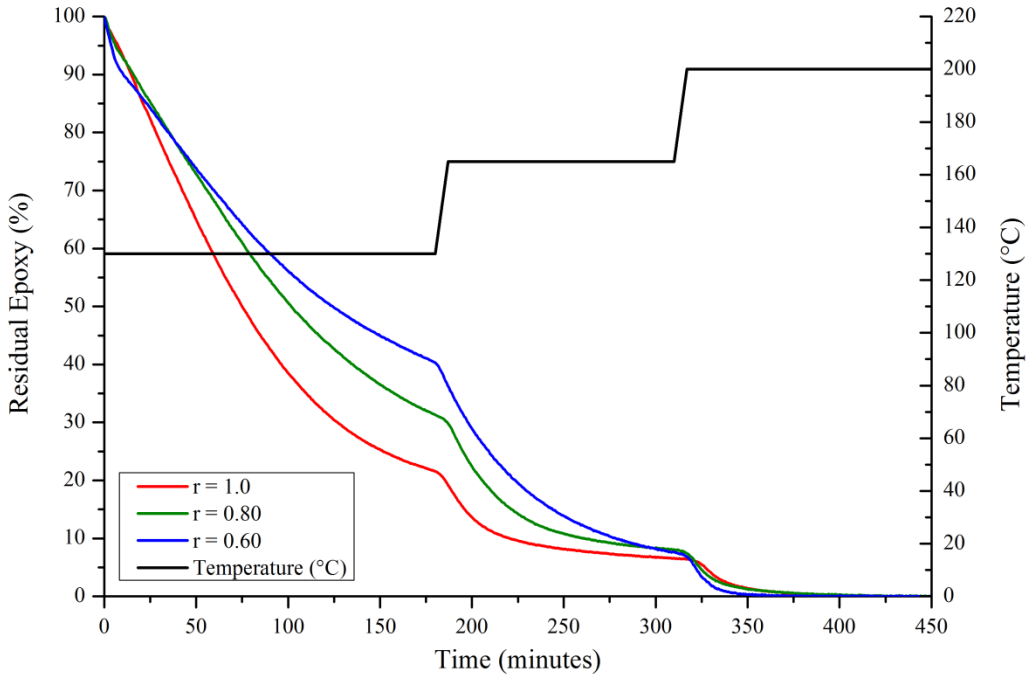

Figure 5.12 Residual epoxy concentration as a function of time following a three step cure cycle for a multi-component epoxy resin system at stoichiometric ratios of r = 1.0, 0.8 and 0.6.

After the initial three hour dwell at 130°C, the temperature increased to 165°C. It is at this point that all three system show a significant increase in the rate of epoxy consumption, although the rates differ between systems with r = 0.6 showing a much faster epoxy consumption rate. It is also interesting to note that by the end of the 165°C dwell the remaining epoxy group percentage for all three systems is very similar with ~5% epoxy groups remaining in each system. Like with the initial dwell at 130°C the rate of reaction slows towards the end of the two-hour dwell at 165°C as the resins tend towards vitrification. The temperature increase to 200°C leads to the epoxy conversion increases further, and after two hours at 200°C the residual epoxy percentage in each system is immeasurable, suggesting the resins are fully cured. When r <1.0 there is an insufficient amine concentration for total epoxy consumption. Thus for all epoxy groups to be consumed in r = 0.8 and 0.6 systems alternative reactions must occur; namely etherification.

The mid-infra-red FTIR peak at 1618-1628 cm^{-1} is attributed to the primary amine absorption. The peak area was used to characterise the change in primary amine

concentration with time following the cure cycle. However, as discussed as some length in section 4.2 (p 121) the change in peak area of this peak was more representative of the change in total amine concentration as opposed to the change in primary amine concentration. For all three base resin systems, the change in the primary amine peak area depleted on a 1:1 ratio with the depletion of epoxy groups. The results for epoxy and primary amine residual percentages (Figure 5.12 and 5.13) show a comparable rate of change when r = 1.0, especially at the start of cure. This follows the results from chapter 4 that also showed a comparable rate of change between the two peak areas, suggesting that the 'primary amine' peak is in fact a measure of the total residual unreacted amines present in the system.

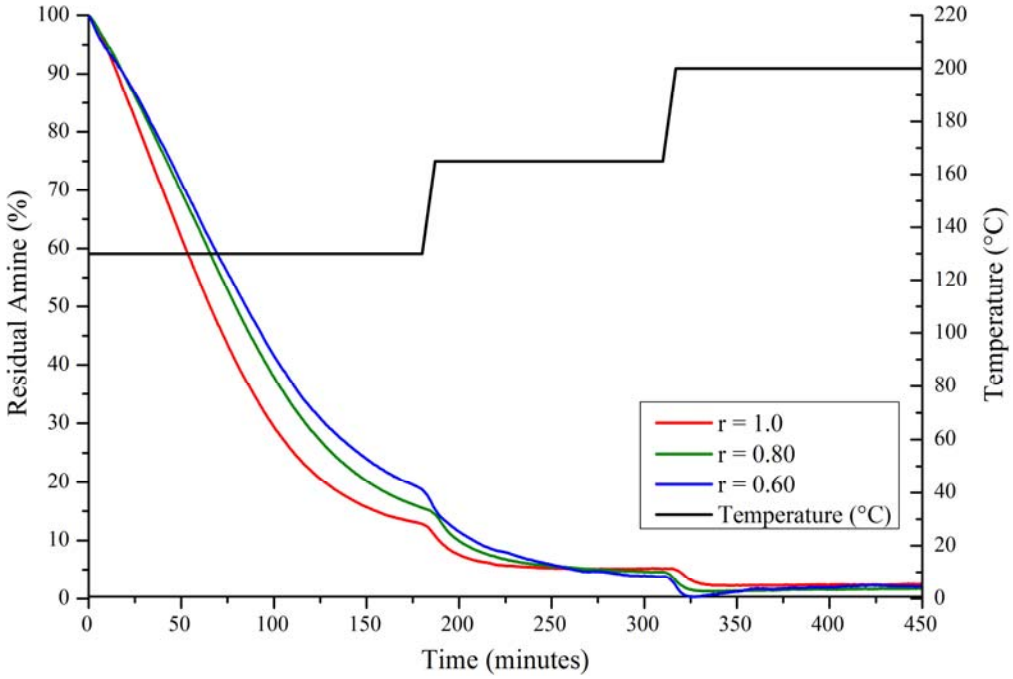

Figure 5.13 Residual amine concentration as a function of time following a three step cure cycle for a multi-component (MC) epoxy resin system at stoichiometric ratios of r = 1.0, 0.8 and 0.6.

Assuming the residual primary amine peak area is in fact the total residual amine peak area provides support to the main trend observed in Figure 5.13; that is with an increase in stoichiometric ratio the rate of amine consumption is faster. When r = 0.6 the concentration of primary amines should deplete quicker than at higher stoichiometric ratios as there is fewer amine groups in the resin system. Consequently, this should lead to more unreacted epoxy groups at any given point, as shown in Figure 5.12. Secondary amines are an order of magnitude less reactive towards

epoxies than primary amines [32]. Thus, it follows that once the primary amines are consumed the rate of reaction slows. Figure 5.13 supports this, as the rate of amine consumption is quicker at higher stoichiometric ratios, suggesting more primary amines are available to react in the initial resin system.

Further observation of Figure 5.13 shows for all stoichiometries a residual amine percentage of ~3% after the full cure cycle. Possible explanations for this are the error associated with measuring the area of an overlapping peak, as is the case with the primary amine peak measured using mir-FTIR. It is also possible that the measured areas are accurate and that a small residual unreacted amine concentration exists within the fully cured epoxy resins. This could occur due to steric hindrance restricting molecular interactions.

5.2.3. Rheology

5.2.3.1. Gel Point and Processing Window

Rheology was conducted on the three MC resins at 130°C. The resultant viscosity profiles can be seen in Figure 5.14 and the times attributed to the processing window (PW) and G'/G'' crossover in Table 5.8. As briefly discussed in section 5.1.3 (p 146) and seen in Figure 5.14, a reduction in stoichiometry results in a slower increase in viscosity through crosslinking; ultimately leading to a longer PW.

Lowering the stoichiometry reduces the number of available amine groups for epoxy conversion, which in turn reduces the rate of reaction. This was seen from the isothermal DSC results presented in Figure 5.6 (p 157) and in Tables 5.5-5.7 (p 163), which showed as the stoichiometry reduced so did the rate of reaction. Furthermore, the FTIR results for epoxy conversion shown in Figure 5.12 (p 167) showed a slower epoxy conversion with a reduction in stoichiometry, in agreement with the rheology results shown above.

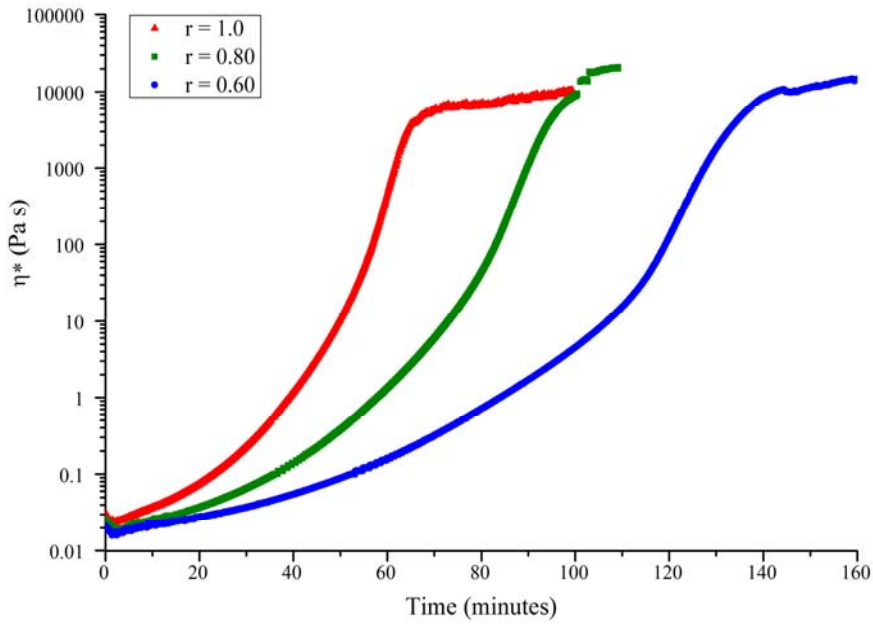

Figure 5.14 Viscosity profile at 130°C for a multi-component (MC) resin at three distinct stoichiometric ratios; r = 1.0, r = 0.8 and r = 0.6.

Table 5.8 The processing window and G'/G'' crossover times at 130°C for a multi-component resin at three distinct stoichiometric ratios; r = 1.0, r = 0.8 and r = 0.6.

Stoichiometry	Gel time (minutes)	
	Processing Window (100 Pa s)	G'/G" Crossover
1.0	58 ± 2	63 ± 2
0.8	83 ± 3	88 ± 2
0.6	120 ± 3	124 ± 3

5.2.3.2. Conversion at the Gel Point

The theoretical gel point conversions along with the calculated conversion from DSC data (see p 133 for details on this technique) and FTIR data are presented in Table 5.9. Owing to the same quantities of base resins used in each formulation both the amine and average epoxy functionality remain constant. The only variable to change is the stoichiometric ratio, r. Varying r has a significant effect on the predicted gel point conversion; thus a reduction from r = 1.0 to r = 0.6 leads to an increase in the degree of epoxy conversion required for gelation, from 38% to 49%.

Table 5.9 The theoretical and measured gel point conversions by DSC and FTIR for a multi-component (MC) resin at three distinct stoichiometric ratios; r = 1.0, r = 0.8 and r = 0.6.

Stoichiometric Ratio	Conversion at Gel Point			Residual dH (J g^{-1})
	Theoretical	Measured (DSC)	Measured (FTIR)	
1.0	0.38	0.32 ± 0.02	0.40	409 ± 11
0.8	0.42	0.28 ± 0.02	0.43	465 ± 13
0.6	0.49	0.17 ± 0.01	0.49	557 ± 6

Gel point conversion measurements from FTIR data follow this trend with values of 0.40, 0.43 and 0.49 for r = 1.0, 0.8 and 0.6 respectively, thus supporting the use of FTIR to determine epoxy conversion. The measured values by DSC however show that a reduction in stoichiometry leads to a reduction in the degree of conversion at the gel point, with a gel point conversion of 17% at r = 0.6. This value is clearly incorrect and highlights the inaccuracy in using DSC to determine the gel point conversion. As previously discussed in section 5.2.1.1 (p 154) an increase in dH_t with a reduction in stoichiometry for TGPAP and TGDDM resins is likely because of more reactions occurring per unit weight. It is interesting to note that the residual enthalpy of reaction (Table 5.9) also increases with a reduction in stoichiometry. Initially this is surprising considering that the theoretical gel point conversion increases as stoichiometry reduces. However, it can be explained by examining the curing conditions pre and post gelation. When using a low curing temperature, such as 130°C (pre gelation), etherification is unlikely and so amine addition drives epoxy conversion. When subjected to higher curing temperatures (post gelation) etherification competes with amine addition and can become a dominant reaction mechanism, especially in amine-depleted systems. Therefore, during a temperature ramp to find the residual enthalpy of reaction all epoxy groups can react, regardless of the stoichiometric ratio. Since there are more epoxy groups per unit weight of the total formulation (epoxy + amine) reacting as the stoichiometry reduces, the residual enthalpy of reaction is greater, leading to a misrepresentation of the gel point conversion.

5.2.3.3. Viscosity Modelling

Viscosity modelling was conducted using the theoretical gel point conversions. Models were fit to the three MC systems using Equation 4.5 (p 147). Graphical representation of the viscosities and models as a function of time at 130°C for each system are shown in Figure 5.15. It can be seen from the figure that as the stoichiometric ratio reduces the model deviates from the data. However all three models show relatively good fit with the data towards the gel point (~1000 Pa s), suggesting that the NLR favours generating fitting parameters which result in a good fit for the gel-region of the curves. That said, with a reduction in stoichiometry the viscosity does not rise as dramatically with gelation (see Figure 5.15c), owing to which the model shows poorer fit at gelation compared to r = 1.0.

The minimum viscosities and fitting parameters associated with the three stoichiometric ratios are also shown in Table 5.10. With a reduction in stoichiometry the minimum viscosity reduces on account of a lower quantity of DDS powder in the resin system. It can also be seen for the three stiochiometries that parameter B is positive and increases as the stoichiometry reduces whereas parameter B is negative and decreases as stoichiometry reduces. However, there is no trend between the variation in parameters B and C with stoichiometry. This differs to the fitting parameters of the base resins studied in chapter 4, where the fitting parameters showed a linear relationship with change in epoxy resin functionality.

Table 5.10 The effects of varying the stoichiometric ratio in a multi-component resin system, MC, on minimum viscosity and fitting parameters at 130°C.

Stoichiometry	Minimum viscosity (Pa s)	B	C
1.0	0.024	4.63	-4.17
0.8	0.020	6.55	-8.32
0.6	0.016	11.23	-17.71

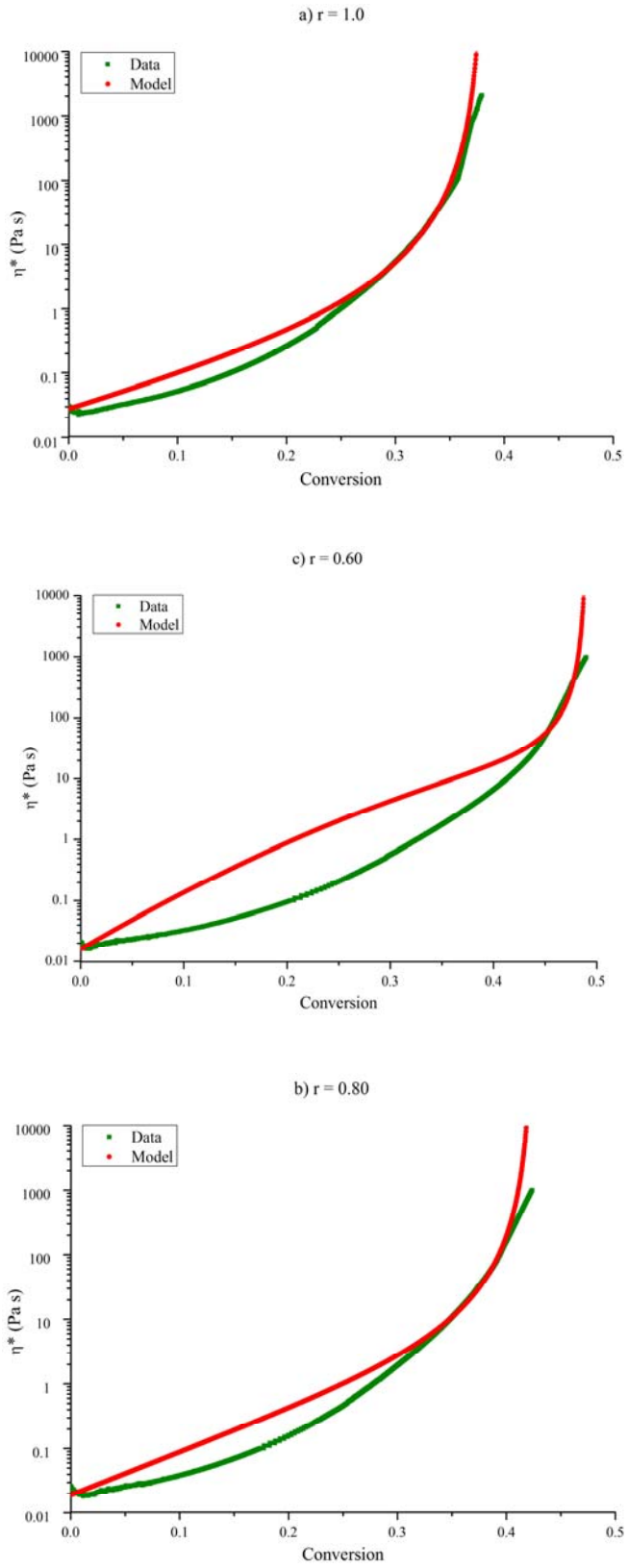

Figure 5.15 Rheological modelling of a multi-component (MC) resins at 130°C, with stoichiometric ratios of (a) r = 1.0, (b) r = 0.8 and (c) r = 0.6.

5.2.4. Glass Transition Temperature

In section 5.1 the effects of altering stoichiometric ratio on the T_g were briefly discussed, however little explanation was given as to why the T_g changes with stoichiometric ratio. Table 5.11 shows the T_g values of the cured MC resin at the three stoichiometric ratios used. As the stoichiometric ratio reduces the T_g of the polymer increases.

Table 5.11 The change in glass transition temperature with stoichiometric ratio for a multi-component (MC) epoxy resin mixed with DDS.

Stoichiometric Ratio	Glass Transition Temperature (°C)
1.0	255 ± 1
0.8	262 ± 1
0.6	265 ± 1

The T_g of a thermosetting polymer can be directly related to the crosslink density of the material [199], along with molecular structure [39] and degree of reactive group conversion [35]. The three resin systems consisted of the same blend of DGEBF, TGDDM and TGPAP and all resins were postcured at 200°C for five hours to ensure the polymers were fully cured. In this case any variation in T_g can be related to the crosslink density. Higher T_gs are attributed to polymers with higher crosslink densities. Increasing the degree of conversion and reducing the molecular distance between crosslinks both increases the crosslink density of a polymer. As all resins were fully cured one has to assume that the increase in T_g seen with a reduction in stoichiometry is caused by a reduction in the molecular distance between crosslinks. There is evidence in the literature that suggests a slight excess of epoxy is beneficial in maximising the T_g in higher functionality epoxy resins. Guerrero et al. [70] studied TGDDM cured with an anhydride by DMTA and found the maximum T_g (after post curing to be 200°C) with a stoichiometry between r = 0.8 and 0.9. They suggested that a slight excess of epoxy promoted etherification and that this resulted in a higher crosslink density. Etherification is a prominent reaction between epoxy groups and hydroxyl groups; especially at high temperatures [205] and in DGA based epoxy resins [40] such as TGDDM and TGPAP where epoxy groups are in close proximity.

It is interesting to note that in Guerrero's study, a stoichiometric ratio below r = 0.8 resulted in a reduction in the crosslink density and therefore T_g. They reported that below r = 0.8 there was a marked increase in the number of residual unreacted epoxy groups in the final structure and that this increased as the stoichiometric ratio reduced further. This differs to the results shown in Table 5.11, whereby the T_g continues increasing with a reduction in stoichiometry to r = 0.6. Furthermore, FTIR results shown in Figure 5.12 (p 167) show no residual epoxy groups remained in the final structure, hence a reduction in stoichiometry does not hinder complete reaction. This is most likely due to etherification that occurs in a depleted amine system.

In an attempt to quantify etherification, mid-infra-red (mir) FTIR was conducted on the three resins following the cure cycle developed within our group. It has been reported in various literature that the absorbance peak at 1120 cm^{-1} can be attributed to the ether linkage (C-O-C) in epoxy resins [195], [220]. Attempts were made to quantify the peak both in terms of peak area and height with respect to time for the three resins, however there was no observable trends. Whilst etherification is the most probably cause for epoxy consumption in the amine depleted systems, mir-FTIR was inconclusive. Near-infra-red FTIR may be more accurate in monitor the change in the ether peak with time.

Further comparison between the effects of stoichiometry on T_g presented in this study and those available in literature yield contradictory results. Levchik et al. [44] cured TGDDM with DDS at two stoichiometric ratios; r = 0.50 and 0.85. Using DSC they found the T_g of the two systems and reported values of 175 °C and 215 °C respectively. Although these results initially seem to contradict the work presented in Table 5.11 it should be noted that the resins in Levchik's work were cured at 180°C. In chapter 4 it was reported that curing isothermally at 180°C resulted in a conversion of ~88% for TGDDM; 8% less than the measured conversion when cured isothermally at 200°C for the same period of time. Whilst Levchik et al. did not report on the degree of conversion for their TGDDM systems, Varley et al. [205] stated that when postcured at 205°C, etherification in TGDDM is far more significant than amine based reactions. This would suggest that the resin systems in Levchik's work were not fully cured and that the unreacted groups remaining in their systems would have gone on to

react via etherification had the resins been subjected to a higher curing temperature, ultimately leading to an increase in the T_g of the two resins.

5.3. Further Study on the Influence of a Bi-functional Epoxy Resin within a Multi-component Epoxy Resin System

The addition of a bi-functional epoxy resin to a multi-component resin system was studied in section 5.1, however it was concluded that the addition of DGEBF up to 25% was too narrow a range to fully understand the benefits of its incorporation. Therefore a second FED was created with two variables; the ratio of DGEBF in a DGEBF/TGPAP mix and TGDDM level. The variables and limits of the FED can be seen in Table 5.12 and a schematic in Figure 5.16. Owing to the use of two distinct FED's used in this thesis, they will henceforth be referred to as FED 1 and FED 2. As with the schematic of FED 1 (p 143) each of the nodes represents a resin system that requires mixing and testing. For each of the nodes one sample was mixed, except the central green node of which there were three.

Table 5.12 The limits for a factorial experimental design examining DGEBF in a DGEBF/TGPAP mix and TGDDM content.

Material	Limits
DGEBF in a DGEBF/TGPAP Mix	0-100 wt%
TGDDM	0–50 wt%

In FED 1 and in section 5.2 (p 154) a low stoichiometric ratio was found to increases the glass transition temperature of high-functionality resin systems whilst also extending the processing window. In FED 2 the stoichiometric ratio was fixed at r = 0.68; the -1 point from FED 1. In hindsight, the stoichiometry should have been investigated to a lower ratio to ensure optimisation of the resin formulation. Whilst this was not done for FED 2, further research into the effects of a lower stoichiometry in an epoxy-DDS system was subsequently investigated through FED analysis using a

TGPAP/DGEBF system, studied by two first year PhD under my supervision. The results of which will be integrated throughout section 5.3.

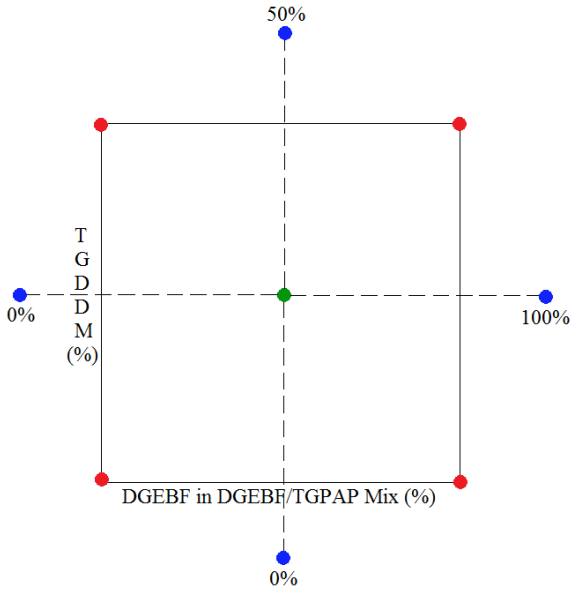

Figure 5.16 A schematic diagram of an FED studying the effect of DGEBF in a DGEBF/TGPAP mix against TGDDM level.

5.3.1. Rheology

5.3.1.1. Room Temperature Viscosity

The room temperature viscosity was measured for FED 2 and the respective contour plot can be seen in Figure 5.17. As was reported in FED 1 the TGDDM content had the largest effect on room temperature viscosity, although in FED 1 TGDDM was studied as a dependant variable and as such quantifying its true effects on viscosity could not be shown. Figure 5.17 displays the effects of TGDDM as an independent variable and it can be seen that it has a significant effect on the viscosity, with its inclusion from 0-50% increasing the viscosity from <20 Pa s to >240 Pa s at high DGEBF levels.

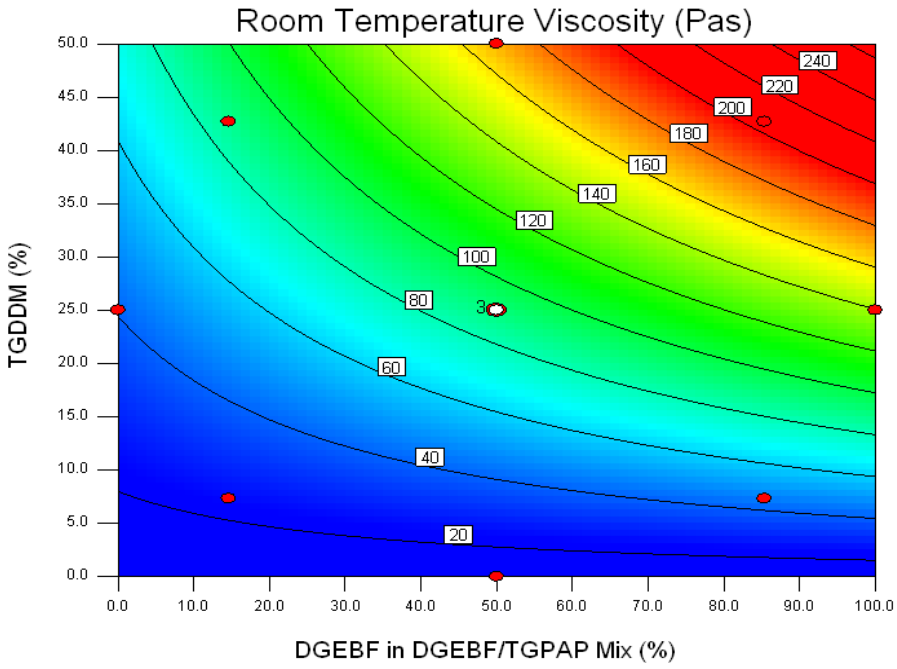

Figure 5.17 Contour plot for the change in room temperature viscosity across an FED examining the influence of DGEBF from 0-100%. The red nodes represent real data points.

Conclusions drawn from the results in Figure 5.17 are similar to those from FED 1, whereby the addition of TGDDM should be minimised for composite manufacturing in order to maximise resin flow. At low TGDDM levels, the variation in viscosity between DGEBF and TGPAP is minimal and as such varying the quantity of either will have minimal effect on the processing viscosity.

5.3.1.2. Processing Window

Figure 5.18 shows a contour plot of the processing window for FED 2. The most apparent trend from the plot is that increasing the DGEBF content increases the PW, as was found in FED 1. At 0% TGDDM, the PW increases by ~115 minutes from 0-100% DGEBF, whereas at 50% TGDDM it increases by ~50 minutes. The increase in PW with DGEBF content is a result of a reduction in the average epoxy functionality of the multi-component resin system. TGDDM and TGPAP have functionalities of 4 and 3 respectively, thus each monomer has a greater contribution to the network formation, whereas DGEBF has a functionality of 2 and is therefore reliant on the DDS (functionality of 4) to develop a three dimensional polymer

network. Owing to which, DGEBF monomers are more likely to form polymer chains that do not contribute to the molecule of infinite molecular mass required for gelation.

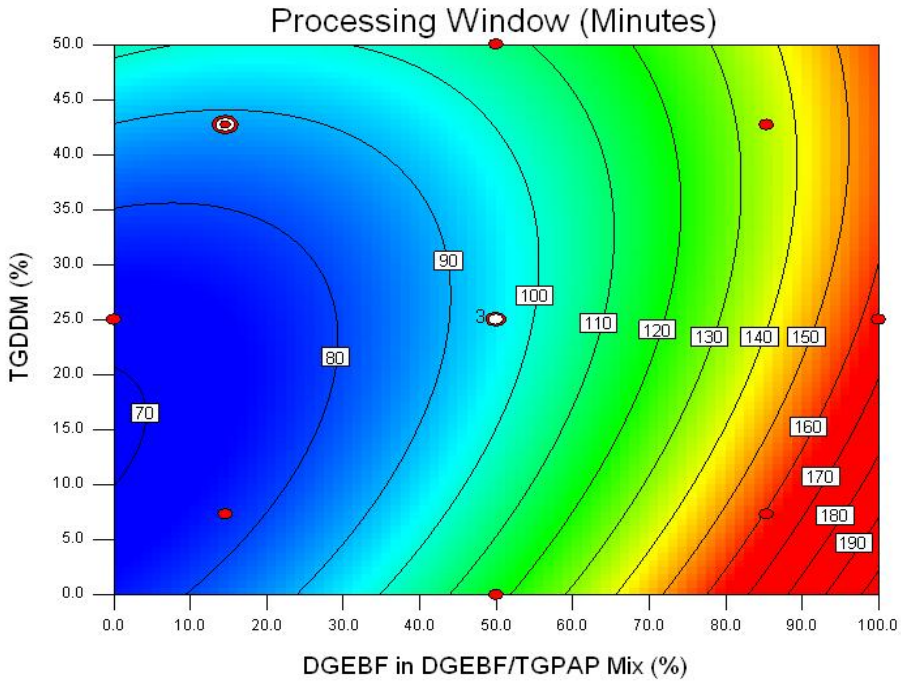

Figure 5.18 Contour plot for the change in processing window across an FED examining the influence of DGEBF from 0-100%.

In FED 1 (p 146) it was reported that the addition of DGEBF to formulations containing high levels of TGDDM had little to no effect on the PW. This was attributed to equilibrium between the polymerisation of DGEBF, which increases the PW, and the lower activation energy of the epoxy-amine reactions in DGEBF that reduce the PW. Further evidence supporting this theory is provided in the PW contour plot of FED 2 (Figure 5.18). At 50% TGDDM an increase in DGEBF content of up to ~50% shows little change in the PW, with values ranging from ~100-105 minutes. Once the DGEBF content exceeds 50% the PW increases at a much faster rate, suggesting that the equilibrium between the polymerisation mechanisms and activation energies no longer exists. With this in mind, the inclusion of DGEBF in to a formulation containing 50% TGDDM must be higher than 50% for any noteworthy processing benefits, as the sole advantage of incorporating DGEBF instead of TGPAP is to increase the PW.

5.3.2. Glass Transition Temperature

The contour plot in Figure 5.19 shows T_g^∞ for FED 2, with values ranging from 270°C to 190°C across the contour plot. The lower T_gs resulting from the increase in the DGEBF content are due to a reduction in the crosslink density, similarly found in FED 1. Comparison between the T_g values reported in Figure 5.19 and those from FED 1 at the same stoichiometry (r = 0.68) (Figure 5.4c, p 152) show a maximum T_g of 270°C in both plots. That said, the results from the two FED's contrast as to the optimum formulation for maximising the T_g. FED 1 suggests higher TGDDM levels result in the optimum T_g whereas FED 2 suggests increasing TGPAP is beneficial, albeit the variation in T_g^∞ between the two resins at r = 0.68 is ± 5°C.

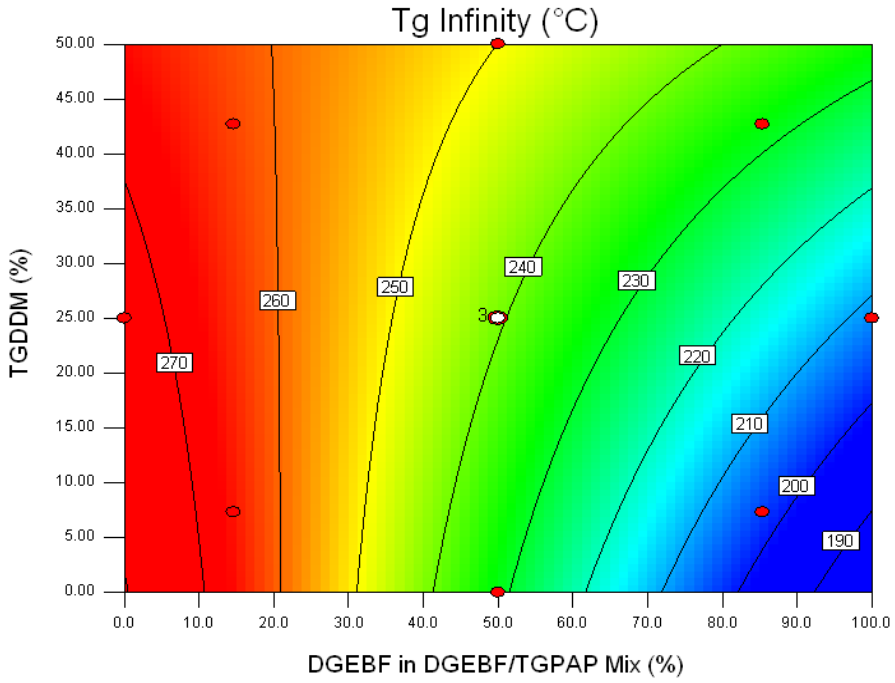

Figure 5.19 Contour plot for the change in T_g^∞ (from DMTA tan δ peaks) across an FED examining the influence of DGEBF from 0-100%.

At 100% DGEBF and without the addition of TGDDM, T_g^∞ is predicted to be ~185°C. T_g^∞ of DGEBF at r = 1.0 was found to be 193°C. The similarity between the predicted T_g^∞ of 100% DGEBF at r = 0.68 and that found at r = 1.0 is surprising considering results from the literature which suggest that for bi-functional resins cured with a multi-functional amine hardener the optimum stoichiometry is r = 1.0 [69], [192], [221]. This is due to the linearity of bi-functional epoxy resins, which restrict their

crosslinking potential. The fact that at a reduced stoichiometry DGEBF still generates a high T_g suggests crosslinking occurs by etherification; a reaction which has been reported to be less prevalent in bi-functional epoxies owing to the lack of epoxy groups in close proximity as found in DGA-derived epoxy resins such as TGPAP and TGDDM [40]. It can therefore be concluded that the T_g^∞ of any resin within the range studied at r = 0.68 is similar to if not higher than that of the same resin cured at r = 1.0.

As mentioned at the beginning of this section, a further FED was constructed to examine the effects of stoichiometric ratio beyond that which was used in this research. The FED examined stoichiometry from r = 1.0 to r = 0.42 across a DGEBF/TGPAP mix from 0-100%. Figure 5.20 shows the resultant contour plot for T_g^∞. The maximum-recorded T_g^∞ from the FED was 256°C, some 12°C lower than the highest T_g^∞ recorded for FED 2. This was due to different TGPAP and DGEBF resins used for this FED, which owing to the lower T_gs presented, suggests a lower crosslink density; most likely due to a higher concentrations of high molecular weight impurities. Despite the difference in magnitude, the T_gs follow the same pattern as those from FED 2.

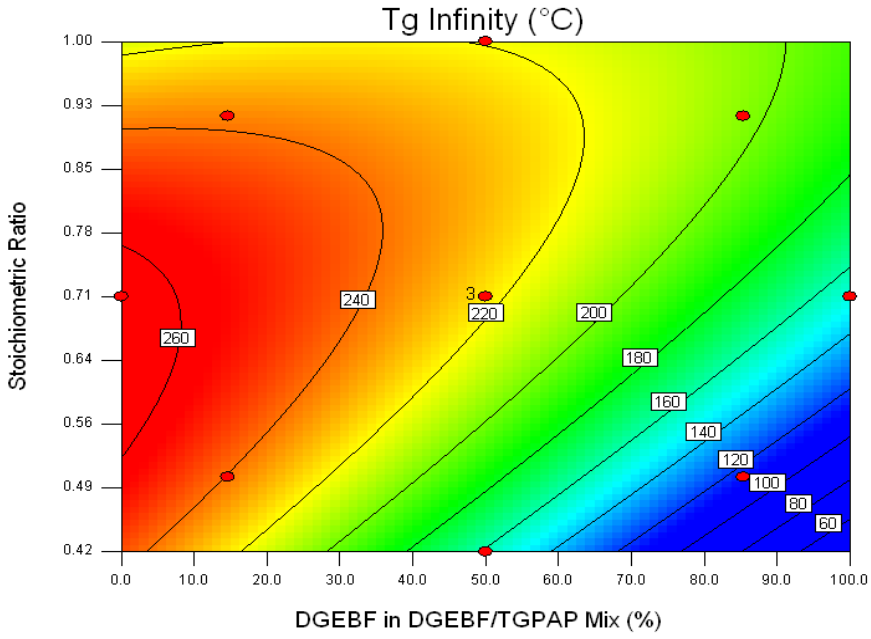

Figure 5.20 A contour plot for T_g infinity from an FED studying the effects of stoichiometric ratio across a DGEBF/TGPAP mix.

At high TGPAP contents the FED predicts that a stoichiometry between r = 0.77 and r = 0.53 results in the optimum T_g^{∞}. Whilst the stoichiometry used in this section of the thesis (r = 0.68) falls within this range, the region of the contour plot falls outside the +1 and -1 values of the FED and are extrapolations from the FED model. Further work is required studying the effects of stoichiometry on TGPAP, with specific focus directing towards variations in T_g with a reduction in stoichiometry below r = 0.77.

5.3.3. Conclusions

The addition of DGEBF from 0-100% increases the PW by over 300% in a system devoid of TGDDM. The same trend exists at high TGDDM levels albeit over a smaller range. Thus, purely from a processing standpoint, maximising the amount of DGEBF in a resin system is desirable. However, the addition of any amount of DGEBF comes at a price; namely a reduction in the T_g of the polymer and therefore a reduction in its maximum operating temperature. With this in mind, determining the maximum operating temperature required for a resin is the primary consideration needed in setting the maximum allowable DGEBF content in a resin system.

Based on the work in this study the inclusion of TGDDM in a multi-component resin system should be minimised. For systems that require a high T_g TGPAP should be used owing to its much lower viscosity and similar T_g. Whilst the inclusion of TGDDM in a TGPAP system increases the PW, the range over which it does so is minimal compared to the effects of adding DGEBF to a TGPAP system.

From these conclusions, four resin systems were carried forward for further work with the majority of focus directed towards two of these systems. The four resin systems are shown by the yellow points in Figure 5.21. The figure also depicts a restriction to the possible resin formulations used in further study. It was arbitrarily decided that a T_g of 220°C was a minimum requirement for a 'high operating temperature resin system', as this equates to a maximum operating temperature in excess of 200°C (as set by the onset in drop of the storage modulus). Based on these criteria, the two main resin systems taken for further study include 100% TGPAP and a binary mixture containing 60% DGEBF and 40% TGPAP; shown in Figure 5.21 by the yellow points along the bottom of the contour plot. The addition of a thermoplastic toughener is

certain to increase the viscosity of the resins [93] and therefore hinder resin flow. As such, the inclusion of DGEBF is studied owing to the additional resin flow time it provides.

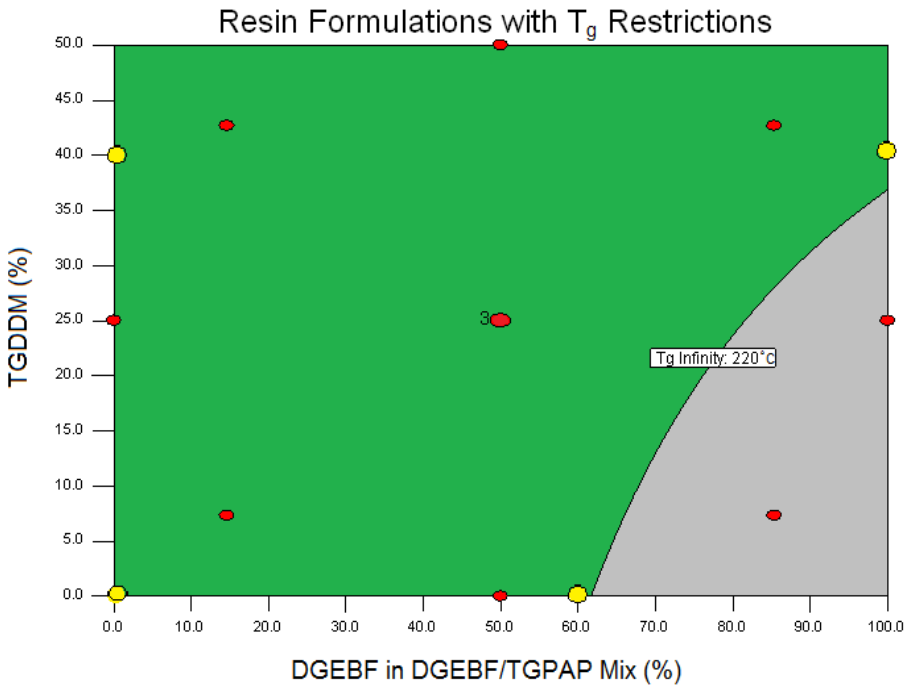

Figure 5.21 A plot of the resin systems taken forward for further study and the imposed glass transition temperature restriction. The yellow nodes are the formulations used in further study. The grey region shows the region of the plot with a T_g < 220°C.

The two other systems taken forward are multi-component resin systems containing 40% TGDDM and 100% TGPAP, and 40% TGDDM and 100% DGEBF in the DGEBF/TGPAP mix. The systems were chosen for the sole purpose of studying the resin fracture toughness with the addition of TGDDM. Based on the information available thus far, the inclusion of TGDDM provides no noteworthy benefits in comparison to TGPAP; however, it may be that its inclusion has a significant positive effect on toughening. The addition of 40% was selected owing to the self-imposed minimum T_g restrictions (see Figure 5.21). At 100% DGEBF in the DGEBF/TGPAP mix, the addition of 40% TGDDM results in a T_g^{∞} in excess of 220°C. The same quantity of TGDDM was incorporated into a TGPAP resin system to allow for direct comparison of fracture toughness results between TGDDM in DGEBF and TGPAP systems.

6. Addition of a Thermoplastic Toughener

The resin systems used in this section are shown in Table 6.1. The abbreviated form of each system refers to the quantity and starting letter of the major resin component. Formulations involving TGDDM use the abbreviation, t. Any subsequent addition to this letter refers to the weight-quantity of DGEBF or TGPAP in the DGEBF/TGPAP mix or weight percent of PES added

Table 6.1 Resin formulations and their abbreviations used in Chapter 6.

Resin System	Abbreviation
100 wt% TGPAP	100T
60 wt% DGEBF, 40 wt% TGPAP	60D
40 wt% TGDDM, 100 wt% TGPAP	40t-100T
40 wt% TGDDM, 100 wt% DGEBF	40t-100D
wt% PES	P
(for example) 100 wt% TGPAP with 10-50 wt% PES	100T-10-50P

One of the most suitable thermoplastics for improving fracture toughness of an epoxy resin is polyethersulphone (PES). This is primarily due to its high thermal stability and easy processability in melt or in solution [122]. PES is commercially available at different molecular weights and with different functional end groups. Functional end groups are often added to PES to aid its dissolution in thermosets. The PES used in this study was VW-10200RP supplied by Solvay Advanced Polymers. It is a high number average molecular weight PES (46500 g mol^{-1}), functionalised with hydroxyl groups. This PES was used owing to the fracture toughness results found within our research group. Stein [222] investigated various molecular weights and functionalities

of PES within a TGPAP/TGDDM-DDS resin system and found the greatest improvement in fracture toughness were achieved when the resin incorporated the high molecular weight OH functionalised PES.

The quantity of PES added to each resin system varied and was dependent on the maximum wt% of PES it was possible to dissolve in each resin system. TGDDM based systems (40t-100T and 40t-100D) included 40% PES. Owing to the results of previous sections the use of TGDDM seems undesirable, however to determine whether it has any fracture toughness benefits the results from these two systems will be compared to those of the 100T and 60D systems. The two main resin systems, 100T and 60D, had 0%, 10%, 30% and 50% PES added in order to study the effects of varying the PES inclusion on the morphology, T_g, processability and fracture toughness.

Existing studies have investigated the effects of adding PES over a wide range, with some focusing on the addition of 10% [223] or 20% [110], [224]; whilst others have added as much as 40% [112], [124] or 50% [113]. What appears to be unique to this study is the use of melt mixing to dissolve the PES in the epoxy resin. The aforementioned papers all used solvent mixing because of the high viscosity generated when dissolving PES in epoxy resin. Solvent mixing was avoided in this work owing to the detrimental effects residual solvent has on the mechanical properties of the cured polymer. Furthermore its use results in additional processing time taken for solvent to evaporate from the liquid resin prior to curing and environmental concerns which make it commercially unfavourable [184].

Prior to curing, samples were degassed in a vacuum oven at 130°C for 30 minutes. This temperature was required owing to the high viscosity of resin systems containing 30-50% PES. All resins were cured following the cycle developed within our group, which involved a final dwell at 200°C for 2 hours.

6.1. Rheology

The viscosity profiles at 130°C for the 100T and 60D systems with PES addition are shown in Figure 6.1 and Figure 6.2 respectively. The gel times and minimum viscosities for all systems are summarised in Table 6.2. It has been widely reported that the addition of PES to epoxy resins leads to a significant increase in the viscosity [9], [28], [49], [100], [225]. In this work, the effects of PES on viscosity agree with those reported in literature. Owing to the similarity between the viscosities of the untoughened 100T and 60D resins, the inclusion of PES has similar effects on both systems, whereby the addition of 10% leads to an initial increase in viscosity by an order of magnitude and subsequent additions of 20% led to a further increase in viscosity, by approximately an order of magnitude. There are small differences at each PES loading level between the viscosities of the 100T and 60D systems, with the 60D resins having a lower viscosity. This is due to the different weight percent of DDS added to maintain the same stoichiometry.

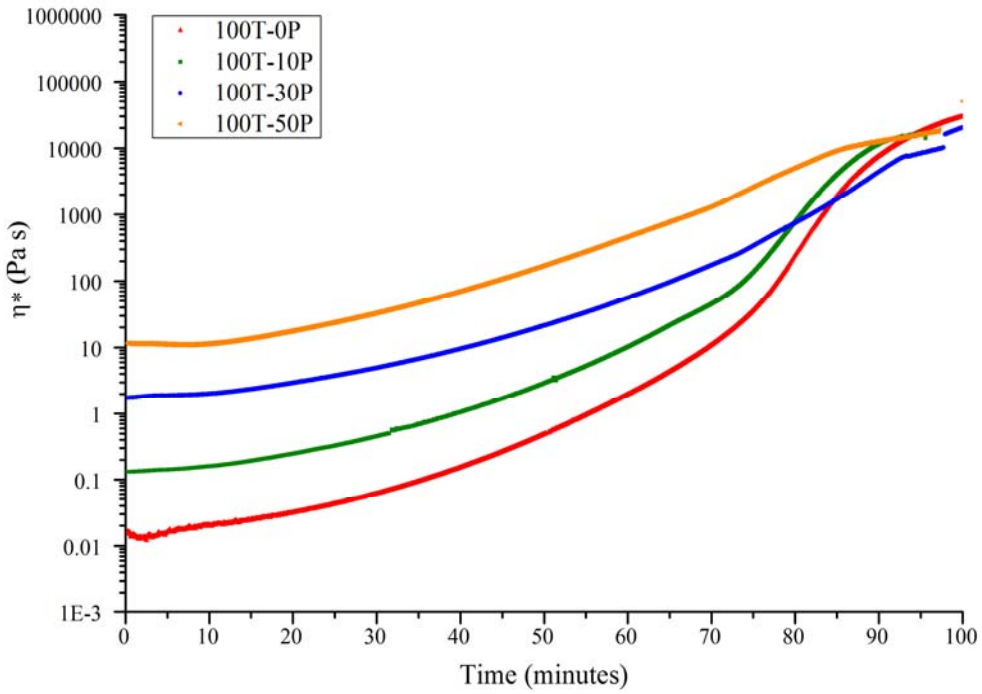

Figure 6.1 Viscosity profiles at 130°C for the 100T system with increasing levels of PES.

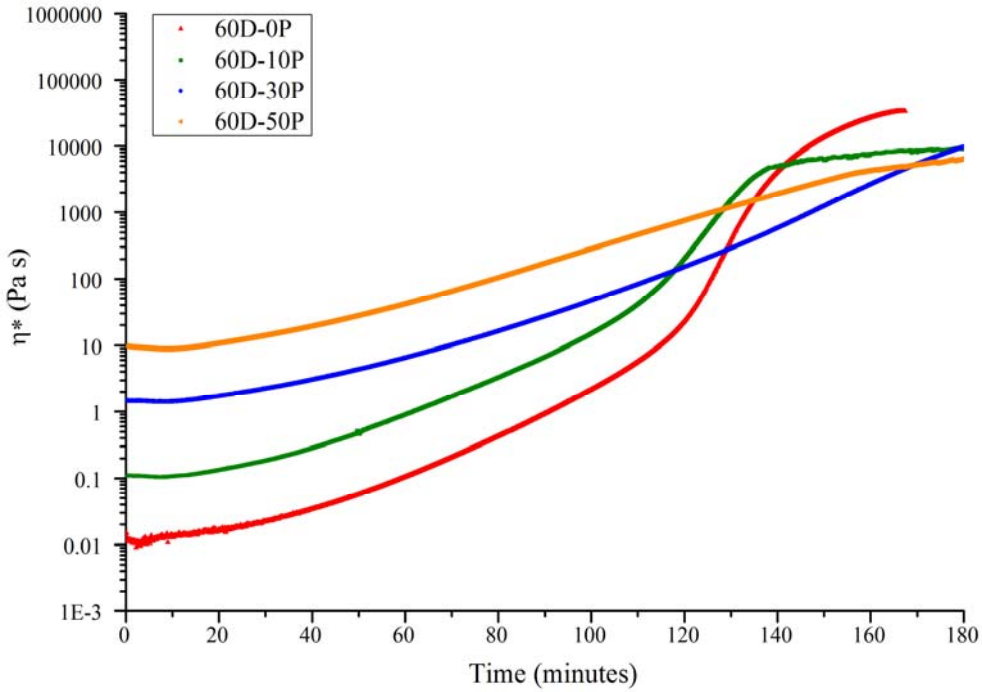

Figure 6.2 Viscosity profiles at 130°C for the 60D system with increasing levels of PES.

The addition of PES to both systems reduced the processing window (PW); with 50% PES reducing the PW of the 100T and 60D systems by 43% and 37% over the untoughened resins, respectively. However, the PW is only an indication of the time in which the resin will flow. For untoughened systems the PW and the G'/G'' crossover are relatively close together. Table 6.2 shows the proportion of the pre-gel time in between 100 Pa s and the G'/G'' crossover for each system. In the untoughened systems this time is 5% and 2% of the total pre-gel time for 100T-0P and 60D-0P, signifying that once the viscosity reaches 100 Pa s the polymer is approaching gelation. However, this time increases with the addition of PES. The proportion of the pre-gel time above 100 Pa s is 43% and 50% for the 100T-50P and 60D-50P systems respectively. Therefore whilst the inclusion of PES reduces the time the resin viscosity is below the 100 Pa s PW, it does not necessarily reduce the time for the G'/G'' crossover.

Table 6.2 Minimum viscosities and gel times for the 100T and 60D systems with increasing levels of PES.

Resin	PES (%)	Minimum Viscosity (Pa s)	Apparent Gel Time (minutes)		Fraction of Pre-gel Time Above 100 Pa s
			Processing Window (100 Pa s)	G'/G" Crossover	
100T	0	0.01	78 ± 2	82 ± 2	5%
	10	0.15	74 ± 2	80 ± 1	8%
	30	1.70	65 ± 3	85 ± 2	24%
	50	11.00	44 ± 2	77 ± 2	43%
60D	0	0.01	126 ± 2	129 ± 2	2%
	10	0.10	116 ± 2	127 ± 2	9%
	30	1.45	113 ± 3	157 ± 3	28%
	50	8.80	79 ± 3	159 ± 3	50%

Comparison between the two 10 wt% toughened resins and the untoughened resins best highlight this effect. The addition of 10 wt% PES reduces the 100 Pa s PW however it has no significant effect on the G'/G'' crossover. Fernandez et al. [226] added 10 wt% PES to a TGDDM-DDM system and found little change in gel time at various temperatures, in agreement with the results for the addition of 10 wt% PES in both the 100T and 60D systems. These results suggest that the inclusion of 10 wt% PES had little effect on the rate of reaction. However, Man et al. [78] studied the inclusion of up to 20 wt% PES addition to a TGPAP-DDS system, concluding that any PES loading reduced the rate of reaction. Whilst the results for 10 wt% PES loading in this study suggest no effect on the rate of reaction, the addition of 30% and 50% show different results. The addition of 50% PES to the 60D system increases the G'/G'' crossover time by ~30 minutes compared to the untoughened system, indicative that the incorporation of PES slows the rate of reaction. Chen et al. [224] examined the kinetic effects of incorporating hydroxyl-terminated PES into a DGEBA-DDS formulation. They suggested the increase in viscosity due to PES addition may decrease the curing rate, however owing to the functionality of PES, they proposed it may increase the rate of reaction through etherification with epoxy groups. They went on to conclude that higher molecular weight PES decreased the rate of reaction and

that the rate continued to decrease as the PES quantity increased. Owing to a similar high molecular weight PES used in this thesis, it is not surprising that the gel time increased in 60D systems with increasing levels of PES.

This behaviour is not seen in the 100T systems, where the addition of PES shows no apparent trend; with the incorporation of 30% PES increasing the crossover time by 3 minutes and 50% PES reducing the crossover time by 5 minutes compared to the untoughened resin. The lack of any great variation in gel time with PES addition suggests that its inclusion in the 100T system has little effect on the rate of reaction, unlike the 60D systems, and that any variation in gel time may be due to experimental error. This difference between the 60D and 100T systems may be due to the effects of phase separation. It was found (and reported in section 6.2, p 190) that all toughened 100T systems phase separated whereas the 60D systems did not. Phase separation leads to an epoxy rich phase and PES rich phase. The formation of an epoxy rich phase potentially increases the rate of reaction on two counts:

1. The removal of the high molecular weight PES from the epoxy rich phase (and similarly removal of epoxy from the PES rich phase) reduces the molecular distance between reactive groups of the epoxy resin and amine hardener, therefore increasing the likelihood of epoxy-amine interactions thus promoting reaction.
2. The formation of two chemical distinct phases results in two distinct viscosities, the thermoplastic phase of a high viscosity and the epoxy phase with a variable viscosity dependent on degree of conversion. Assuming that phase separation initiates at an early stage of conversion, the viscosity of the epoxy rich phase will reduce as phase separation proceeds resulting in an increased likelihood of epoxy-amine interactions and therefore increased rate of reaction.

6.2. Variations in Glass Transition Temperature and Morphology with PES Content

6.2.1. 100% TGPAP with PES

DSC analysis of the untoughened resin and the 50% PES-containing resin revealed that neither of the systems were fully cured (Table 6.3) (see section 3.5.2 for details). As such, specimens of each resin formulation were postcured at 200°C for an additional five hours. DSC confirmed the resins were fully cured as no visible deflection in the baseline could be seen. Comparisons between the cured and postcured resins yield some interesting results and will be discussed in due course.

Table 6.3 Degree of conversion after the cure cycle for 100T-0P and 100T-50P.

Resin Formulation	Degree of Conversion (%)
100T-0P	95 ± 1
100T-50P	95 ± 2

The DMTA results for the 100T systems (Figure 6.3) show two distinct peaks in the tan δ curves for toughened systems; indicative of a phase separated morphology. The untoughened system shows only one peak at 268°C; indicative of a single phase morphology. For all PES-containing systems, the second peak occurs at a similar temperature to that of the single peak in 100T-0P. As such, it is attributed to the T_g of the 'epoxy rich' phase, or alpha phase, $T_{g\alpha}$. The second peak in tan δ occurs at a lower temperature and is in the same temperature region for all toughened systems. The T_g of PES used in this study is 220°C (provided by manufacturers); similar to that of the second tan δ peak. As such this peak is attributed to the T_g of the 'PES rich' phase, or beta phase, $T_{g\beta}$. $T_{g\beta}$ increases in height with an increase in PES content, indicating more PES present in the phase. The $T_{g\beta}$ also shifts to a higher temperature with an increase in PES content, from ~220°C in 100T-10P to ~228°C in 100T-50P. This shift is due to an increase in the volume of epoxy remaining in the PES rich phase. As seen

in Figure 6.3, $T_{g\alpha}$ is at a much higher temperature than $T_{g\beta}$. Thus, incorporation of epoxy within the PES rich phase raises $T_{g\beta}$ towards $T_{g\alpha}$.

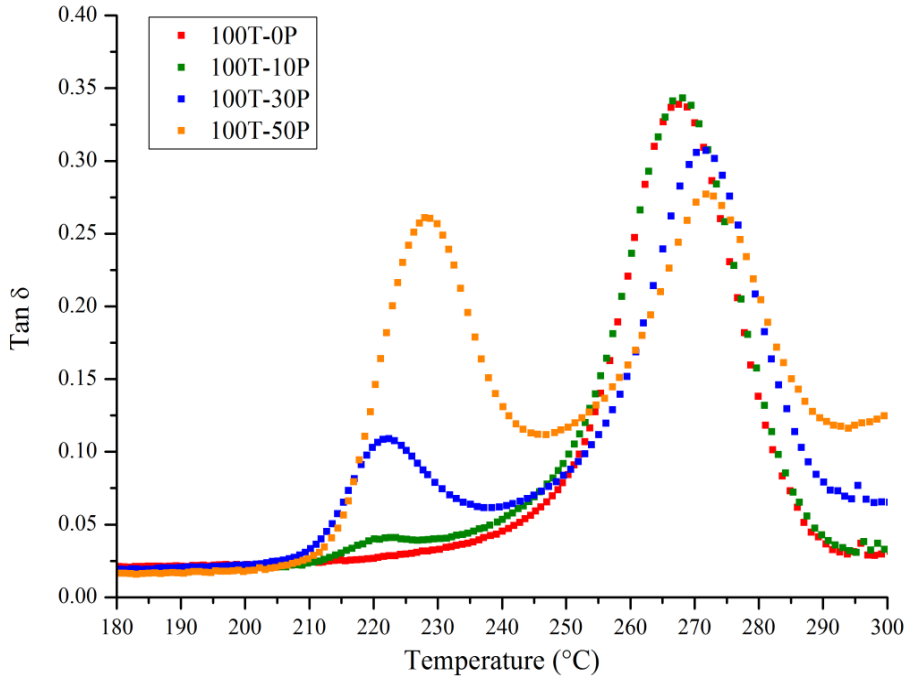

Figure 6.3 Tan δ as a function of temperature for 100T resins loaded at 0%, 10%, 30% and 50% PES following the cure cycle.

$T_{g\alpha}$ of the 100T systems vary according to PES content. An increase in the amount of PES in the system increases $T_{g\alpha}$ (Table 6.4), with the addition of 50% PES increases $T_{g\alpha}$ by nearly 5°C compared to the untoughened resin. Although this is a small increase, it is the opposite of what would be expected. One could assume a higher degree of PES remaining in the epoxy phase would (through a simple rule of mixtures) lead to a lower $T_{g\alpha}$. A possible explanation for this trend relates to the hydroxyl functionality of the PES. Hydroxyl groups can react with epoxy groups via etherification, a reaction known to occur in depleted amine systems and at high temperatures. The incorporation of high PES levels (functionalised with hydroxyl groups) most likely increases the crosslink density through promoting etherification between epoxy groups of the resin and the hydroxyl groups attached to the PES [224].

Table 6.4 The variations in glass transition temperatures with the addition of PES for 100T systems, both cured and postcured.

Resin	PES Content (%)	Cure Cycle		Post Cured	
		$T_{g\beta}$ (°C)	$T_{g\alpha}$ (°C)	$T_{g\beta}$ (°C)	$T_{g\alpha}$ (°C)
100T	0	-	268	-	270
	10	221	268	234	270
	30	222	272	239	273
	50	228	273	239	273

As previously stated, specimens of each resin were postcured for five hours at 200°C to ensure they were fully cured. The resultant tan δ plots can be seen in Figure 6.4 and the corresponding peak temperatures in Table 6.4. There is little difference between $T_{g\alpha}$ of the cured and post cured resins at all PES levels. However, there is a significant difference between the $T_{g\beta}$'s of the cured and postcured systems. Post curing for five hours increases the $T_{g\beta}$ for all compositions. In 100T-10P it rose by ~13°C and in 10T-30P and 100T-50P it rose by ~16°C and ~10°C, respectively. As stated previously the T_g of pure PES is 220°C, therefore if the T_g of the PES rich phase is greater than this it must be assumed that there is a significant amount of epoxy remaining in the PES rich phase. In addition, the large differences between the $T_{g\beta}$ of the cured and postcured systems suggest that the rate of reaction of the epoxy trapped in the PES rich phase is much slower than that of the epoxy in the epoxy rich phase. This is most likely due to the high viscosity of the PES restricting molecular motion of the epoxy resin.

Figure 6.4 and Table 6.4 also show that the $T_{g\beta}$ of 100T-30P and 100T-50P occur at almost identical temperatures, meaning a similar epoxy PES ratio present in the PES rich phase, and therefore a similar degree of phase separation despite 100T-50P having a significantly higher viscosity. Horiuchi [225] suggested that higher loading levels increases the viscosity which in turn hinders phase separation, trapping more PES in the epoxy phase and vice versa. DMTA results of the post cured 100T-30P and 100T-50P would disagree with this statement. However, Horiuchi's statement does

hold for 100T-10P. $T_{g\beta}$ of this system is lower than the systems containing 30% and 50% PES, suggesting the PES phase is purer in 100T-10P.

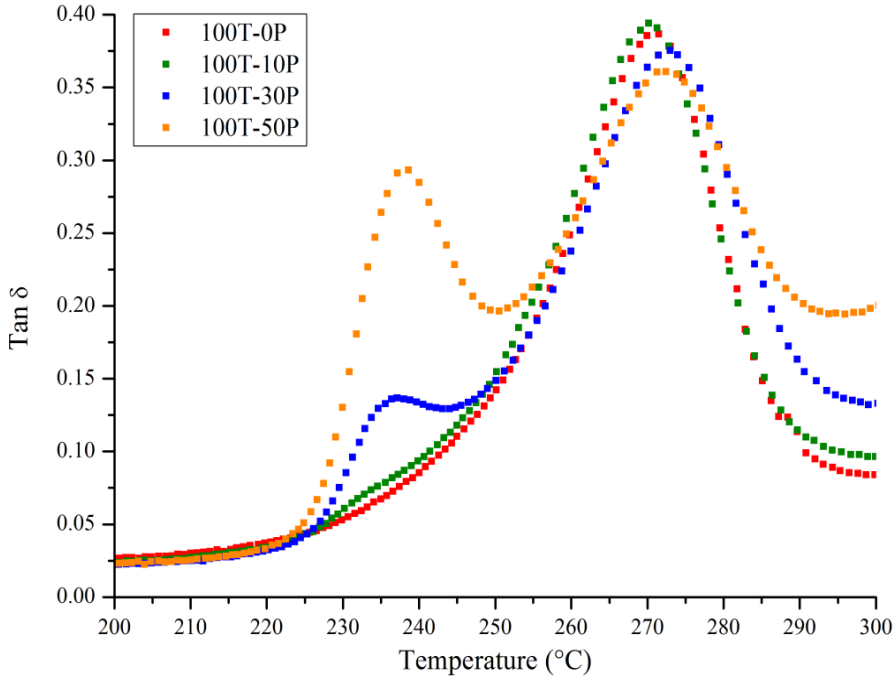

Figure 6.4 Tan δ as a function of temperature for 100T resins loaded at 0%, 10%, 30% and 50% PES after being post cured for five hours at 200°C.

Figure 6.5 shows the scanning electron microscopy (SEM) images of the 100T resin systems. The untoughened 100T system (Figure 6.5a) has no visible morphology; however with the addition of PES two distinct phases can be observed. The surface of the 10% PES-containing system (Figure 6.5b) resembles a pitted texture, akin to a particulate morphology and comparable to results published elsewhere [110].

A particulate morphology is indicative of phase separation through nucleation and growth [227]; a method of phase separation that occurs in the metastable region of the phase diagram (point a in Figure 6.6). It has been reported that the addition of PES quantities below 15% result in this morphology [110] and increasing the amount of PES beyond 15% changes the morphology and the mechanism by which it develops. This is confirmed through the SEM image of 100T-30P, which shows a co-continuous morphology (Figure 6.5c). A co-continuous morphology forms by thrusting the initially stable homogenous mixture into the unstable region of the phase diagram, at which point phase separation occurs through spinodal decomposition.

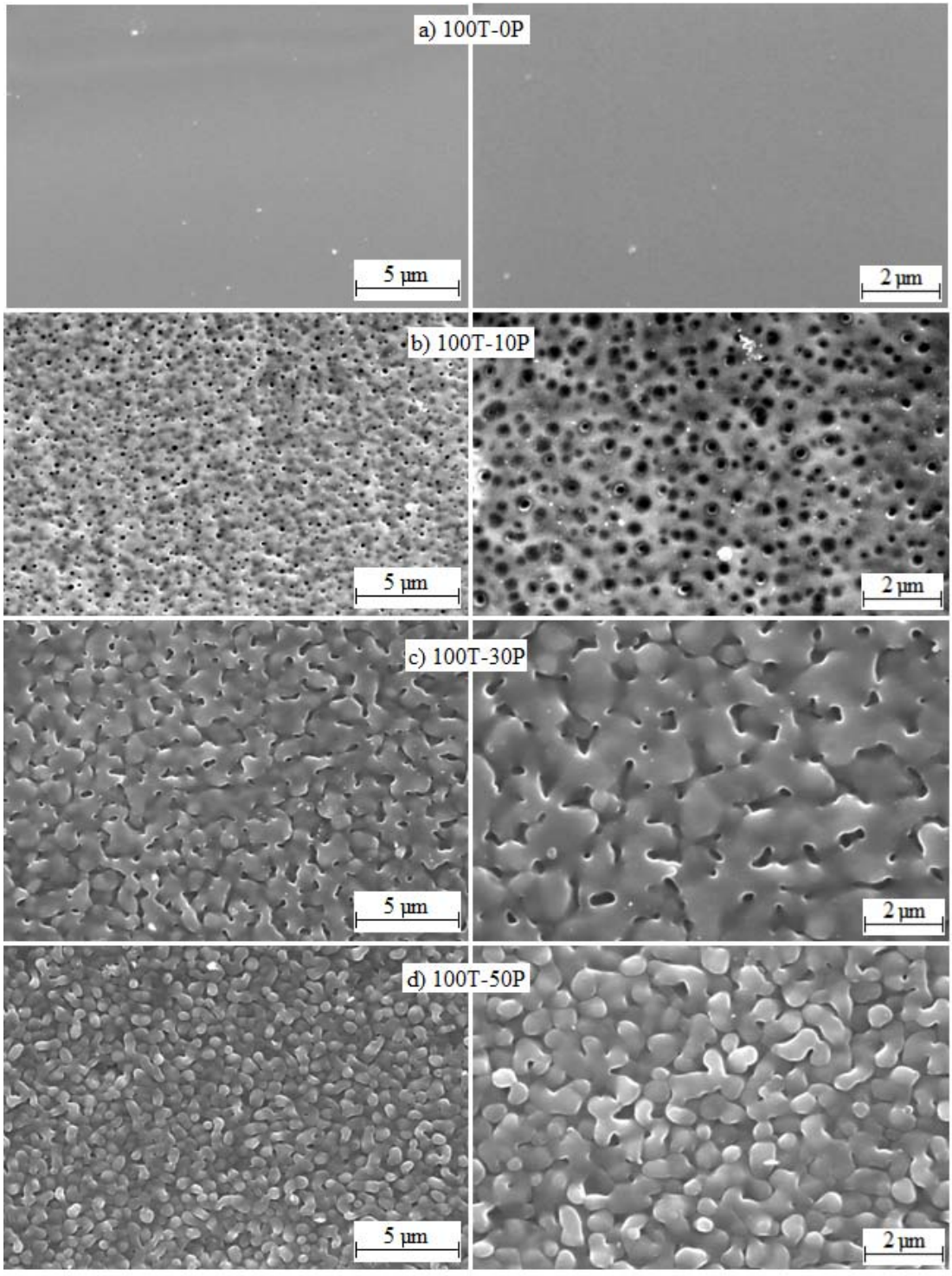

Figure 6.5 SEM images of the acid etched fracture surface of resin systems based on 100T, where (a) = 0% PES, (b) = 10% PES, (c) = 30% PES and (d) = 50% PES.

It is possible that nucleation and growth begins before spinodal decomposition however, as chemical conversion continues the mixture decreases in stability before gelation; resulting in a co-continuous morphology.

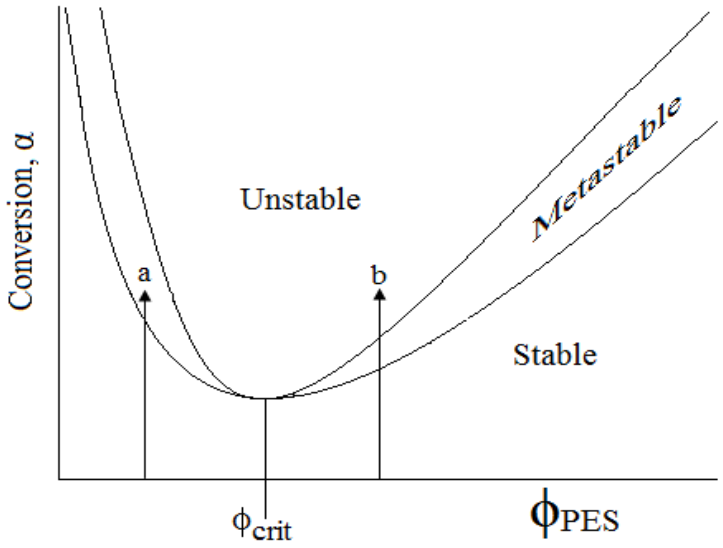

Figure 6.6 A schematic phase diagram, where (a) = metastable region resulting in phase separation through nucleation and growth and (b) = phase separation through spinodal decomposition.

Williams et al. [115] stated the morphological development is dependent on the PES concentration in relation to ϕ_{crit} (Figure 6.6). For concentrations below ϕ_{crit} phase separation will produce a dispersed PES phase or particulate morphology whereas above it phase inversion will take place. Both of these morphologies develop in the metastable region of the phase diagram. Whilst they are the most likely morphological outcome for high and low PES contents they are not guaranteed as the resin may gel in the stable region leading to homogenous morphology or in the unstable region, leading to a co-continuous morphology. In the region close to ϕ_{crit} a co-continuous phase will definitely form. Based on this it can be suggested that 10% PES is below ϕ_{crit} and 30% PES is similar to ϕ_{crit}. 100T-50P also shows a co-continuous morphology although the domain size is much smaller than in 100T-30P. This indicates phase separation was quenched sooner in 100T-50P, most likely due to the higher degree of epoxy conversion required to initiate phase separation. (point b in Figure 6.6). Ireland and Road [113] studied phase separation in a TGPAP-DDS-PES system and saw similar morphologies as those in this work for all levels of PES studied. Furthermore, Mimura

et al. [110] reported a particulate morphology at 10% PES and a co-continuous morphology at 20% PES in agreement with the results in this study.

6.2.2. 60% DGEBF - 40% TGPAP with PES

Once cured, all 60D systems had a T_g of ~205°C; some 15-20°C below the expected T_g^{∞}. As with the 100T systems, DSC results revealed the resins were not fully cured (Table 6.5) and as such specimens of each resin were exposed to five hours post cure at 200°C.

Table 6.5 Degree of conversion for 60D-0P and 60D-50P following the cure cycle.

Resin Formulation	Conversion (%)
60D-0P	96 ± 1
60D-50P	94 ± 1

The 60D systems showed a significant increase in T_g once post cured with values of ~225°C for all PES levels. Figure 6.7 shows the tan δ curves for the 60D systems (once post cured) with the inclusion of various amounts of PES. Unlike the 100T systems that showed two peaks with the addition of PES, the 60D system shows only one peak for all compositions; indicative of a homogenous morphology. Despite the lack of phase separation, the inclusion of PES does not affect the glass transition temperature; with all four systems having the same T_g ± 1.2°C (Table 6.6). This would suggest a similar degree of crosslinking regardless of PES content. Furthermore, there would be a difference in the peak widths should the crosslink density have been effected by PES addition. Alterations to peak width indicate changes to the network structure [228], [229] such as crosslink density. All four systems have visibly very similar peak widths suggesting the incorporation of PES has no significant effect on network structure.

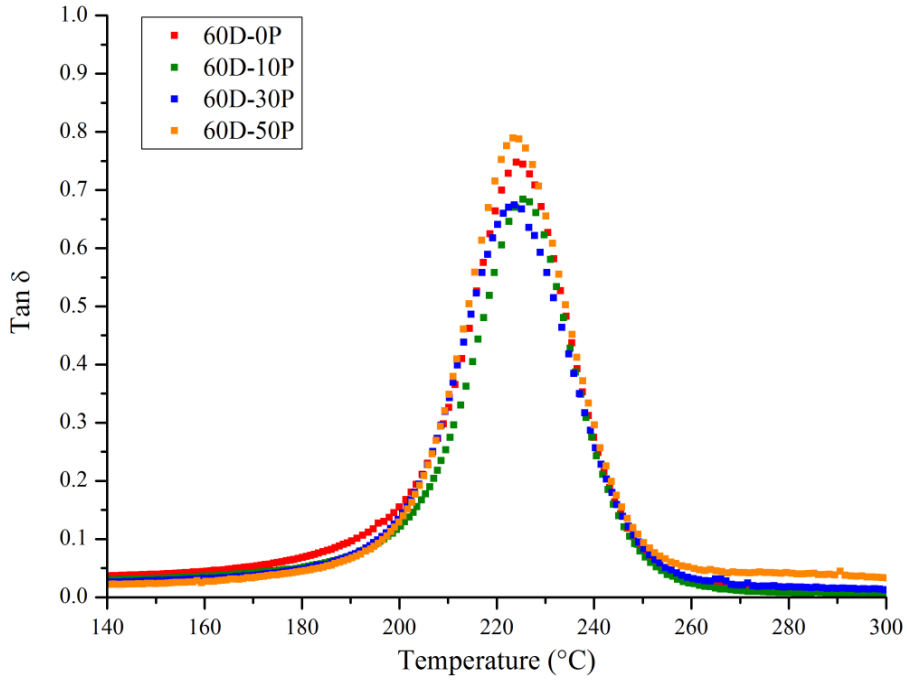

Figure 6.7 Tan δ as a function of temperature for 100T resins loaded at 0%, 10%, 30% and 50% PES after being post cured for five hours at 200°C.

Table 6.6 The variations in glass transition temperatures with the addition of PES for 60D systems.

Resin	PES Content (%)	T_g (°C)
60D	0	225
	10	224
	30	223
	50	223

SEM of the 60D systems (Figure 6.8) revealed no phase separation for all PES contents, as was predicted from the DMTA results. That said the images show an increase in small white spots with an increase in PES content. It is likely the spots are due to the sputter coated carbon; however, it seems somewhat coincidental that the spot density increases with an increase in PES. The white spots could potentially be due to the formation of nanoscale phase separation, although no further investigation was conducted.

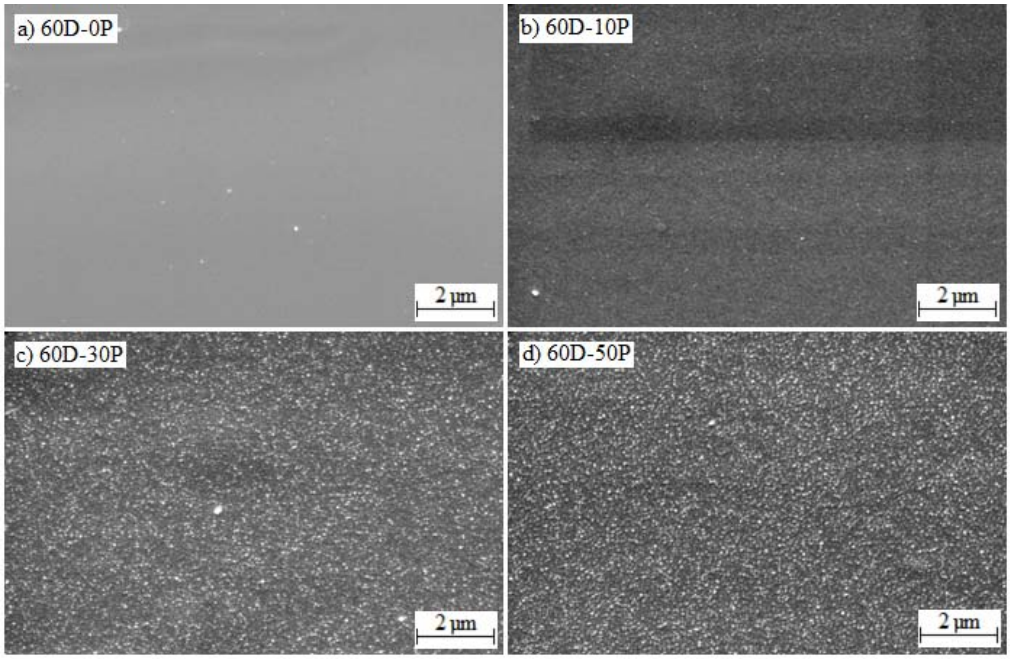

Figure 6.8 SEM images of the acid etched fracture surface of resin systems based on 60D, where (a) = 0% PES, (b) = 10% PES, (c) = 30% PES and (d) = 50% PES.

6.2.3. Effect of DGEBF Level in Development of Two Tan Delta Peaks

Owing to the variation in morphology between the toughened 100T and 60D systems the effects of varying the ratio of TGPAP to DGEBF was studied. An additional three systems were mixed and cured and are known as 80T-20D, 70T-30D and 60T-40D, where T refers to the TGPAP wt% and D to the DGEBF wt%. All were cured with 50% PES. Figure 6.9 shows the DMTA tan δ plots for these systems along with 100T and 60D at 50% PES for comparison. As expected, based on the results from FED 2 there is a linear increase in $T_{g\alpha}$ with increasing TGPAP content. This suggests that despite the addition of PES (and the variations in resultant morphology) the crosslinking of the epoxy phase remains unaffected.

The 80T-20D system clearly shows two distinct peaks. The peak attributed to PES ($T_{g\beta}$) is at a lower temperature and is smaller in height than the PES peak of the 100T-50P system, suggesting a smaller amount of PES has phase separated. This is not surprising considering the higher quantity of DGEBF in the resin that seemingly suppresses phase separation. The fact that $T_{g\beta}$ is at a lower temperature than that of the

100T system could indicate that the phase is richer in PES, especially with the peak height being similar to that of pure PES. However, it is more likely that it has a similar PES purity to the PES phase in 100T and that the reduction in peak temperature is due to the lower T_g of the epoxy contained within the phase.

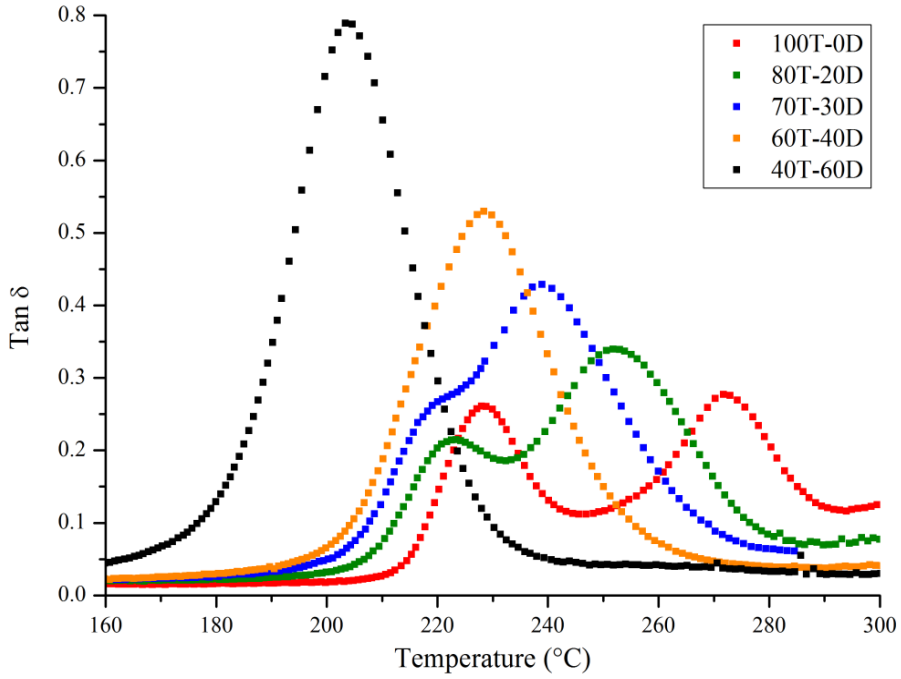

Figure 6.9 Tan δ as a function of temperature for varying DGEBF/TGPAP ratios; all systems including 50% PES.

The 70T-30D system shows a peak at ~240°C with a shoulder on the peak at ~220°C. A shoulder usually indicates a second peak overlapping with the first; however, without a definitive peak it is difficult to predict the extent of phase separation. The 60T-40D system shows a single peak with no shoulder; therefore a blend of DGEBF and TGPAP between 60T-40D and 70T-30D results in equilibrium between the thermodynamic and kinetic factors that respectively drive and suppress phase separation.

The fracture surface of 70T-30D-50P was studied using SEM (Figure 6.10), as this was the highest DGEBF-containing resin to show signs of phase separation. Comparison between the morphologies of 70T-30D-50P and 100T-50P reveals with an increase in DGEBF content a different morphology develops. As previously stated, the morphology of 100T-50P is co-continuous whereas SEM images of 70T-30D-50P

show small spherical domains, ~0.3 μm in diameter, more similar in structure to 100T-10P. The SEM images of 70T-30D-50P indicate the morphology is phase inverted, suggesting that the resin gelled in the metastable region of the phase diagram to the right hand side of $\phi_{crit.}$ The variation in morphology between the two 50% PES-loaded resins suggests a higher degree of phase separation with an increase in TGPAP content, most likely due to the favourable thermodynamic factors driving phase separation.

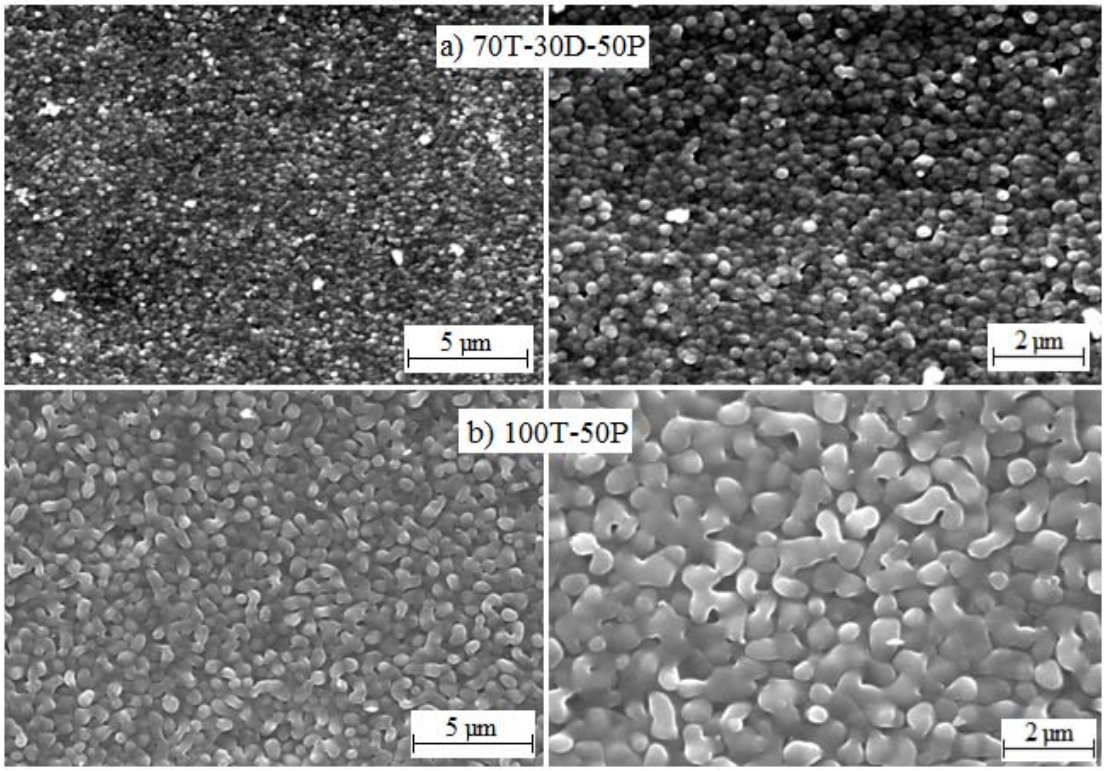

Figure 6.10 SEM images of the acid etched fracture surface of a) 70T-30D-50P and b) 100T-50P.

6.3. Variations in Glass Transition Temperature and Morphology with the Addition of TGDDM

40% TGDDM was added to two resin systems; 100% TGPAP in the TGPAP/DGEBF mix (40t-100T) and 100% DGEBF in the TGPAP/DGEBF mix (40t-100D). Both systems were toughened with 40% PES. The DMTA tan δ plots for each system are shown in Figure 6.11. The 40t-100T-40P system shows two peaks; one at ~270°C and one at ~220°C. The peak at 220°C is the same as that of PES, indicating phase separation. The epoxy peak at 270°C is in the same temperature region as the 100T

systems; which is to be expected based on the results form FED 2. 40t-100D has a single DMTA peak at ~220°C making DMTA redundant in determining the morphology as this epoxy and PES peaks would be overlapping. Figure 6.12b provides SEM evidence of phase separation in 40t-100D.

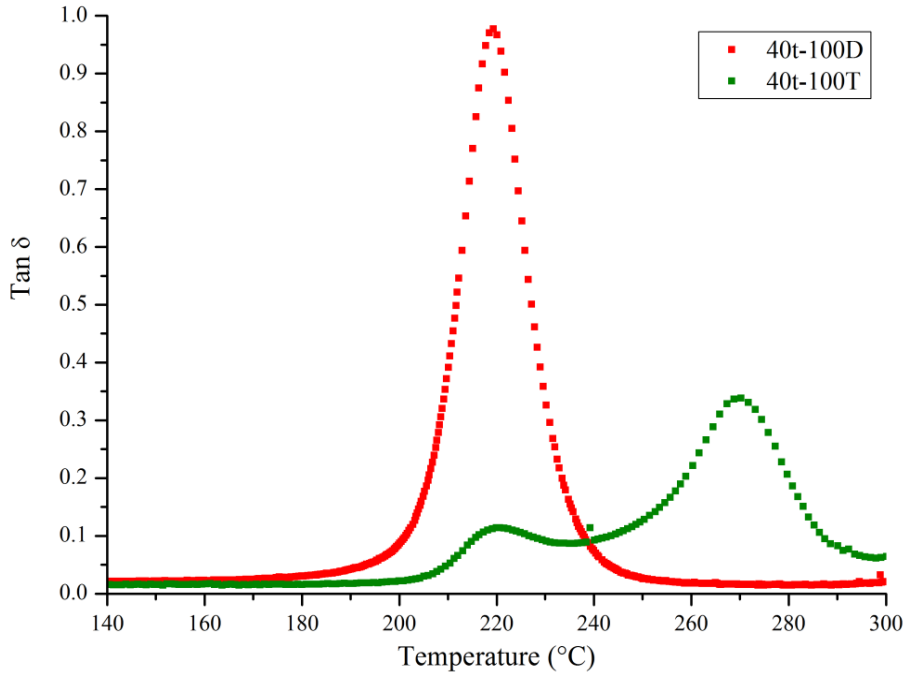

Figure 6.11 Tan δ as a function of temperature for two resin systems containing TGDDM and 40% PES.

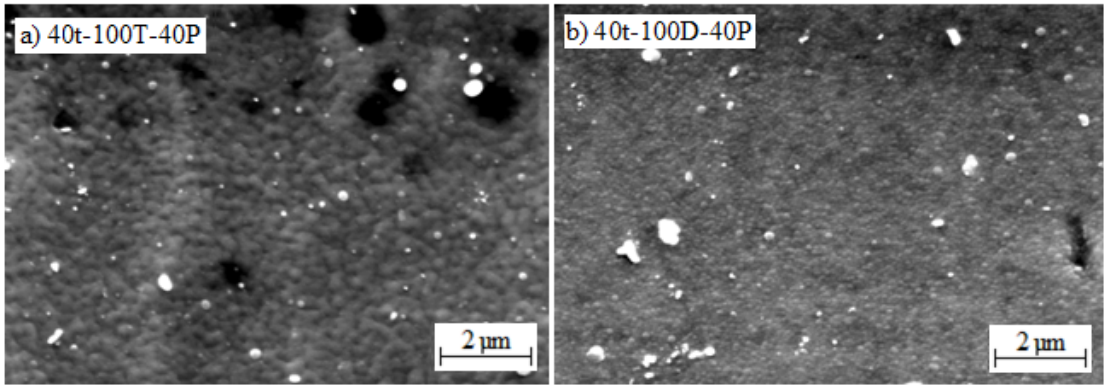

Figure 6.12 SEM images of the acid etched fracture surface of a) 40t-100T-40P and b) 40t-100D-40P.

Unlike the 100T systems or the 30D system, the phase separated PES is on a much smaller scale, with individual domains difficult to distinguish. This is not surprising considering the work of Bucknall and Partridge [230], who reported a co-continuous

morphology when TGPAP was mixed with PES and cured with DDS, and no phase separation when TGDDM and PES were cured with DDS. They went on to support their own work in a further study examining blends of TGPAP and TGDDM and their effect on phase separation with PES [124]. They reported the addition of as little as 20% TGDDM to TGPAP resulted in no visible phase separation either by SEM or DMTA analysis when cured with DDS. Similar to30D-50P, the SEM image of 40t-100T-40P suggests a nanoscale phase separation. However the $T_{g\beta}$ of 40t-100T-40P (seen in Figure 6.11) would suggest a highly 'rich' PES phase as it is has the same T_g as PES, unlike the 100T systems (p 193) which showed $T_{g\beta}$ is somewhat higher than that of pure PES, indicating the presence of a high proportion of epoxy remaining in the PES rich phase.

DMTA results for the 40t-100D-40P system are inconclusive towards phase separation owing to the tan δ peak of the epoxy overlapping with that of the pure PES. However, SEM imaging reveals nanoscale phase separation, as seen in Figure 6.12b.

6.4. An Explanation of Phase Separation

The difference between the morphologies of the two main resin systems can be explained using schematic phase diagrams, as seen in Figure 6.13. The horizontal dotted line signifies the theoretical gel point, beyond which point phase separation ceases. The two curved lines represent the binodal and spinodal curves. Above the binodal curve the system is in a metastable phase, and phase separation may occur through nucleation and growth; however above the spinodal curve the system is unstable and phase separation occurs through spinodal decomposition [115]. As seen from the SEM images of 100T systems (Figure 6.5, p 194) phase separation occurs in all PES-containing systems.

This suggests gelation occurs at a conversion beyond which the system is thrust into the metastable or unstable region of the phase diagram. In other words the cloud-point conversion (the epoxy-conversion point at which phase separation initiates and schematically represented as the binodal curve), is for some levels of PES, lower than the gel point conversion. Furthermore, the SEM images of the 100T-10P system indicate a particulate morphology; suggestive of phase separation induced by

nucleation and growth. This indicates that phase separation occurred in the metastable region of the phase diagram and did not proceed in to the unstable region. Based on this the spinodal curve must cross the gel point conversion line at a PES content greater than 10 wt%. SEM revealed 100T-50P was co-continuous and as such, the system gelled in the unstable region of the phase diagram. Therefore, the PES content required for the unstable region of the phase diagram to be inaccessible to 100T is greater than 50 wt%.

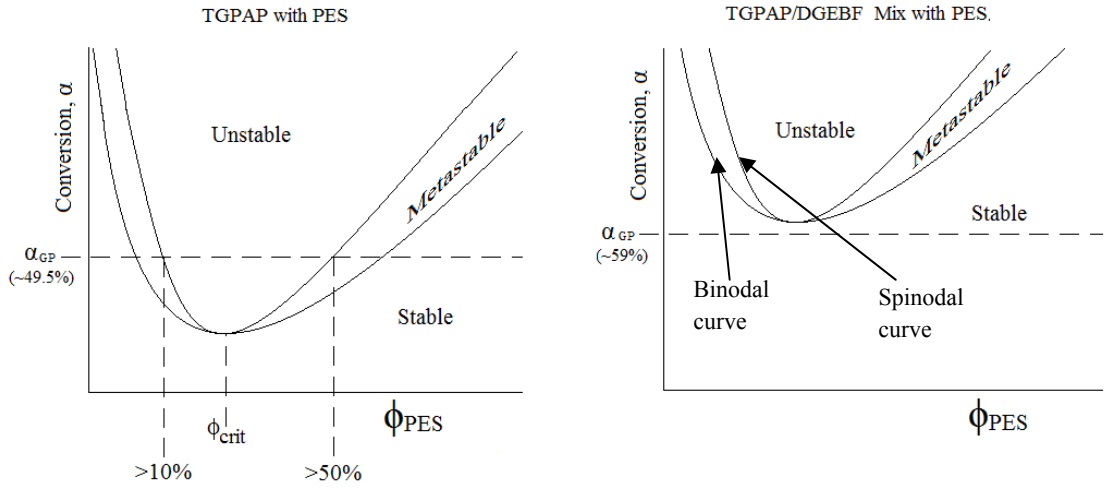

Figure 6.13 Schematic phase diagrams showing the relationship between the gel point conversion (α_{GP}) and binodal and spinodal curves for (a) 100T and (b) 60D with PES.

Despite the seemingly favourable kinetic factors driving phase separation in 60D systems, all PES-containing systems are single phase, indicating that the cloud-point conversion is higher than the gel point conversion, meaning the system gels in the stable region of the phase diagram, thus preventing phase separation. From a kinetic standpoint, the 60D systems are more likely to phase separate than the 100T systems. Table 6.2 (pg 188) showed that the 60D system had a longer processing window than 100T for all compositions, allowing more time during which phase separation can occur. That said the results of this study are not surprising if one consults the literature. Several researchers have reported a homogeneous morphology when DGEBA (chemically similar to DGEBF) is toughened with PES and cured with DDS [49], [225]. Furthermore, research has shown that TGPAP and PES phase separate when cured with DDS [112], [231] complementing the results in this thesis. It must be

remembered however that phase separation is governed by both kinetic and thermodynamic factors [230].

An initial insight in to the thermodynamic differences between the two epoxies begins with the initial miscibility between the epoxy resins and the PES toughener. Miscibility between two materials is dependent on the similarity between their solubility parameters. Materials with similar solubility parameters are more likely to be miscible. Consultation of the literature reveals that PES has a solubility parameter of 23.1 $MPa^{0.5}$ and TGPAP 21.8 $MPa^{0.5}$ [49]. The solubility parameter of DGEBF could not be found in the literature; as such it was calculated using Fedors method [118] and was found to be 23.5 $MPa^{0.5}$. These values would suggest that PES is more miscible with DGEBF compared to TGPAP and could potentially explain why there is no phase separation in the 60D systems. However, Bucknall and Partridge [231] reported the solubility parameter for DGEBA to be 20.5 $MPa^{0.5}$. This lower value suggests DGEBA is less miscible with PES than both DGEBF and TGPAP, and yet the literature reveals that DGEBA-DDS-PES resins show no phase separation [231]. This would suggest that any discrepancies between the miscibility gaps of epoxy resin and PES used in this study are insignificant and that alternative thermodynamic factors are governing the morphological development.

To understand the thermodynamics of phase separation attention is given to the stability of a system, which is governed by the free energy of mixing, ΔG_m, where ΔH_m = enthalpy of mixing, T = temperature and ΔS_m = entropy of mixing.

$$\Delta G_m = \Delta H_m - T\Delta S_m \qquad (2.8)$$

In a miscible system, ΔG_m must be negative. For the epoxy-PES systems studied, we know this to be true as the PES dissolved in the epoxy prepolymer, however with epoxy conversion, the toughened 100T systems became immiscible. This occurs when $\Delta G_m > 0$, thus it is this point that phase separation is possible i.e. the point that $\Delta G_m = 0$ equates to the cloud point conversion (or binodal curve). This change in the free energy is due to change in the entropy of mixing.

The simplest model examining ΔS_m, which introduces the most important element needed for polymer blends, is that developed by Flory [116] and Huggins [117] originally for the treatment of polymer solutions. The entropy of mixing (ΔS_m) associated with mixing n_1 moles of thermoset with n_2 moles of thermoplastic is expressed as:

$$\Delta S_m = -R\left(n_1 \ln \phi_1 + n_2 \ln \phi_2\right) \tag{2.10}$$

Where R = the gas constant, and ϕ_i = the volume fraction of component *i* in the mixture. Since $\phi < 1$, ΔS_m is positive as required. ΔS_m can be better understood through transforming Equation 2.5 to give ΔS_m per volume, V of solution. By calling V_1 and V_2 the molar volumes of thermoset and thermoplastic, and $V = n_1 V_1 + n_2 V_2$, the total volume of the system, the entropy of mixing per unit volume may be written as:

$$\Delta S = \frac{\Delta S_m}{V} = -R\left(\frac{n_1 \ln \phi_1}{V_1} + \frac{\ln \phi_2}{V_2}\right) \tag{2.11}$$

While V_2 (PES) remains constant during the polymerisation of the epoxy, V_1 increases with chemical conversion (p), following a particular law that depends on the functionalities of the reactants. As the molar volume, V_i, is related to molecular weight and density ($V_i = M_i/\rho_i$), then V_1 increases as the reaction proceeds, (the epoxy molecular weight M_1 increases). For this reason, phase separation is the result of a decrease in the entropic contribution to the free energy of mixing during polymerisation. Thus, as the polymer molecular weight increases, the entropic stabilisation of the blend decreases, and phase separation becomes more likely.

In 100T systems, the increase in volume (V_1) with conversion is far greater than in the 60D systems owing to the higher functionality of the epoxy prepolymer. As such, ΔG_m increases at a much faster rate in 100T and becomes positive before gelation resulting in phase separation. However, the degree of phase separation is not solely determined by the epoxy functionality. If it was, TGDDM based resins would show the highest degree of phase separation. Results from this study and those published elsewhere

[231] show that the inclusion of TGDDM suppresses phase separation with PES. A possible explanation for this was given by Bucknall and Partridge [230] who suggested etherification may be occurring between the terminated hydroxyl groups of PES and epoxy groups of TGDDM. This would produce a block copolymer that would increase the solubility and therefore hinder phase separation. However, if this was the case it would be more prevalent in the 100T systems according to the work of Varley et al. [205] who reported etherification was more likely in TGPAP than TGDDM systems.

A more likely explanation for the lack of phase separation in TGDDM-PES systems relates to the gel point conversion. Owing to the higher functionality of the epoxy prepolymer, TGDDM (with DDS at r = 1.0) gels at ~0.33 epoxy conversion whereas TGPAP gels at ~0.41 conversion. Thus, at gelation (the point at which phase separation ceases) the number of reacted epoxy groups is greater in TGPAP and the average molecular mass is greater; which lowers ΔS_m and increases the free energy of mixing, driving phase separation. Therefore the final morphology is the result of the competition between the increase in molecular weight of the epoxy resin leading to phase separation, and the simultaneous crosslinking which suppresses it [28].

6.5. Fracture Toughness

Fracture toughness testing of the cured resins was conducted in accordance with ASTM D 5045-99 [181]. The critical-stress-intensity factor (fracture toughness), K_{1c}, and the critical strain energy release rate at fracture initiation (fracture energy), G_{1c}, were determined. K_{1c} indicates a materials resistance to fracture under plain strain conditions whereas G_{1c} indicates the energy required to fracture. A minimum of five specimens for each material were tested, as consultation of the literature revealed high standard deviations for the test [101], [110], [182].

6.5.1. Fracture Toughness of the 100T and 60D Systems

Theoretically, phase separation leads to an improvement in fracture toughness owing to the prevention of crack tip growth. Upon reaching the phase separated thermoplastic phase, the crack tip branches and continues propagating along a path requiring the

least amount of energy; through the brittle epoxy phase. In a particulate morphology this is possible, however once a co-continuous morphology forms the crack cannot propagate without passing through the PES rich phase. Mimura et al. [110], using optical microscopy, observed increased branching at the crack tip with an increase in PES from 0-20%. The increased branching coincided with a change in morphology, from homogeneous to particulate to co-continuous. This lead to an increase in fracture toughness of 100% compared to the untoughened resin.

Mimura's results differed from those found in this study as shown by the K_{1c} results for the 100T and 60D systems in Figure 6.14. An increase in PES led to an increase in the fracture toughness for both systems, with the fracture toughness of the 60D system increasing linearly from 10% to 50% PES. This is not surprising considering the lack of phase separation, however little difference was found between the fracture toughness of the 100T and 60D resins at each level of PES up to 30% PES inclusion; suggesting that the phase separated morphology found in the 10% and 30% PES-containing 100T systems had little effect on the toughness. Similar results were found by Bucknall and Partridge [124] who examined the toughening and morphological effects of PES in TGPAP and TGDDM; reporting modest improvements in fracture toughness up to 25% PES, irrespective of the morphology. They went on to support their own work [230] showing little difference in K_{1c} values regardless of epoxy formulation and morphology, with values ranging between 0.6 and 0.9 MN $m^{-1.5}$ for all systems up to 40% PES. Yoon [232] also reported similar results to those seen in Figure 6.14, with slight improvements found in fracture toughness for a co-continuous morphology between PES and DGEBA.

The lack of fracture toughness improvement between a homogenous and phase separated morphology up to 30% PES indicates crack propagation through the PES rich phase is just as easy as through the epoxy rich phase, suggesting that the localised concentrations of PES provide no improvement in fracture toughness. However, increasing the PES content to 50% significantly affects the fracture toughness. 100T-50P has superior fracture toughness in comparison to the other resins; with an improvement of 46% compared to 60D-50P and 62% compared to 100T-30P. The critical strain energy release rate, G_{1c}, for the 100T and 60D systems is shown in

Figure 6.15. An increase in PES results in an increase in G_{1c} for both systems. At 0% and 10% PES the G_{1c} values are similar for the two systems.

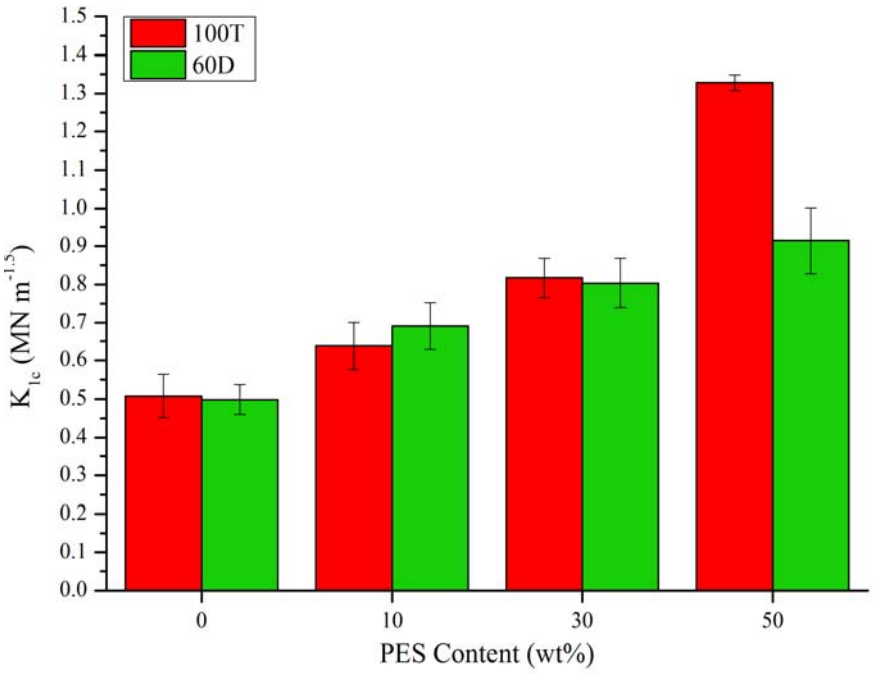

Figure 6.14 The critical stress intensity factor, K_{1c}, of 100T and 60D systems with the addition of PES from 0-50 wt%

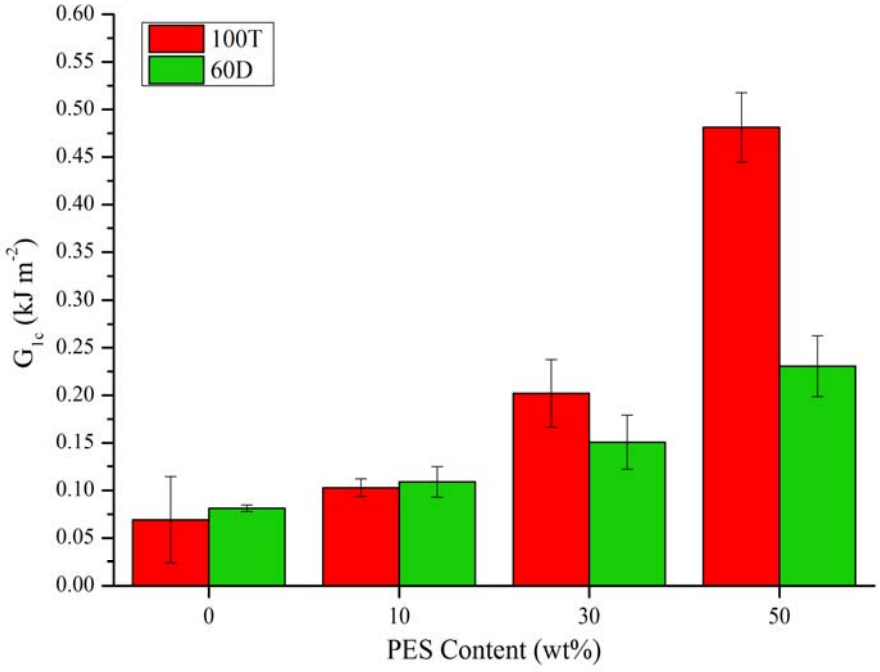

Figure 6.15 The critical strain energy release rate, G_{1c}, of 100T and 60D systems with the addition of PES from 0-50 wt%

At 30% PES there is a small difference whereby 100T-30P (showing phase separation) has a higher average G_{1c} value, although the error bars would suggest this is within experimental error. At 50% PES the same dramatic increase in G_{1c} is observed in the 100T system as was observed for K_{1c}. The energy dissipated during fracture in this system is 685% higher than that of the untoughened resin, 240% higher than the 100T-30P system and 209% higher than the equivalent 60D system that showed no phase separation.

Hourston et al. [68] reported G_{1c} values in the region of 0.3 kJ m^{-2} for untoughened epoxy systems based on a combination of DGEBA, TGPAP and TGDDM. These values increased with the addition of 20% PEI, depending on the resin formulation, to within the range 0.4-1.1 kJ m^{-2}. Their G_{1c} values for untoughened systems are >300% higher than the untoughened systems in this study. Variations between Hourston's results for untoughened resins and those in this study are most likely due to testing conditions. Hourston tested specimens with a notch depth of 2 mm, a span between supports of 50 mm and a crosshead loading speed of 1 mm min^{-1}, whereas in this study a notch depth of between 4.5-5.5 mm was used with a support span of 40 mm and a crosshead loading speed of 10 mm min^{-1}. Similarly high G_{1c} results to those reported by Hourston have been reported by others [28], [114]. The common variable between the studies was a loading speed of 1 mm min-1, suggesting that the fracture toughness is dependent on the rate of deformation. Kanchanomai et al. [233] studied the loading rate on K_{1c} and G_{1c} for a toughened epoxy resin and found K_{1c} reduces from 4 MN $m^{-1.5}$ at 1 mm min^{-1} to 2.5 MN $m^{-1.5}$ at 10 mm min^{-1} and G1c reduced from 4 kJ m^{-2} at 1 mm min^{-1} to 2 kJ m^{-2} at 10 mm min^{-1}.

6.5.2. Fracture Toughness of Alternative Resin Systems

The fracture toughness of the two toughened resin systems based on TGDDM (40t-100T-40P and 40t-100D-40P) and the system containing 30% DGEBF (30D-50P) were measured and compared to the toughness of the two main resin systems. The K_{1c} values for the systems are shown as a line and scatter graph in Figure 6.16. The two line plots are the resin systems already discussed; 100T and 60D with various PES inclusions. The 30D-50P system has a K_{1c} of 1.10 ± 0.05 MN $m^{1.5}$; half way between

the K_{1c} values of the 100T and 60D systems containing the same quantity of PES. It is interesting to compare the K_{1c} values against the respective morphologies as seen using SEM. The significant increase in fracture toughness from 60D to 100T at 50% PES is attributed to the phase separated network in the 100T resin, with domains ranging in size from ~0.5-0.8 μm.

30D-50P was found to have domain sizes of ~0.3 μm; half the size of those in the 100T system. As such, the measured K1c of 30D-50P sits half way between the values measured for the homogenous resin (60D-50P) and 100T-50P, which showed larger domains. These three points aptly highlight the effects of domain size on the fracture toughness. Figure 6.17 shows that G_{1c} significantly increased between the 100T and 60D systems at 50% PES; following the trend of the K_{1c} values.

However, 30D-50P does not follow the same trend, as it required a similar energy to fracture as 60D-50P; suggesting that irrespective of the phase separated morphology seen through SEM, the energy required to fracture is no greater than a homogenous morphology containing the same level of PES. This would point towards the existence of a critical domain size, below which a phase separated morphology provides little to no additional benefit towards G_{1c}.

The two resin systems containing TGDDM show no significant improvement in fracture toughness when compared to the 100T system. K_{1c} values are 0.92 ± 0.06 MN $m^{-1.5}$ for 40t-100T-40P and 0.86 ± 0.07 MN $m^{-1.5}$ for 40t-100D-40P. K_{1c} of 40t-100T-40P is slightly higher than 40t-100D-40P, most likely due to the slightly higher levels of phase separation. Despite the domain sizes of each system being immeasurable through SEM it is clear that the effect of phase separation is more significant in the TGPAP-containing TGDDM system. From Figure 6.16 it can be seen that K_{1c} of the DGEBF-containing TGDDM system is equal to the expected fracture toughness of the 60D system at 40% PES loading, signifying that the nanoscale phase separation observed in this system provides no additional fracture resistance to that of a homogenous morphology.

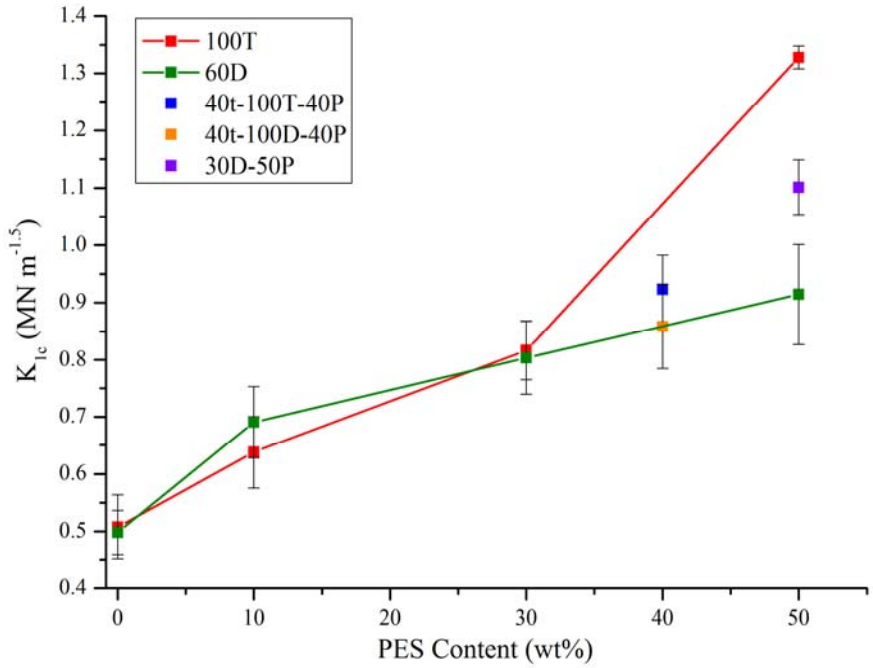

Figure 6.16 The critical stress intensity factor, K_{1c}, of 40t-100T-40P, 40t-100D-40P and 30D-50P systems compared to those of the 100T and 60D systems.

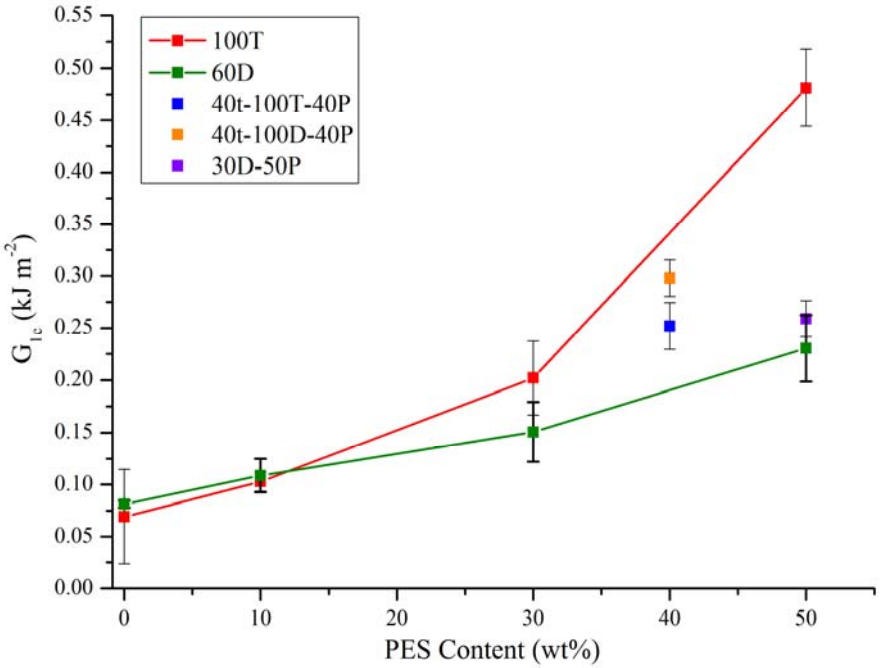

Figure 6.17 **The critical strain energy release rate, G_{1c}, of 40t-100T-40P, 40t-100D-40P and 30D-50P systems compared to those of the 100T and 60D systems.**

The G_{1c} values for the two TGDDM systems also fall within the range of the 100T and 60D systems indicating the inclusion of TGDDM is of no benefit in comparison to a formulation based solely on TGPAP. However, the addition of TGDDM does appear

to be of some benefit in comparison to DGEBF, as both TGDDM-containing resins have a notably higher G_{1c} than G_{1c} for a 60D-40P system. Initial analysis would suggest that the morphological development of the two systems led to this improvement. However, if this were true a similar trend would have been observed for K_{1c}. Furthermore, phase separation was greater in 40t-100T-40P and yet it has a lower G_{1c} than 40t-100D-40P; suggesting the reduced phase separation seen in 40t-100D-40P is somehow beneficial towards improving G_{1c}. A potential reason for this could be the interaction between PES and TGDDM. It is possible etherification bonding has occurred between epoxy groups and the functionalised end groups of PES resulting in the formation of block copolymers. If this increased the energy dissipated during fracture then a homogeneous morphology would result in an improved G_{1c} owing to the increased volume of PES bonded with TGDDM.

This is further supported by comparing the G_{1c} results from both TGDDM systems with that of 30D-50P. Despite the TGDDM systems containing 10% less PES, they have a G_{1c} equal to if not higher than 30D-50P. 30D-50P showed a greater level of phase separation which, when coupled with its higher PES content led to a higher K_{1c}. The fact that the trend is not found in the G_{1c} values suggests there is an interaction between PES and TGDDM resulting in a higher energy required for crack propagation.

Based on the results presented above several conclusions are made regarding the fracture resistance and energy required for fracture:

- Both the K_{1c} and G_{1c} increase upon the addition of PES regardless of the resin used.
- For a phase separated morphology to be of any benefit towards fracture resistance in an epoxy-PES system, a co-continuous morphology is required.
- The extent to which the co-continuity affects K_{1c} is determined by the domain size, which in turn is effected by the PES loading level. Smaller domains occur with high loading levels, resulting in a higher K_{1c}.
- The extent to which phase separation affects G_{1c} is determined by the type of morphology, with a co-continuous morphology having the greatest effect. Phase

inversion has no significant effect on G_{1c} when compared to a single phase polymer.

- The inclusion of TGDDM has no significant advantage in improving K_{1c} over resin formulations based solely on TGPAP.
- The inclusion of TGDDM is beneficial towards improving G_{1c}; however, its effectiveness decreases if the PES phase separates.

6.6. Conclusions

High PES loading levels resulted in a significant increase in viscosity, with 50% PES resulting in a viscosity of ~10 Pa s for both systems at 130°C. The incorporation of PES had little effect on the pre-gel kinetics of 100T with all four formulations gelling in roughly the same time. However, in 60D systems, loading of PES slowed the kinetics with the 30% and 50% PES systems gelling ~30 minutes after the untoughened system. From a composite manufacturing standpoint, the incorporation of such high quantities of PES may result in the inability to generate sufficient flow to produce a high quality laminate. Bin et al. [234] suggested that the ideal viscosity for resin infusion is below 3.0 Pa s and a gel time greater than 60 minutes. When taking in to account the degassing of the resins (30 minutes at 130°C) the gel times for the 100T systems are significantly shorter than 60 minutes, whereas the 60D systems are longer. It is predicted the 60D resins will flow better than the 100T systems for all PES levels, however the 60D-50P may struggle to flow sufficiently owing to its high initial viscosity. This is reported in some detail in Appendix B.

As expected the 60D systems had a lower T_g than the 100T systems, however once post cured the T_g was greater than 220°C; the value arbitrarily selected as the minimum allowable T_g for the resins studied in this thesis. The incorporation of PES had mixed effects on DMTA results, with the toughened 100T systems showing two tan δ peaks, indicative of phase separation, whereas the 60D systems were all homogeneous. Variations in DGEBF/TGPAP composition were studied (loaded at 50% PES) to assess the effects on phase separation. It was found up to 30% DGEBF could be added to TGPAP and still obtain a phase separated morphology. The

inclusion of TGDDM retarded phase separation although it was still visible on a smaller scale than in the 100T systems.

The fracture toughness of the resins increased with PES content although there was no significant difference between the 100T and 60D systems up to 30% PES. Furthermore, the addition of 10% PES showed little improvement in fracture resistance compared to the untoughened resin. Only when 50% PES was incorporated did the fracture toughness of the 100T system vary significantly from the 60D system. The inclusion of TGDDM had no noteworthy benefits on the fracture toughness regardless of the morphology.

7. Conclusions and Further Work

7.1. Conclusions

The main objective of this thesis was to optimise a low viscosity multi-component epoxy resin formulation suitable for use as an aerospace grade composite matrix. The formulation should allow for the addition of high levels of thermoplastic to improve the fracture toughness of the resin whilst also maintaining resin processability.

From the experimental work undertaken the following conclusions are drawn:

- DGEBF is a suitable reactive diluent for high performance epoxy resins. The processing window of DGEBF is significantly longer than TGDDM and TGPAP whilst its viscosity is also lower than TGDDM.
- Reducing the stoichiometric ratio between epoxy and amine groups in a multi-component resin leads to an increase in the glass transition temperature (T_g) and gel time, two desirable properties for composites manufacturing. The optimum stoichiometric ratio is r = 0.68.
- Up to 60 wt% DGEBF can be added to TGPAP at r = 0.68 and maintain a T_g above 220°C whilst increasing the processing window by ~55 minutes.
- Adding high levels of PES significantly increases the viscosity of resin systems. The inclusion of DGEBF in resin formulations reduces phase separation between the epoxy and PES phases. The inclusion of 60 wt% DGEBF leads to no phase separation.
- Phase separation has no effect on the fracture toughness when up to 30 wt% PES is added to a resin system. Only when 50 wt% PES is added does the fracture toughness of a phase separated system significantly increase beyond the single phase system.

- The inclusion of TGDDM prepolymer has no discernible benefits on the gel time, maximum operating temperature or fracture toughness of a multi-component resin formulation.

7.1.1. Two Component Resins

The three prepolymers, TGDDM, TGPAP and DGEBF were mixed with 4,4'-DDS hardener at a stoichiometric ratio of r = 1.0, i.e. equal concentrations of reactive epoxy and amine active hydrogens. Reaction kinetics were determined from isothermal DSC runs by fitting Kamal's autocatalytic model to the rate of reaction curves using non-linear regression analysis (NLR). Activation energies (E_a) were calculated from the k_1 and k_2 values for the three resins and it was found the E_a values for TGDDM were 75 and 73 kJ mol^{-1}, whereas those for TGPAP were 68 and 28 kJ mol^{-1} and for DGEBF they were 59 and 58 kJ mol^{-1}. The E_a values for TGDDM are much higher, in keeping with the slower rate of reaction. E_{a2} for TGPAP was considerably lower than any other measured E_a. There is some published support for this result [40], [203], which suggests that the low value is due to the catalytic effect of the hydroxyl groups generated through primary amine addition along with the tertiary amines present in the TGPAP backbone. The E_a results suggest etherification is more significant in TGPAP compared to TGDDM.

Fourier transform infra-red (FTIR) spectroscopy was used to monitor changes in the epoxy and primary amine peaks as a function of time at 130°C. Time resolved FTIR showed the epoxy percentages reduced with time for the three resins, with the rate of depletion occurring at a similar rate in TGPAP and DGEBF. The rate of epoxy consumption was much slower in TGDDM; in agreement with the slower rate of reaction found from DSC kinetics.

The rate of change in the 1620 cm^{-1} peak area mirrored that of the epoxy consumption. It was concluded that this peak area was in fact a measure of the total amine groups remaining in the system and not the total primary amine groups as is reported in the literature. This indicates that mid-infra-red FTIR is incapable of distinguishing between primary and secondary amines and that for a more accurate measure of amine conversion near infra-red FTIR should be used

Isothermal rheology was conducted on the three base resins at 130°C. The processing windows for TGDDM, TGPAP and DGEBF were 61 ± 2, 49 ± 2 and 89 ± 3 minutes respectively. Gel point conversions were measured using DSC and time resolved FTIR spectroscopy. DSC measurements of the gel point conversion in TGPAP and TGDDM were significantly below the values predicted by the Flory equation and were attributed to an inaccuracy in the use of DSC to determine the degree of conversion at a given point. FTIR measurements of the gel point conversion were in better agreement with the theoretical conversions than the DSC results.

The glass transition temperature (T_g) values of the fully cured resins were determined from the peak in DMTA tan δ curves. T_g^∞ for DGEBF, TGPAP and TGDDM were 193°C, 254°C and 270°C respectively and were in good agreement with values found in the literature. Increasing the epoxy functionality from 2 in DGEBF to 4 in TGDDM results in an increase in T_g of 77°C. The rise in T_g is due to an increase in the crosslink density which occurs owing to the increase in functionality of the epoxy prepolymer and a reduction in epoxy equivalent weight

7.1.2. Multi-component Resins and Stoichiometry

A three level factorial experimental design (FED) studied varying the quantities of the three prepolymers and the stoichiometric ratio within a predefined experimental space. Regardless of resin formulation, an increase in the stoichiometric ratio reduced the processing window. Increasing the DGEBF concentration increased the processing window at high TGPAP levels whilst it had no effect at high TGDDM levels.

For all stoichiometric ratios, T_g^∞ of the multi-component resins reduced as DGEBF content increased. Furthermore, the T_g^∞ increased as the stoichiometry reduced, suggesting that a less than equal numbers of reactive amine-hydrogens and epoxy groups leads to an increase in the crosslink density. An in-depth study of a multi-component (MC) resin system at three stoichiometries, r = 0.6, 0.8 and 1.0, revealed T_g^∞ increased from 255°C at r = 1.0 to 265°C at r = 0.6. FTIR and DSC results suggested that despite the reduced stoichiometry all epoxy groups were consumed during the cure, indicating etherification had occurred and that an increase in

etherification led to an increase in the T_g due to a reduction in the molar mass between crosslinks.

Theoretical conversions at the gel point increased with stoichiometry, with values of 0.38, 0.42 and 0.49 for r = 1.0, 0.8 and 0.6 respectively. FTIR measurements increased with stoichiometry and were in good agreement with the theoretical conversions. Poor agreements were again found using DSC.

A second FED studied the addition of DGEBF over the range 0-100% at a stoichiometry of r = 0.68. Four resin systems were chosen for further work, all at a stoichiometric ratio of r = 0.68. The formulations were 100% TGPAP, a binary mixture of 60%DGEBF-40%TGPAP and two TGDDM-containing formulations, one with 40%TGDDM-100%TGPAP in the TGPAP/ DGEBF mix and a second with 40%TGDDM-60%DGEBF in the TGPAP/DGEBF mix. 220°C was arbitrarily chosen as the minimum T_g allowable for an aerospace matrix, hence 60% DGEBF was the maximum amount of DGEBF allowed in a multi-component system.

7.1.3. Toughening

Abbreviations of the resin systems refer to the weight percent and starting letter of the major resin component. TGPAP = T, DGEBF = D and TGDDM = t. Up to 50 wt% polyethersulphone (PES) was added to the resins without the addition of solvent. The TGDDM-containing formulations could only dissolve up to 40 wt% PES on account of the initial high viscosity of the resin. The two main resin systems, 100T and 60D were studied at four PES levels; 0%, 10%, 30% and 50%. 40t-100T and 40t-60D were loaded at 40 wt% PES.

Isothermal rheology of the two main systems at 130°C showed that as the PES content increased, the initial viscosity increased. The addition of 10 wt% PES increased the initial viscosity by an order of magnitude, with subsequent additions of 20 wt% PES increasing the viscosity by a further order of magnitude.

The PW of the systems reduced with PES content because of the higher initial viscosity. G'/G'' crossover (referred to as the apparent gel point) for the 100T systems

remained consistent regardless of PES content. In contrast, the gel times of 60D increased by 30 minutes with 50 wt% PES. The increase in gel time with PES addition in 60D resins is attributed to a lack of phase separation, resulting in a slower rate of reaction compared to the 100T resins which did phase separate.

DMTA of the 100T systems showed two distinct tan δ peaks unlike the solitary peak seen for the 60D systems. The lower temperature peak at approximately 220°C was the PES rich phase and the peak occurring at ~270°C was the epoxy rich phase. As the PES content increased the T_g of the PES rich phase also increased from 220°C at 10% PES to 228°C at 50% PES. The increase is due to a higher residual epoxy content in the PES rich phase. The epoxy peak increased slightly with PES content suggests the inclusion of PES increased the crosslink density, most likely through promoting etherification between epoxy groups and the hydroxyl-terminated PES.

All 60D systems had a single tan δ peak at ~223°C. SEM showed no signs of phase separation for any of the 60D systems whereas all the toughened 100T systems were phase separated. 100T-10P had a particulate morphology, and both 100T-30P and 100T-50P a co-continuous morphology, although the domain sizes between the two co-continuous morphologies differed. The fracture toughness of the 100T and 60D systems both increased with PES content. No difference in the fracture toughness of the two systems existed up to 30% PES. At 50% PES K_{1C} of the 100T system was much higher than the 60D system owing to the phase separated morphology seen in 100T.

7.2. Future Work

- In this study, all resins were cured until completion to maximise the glass transition temperature, however in doing so it is possible that other properties were sacrificed. The effects of degree of epoxy conversion on properties such as flexural strength, tensile strength and fracture toughness should be studied, especially in TGDDM and TGPAP systems.

- Mid infra-red FTIR was used in this study to monitor the cure of epoxy-DDS systems. However, difficulties arose in monitoring individual amine peaks and

changes to the ether peak. Near infra-red FTIR should be used to study the development of the epoxy-amine network, with specific focus on varying the stoichiometric ratio and how it affects the rate of etherification and the residual amine group and epoxy group concentrations. Furthermore, the effects of altering the stoichiometry on the mechanical properties should be studied. Properties such as flexural strength, tensile strength and fracture toughness may alter due to the difference in molecular bonds formed with a reduced stoichiometry.

- The effects of stoichiometric ratio on reaction kinetics were apparent in this study; however, modelling of the rate of reaction curves using Kamal's autocatalytic model proved a poor fit when the stoichiometric ratio was below r = 1.0. Future modelling of the rate of reaction should focus on developing a more sophisticated model, one taking into account etherification.

- The inclusion of 50% PES in liquid resin without the use of solvent mixing was successful in this study and is attributable to the low viscosities of DGEBF and TGPAP. Whilst PES may not be the optimum-toughening agent, it confirms it is possible to add high quantities of an additive (resulting in high viscosity resins) and still manufacture high quality composites. Additional work should be undertaken looking at the addition of alternative toughening agents up to previously unstudied quantities. Commonly studied engineering thermoplastics such as polysulphone (PSF), polyetherimide (PEI) and poly (ether ether ketone) (PEEK) could be incorporated in epoxy matrices at high loading levels.

- A future study should look at the optimised resin formulations from this thesis and their compatibility with various composite manufacturing techniques. The processability (including the modelling of resin flow speeds and optimising cure cycles) should be studied along with mechanical properties of the composites and comparisons drawn with properties of the resins from this thesis.

References

[1] Mallick P. Fiber-reinforced composites; Materials, manufacturing and design. Third edition. Taylor and Francis Group. 2008.

[2] Campbell F. Manufacturing processes for advanced composites. Elsevier Advanced Technology. 2004.

[3] Jain P. Effect of structure on thermal behaviour of epoxy resins. *European Polymer Journal* 2003; 39(1): 181–187.

[4] Varma I and Gupta V. Thermosetting resin-properties. *Comprehensive Composite Materials* 2000; 2(1): 1–56.

[5] Neville K and Lee H. Handbook of epoxy resins. McGraw- Hill Book Company, Inc. 1967.

[6] Wan J, Li B-G, Fan H, Bu Z-Y, and Xu C-J. Nonisothermal reaction, thermal stability and dynamic mechanical properties of epoxy system with novel nonlinear multifunctional polyamine hardener. *Thermochimica Acta* 2010; 511(1-2): 51–58.

[7] May C and Nixon A. Reactive diluents for epoxy adhesives. *Industrial & Engineering Chemistry* 1961; 53(4): 303–304.

[8] Coyard H, Deligny P, and Tuck N. Resins for surface coatings: acrylics and epoxies. Wiley and Sons. 2001.

[9] Yang G, Zheng B, Yang J, Xu G, and Fu S. Preparation and cryogenic mechanical properties of epoxy resins modified by poly (ethersulphone). *Journal of Polymer Science Part A: Polymer Chemistry* 2008; 46(13): 612–624.

[10] Hexcel. M21 prepreg data sheet, 2012. [Online]. Available: http://www.hexcel.com/Resources/DataSheets/Prepreg-Data-Sheets/M21_global.pdf. [Accessed: 27-Sep-2012].

[11] Gurit. Guide to Composites, 2004. [Online]. Available: http://www.gurit.com/guide-to-composites.aspx. [Accessed: 25-Sep-2012].

[12] Boeing. About the 787 family. [Online]. Available: http://www.boeing.com/commercial/787family/background.html. [Accessed: 08-Feb-2012].

[13] Mathur R, Bahl O, and Mittal J. Advances in the development of high-performance carbon fibres from pan precursor. *Composites Science and Technology* 1994; 51(2): 223–230.

[14] Kaiser M, Garschke C, and Fox B. Out of autoclave manufacture of structural aerospace composite materials, in *SAMPE Europe 28th International Conference and Forums*, 2007, 468–473.

[15] Davies L, Day R, Bond D, Nesbitt A, Ellis J, and Gardon E. Effect of cure cycle heat transfer rates on the physical and mechanical properties of an epoxy matrix composite. *Composites Science and Technology* 2007; 67(9): 1892–1899.

[16] Donnet J-B and Bansal RC. Carbon Fibers. Second edition. Marcel Dekker. 1990.

[17] Campbell F. Polymer matrix composites in *Manufacturing technology for aerospace structural materials*. 2006, Chapter 7.

[18] Hodgkin JH. Thermosets : epoxies and polyesters. *Encyclopedia of Materials: Science and Technology*. Elsevier Ltd. 2001. 9215–9221.

[19] Brydson J. Plastic materials. Seventh edition. Butterworth-Heinemann, Oxford, UK. 1999.

[20] Wan J, Li C, Bu Z-Y, Xu C-J, Li B-G, and Fan H. A comparative study of epoxy resin cured with a linear diamine and a branched polyamine. *Chemical Engineering Journal* 2012; 188(1): 160–172.

[21] Ellis B. Chemistry and technology of epoxy resins. Blackie Academic Professional. 1993.

[22] Thomas R, Durix S, Sinturel C, Omonov T, Goossens S, Groeninckx G, Moldenaers P, and Thomas S. Cure kinetics, morphology and miscibility of modified DGEBA-based epoxy resin – Effects of a liquid rubber inclusion. *Polymer* 2007; 48(6): 1695–1710.

[23] Rosu D. Investigation of the curing reactions of some multifunctional epoxy resins using differential scanning calorimetry. *Thermochimica Acta* 2001; 370(1-2): 105–110.

[24] Ohashi K, Hasegawa K, Fukuda A, and Uede K. Curing behavior of epoxy resin having hydroxymethyl group. *Journal of Applied Polymer Science* 1992; 44(3): 419–423.

[25] Dowd R. Epoxy Resin technology. Interscience Publishers. 1968.

[26] Zhang D, Jia D, and Chen S. Kinetics of curing and thermal degradation of hyperbranched epoxy (HTDE)/diglycidyl ether of bisphenol-A epoxy hybrid resin. *Journal of Thermal Analysis and Calorimetry* 2009; 98(3): 819–824.

[27] Verrey J, Winkler Y, Michaud V, and Manson J. Interlaminar fracture toughness improvement in composites with hyperbranched polymer modified resin. *Composites Science and Technology* 2005; 65(10): 1527–1536.

[28] Blanco I, Cicala G, Faro C Lo, and Recca A. Development of a toughened DGEBS/DDS system toward improved thermal and mechanical properties by the addition of a tetrafunctional epoxy resin and a novel thermoplastic. *Journal of Applied Polymer Science* 2003; 89(1): 268–273.

[29] Xu Y and Hoa S Van. Mechanical properties of carbon fiber reinforced epoxy/clay nanocomposites. *Composites Science and Technology* 2008; 68(3-4): 854–861.

[30] Mijovic J. Cure kinetics of neat versus reinforced epoxies. *Journal of Applied Polymer Science* 1986; 31(1): 1177–1187.

[31] Thoseby MR, Dobinson B, and Bull CH. Recent advances with glycidylamine resins. *British Polymer Journal* 1986; 18(5): 286–291.

[32] St John A and George G. Diglycidyl amine-epoxy resin networks: kinetics and mechanisms of cure. *Progress in Polymer Science* 994; 19(1): 755–795.

[33] Pascault J-PP and Williams RJJ. General concepts about epoxy polymers in *Epoxy polymers*. Wiley and Sons, 2010, Chapter 1.

[34] Kim DH and Kim SC. Vitrification effect on the curing reaction of epoxy resin. *Polymer Bulletin* 1987; 18(1): 533–539.

[35] Wisanrakkit G and Gillham JK. The glass transition temperature (Tg) as an index of chemical conversion for a high-Tg amine/epoxy system: Chemical and diffusion-controlled reaction kinetics. *Journal of Applied Polymer Science* 1990; 41(1112): 2885–2929.

[36] Grillet A, Galy J, Pascault J, and Bardin I. Effects of the structure of the aromatic curing agent on the cure kinetics of epoxy networks. *Polymer* 1989; 30(507): 2094–2103.

[37] Jagadeesh KS and Siddaramaiah. Kinetics of curing epoxy formulations with diaminodiphenyl ether. *Polymer International* 1991; 26(2): 129–132.

[38] Dusek K and Matejka L. Curing of diglycidylamine-based epoxides with amines: Kinetic model and simulation of structure development. *Journal of Polymer Science Part A: Polymer Chemistry* 1995; 33(3): 461–472.

[39] Min B-G, Stachurski ZH, and Hodgkin JH. Cure kinetics of elementary reactions of a DGEBA/DDS epoxy resin: 1. Glass transition temperature versus conversion. *Polymer* 1993; 34(23): 4908–4912.

[40] Bonnaud L, Pascault JP, and Sautereau H. Kinetic of a thermoplastic-modifed epoxy-aromatic diamine formulation: modeling and influence of a trifunctional epoxy prepolymer. *European Polymer Journal* 2000; 36(1): 1313–1321.

[41] Lee; H and Neville K. Epoxy Resins, Their Applications and Technology. McGraw- Hill Book Company, Inc. 1957.

[42] Zabihi O, Hooshafza A, Moztarzadeh F, Payravand H, Afshar A, and Alizadeh R. Isothermal curing behavior and thermo-physical properties of epoxy-based thermoset nanocomposites reinforced with Fe2O3 nanoparticles. *Thermochimica Acta* 2012; 527(1): 190–198.

[43] Varley R, Hodgkin J, and Simon G. Toughening of a trifunctional epoxy system: Part VI. Structure property relationships of the thermoplastic toughened system. *Polymer* 2001; 42(1): 3847–3858.

[44] Levchik S, Camino G, and Luda M. Mechanistic study of thermal behaviour and combustion performance of epoxy resins. II. TGDDM/DDS system. *Polymer Degradation and Stability* 1995; 48(1): 359–370.

[45] Francis B, Rao VL, Vanden Poel G, Posada F, Groeninckx G, Ramaswamy R, and Thomas S. Cure kinetics, morphological and dynamic mechanical analysis of diglycidyl ether of bisphenol-A epoxy resin modified with hydroxyl terminated poly(ether ether ketone) containing pendent tertiary butyl groups. *Polymer* 2006; 47(15): 5411–5419.

[46] Ogasawara T, Ishida Y, and Kasai T. Mechanical properties of carbon fiber/fullerene-dispersed epoxy composites. *Composites Science and Technology* 2009; 69(1): 2002–2007.

[47] Liu W, Hoa S V, and Pugh M. Organoclay-modified high performance epoxy nanocomposites. *Composites s* 2005; 65(1): 307–316.

[48] Tripathi G and Srivastava D. Effect of carboxyl-terminated poly(butadiene-co-acrylonitrile) (CTBN) concentration on thermal and mechanical properties of binary blends of diglycidyl ether of bisphenol-A (DGEBA) epoxy resin. *Materials Science and Engineering: A* 2007; 443(1-2): 262–269.

[49] Bucknall CB, Gomez CM, and Quintard I. Phase separation from solutions of poly (ether sulphone) in epoxy resins. *Polymer* 1994; 35(2): 353–359.

[50] Long T and Turner R. Applied polymer science: 21st Century. First edition. Elsevier Ltd. 1985. 979–997.

[51] Smith C. The glass transition temperature and its measurement in epoxy glass laminates. *Circuit World* 1986; 12(2): 62–64.

[52] Nielsen LE. Cross-linking-effect on physical properties of polymers. *Journal of Applied Polymer Science, Part C: Polymer Review* 1969; 3(1): 69–103.

[53] Lazaa JM, Julian CA, Larraurib E, Rodrigueza M, and Leona LM. Thermal scanning rheometer analysis of curing kinetic of an epoxy resin : 2 . An amine as curing agent. *Polymer* 1998; 40(1): 35–45.

[54] Gillham JK. The formation and properties of network polymeric materials. *Polymer Engineering & Science* (19): 676–82.

[55] Enns JB and Gillham JK. Effect of the extent of cure on the modulus , glass transition , water absorption , and density of an amine-cured epoxy. *Journal of Applied Polymer Science* 1983; 28(1): 2831–2846.

[56] Varley RJ, Hodgkin JH, Hawthorne DG, and Simon GP. Toughening of a trifunctional epoxy system. II. Thermal characterization of epoxy/amine cure. *Journal of Applied Polymer Science* 1996; 60(12): 2251–2263.

[57] Deng Y and Martin GC. Diffusion phenomena during cyanate resin cure. *Polymer* 1996; 37(16): 3593–3601.

[58] Meyer F, Sanz G, Eceiza A, Mondragon I, and Mijovic J. The effect of stoichiometry and thermal history during cure on structure and properties of epoxy networks. *Polymer* 1995; 36(7): 1407–1414.

[59] Miller DR and Macosko CW. A new derivation of post gel properties of network polymers. *Macromolecules* 1974; 9(2): 206–211.

[60] Macosko CW and Miller DR. A new derivation of average molecular weights of nonlinear polymers. *Macromolecules* 1976; 9(2): 199–206.

[61] Flory P. Principles of polymer chemistry. Cornell University Press, Ithaca, New York. 1953.

[62] Barton JM. Monitoring the cross-linking of epoxide resins by thermoanalytical techniques. *Journal of Macromolecular Science: Part A - Chemistry: Pure and Applied Chemistry* 1974; A8(1): 25–32.

[63] Varley R, Hodgkin J, and Hawthorne D. Toughening of a trifunctional epoxy system Part III. Kinetic and morphological study of the thermoplastic modified cure process. *Polymer* 2000; 41(2000): 3425–3436.

[64] Hourston D and Lane J. The toughening of epoxy resins with thermoplastics: 1. Trifunctional epoxy resin-polyetherimide blends. *Polymer* 1992; 33(7): 1379–1383.

[65] Ratna D. Phase separation in liquid rubber modified epoxy mixture. Relationship between curing conditions, morphology and ultimate behavior. *Polymer* 2001; 42(1): 4209–4218.

[66] Hodgkin JH, Simon GP, and Varley RJ. Thermoplastic toughening of epoxy resins: A critical review. *Polymers for Advanced Technologies* 1998; 9(1): 3–10.

[67] Rose N, Le Bras M, Bourbigot S, and Delobel R. Thermal oxidative degradation of epoxy resins: Evaluation of their heat resistance using invariant kinetic parameters. *Polymer Degradation and Stability* 1994; 45(3): 387–397.

[68] Hourston DJ, Lane JM, and Zhang HX. Toughening of epoxy resins with thermoplastics: 3. An investigation into the effects of composition on the properties of epoxy resin blends. *Polymer International* 1997; 42(4): 349–355.

[69] Fernandez-Nograro F, Valea A, Llano-ponte R, and Mondragon I. Dynamic and mechanical properties of DGEBA/poly(propylene oxide) amine based epoxy resins as a function of stoichiometry. *European Polymer Journal* 1996; 32(2): 257–266.

[70] Guerrero P, De la Caba K, Valea M, Corcuera A, and Mondragon I. Influence of cure schedule and stoichiometry on the dynamic mechanical behaviour of tetrafunctional epoxy resins cured with anhydrides. *Polymer* 1996; 37(11): 2195–2200.

[71] Calventus Y, Montserrat S, and Hutchinson JM. Enthalpy relaxation of non-stoichiometric epoxy-amine resins. *Polymer* 2001; 42(16): 7081–7093.

[72] Boye J, Martinez JJ, Demont P, and Lacabanne C. Molecular mobility associated with the Tg in DGEBA-DDM networks. *Thermochimica Acta* 1991; 192(1): 147–154.

[73] Morgan R, Kong F, and Walkup C. Structure-property relations of polyethertriamine-cured bisphenol-A-diglycidyl ether epoxies. *Polymer* 1984; 25(1): 375–386.

[74] Nikolic G, Zlatkovic S, Cakic M, Cakic S, Lacnjevac C, and Rajic Z. Fast fourier transform IR characterization of epoxy GY systems crosslinked with aliphatic and cycloaliphatic EH polyamine adducts. *Sensors* 2010; 10(1): 684–96.

[75] Liu H, Uhlherr A, Varley RJ, and Bannister MK. Influence of substituents on the kinetics of epoxy/aromatic diamine resin systems. *Journal of Polymer Science Part A: Polymer Chemistry* 2004; 42(13): 3143–3156.

[76] Jungang G, Shigang S, Yangfang L, and Deling L. Curing kinetics and thermal property characterization of bisphenol-F epoxy resin and DDS system. *International Journal of Polymeric Materials* 2004; 53(4): 341–354.

[77] Sourour S and Kamal MR. Differential scanning calorimetry of epoxy cure: isothermal cure kinetics. *Thermochimica Acta* 1976; 14(1): 41–59.

[78] Man Z, Stanford JL, and Dutta BBK. Reaction kinetics of epoxy resin modified with reactive and nonreactive thermoplastic copolymers. *Journal of Applied Polymer Science* 2009; 112(1): 2391–2400.

[79] Karayannidou EG, Achilias DS, and Sideridou ID. Cure kinetics of epoxy–amine resins used in the restoration of works of art from glass or ceramic. *European Polymer Journal* 2006; 42(12): 3311–3323.

[80] Thakkar J, Patel R, and Patel V. Kinetic study on the effect of addition of epoxy diluents and/or fortifier on the curing characteristics of DGEBA by differential scanning calorimetry. *European Polymer Journal* 1987; 23(10): 799–802.

[81] Sidyakin P. An infrared spectroscopic study of the curing of epoxide resins with amines. *Polymer Science USSR* 1972; A14(5): 1087–1098.

[82] González MG, Cabanelas JC, and Baselga J. Applications of FTIR on epoxy resins – Identification , monitoring the curing process , phase separation and water uptake in *Infrared Spectroscopy - Materials Science, Engineering and Technology* vol. 2. InTech, 2012, 13.

[83] Cai H, Li P, Sui G, Yu Y, Li G, Yang X, and Ryu S. Curing kinetics study of epoxy resin/flexible amine toughness systems by dynamic and isothermal DSC. *Thermochimica Acta* 2008; 473(1-2): 101–105.

[84] Perrin FX, Nguyen TMH, and Vernet JL. Chemico-diffusion kinetics and TTT cure diagrams of DGEBA–DGEBF/amine resins cured with phenol catalysts. *European Polymer Journal* 2007; 43(12): 5107–5120.

[85] Dusek K and Matejka L. Curing of diglycidylamine-based epoxides with amines: Kinetic model and simulation of structure development. *Journal of Polymer Science Part A: Polymer Chemistry* 1995; 33(3): 461–472.

[86] Cole KC, Hechler JJ, and Noel D. A new approach to modeling the cure kinetics of epoxy/amine thermosetting resins. 2. Application to a typical system based on bis[4-(diglycidylamino)phenyl]methane and bis(4-aminophenyl) sulphone. *Macromolecules* 1991; 24(11): 3098–3110.

[87] Garschke C, Parlevliet PP, Weimer C, and Fox BL. Cure kinetics and viscosity modelling of a high-performance epoxy resin film. *Polymer Testing* 2013; 32(1): 150–157.

[88] Chern C-S and Poehlein GW. A kinetic model for curing reactions of epoxides with amines. *Polymer Engineering and Science* 1987; 27(11): 788–795.

[89] Hamerton I. Recent development in epoxy resins. *Rapra Review Reports* 1996; 8(7): Report 91.

[90] Mustata F and Bicu I. Rheological and thermal behaviour of DGEBA/EA and DGEHQ/EA epoxy systems crosslinked with TETA. *Polymer Testing* 2001; 20(5): 533–538.

[91] Manjunatha C, Taylor A, Kinloch A, and Sprenger S. The tensile fatigue behaviour of a silica nanoparticle-modified glass fibre reinforced epoxy composite. *Composites Science and Technology* 2010; 70(1): 193–199.

[92] Wu S, Sears MT, Soucek MD, and Simonsick WJ. Synthesis of reactive diluents for cationic cycloaliphatic epoxide UV coatings. *Polymer* 1999; 40(20): 5675–5686.

[93] Rahman MM, Hosur M, Ludwick AG, Zainuddin S, Kumar A, Trovillion J, and Jeelani S. Thermo-mechanical behavior of epoxy composites modified with reactive polyol diluent and randomly-oriented amino-functionalized multi-walled carbon nanotubes. *Polymer Testing* 2012; 31(6): 777–784.

[94] Harani H, Fellahi S, and Bakar M. Toughening of epoxy resin using hydroxyl-terminated polyesters. *Journal of Applied Polymer Science* 1999; 71(1): 29–38.

[95] Pham H and Marks M. Epoxy resins. *Ulmann's encyclopedia of industrial chemistry*. 2012. 156–243.

[96] Van Overbeke E, Devaux J, Legras R, Carter J., McGrail P., and Carlier V. Phase separation in epoxy-copolyethersulphone blends: morphologies and local characterisation by micro-Raman spectroscopy. *Polymer* 2003; 44(17): 4899–4908.

[97] Alessi S, Dispenza C, and Spadaro G. Thermal properties of E-beam cured epoxy/thermoplastic matrices for advanced composite materials. *Macromolecular Symposia* 2007; 247(1): 238–243.

[98] Perrin F-X, Nguyen TMH, and Vernet J-L. Modeling the cure of an epoxy-amine resin with bisphenol A as an external catalyst. *Macromolecular Chemistry and Physics* 2007; 208(1): 55–67.

[99] Overbeke E Van, Carlier V, Devaux J, Carter JT, Mcgrail PT, and Legras R. The use of Raman spectroscopy to study the reaction between an amine-terminated thermoplastic and epoxy resins. *Polymer* 2000; 41(1): 8241–8245.

[100] Wong DWY, Lin L, McGrail PT, Peijs T, and Hogg PJ. Improved fracture toughness of carbon fibre/epoxy composite laminates using dissolvable thermoplastic fibres. *Composites Part A: Applied Science and Manufacturing* 2010; 41(6): 759–767.

[101] Hsieh T, Kinloch A, Masania K, Sohn Lee J, Taylor A, and Sprenger S. The toughness of epoxy polymers and fibre composites modified with rubber microparticles and silica nanoparticles. *Journal of Materials Science* 2009; 45(5): 1193–1210.

[102] Russell B and Chartoff R. The influence of cure conditions on the morphology and phase distribution in a rubber-modified epoxy resin using scanning electron microscopy and atomic force microscopy. *Polymer* 2005; 46(3): 785–798.

[103] Calabrese L and Valenza A. Effect of CTBN rubber inclusions on the curing kinetic of DGEBA – DGEBF epoxy resin. *European Polymer Journal* 2003; 39(1): 1355–1363.

[104] Wise CW, Cook WD, and Goodwin AA. CTBN rubber phase precipitation in model epoxy resins. *Polymer* 2000; 41(1999): 4625–4633.

[105] Brantseva TV. Modification of epoxy resin by polysulphone to improve the interfacial and mechanical properties in glass fibre composites. II. Adhesion of the epoxy-polysulphone matrices to glass fibres. *Journal of Adhesion Science and Technology* 2004; 18(11): 1293–1308.

[106] Xie X and Yang H. Phase structure control of epoxy/polysulphone blends — effects of molecular weight of epoxy resins. *Materials & Design* 2001; 22(1): 7–9.

[107] Chang I. Thermoplastic matrix continuous filament composites of Kevlar aramid or graphite fiber. *Composites Science and Technology* 1985; 24(1): 61–79.

[108] Bucknall CB and Gilbert AH. Toughening tetrafunctional epoxy resins using polyetherimide. *Polymer* 1989; 30(1): 213–217.

[109] Moosburger-Will J, Jäger J, Horn S, and Wellhausen C. Investigation of phase morphology of polyetherimide-toughened epoxy resin by scanning probe microscopy. *Polymer Testing* 2012; 31(8): 1008–1018.

[110] Mimura K, Ito H, and Fujioka H. Improvement of thermal and mechanical properties by control of morphologies in PES-modified epoxy resins. *Polymer* 2000; 41(12): 4451–4459.

[111] Qipeng G. Phase behaviour in epoxy resin containing phenolphthalein poly(ether ether sulphone). *Polymer* 1993; 34(1): 70–76.

[112] Kim B, Chiba T, and Inoue T. Morphology development via reaction-induced phase separation in epoxy/poly (ether sulphone) blends: morphology control using poly (ether sulphone) with functional. *Polymer* 1995; 36(1): 43–47.

[113] Akay M and Cracknell J. Epoxy resin-polyethersulphone blends. *Journal of Applied Polymer Science* 1994; 52(1): 663–688.

[114] Mackinnon A, Jenkins S, Mcgrail P, and Pethrick R. Cure and physical properties of thermoplastic modified epoxy resins based on polyethersulphone. *Journal of Applied Polymer Science* 1995; 58(1): 2345–2355.

[115] Williams RJJ, Rozenberg BA, and Pascault JJ. Reaction-induced phase separation in modified thermosetting polymers. *Advances in Polymer Science* 1997; 128(1): 95–156.

[116] Flory PJ. Thermodynamics of high polymer solutions. *The Journal of Chemical Physics* 1942; 10(1): 51.

[117] Huggins ML. Solutions of long chain compounds. *The Journal of Chemical Physics* 1941; 9(5): 440.

[118] Fedors RF. A method for estimating both the solubility parameters and molar volumes of liquids. *Polymer Engineering and Science* 1974; 14(2): 472–472.

[119] Man Z. Formation and properties of epoxy resins containing PES copolymer modifiers, PhD Thesis: The University of Manchester, 2003.

[120] Kim BSB, Chiba T, and Inoue T. Phase separation and apparent phase dissolution during cure process of thermoset/thermoplastic blend. *Polymer* 1995; 36(1): 67–71.

[121] Mackinnon A, Jenkinst S, Mcgrail P, and Pethrick R. Dielectric, mechanical and rheological studies of phase separation and cure of a thermoplastic modified epoxy resin: Incorporation of reactively terminated polysulphones. *Polymer* 1993; 34(15): 3252–3263.

[122] Zhou X-M and Jiang Z-H. Sequence analysis of poly (ether sulphone) copolymers by13C NMR. *Journal of Polymer Science Part B: Polymer Physics* 2005; 43(13): 1624–1630.

[123] Raghava R. Development and characterization of thermosetting- thermoplastic polymer blends for applications in damage- tolerant composites. *Journal of Polymer Science Part B: Polymer Physics* 1988; 26(1): 65–81.

[124] Bucknall C and Partridge I. Phase separation in epoxy resins containing polyethersulphone. *Polymer* 1983; 24(5): 639–644.

[125] Blanco I, Cicala G, Motta O, and Recca A. Influence of a selected hardener on the phase separation in epoxy/thermoplastic polymer blends. *Journal of Applied Polymer Science* 2004; 94(1): 361–371.

[126] Fernandez B, Arbelaiz A, Diaz E, and Mondragon I. Influence of polyethersulphone modification of a tetrafunctional epoxy matrix on the fracture behavior of composite laminates based on woven carbon fibers. *Polymer Composites* 2004; 25(5): 480–488.

[127] Raghava RS. Role of matrix-particle interface adhesion on fracture toughness of dual phase epoxy-polyethersulphone blend. *Journal of Polymer Science Part B: Polymer Physics* 1987; 25(5): 1017–1031.

[128] Mondragon I, Oyanguren PA, Aizpurua B, Galante MJ, Riccardi CC, and Corta OD. Design of the ultimate behavior of tetrafunctional epoxies modified with polysulphone by controlling microstructure development. *Journal of Polymer Science Part B: Polymer Physics* 1999; 37(19): 2711–2725.

[129] Purslow D and Childs R. Autoclave moulding of carbon fibre-reinforced epoxies. *Composites* 1986; 17(2): 127–136.

[130] Molyneux M. Prepreg, tape and fabric technologoy. *Composites* 1983; 14(2): 87–91.

[131] Goren A and Atas C. Manufacturing of polymer matrix composites using vacuum assisted resin infusion molding. *Archives of materials science and engineering* 2008; 34(2): 117–120.

[132] Peila R, Seferis JC, Karaki T, and Parker G. Effects of nanoclay on the thermal and rheological properties of a vartm (vacuum assisted resin transfer molding) epoxy resin. *Journal of Thermal Analysis and Calorimetry* 2008; 96(2): 587–592.

[133] Kuentzer N, Simacek P, Advani S, and Walsh S. Correlation of void distribution to VARTM manufacturing techniques. *Composites Part A: Applied Science and Manufacturing* 2007; 38(3): 802–813.

[134] Grujicic M, Chittajallu K, and Walsh S. Non-isothermal preform infiltration during the vacuum-assisted resin transfer molding (VARTM) process. *Applied Surface Science* 2005; 245(1-4): 51–64.

[135] Wei L, Wong A, Leach D, and Aerospace H. Advances in benzoxazine resins for aerospace applications, 2010. [Online]. Available: http://www.henkelna.com/us/content_data/232112_Advances_in_Benzoxazine_Resins_for_Aerospace_Applications.pdf. [Accessed: 05-Feb-2011].

[136] Williams C, Summerscales J, and Grove S. Resin infusion under flexible tooling (RIFT): a review. *Composites Part A: Applied Science and Manufacturing* 1996; 27(7): 517–524.

[137] Campbell F. Liquid molding: You get a good preform and tool...you get a good part in *Manufacturing processes for advanced composites*. Elsevier Ltd, 2003, Chapter 9.

[138] Karal M. AST composite wing program - Executive summary, 2001.

[139] Tong L, Mouritz A, and Bannister M. Preform consolidation in *3D fibre reinforced polymer composites* vol. i. Elsevier Ltd, 2002, Chapter 3.

[140] Hinrichsen J and Bautista C. The challenge of reducing both airframe weight and manufacturing cost. *Air & Space Europe* 2001; 3(3-4): 119–121.

[141] Antonucci V, Giordano M, Nicolais L, Calabrò A, Cusano A, Cutolo A, and Inserra S. Resin flow monitoring in resin film infusion process. *Journal of Materials Processing Technology* 2003; 143-144(1): 687–692.

[142] Park J and Kang MK. A numerical simulation of the resin film infusion process. *Composite Structures* 2003; 60(4): 431–437.

[143] Garschke C, Weimer C, Parlevliet PP, and Fox BL. Out-of-autoclave cure cycle study of a resin film infusion process using in situ process monitoring. *Composites Part A: Applied Science and Manufacturing* 2012; 43(6): 935–944.

[144] Marsh G. Resin film infusion-composites cost reducer. *Reinforced Plastics* 2002; (1): 44–49.

[145] Qi B, Raju J, Kruckenberg T, and Stanning R. A resin film infusion process for manufacture of advanced composite structures. *Composite Structures* 1999; 47(1999): 471–476.

[146] Roller M. Characterization of the time-temperature-viscosity behavior of curing B-staged epoxy resin. *Polymer Engineering & Science* 1975; 15(6): 406–414.

[147] Liu L, Zhang B, Wang D, and Wu Z. Effects of cure cycles on void content and mechanical properties of composite laminates. *Composite Structures* 2006; 73(3): 303–309.

[148] Costa ML, Almeida SF, and Rezende MC. The influence of porosity on the interlaminar shear strength of carbon/epoxy and carbon/bismaleimide fabric laminates. *Composites Science and Technology* 2001; 61(1): 2101–2108.

[149] Zhu H, Li D, Zhang D, Wu B, and Chen Y. Influence of voids on interlaminar shear strength of carbon/epoxy fabric laminates. *Transactions of Nonferrous Metals Society of China* 2009; 19(1): 470–475.

[150] Chambers A, Earl J, Squires C, and Suhot M. The effect of voids on the flexural fatigue performance of unidirectional carbon fibre composites developed for wind turbine applications. *International Journal of Fatigue* 2006; 28(10): 1389–1398.

[151] Jeong H. Effects of voids on the mechanical strength and ultrasonic attenuation of laminated composites. *Journal of Composite Materials* 1997; 31(3): 276–292.

[152] Judd N and Wright W. Voids and their effects on the mechanical properties of composites-An appraisal. *SAMPE Journal* 1978; 14(1): 10–14.

[153] Boey F. Void reduction in autoclave processing of thermoset composites Part 1: High pressure effects on void reduction. *Composites* 1992; 23(4): 261–265.

[154] De Almeida SFM and Neto ZDSN. Effect of void content on the strength of composite laminates. *Composite Structures* 1994; 28(2): 139–148.

[155] Dell'Anno G, Cartié DD, Partridge IK, and Rezai A. Exploring mechanical property balance in tufted carbon fabric/epoxy composites. *Composites Part A: Applied Science and Manufacturing* 2007; 38(11): 2366–2373.

[156] Khan LA, Nesbitt A, and Day RJ. Hygrothermal degradation of 977-2A carbon/epoxy composite laminates cured in autoclave and Quickstep. *Composites Part A: Applied Science and Manufacturing* 2010; 41(8): 942–953.

[157] Campbell F. Curing: It's a matter of time (t), temperature (T) and pressure (P) in *Manufacturing Processes for Advanced Composites*. Elsevier Ltd, 2003.

[158] Brosius D. Economic comparison of autoclave and quickstep process for high volume advanced composite automative components, Quickstep Technologies Pty. Ltd., 2004.

[159] Olivier R, Cottu JP, and Ferret B. Effects of cure cycle pressure and voids on some mechanical properties of carbon / epoxy laminates. *Composites* 1995; 26(7): 509–515.

[160] Hernández S, Sket F, Molina-Aldareguı´a J., González C, and LLorca J. Effect of curing cycle on void distribution and interlaminar shear strength in polymer-matrix composites. *Composites Science and Technology* 2011; 71(10): 1331–1341.

[161] Akay M, Kong S, and Stanley A. Influence of moisture on the thermal and mechanical properties of autoclaved and oven-cured kevlar-49/epoxy laminates. *Composite Science and Technology* 1997; 57(1): 565–571.

[162] Papargyris D, Day R, Nesbitt A, and Bakavos D. Comparison of the mechanical and physical properties of a carbon fibre epoxy composite manufactured by resin transfer moulding using conventional and microwave heating. *Composites Science and Technology* 2008; 68(7-8): 1854–1861.

[163] Nightingale C and Day R. Flexural and interlaminar shear strength properties of carbon fibre/epoxy composites cured thermally and with microwave radiation. *Composites Part A: Applied Science and Manufacturing* 2002; 33(7): 1021–1030.

[164] Rao S and Rao R. Cure studies on bifunctional epoxy matrices using a domestic microwave oven. *Polymer Testing* 2008; 27(5): 645–652.

[165] Rahmat A, Heatley F, and Day RJ. Comparison of microwave and thermal cure of unsaturated polyester resin. *Plastics, Rubber and Composites* 2003; 32(6): 257–264.

[166] Herring ML, Mardel JI, and Fox BL. The effect of material selection and manufacturing process on the surface finish of carbon fibre composites. *Journal of Materials Processing Technology* 2010; 210(1): 926–940.

[167] Corbett T, Forrest M, Gac P, and Fox B. Characterization of melded carbon fibre/epoxy laminates. *Composites: Part A* 2007; 38(1): 1860–1871.

[168] Gardiner G. Out-of-autoclave prepregs : Hype or revolution? *Composites World*. 2011.

[169] Montgomery, Douglas C. Design and analysis of experiments. Fifth edition. John Wiley andd Sons, Inc. 2001.

[170] Expert D. Design Expert 7: Software help sheet. 2007; (1): 1–10.

[171] Mustata F and Bicu I. Synthesis, characterization, and properties of multifunctional epoxy maleimide resins. *Macromolecular Materials and Engineering* 2006; 291(6): 732–741.

[172] Lopez J, Lopez-Bueno I, and Nogueira P. Effect of poly (styrene- co-acrylonitrile) on the curing of an epoxy/amine resin. *Polymer* 2001; 42(1): 1669–1677.

[173] Hohne GWH, Hemminger WF, and Flammersheim H-J. Differential scanning calorimetry. Second edition. 2003.

[174] Silverstein R. and Webster F. Spectrometric identification of organic compounds. Sixth edition. John Wiley & Sons, New York. 1989.

[175] Cherdoudâ- Chihani A, Mouzali M, and Abadie M. Study of crosslinking acid copolymer/DGEBA systems by FTIR. *Journal of Applied Polymer Science* 2003; 87(1): 2033–2051.

[176] Jones N and Herling F. Characteristic group frequencies in the infrared spectra of steroids. *Journal of Organic Chemistry* 1954; 19(1): 1252–1268.

[177] Osswald T and Menges G. Materials science of polymers for engineers. Hanser Publishers. 1996.

[178] Sepe M. Thermal analysis of polymers. Rapra Review Reports. 1997.

[179] Mezger T. The rheology handbook: For users of rotational and oscillatory rheometers. Second edition. Vincentz Network GmbH and Co KG. 2006.

[180] Test Standard - ASTM D4473-95a: Standard practice for measuring the cure behaviour of thermosetting resins using dynamic mechanical procedures. .

[181] Test Standard - ASTM D 5045-99: Standard test methods for plane-strain fracture toughness and strain energy release rate of plastic materials. .

[182] M C, Hourston DJ, and Sun W. The morphology and fracture behaviour of a miscicible epoxy resin-polyetherimde blend. *European Polymer Journal* 1995; 31(2): 199–201.

[183] Jose J, Joseph K, Pionteck J, and Thomas S. PVT behavior of thermoplastic poly(styrene-co-acrylonitrile)-modified epoxy systems: relating polymerization-induced viscoelastic phase separation with the cure shrinkage performance. *The Journal of Chemical Physics B* 2008; 112(47): 14793–803.

[184] Ishii Y and Ryan AJ. Processing of poly(2,6-dimethyl-1,4-phenylene ether) with epoxy resin. 1. reaction-induced phase separation. *Macromolecules* 2000; 33(1): 158–166.

[185] Sawyer L and Grubb D. Polymer Microscopy. Chapman and Hall, New York. 1989.

[186] Joy D. Beam interactions, contrast and resolution in the SEM. *Journal of Microscopy* 1984; 136(2): 241–258.

[187] Gupta A, Cizmecioglu M, Coulter D, Liang RH, Yavrouian A, Tsay FD, and Moacanin J. The mechanism of cure of tetraglycidyl diaminodiphenyl methane with diaminodiphenyl sulphone. *Journal of Applied Polymer Science* 1983; 28(6): 2131–2131.

[188] Mijovic J, Kim J, and Slaby J. Cure kinetics of epoxy formulations of the type used in advanced composites. *Journal of applied polymer science* 1984; 29(2): 1449–1462.

[189] Rozenberg B. Epoxy Resins and Composites II in *Advances in Polymer Science*. Springer-Verlag, 1986.

[190] Horie K, Hiura H, Sawada M, Mita I, and Kambe H. Calorimetric investigation of polymerization reactions. III. Curing reaction of epoxides with amines. *Journal of Polymer Science: Part A-1* 1970; 8(6): 1357–1372.

[191] Riccardi C, Adabbo H, and Williams R. Curing reaction of epoxy resins with diamines. *Journal of Applied Polymer Science* 1984; 29(1): 2481–2492.

[192] Simon SL and Gillham JK. Reaction kinetics and TTT cure diagrams for off-stoichiometric ratios of a high-Tg epoxy/amine system. *Journal of Applied Polymer Science* 1992; 46(7): 1245–1270.

[193] Ratna D, Varley R, and Simon G. Processing and chemorheology of epoxy resins and their blends with dendritic hyperbranched polymers. *Journal of Applied Polymer Science* 2004; 92(1): 1604–1610.

[194] Lee S, Chiu M, and Lin H. Kinetic model for the curing reaction of a tetraglycidyl diamino diphenyl methane/diamino diphenyl sulphone (TGDDM/DDS) epoxy resin system. *Polymer Engineering & Science* 1992; (15): 1037–1046.

[195] Ramírez C, Rico M, Torres A, Barral L, López J, and Montero B. Epoxy/POSS organic–inorganic hybrids: ATR-FTIR and DSC studies. *European Polymer Journal* 2008; 44(10): 3035–3045.

[196] Lee JY, Choi HK, Shim MJ, and Kim SW. Kinetic studies of an epoxy cure reaction by isothermal DSC analysis. *Thermochimica Acta* 2000; 343(1): 6–12.

[197] Aziz M. A Study on the effect of hardener on the mechanical properties of epoxy resin, University of Technology, Republic of Iraq, 2010.

[198] Brown A. A step-by-step guide to non-linear regression analysis of experimental data using a Microsoft Excel spreadsheet. *Computer Methods and Programs in Biomedicine* 2001; 65(3): 191–200.

[199] Naé HN. Cure and thermal properties of brominated epoxy systems. *Journal of Applied Polymer Science* 1987; 33(4): 1173–1185.

[200] Shechter L and Wynstra J. Glycidyl ether reactions with alcohols, phenols, carboxylic acids, and acid anhydrides. *Industrial & Engineering Chemistry* 1956; 48(1): 86–93.

[201] Chapman N, Isaacs N, and Parker R. The mechanism of epoxide reactions. Part I. The reactions of 1, 2-epoxyethylbenzene, 1, 2-epoxy-3-phenylpropane, and 1, 2-epoxy-3-phenoxypropane with some secondary amines. *Journal of the Chemical Society* 1960; (1): 1925–1934.

[202] Ehlers J-E, Rondan N, Huynh L, Pham H, Marks M, and Truong T. Theoretical study on mechanisms of the epoxy−amine curing reaction. *Macromolecules* 2007; 40(12): 4370–4377.

[203] Carrasco F, Pagès P, Lacorte T, and Briceño K. Fourier transform IR and differential scanning calorimetry study of curing of trifunctional amino-epoxy resin. *Journal of Applied Polymer Science* 2005; 98(4): 1524–1535.

[204] Xu L and Schlup J. Etherification versus amine addition during epoxy resin/amine cure: An in situ study using near-infrared spectroscopy. *Journal of applied polymer science* 1998; 67(1): 895–901.

[205] Varley RJ, Hodgkin JH, and Simon GP. Toughening of trifunctional epoxy system. V. Structure-property relationships of neat resin. *Journal of applied polymer Science* 2000; 77(1): 237–248.

[206] Chiao L. Mechanistic reaction kinetics of 4, 4’-diaminodiphenyl sulphone cured tetraglycidyl-4, 4'-diaminodiphenylmethane epoxy resins. *Macromolecules* 1990; 1290(23): 1286–1290.

[207] George G, Cash G, and Rintoul L. Cure monitoring of aerospace epoxy resins and prepregs by fourier transform infrared emission spectroscopy. *Polymer International* 1996; 41(2): 169–182.

[208] Mijovic J and Andjelic S. A study of reaction kinetics by near-infrared spectroscopy. 1. Comprehensive analysis of a model epoxy/amine system. *Macromolecules* 1995; 28(1): 2787–2796.

[209] Tong L, Mouritz A, and Bannister M. Preform consolidation in *3D fibre reinforced polymer composites* vol. i. Elsevier Ltd, 2006, 3.

[210] Li W, Wong A, and Leach D. Advances in Benzoxazine resins for Aerospace applications, *http://www.henkelna.com/us/content_data/232112_Advances_in_Benzoxazine_Resins_for_Aerospace_Applications.pdf*, 2010. [Online]. Available: http://www.henkelna.com/us/content_data/232112_Advances_in_Benzoxazine_Resins_for_Aerospace_Applications.pdf. [Accessed: 30-Apr-2013].

[211] Mortimer S, Ryan a. J, and Stanford JL. Rheological Behavior and Gel-Point Determination for a Model Lewis Acid-Initiated Chain Growth Epoxy Resin. *Macromolecules* 2001; 34(9): 2973–2980.

[212] Lachenal G. Evaluation of the curing state of epoxy thermoset systems. *Macromolecular Symposia* 1997; 136(1): 129–136.

[213] Bakker CJ De, John NAS, and Georget GA. Simultaneous differential scanning analysis of the curing of tetraglycidyldiaminodiphenylmethane with diaminodiphenylsulphone. *Polymer* 1993; 34(4): 716–725.

[214] Kenny J. Application of modeling to the control and optimization of composites processing. *Composite Structures* 1994; 27(1-2): 129–139.

[215] Loos AC, Rattazzi D, and Batra RC. A three-dimensional model of the resin film infusion process. *Journal of Composite Materials* 2002; 36(10): .

[216] Hickey CMD and Bickerton S. Cure kinetics and rheology characterisation and modelling of ambient temperature curing epoxy resins for resin infusion/VARTM and wet layup applications. *Journal of Materials Science* 2012; 48(2): 690–701.

[217] Barton J. Monitoring the cross-linking of epoxide resins by thermoanalytical techniques. *Journal of Macromolecular Science: Part A - Chemistry: Pure and Applied Chemistry* 1974; (1): 37–41.

[218] Bakar M, Duk R, Przybylek M, and Kostrzewa M. Mechanical and Thermal Properties of Epoxy Resin Modified with Polyurethane. *Journal of Reinforced Plastics and Composites* 2008; 28(17): 2107–2118.

[219] Dušek K. Cross-linking of epoxy resins. *Rubber–modified thermoset resins Advances in Chemistry* 1984; (1): 3–14.

[220] Hodd K a. Epoxy Resins. *Comprehensive Polymer Science and Supplements* 1989; 5(1): 667–699.

[221] Palmese G and McCullough R. Effect of epoxy–amine stoichiometry on cured resin material properties. *Journal of Applied Polymer Science* 2003; 46(1): 1863–1873.

[222] Stein J. Toughening of epoxy resins with a thermoplastic and a block copolymer, University of Manchester, 2013.

[223] Yamanaka K and Takashi I. Structure development in epoxy resin modified with poly(ether sulphone). *Polymer* 1989; 30(1): 662–667.

[224] Chen J, Chen W, and Cheng M. The curing reaction of poly(ether-sulphone)-modified epoxy resin. *Macromolecular Chemistry and Physics* 1995; 196(11): 3447–3458.

[225] Horiuchi S, Street a. C, Ougizawa T, and Kitano T. Fracture toughness and morphology study of ternary blends of epoxy, poly(ether sulphone) and acrylonitrile-butadiene rubber. *Polymer* 1994; 35(24): 5283–5292.

[226] Fernandez B, Corcuera M, Marieta C, and Mondragon I. Rheokinetic variations during curing of a tetrafunctional epoxy resin modified with two thermoplastics. *European polymer Journal* 2001; 37(1): 1863–1869.

[227] Zhang J, Guo Q, Huson M, Slota I, and Fox B. Interphase study of thermoplastic modified epoxy matrix composites: Phase behaviour around a single fibre influenced by heating rate and surface treatment. *Composites Part A: Applied Science and Manufacturing* 2010; 41(6): 787–794.

[228] Timmerman J. Nanoclay reinforcement effects on the cryogenic microcracking of carbon fiber/epoxy composites. *Composites Science and Technology* 2002; 62(9): 1249–1258.

[229] Hillermeier RW and Seferis JC. Interlayer toughening of resin transfer molding composites. *Composites Part A: Applied Science and Manufacturing* 2001; 32(5): 721–729.

[230] Bucknall C and Partridge I. Addition of polyethersulphone to epoxy resins. *The British polymer journal* 1983; 15(1): 71–75.

[231] Bucknall CB and Partridge IK. Phase separation in crosslinked resins containing polymeric modifiers. *Polymer Engineering and Science* 1986; 26(1): 54–62.

[232] Yoon T, Priddy D, Lyle G, and Mcgrath JE. Mechanical and morphological investigation of reactive polysulphone toughened epoxy networks. *Macromolecular Symposia* 1995; 686(1): 673–686.

[233] Kanchanomai C, Rattananon S, and Soni M. Effects of loading rate on fracture behavior and mechanism of thermoset epoxy resin. *Polymer Testing* 2005; 24(7): 886–892.

[234] Bin L, Lixin C, Jianna D, Huixin Z, and Fengfei L. A thermosetting phenolic film and its application in the resin film infusion. *Journal of Composite Materials* 2011; 46(3): 285–290.

[235] Halmshaw R. Non-destructive testing. 2nd edition. Edward Arnold. 1991. 132.

[236] Afendi M, Banks WM, and Kirkwood D. Bubble free resin for infusion process. *Composites Part A: Applied Science and Manufacturing* 2005; 36(6): 739–746.

[237] Test Standard - ASTM D 3171-09: Standard test methods for constituent content of composite materials. 2009.

[238] Deng S. Influence of fibre cross-sectional aspect ratio on mechanical properties of glass-fibre/epoxy composites II. Interlaminar fracture and impact behaviour. *Composites Science and Technology* 1999; 59(11): 1725–1734.

[239] Test Standard - ASTM 5528-01; Standard test method of mode I interlaminar fracture toughness of unidirectional fiber-reinforced polymer matrix composites. 2007.

[240] Jar P-YB, Mulone R, Davies P, and Kausch H-H. A study of the effect of forming temperature on the mechanical behaviour of carbon-fibre/peek composites. *Composites Science and Technology* 1993; 46(1): 7–19.

[241] Imanaka M, Motohashi S, Nishi K, Nakamura Y, and Kimoto M. Crack-growth behavior of epoxy adhesives modified with liquid rubber and cross-linked rubber particles under mode I loading. *International Journal of Adhesion and Adhesives* 2009; 29(1): 45–55.

[242] Coronado P, Argüelles A, Viña J, Mollón V, and Viña I. Influence of temperature on a carbon–fibre epoxy composite subjected to static and fatigue loading under mode-I delamination. *International Journal of Solids and Structures* 2012; 49(21): 2934–2940.

[243] Hu X and Mai Y. Mode I delamination and fibre bridging in carbon-fibre/epoxy composites with and without PVAL coating. *Composite Science and Technology* 1993; 46(1): 147–156.

[244] Test Standard - ASTM 2344/D: Standard test method for short-beam strength of polymer matrix composite materials and their laminates. 2013.

[245] Test Standard - EN ISO 178:2010: Plastics - determination of flexural properties. .

[246] Mills A. Development of an automated preforming technology for resin infusion processing of aircraft components. *Journal of Aerospace Engineering* 2006; 220(5): 499–505.

[247] Abraham D, Matthews S, and McIlhagger R. A comparison of physical properties of glass fibre epoxy composites produced by wet lay-up with autoclave consolidation and resin transfer moulding. *Composites Part A: Applied Science and Manufacturing* 1998; 29(7): 795–801.

[248] Dow M and Benso D. Development of stitched , braided and woven composite structures in the ACT program and at langley research centre, NASA, 1997.

[249] Tang J-M, Lee WI, and Springer GS. Effects of cure pressure on resin flow, voids, and mechanical properties. *Journal of Composite Materials* 1987; 21(5): 421–440.

[250] Stringer LG. Optimization of the wet lay-up/vacuum bag process for the fabrication of carbon fibre epoxy composites with high fibre fraction and low void content. *Composites* 1989; 20(5): 441–452.

[251] De Baere I, Jacques S, Van Paepegem W, and Degrieck J. Study of the mode I and mode II interlaminar behaviour of a carbon fabric reinforced thermoplastic. *Polymer Testing* 2012; 31(2): 322–332.

Appendix A: Composites Experimental

A.1 Composite Lay Up

The composite manufacturing technique utilised in this study was resin film infusion (RFI). Owing to the high viscosity resins being studied a more conventional manufacturing technique such as resin infusion would not be suitable. RFI is a technique that often gets overlooked, whilst in reality it provides an excellent platform for manufacturing high quality composites with relative ease.

Before lay-up began films of epoxy resin were made by pouring the liquid resin into a disposable mould. The mould was placed in a vacuum oven and the resin was degassed under full vacuum at 130°C. This temperature was required due to the high viscosity of the resin systems containing high quantities of PES. To begin the lay-up process an area at the centre of a tool plate was marked out using tacky tape. In the centre of the plate a layer of breathable mesh was placed before perforated release film and peel ply were added (Figure A.1). Note that if at any point the supporting material seemed likely to move the corners were taped down. Five layers of pre-cut dry carbon fibre mat were then placed on top of the peel ply and aligned along the fibre direction. A film of resin (~2 mm thick) was then placed on top of the fibres. Note that the resin layer was at least the same length and width to that of the fibre stack. Once the resin was in place, five layers of carbon fibre mat, peel ply, release film and breathable mesh were all placed on top.

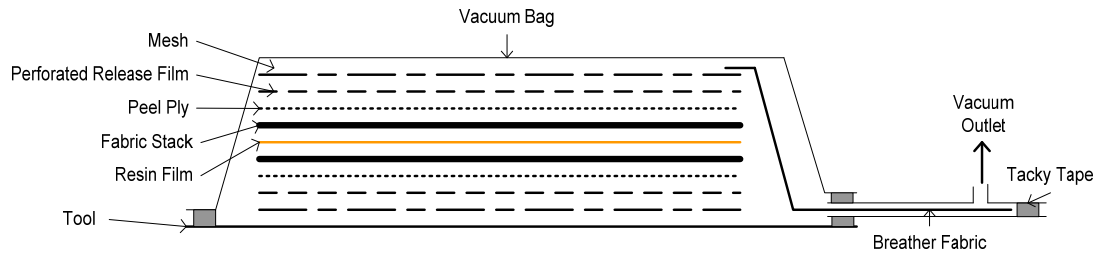

Figure A1. A schematic of the vacuum bag for resin film infusion.

Breathable fabric was then inserted in to a sleeve made from vacuum bagging material of length ~75 cm. One end of the sleeve was sealed using tacky tape whilst the other was placed over the edge of the tacky tape on the tool plate surrounding the stack of

fabric. The bottom half of a vacuum outlet port was then inserted in to the sleeve at the end furthest from the tool plate, whilst the conjoining part was screwed in on the outside of the sleeve. Note that the sleeve served a second function, acting as a bleeder for any excess resin. A sheet of vacuum bagging material was then placed across the tacky tape surrounding the fabric stack and firm pressure was placed along the tacky tape edge insuring good adhesion between the bagging material and the tape. A vacuum was then applied to the stack using the outlet port. Once under complete vacuum the layup was left for ~30 minutes after which, using a pressure gauge, an assessment of the quality of the vacuum seal was undertaken. If the pressure had remained sufficiently low then a thermocouple was taped to the outside of the vacuum bag before the curing process began.

As the composite panels being manufactured were to be used (at least in part) for mode I fracture toughness testing, a small insert of release film measuring 65 mm wide and 300 mm in length were placed so that its edges protruded that of the edges of the panel. This insert will be discussed in more detail in the mechanical testing section of the report. Once in place a second layer of resin was added before the above process was repeated but in reverse order.

A.2 Ultrasonic C-Scan

Ultrasonic inspection is the most common non-destructive technique used to detect the presence of manufacturing defects in composite parts [147]. C-Scan assesses the quality of a material in terms of uniformity which when applied to composite laminates can distinguish areas of resin enrichment and give a qualitative assessment of void content and areas of delamination. By using two jets of water as a transfer medium, sound waves of ultrasonic frequencies are passed through the sample being tested [235]. The strength of the received signal is directly related to both the uniformity of the material it passes through and the frequency of the sound waves. Thinner samples require a higher frequency in order to penetrate the material. As the signal transfers through non-uniform materials signal strength is lost, known as an increase in attenuation [235]. Computer software attached to the C-Scan records the attenuation across the material. Variations in attenuation are visibly displayed as different colours allowing for easy identification of areas of non-uniformity.

C-Scan testing was conducted using a Midas NDT Linear Water Jet using a 1 MHz ultrasonic probe. Samples were scanned in a raster pattern using an index step and grid size both of 225 μm. Attenuation images were generated using Zeus v3.0 computer software.

A.3 Fibre Volume Fraction and Void Content Analysis

Void content analysis is important in high specification composites as high void contents can lead to poor mechanical properties, specifically interlaminar shear strength, flexural strength and compressive strength [147], [150], [163], [236]. Thus, minimising the void content of a composite is paramount in achieving a high quality laminate. It is also important to have the correct fibre volume fraction and hence matrix volume fraction. A matrix fraction that is too low will result in poor adhesion between the matrix and reinforcement leading to premature mechanical failure, whereas high matrix volume fractions can lead to inadequate transfer of applied loads to the reinforcement.

Acid digestion is a method by which an accurate measure of a carbon fibre composite's fibre volume fraction and void fraction can be determined. With knowledge of both of these parameters, an assessment can be made of the quality of the composite. The procedure for these measurements was conducted in accordance with ASTM D 3171-09 [237] and is documented below.

A.3.1 Experimental Procedure

Specimens of each composite to be tested were cut from various locations of each panel (see section composite panel). Three samples weighing ~1 g were used from each panel and the weight of each was recorded to the nearest ± 0.0001 g. The density of each sample was calculated using a Mettler Toledo balance and an ionised water displacement technique. The sample was then placed in a 100 ml glass beaker on a hot plate at 100°C before 20 ml of sulphuric acid was added. Once the solution had darkened hydrogen peroxide was added a drop at a time until the matrix was sufficiently oxidised to increase the production of acid fumes. This was repeated until the fibres floated to the top of the solution and the solution colour appears clear. The beaker was then removed from the hotplate and allowed to cool. The fibres were

washed with distilled water and acetone before being placed in an oven at 100°C to dry for 1 hour.

A.3.2 Calculations

The extracted fibres were weighed and their density measured using the method mentioned above. The volume fraction of fibre, V_f, was calculated using Equation A.1, where M_f = mass of fibres after digestion, M_i= initial mass of the sample, ρ_c = density of the composite and ρ_r = density of the fibre.

$$V_f = \left(\frac{M_f}{M_i}\right) \times 100 \times \frac{\rho_c}{\rho_r} \tag{A.1}$$

The volume fraction of the matrix, V_m, was calculated using Equation A.2, where ρ_m = density of the matrix.

$$V_m = \frac{(M_i - M_f)}{M_i} \times 100 \times \frac{\rho_c}{\rho_m} \tag{A.2}$$

The void volume fraction, V_v, was calculated using Equation A.3.

$$V_v = 100 - (V_f + V_m) \tag{A.3}$$

A.4 Mode I Fracture Toughness

Delamination is one of the most critical damage modes limiting the application of structural composite laminates [238]. The most common methods for assessing delamination growth are mode I and II testing. Mode I interlaminar fracture energy, G_{1C}, is the strain energy release rate at which delamination growth occurs as a result of an opening load or displacement applied to a pre-existing crack [239]. Various methods of improving this property have been, and are currently being, investigated including z-axis reinforcement and the addition of various materials to the polymer matrix [240]–[243]. By improving the toughness between fabric layers, the energy required for crack propagation should increase.

A.4.1 Specimen Preparation

Mode I testing was completed (where possible) in accordance with ASTM 5528-01 [239]. As will be discussed in the results and discussion section in more detail, panels could not be successfully manufactured using unidirectional carbon fibre fabric. Instead panels were manufactured and tested using satin weave fabric. The panels were prepared with one adjustment. A sheet of release film was inserted in to the middle of the composite during the lay-up process and can be seen in Figure A.2. Note that during the manufacturing of panels for model I testing two films of resin were required either side of the insert to achieve sufficient wetting of the fibre mats.

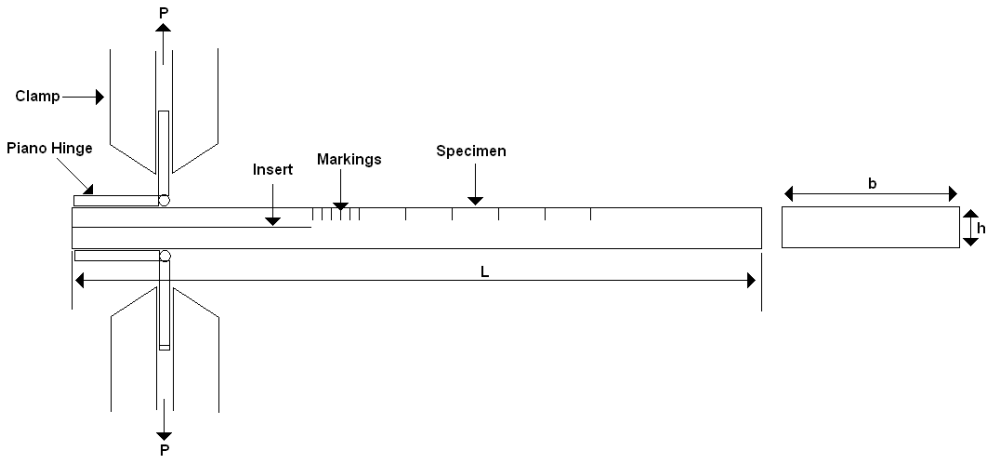

Figure A.2. Schematic of a specimen prepared for mode I fracture toughness testing.

The film measured ~30 cm in length and was ~8 cm wide. It was inserted so that at the front and at both sides the film protruded from the edge of the panel being fabricated in order for its location to be easily identified once the panel was cured. It was inserted so that 70 mm of the film was inside the panel. Once cured the panel was cut in test specimens of dimensions 175 mm × 25 mm. The thickness of the specimens ranged from 3.84–4.03 mm depending on the resin used for manufacturing of the composite. Piano hinges were then attached to the specimens. Beforehand, the area of each sample to which the hinges were to be attached, and the hinges themselves were sandblasted to maximise adhesion. They were then fixed using a room temperature curing epoxy adhesive before being postcured at 80°C for 1 hour. The distance between the hinge butt and the end of the insert was 50 mm. The edges of each specimen were painted

with white spray paint and markings made at every 1mm for the first 5 mm from the insert, followed by markings every 5 mm for the next 20 mm.

A.4.2 Experimental Procedure

The hinges were held between the grips of the loading machine, making sure the sample was central and aligned. The sample was loaded at a speed of 3 mm min^{-1} in order for a natural crack to propagate. The sample was then unloaded and the length of this crack was recorded using the markings made earlier. The crack did not exceed 5mm from the edge of the insert. The sample was then reloaded at the same cross head speed until a total delamination length of 50 mm from the pre-crack. During testing Bluehill computer software, linked to the loading machine, plots a load-displacement curve. Using a computer mouse event markers were made on the graph at points where the crack length increased to the next marking on the side of the sample.

A.4.3 Calculations

G_{1C} values were calculated from the modified beam theory (MBT). For a perfectly built-in sample, G_1 is calculated using Equation A.4, where P = load, ζ = load point displacement, b = sample width and a = delamination length.

$$G_1 = \frac{3P\zeta}{2ba} \tag{A.4}$$

However, samples are not perfectly built-in as rotation may occur at the delamination front. As such, Equation A.4 overestimates the G_1 value. To compensate for this a slightly longer delamination is assumed such that the new delamination length is a + Δ, where Δ may be determined from the generation of a least squares plot of the cube root of compliance, $C^{1/3}$, as a function of delamination length. The compliance is equal to δ/P.

Thus mode I interlaminar fracture toughness is calculated using Equation A.5.

$$G_1 = \frac{3P\zeta}{2b(a+\Delta)} \tag{A.5}$$

A.5 Interlaminar Shear Strength (ILSS)

ILSS is a simple method for determining the maximum shear stress a composite can withstand before delamination failure occurs. Testing was conducted in accordance with ASTM 2344-00 [244] which states that short beam samples should be tested in 3 point bending. Specimens were prepared of dimensions 27 × 10 × 4.5 mm and at least five specimens were tested for each material. Specimens were placed on two side supports of 3 mm diameter (Figure A.3) so that the span between the centres of the supports was 4 times greater than the measured thickness of each material. A 6 mm loading nose was aligned equidistant between the two supports so that the sample lay perpendicular to the nose. The loading nose was programmed to move at a rate of 1 mm min^{-1} and a force versus displacement graph was plotted until either the load drop-off exceeded 30% or the specimen fractured.

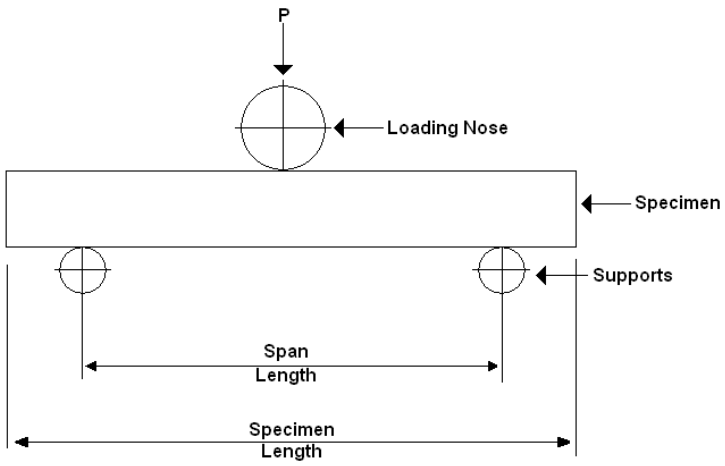

Figure A.3. Set up for interlaminar shear strength (ILSS) testing.

The short beam strength, F, of each sample was calculated from Equation A.6, where P_m = maximum observed load, b = measured width and h = measured thickness.

$$F = 0.75 \times \left(\frac{P_m}{b \times h} \right) \tag{A.6}$$

For statistical analysis, standard deviations were calculated for each material.

A.6 Flexural Properties

A.6.1 Experimental Procedure

The flexural properties of composites were measured in accordance with the British Standard BS ISO 178:2010 [245]. Nominal specimen dimensions were 80 × 10 × 4 ± 0.2 mm. However, owing to the different resin system used in the study the thickness of the samples varied. The standard however accounts for size variations and all specimens were within the range of 3.5-5 mm; as such a width of 10 mm could be used.

Specimens were loaded in three point bending. The radius of the supports and the loading nose was 5 mm, and the span, L, was set to a gap of 64 mm. Specimens were loaded at a crosshead speed of 2 mm min^{-1} and the deflection was recorded. A minimum of five specimens were tested for each material.

A.6.2 Calculations

The flexural-stress was calculated using Equation A.7, where σ_f = the flexural-stress parameter, F = the applied force (N), L is the span (mm), b is the width (mm) and h is the thickness (mm).

$$\sigma_f = \frac{3FL}{2bh^2} \tag{A.7}$$

The flexural-strain , ε_f, was calculated using Equation A.8, s is the deflection (mm).

$$\varepsilon_f = \frac{6sh}{L^2} \tag{A.8}$$

Appendix B: Composite Manufacturing: Processing and Properties

Six resin formulations were used for composite manufacturing; the 100T and 60D systems at PES levels of 0%, 30% and 50%. Consultation of published literature revealed that whilst 50% PES has been incorporated and studied within an epoxy matrix [113], there is no evidence of such a high quantity ever being incorporated within an epoxy matrix used to manufacture composites; most likely due to the extremely high viscosities generated when using such a high content of thermoplastic (Figure 6.1, p 186). However, the rheological data presented in chapter 6 suggests that the systems containing 50% PES do flow, albeit that the viscosity for the majority of the pre-gel cure cycle is above the 100 Pa s processing window. Degassing of the resins further affects the gel time and more importantly, the time the viscosity is below 100 Pa s; a processing requirement not taken into account in the rheological results presented in chapter 6. It is common practice for resins to be degassed prior to composite manufacturing to minimise the level of voids formed during cure [153] as theyact as crack nucleation sites and ultimately lead to poor mechanical performance. The systems containing 30% and 50% PES were degassed at 130°C for 30 minutes owing to their high viscosity. As such, degassing reduces the reported processing windows of the resins by 30 minutes, resulting in the actual PW's for composite manufacturing shown in Table B.1. For 100T-50P and 60D-50P the fraction of the pre-gel cure time with a viscosity >100 Pa s is 70% and 62% respectively. As such, the period in which 100T-50P has a viscosity <100 Pa s is 14 minutes. However, the resin gels after 47 minutes therefore the quality of the resultant composite will shed some light as to whether 100 Pa s is a realistic processing window.

Composites were manufactured using resin film infusion (RFI). RFI has been used for manufacturing advanced composite structures with high mechanical performance and at low cost for aerospace, automotive, military, and civil applications [140], [141]. The technique is similar to resin infusion whereby liquid resin permeates through a dry preform. Unlike resin infusion, the resin used in RFI is placed inside the vacuum bag as a film. The advantage of RFI is that a relatively short flow distance has to be overcome which leads to both improved mould-filling times [142] and eliminates the

need for a low viscosity resin system [143]. Thus, high molecular weight resins can be used resulting in mechanical properties comparable to prepregs [144]. However, for reasons that are discussed later in the chapter, composites made using the untoughened resins (60D-0P and 100T-0P) were manufactured using resin infusion.

Table B.1. Processing windows and gel times for resins used in composite manufacturing taking into account the loss of pre-gel time taken up by degassing.

Resin	PES (%)	Apparent gel time (minutes)		Fraction of Pre-gel Cure Time Above 100 Pa s
		Processing Window (<100 Pa s)	G'/G" crossover	
100T	0	48	52	8%
	30	35	55	36%
	50	14	47	70%
60D	0	96	99	3%
	30	83	127	35%
	50	49	129	62%

Two composite panels were manufactured for each resin system; one for mode I fracture toughness specimens (incorporating a non-adhesive insert for crack initiation) and one for all other tests.

B.1 Effects of Fibre Architecture on Resin Flow

Initially, composite were manufactured using a unidirectional (UD) fabric. The reason being that ASTM 5528-01 [239] for mode I interlaminar fracture toughness suggests using UD fabric for composite testing, as woven fabrics may experience delamination from the mid-plane resulting in greater scatter of data on the R curves and making a true G_{1c} difficult to establish. Composites were manufactured using a specialist UD fabric that contained no woven binder (the orthodox method of keeping the fibres aligned). Instead, a dissolvable thermoplastic binder lay across the top and bottom of the fabric perpendicular to the fibre direction (see Figure B.1). Using this specialist fibre, the three 60D resins were used to manufacture panels by RFI. All preforms were

subjected to a cure cycle developed within our group that included an initial dwell at 130°C until gelation and a final 2 hour dwell at 200°C.

Figure B.1 Photographs of the thermoplastic-bound UD fabric used to manufacture composites.

Observation of all three cured panels revealed that on both the top and bottom there had been little to no wetting of the fibres. It could also be noted that very little bleed out had occurred. A cross section of the panels showed the majority of the resin had not flowed and remained as a cured film in the centre of the preform (Figure B.2).

These results indicated that flow through the fibre in the z-axis was difficult, if not impossible. Under normal circumstances, lack of resin permeation through a dry preform under vacuum can be associated with a high viscosity; however, as the untoughened 60D resin (very low viscosity) failed to wet the preform completely, other factors must be accountable. As a manufacturing technique, RFI relies on resin permeability in the z-axis of a preform. Whilst wet layup techniques such as resin infusion rely to some extent on z-axis permeability they are more heavily reliant on x and y-axis permeability.

Therefore, when manufacturing composites by RFI it is important to use a fabric that allows for resin flow through the z-axis of the preform. Owing to the lack of binder in the fabric used, each layer is completely flat therefore restricting z-axis resin flow. In orthodox UD fabrics, a glass fibre weft binder is woven through the fabric at 90° to the

warp fibre direction. Whilst the binder provides a crimp to the fabric which in turn is detrimental to some mechanical properties of the cured composite [246]–[248], it is the crimp that provides the space (permeability) between the fibre tows that facilitates resin flow. Consequently, a UD fabric with a small (6 mm) binder spacing, (which increased crimp) was used in a further attempt to manufacture high quality composites (Figure B.2).

Figure B.2. Cross-sectional photograph of a cured composite manufactured using a thermoplastic-bound UD fabric. The photo highlights the cured resin film surrounded by dry fibre.

Composites were again manufactured using the three 60D resins. Observation of the cured 60D-0P panel revealed a high quality composite with good bleed out. A cross-section of the panel showed no resin rich areas, indicating resin had successfully flowed in the z-axis. This confirms the lack of flow in the thermoplastic-bound UD fibre was due to the lack of permeability in the z-axis. Composites manufactured using the toughened resins were not as successful. 60D-50P had results similar to that of the panel manufactured using the thermoplastic-bound fabric, whereas 60D-30P showed a marked improvement with resin flowing throughout the entire preform. However, there were regions at the centre of the panel that were clearly resin rich (similar to composites manufactured earlier), indicating that whilst flow was improved, it was not ideal.

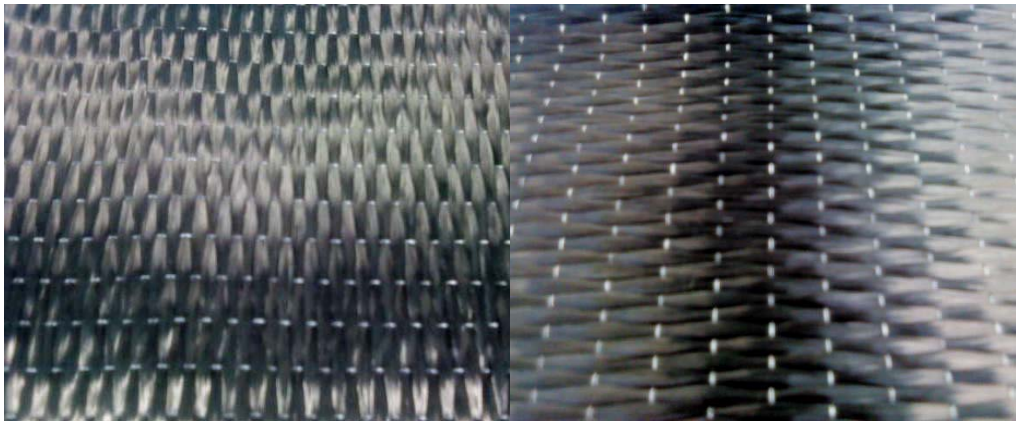

Figure B.3. Pictures of the UD fabric used to manufacture composites using RFI. Binder spacing = 6.0 mm.

In a final attempt to manufacture high quality composites using toughened resin systems, 60D-50P and 60D-30P were used with a 5-harness satin weave fabric (Figure B.3). Owing to the weave of carbon fibre tows the fabric crimp is much higher than the UD fabrics used previously. As such, there is a significant amount of space between the fibre tows in the warp and weft directions, which will enhance z-axis permeability.

Figure B.4. A close up photograph of five-harness satin weave carbon fibre fabric.

Despite the success of manufacturing composites using the untoughened resin and UD fabric, panels were made with 60D-0P and the woven fabric to allow for direct comparison between the resultant mechanical properties. It is also noteworthy that composites manufactured using both untoughened resins were produced using resin infusion and not RFI. Whilst it was possible to use RFI, the low viscosity of the

untoughened resins made it very difficult to transfer the film to the dry preform during layup.

B.2 Assessment of Resin Infusion

Initial visual assessment of the cured panels revealed that the composites were uniform thickness with good bleed out. The surface of 60D-50P showed two dry fibre regions towards the edges of the panel suggesting that resin had not flowed uniformly. This could be due to the high resin viscosity or perhaps the cast resin film was an uneven thickness, which may have led to localised regions in the film with insufficient resin. It is also noteworthy that both the 60D-0P and 60D-30P panels showed small 'shiny flecks' along the overlaps between the weft and warp fibres (see Figure B.5). These areas are most likely dry fibre regions, suggests that whilst resin flow and permeability was excellent, fibre wetting was not.

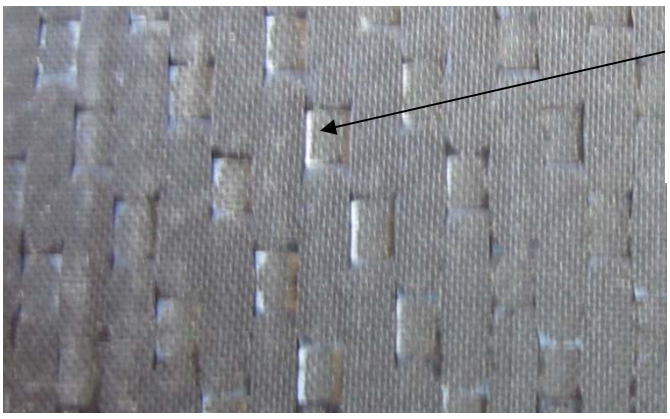

Figure B.5. A photograph of the surface of the cured 60D-0P composite, highlighting the poor surface finish.

Owing to the success of achieving high resin permeability through the woven fabric with the three 60D resin systems, the three 100T resins were used to manufacture composites. Observation of the cured panels revealed resin had flowed and permeated in the z-axis for all three composites. Rather surprisingly, (if one considers the rheology results) 100T-50P flowed through the preform and produced a uniform composite. That said there was a visibly dry section down the centre of the panel on one side, indicating resin had not permeated all the way through the preform. This

suggests (similarly to 60D-50P) that the resin viscosity was too high or an uneven casting of the resin film prior to lay-up.

B.2.1 C-Scan

C-scan was used to assess the homogeneity of the composite panels. The loss of signal strength is known as an increase in attenuation. Variations in attenuation are visibly displayed as different colours allowing for easy identification of areas of non-uniformity. Figure B.6 shows c-scan images of the three 60D panels. The images are displayed using a 15-colour scale corresponding to attenuations of between 0 dB and 45 dB, as shown by the adjacent colour palette. Both the 60D-0P and 60D-30P panels show similar levels of attenuation, with the attenuation varying for the most part between 21 dB and 30 dB. Both panels also show areas with attenuation between 15-8 dB and others of 30-36 dB. This high range of attenuation across both panels suggests a significant non-uniformity. Furthermore, the scattering in attenuation indicates that both composites have a high void content.

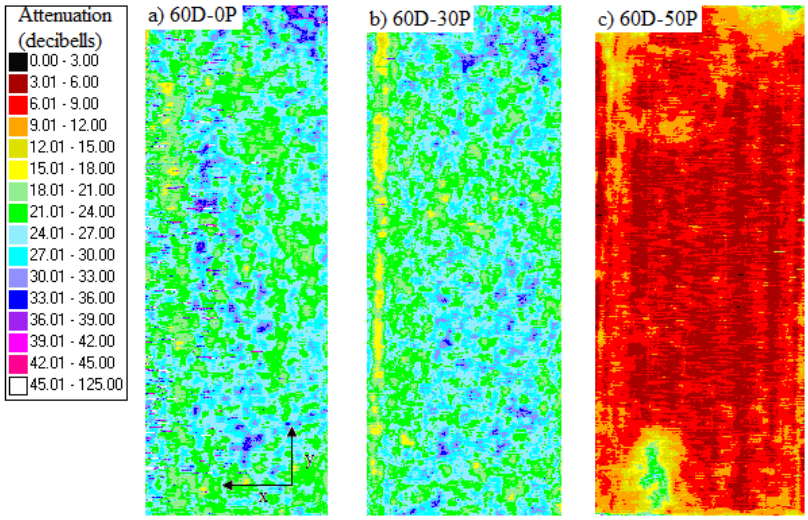

Figure B.6. C-Scan images of composite panels manufactured using (a) 60D-0P, (b) 60D-30P and (c) 60D-50P. Panel dimensions 80 mm (x) and 200 m (y).

60D-50P (shown in B.6c) shows a much lower and more even attenuation across the whole panel, with values for the most part ranging between 3-9 dB. The lack of attenuation for 60D-50P suggests a high quality composite with good fibre wetting. There are areas located at the top right corner and bottom left corner of the panel where attenuation is higher, reaching as high as 21-24 dB. This is due to the dry sports

reported previously. The fact that the attenuation in these regions only ranges between 21-24 dB suggests that the dry spots are only on the surface, indicating the most likely cause for them was an inconsistent thickness in the resin film, resulting in localised regions with insufficient resin to complete fibre wetting. That said the fact that the majority of the panel is of good quality illustrates that a resin formulation containing 50% PES has sufficient flow to manufacture a composite of good quality.

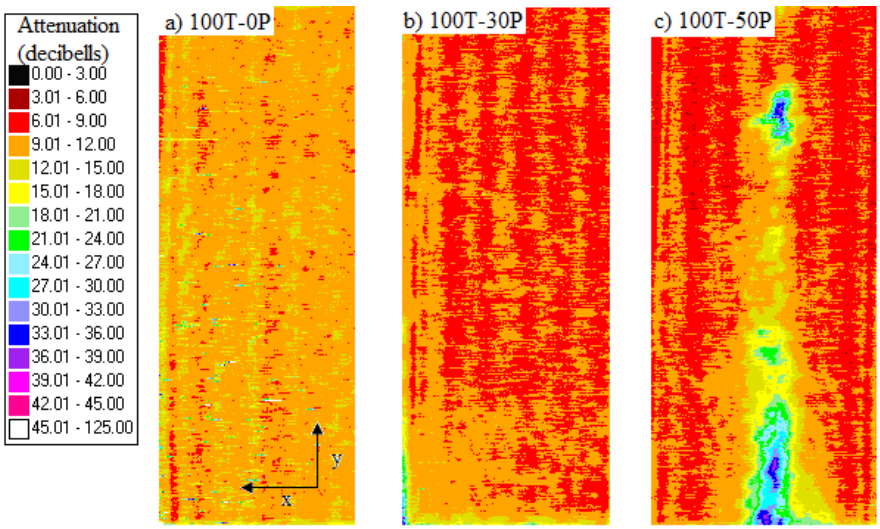

Figure B.7. C-Scan images of composite panels manufactured using (a) 100T-0P, (b) 100T-30P and (c) 100T -50P. Panel dimensions 80 mm (x) and 200 m (y).

Figure B.7 shows the c-scan images of the three cured 100T composites. The attenuation in 100T-0P and 100T-30P are consistent across the two panels. 100T-0P predominately has attenuation ranging from 9-12 dB with patches slightly higher and lower. That said, the range of attenuation over the panel is fairly even and any difference in attenuation is most likely due to slight variation in panel thickness. Similarly, 100T-30P has uniform attenuation only the values are lower, with the majority of the panel having attenuation ranging from 6-12 dB. This range indicates a high quality uniform composite.

The c-scan image for 100T-50P reveals a thin section down the centre of the panel with high attenuation, with areas ranging from 15-36 dB. This corresponds with the visible dry section along one side of the composite surface as mentioned previously. However, the variation in attenuation along the centre of the panel suggests the dry fabric may in places be several layers deep. As was reported for 60D-50P, the most

likely cause for this dry section is an uneven resin film. Despite this flaw, the majority of the panel was uniform with good fibre wetting, allowing for samples to be cut for mechanical testing.

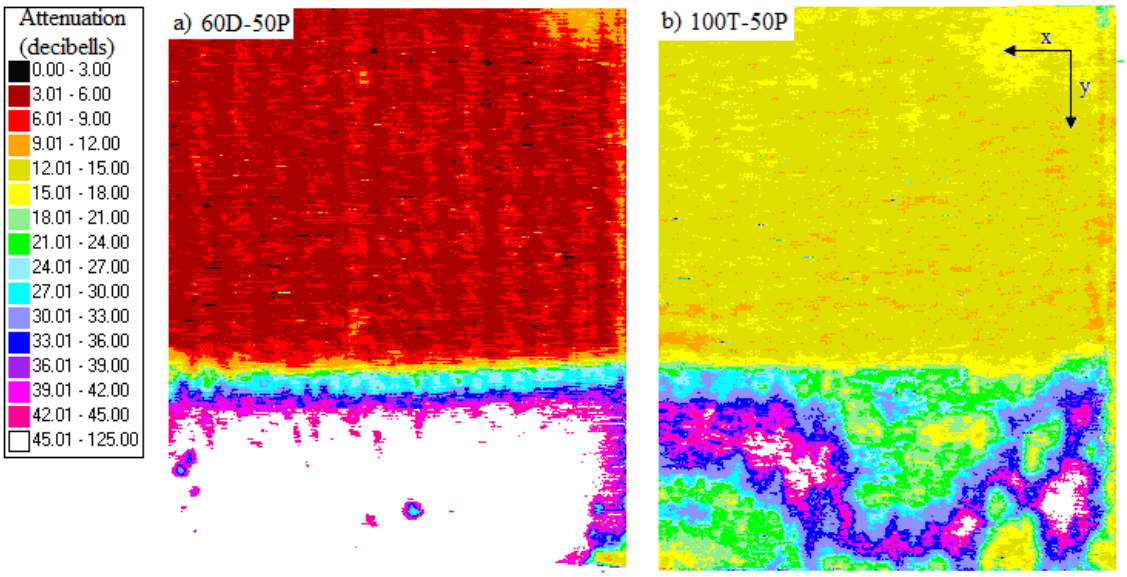

Figure B.8. C-Scan images of composite panels manufactured using (a) 60D-50P and (b) 100T-0P. Panel dimensions 180 mm (x) and 220 m (y).

The fact that both resins containing 50% PES show dry spots indicate that poor resin flow may have been a resin viscosity issue. However, panels made for mode I testing were also c-scanned and the images for 60D-50P and 100T-50P are shown in Figure B.8. Note the bottom third of the c-scan images show high attenuation owing to the polymer insert required for crack initiation in mode I samples. The upper two thirds of both panels show no evidence of any dry spots, and in fact both panels are uniform, indicating that the dry spots reported in the smaller composite panels above were in fact due to an uneven resin film. This confirms that with an accurate casting of the resin film, 50 wt% PES can be used to successfully manufacture composites using a high permeability fabric (such as 5 harness satin weave fabric).

B.2.2 Fibre Volume Fraction and Void Content Analysis

The density of all composites, except 60D-0P and 60D-30P, fall within the range 1.54-1.55 g cm^{-3} (see Figure B.9). The densities of 60D-0P and 60D-30P are ~4% lower at 1.484 ± 0.016 g cm^{-3} and 1.485 ± 0.04 g cm^{-3} respectively. Furthermore, the

standard deviation for the two panels is higher than the other four panels, indicating a lower uniformity.

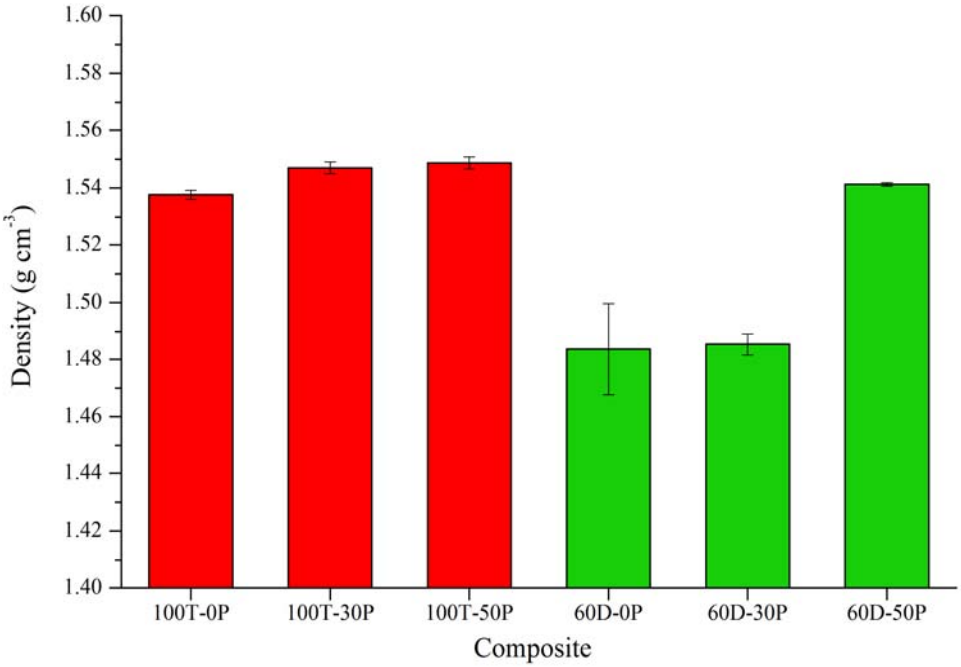

Figure B.9. Panel densities for composites manufactured using 100T and 60D resins loaded at 0%, 30% and 50% PES following original cure cycle.

The fibre volume fractions (V_f) for the composites are shown in Figure B.10 and the void contents in Figure B.11. Fibre volume fractions and void contents were measured for all composites using acid digestion, in accordance with ASTM D 3171-09 [237]. Figure B.10 shows 100T-30P had the lowest V_f of 55.5%. Despite it being comparatively low, the V_f for the 100T-30P composite is of an acceptable standard for high quality composites. It is interesting to note that all the 60D composites have a V_f higher than all 100T composites, suggesting that the longer flow times of the 60D resins allowed for better bleed out, increasing the V_f. 60D-30P had the highest V_f of all the panels, most likely due to the favourable rheological properties of the resin. Table B.1 shows that this resin has a longer processing window than 60D-0P and a similar PW to 60D-50P, yet its initial viscosity is lower than 60D-50P. These two characteristics increase resin flow resulting in a higher V_f.

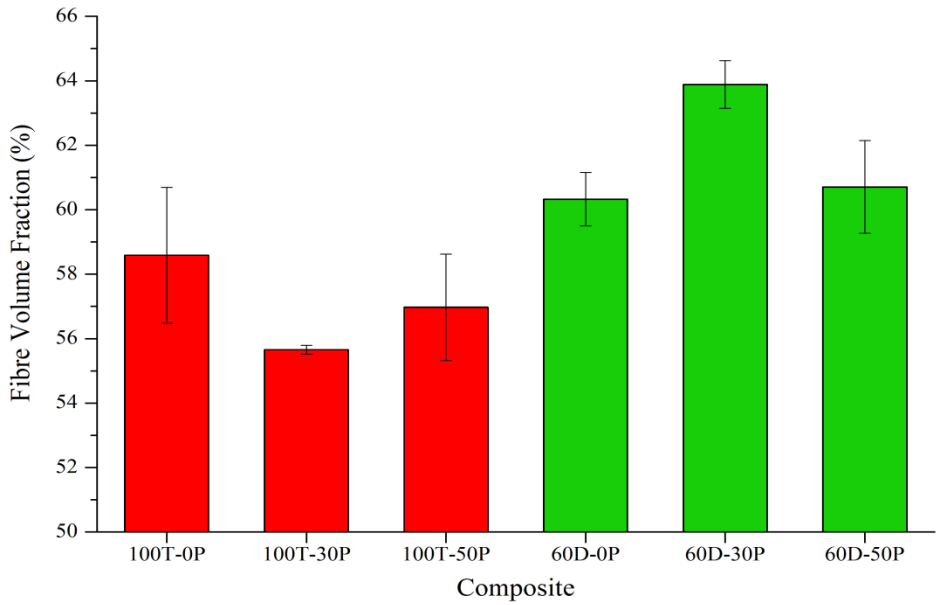

Figure B.10. Fibre volume fractions for composites manufactured using 100T and 60D resins loaded at 0%, 30% and 50% PES following the original cure cycle.

The void contents of all the panels are shown in Figure B.11. The values for all panels except 60D-0P and 60D-30P, were below 3.5%, with 100T-30P having the lowest void content at 1.4%. Whilst these values are relatively low they are still above the maximum 1% void content limit set for aerospace grade composites [147], [151]. That said, Tang [249] suggested that a void content up to 4% has little effect on the mechanical properties indicating that any variation in properties (except 60D-0P and 60D-30P) is a result of the materials present. The most likely reason for the high void contents is the lack of any additional pressure applied during cure; that is, preforms were cured under vacuum-only pressure without additional external pressure from an autoclave. Currently, low void-content aerospace composites are manufactured using autoclave curing at high pressure [153]. The results shown in Figure B.11 support the need for additional pressure in obtaining void contents below 1%. Garschke et al. [143] studied the effects of altering the cure cycle on carbon fibre-epoxy resin composites cured in an oven. They found fibre volume fractions ranging between 52-56% and void contents between 2-5% depending on the cure cycle, results that are in agreement with those of this thesis.

Figure B.11 also shows that panels 60D-0P and 60D-30P have very high void contents, with values in the region of 7.5-8%. This is not surprising if one considers

the c-scan images (Figure B.6), which clearly indicate a high level of non-uniformity. Voids are formed due to entrapment of air during resin formulation, moisture absorption during material storage and processing, inadequate temperature and/or pressure and loss of vacuum in the vacuum bag during cure [148]. As both panels were degassed and cured at the same time the most likely cause for the high void content are loss of vacuum during cure caused by a leak in the vacuum bag. However, manufacturing repeat panels using the two resins led to the same poor composite quality.

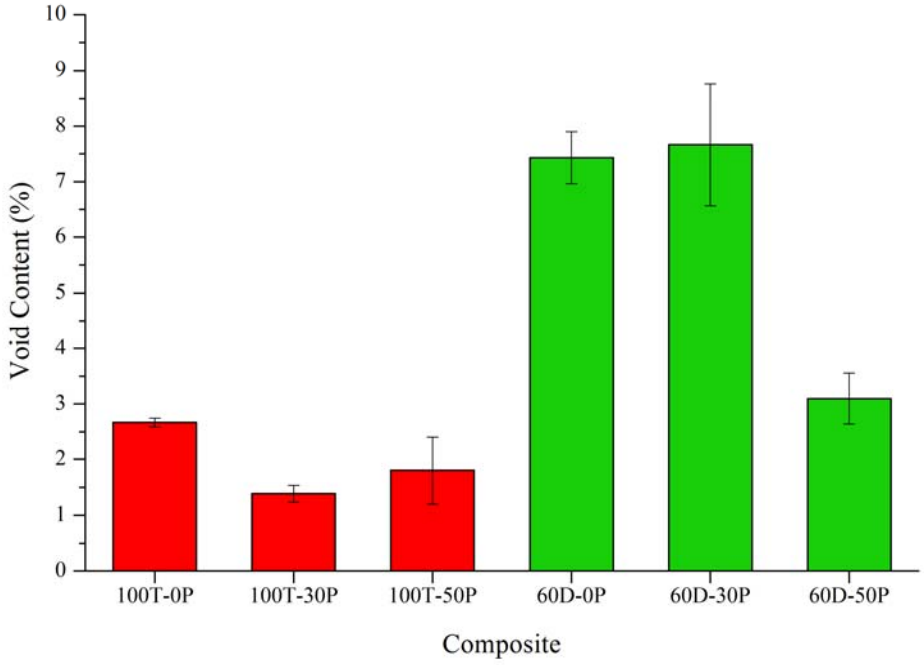

Figure B.11. Void contents (%) for composites manufactured using 100T and 60D resins loaded at 0%, 30% and 50% PES.

During the cure of all composite panels in this thesis, a vacuum pressure was maintained by connecting the vacuum bag to a vacuum outlet. As such, the vacuum was constantly drawing resin from the preform to aid resin flow and to remove excess resin. Stringer [250] suggested a somewhat uncommon source for void formation in cured composites manufactured by wet layup techniques under vacuum pressure. He stated that excessive bleed out of the resin during cure can lead to resin starvation, ultimately resulting in high void contents. Furthermore, he went on to study the effects of viscosity on composite quality in terms of void content and V_f. He concluded that additional vacuum pressure should only be applied to the preform once the resin

viscosity is above a critical level. In his study he reported this to be level to be above 7.5 Pa s, and that the application of additional pressure above a viscosity of 16 Pa s has no added benefits to the composite quality. Additionally, if a resin viscosity was at no point below 16 Pa s composites were found to have a low $V_{f,}$ although the void content remained unaffected.

Stringer's results fit for the most part with those presented in this thesis. From the apparent gel times of the six resins (Table B.1), the 60D systems have a significantly longer gel time compared to the 100T systems, hence giving increased bleed out. Therefore, what initially seemed like a benefit in having a longer processing window with the addition of DGEBF has been detrimental to the composite quality. Furthermore, 60D-0P and 60D-30P have much lower viscosities than 60D-50P and therefore have a longer period where the viscosity is below 7.5 Pa s. Figure B.12 shows the viscosities of the three 60D resins taking into account degassing and the ideal viscosity window proposed by Stringer. What is noteworthy from Figure B.12 is that after degassing both 60D-0P and 60D-30P have in excess of 63 minutes before reaching 7.5 Pa s. According to Stringer, during this period the viscosity is too low, which results in excess bleed out (as was found based on the void content and c-scan images of the two composites). 60D-50P however only has 6 minutes within the 7.5-16 Pa s window where good consolidation can be achieved. There is no point in the cure cycle where the viscosity is below 7.5 Pa s. Owing to this, the void content is much lower, around 3%.

Figure B.13 shows the same details regarding viscosity and processing times but for the 100T resins. The time 100T-0P spends below 7.5 Pa s once degassed is 38 minutes, similar to 60D-30P at 33 minutes. Interestingly the void content of 100T-0P is significantly lower than 60D-30P, despite both systems experiencing similar periods at low viscosity.

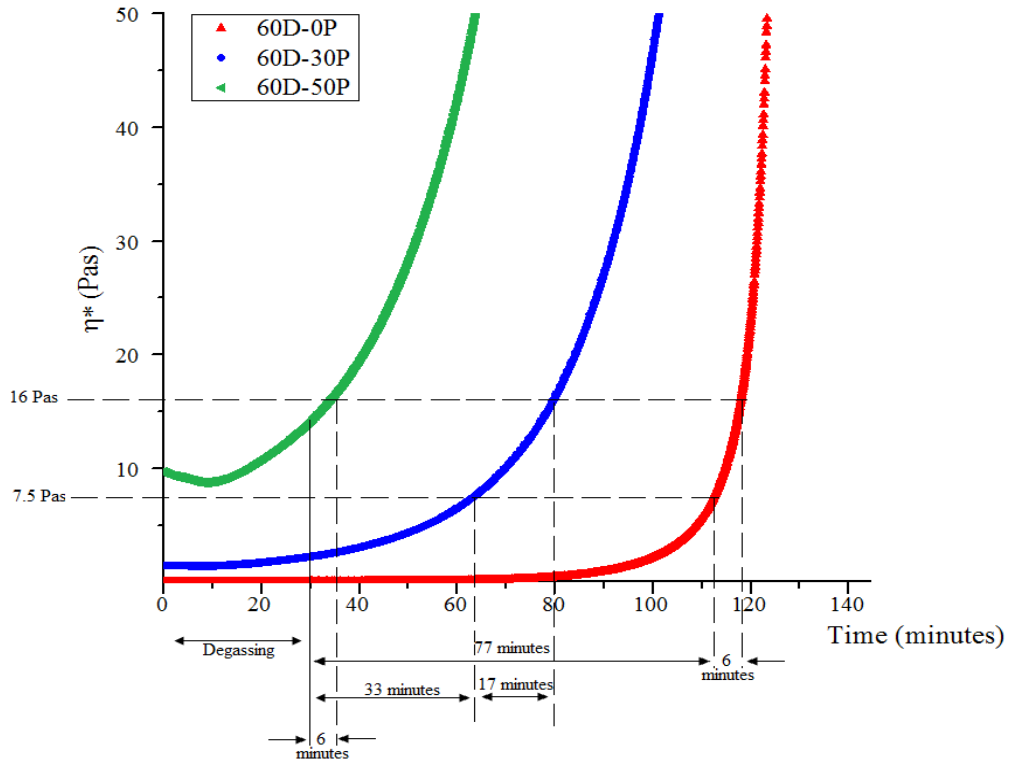

Figure B.12 Viscosity profiles at 130°C for 60D-0P, 60D-30P and 60D-50P at the beginning of cure cycle with limits and timings following the results of Stringer [250]**.**

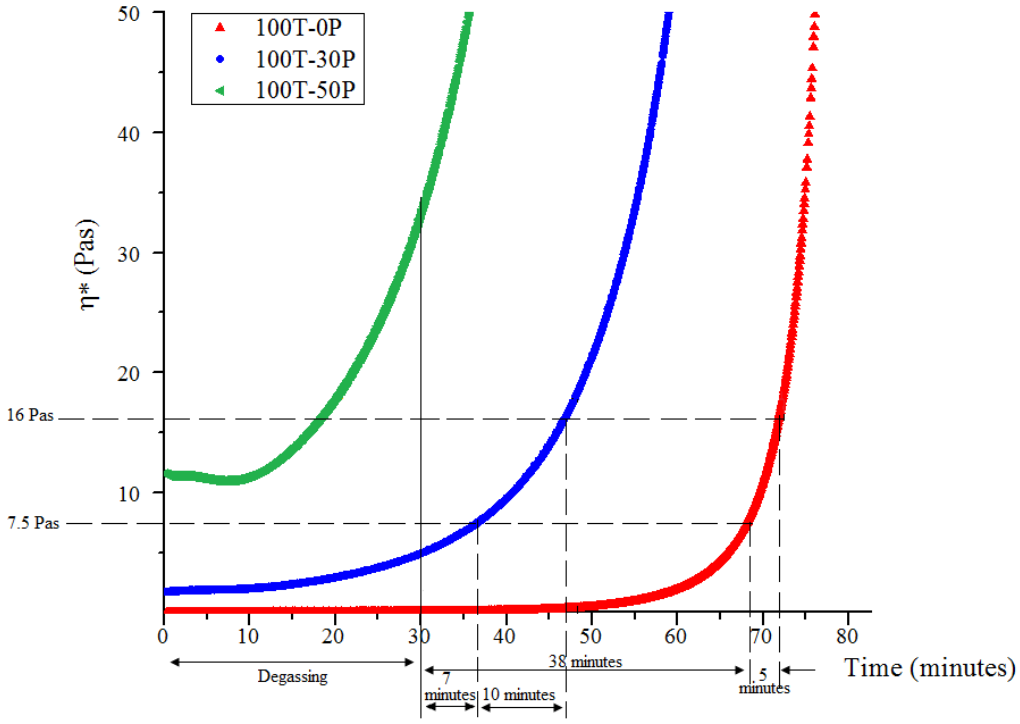

Figure B.13 Viscosity profiles at 130°C for 100T-0P, 100T-30P and 100T-50P at the beginning of cure cycle with limits and timings following the results of Stringer [250]**.**

Based on this, the viscosities suggested by Stringer may only be applicable to his work and that for the resins used in this thesis a different ideal viscosity exists. That said, the highest quality composite, 100T-30P, had a void content of 1.4% and had the shortest period below 7.5 Pa s, which fits with Stringers predictions. Additionally, 100T-30P had the lowest V_f as shown in Figure B.9, further supporting his work which claimed that a shorter time spent at low viscosities would result in a low V_f.

An interesting comparison from the void content and V_f results can be made regarding the two 50% PES resins. 60D-50P has a significantly longer gel time that apparently leads to an increase in V_f from 57% in 100T-50P to 60% in 60D-50P. Whilst this seemingly suggests a longer gel time improves composite quality, the void content results suggest otherwise, as 60D-50P was found to have a void content ~1% higher. This indicates that for high viscosity resins it is very difficult to develop a high V_f, and low void content composite without the application of additional pressure.

B.3 The Effects of Adding a Vacuum-free Dwell

Taking regard of the results reported by Stringer [250], preforms of 60D-0P and 60D-30P were subjected to a 'pre-cure' in an attempt to improve the composite quality. Preforms were held at 130°C until the viscosity increased to 7.5 Pa s before a vacuum was applied. Whilst the same method could be used to improve the other four composites, the quality of these panels was deemed high enough (both in terms of V_f and void content) to provide an accurate representation of the materials mechanical properties. From the rheology results for the resins, the 'pre-cure' period was calculated taking in to account degassing; after which additional pressure was applied via a vacuum pump.

Initial visual assessment of the cured panels suggested that the composites were uniform thickness with good bleed out. Unlike the previous attempt to manufacture composites using 60D-0P and 60D-30P the surface finish was even without any noticeable 'shiny flecks' indicating better fibre wetting. C-scan images of the panels (Figure B.14) revealed a much lower attenuation than was found for the previous attempts, with values for the most part ranging from 6-12 dB, similar to the high quality panels manufactured using the four other resin systems shown earlier.

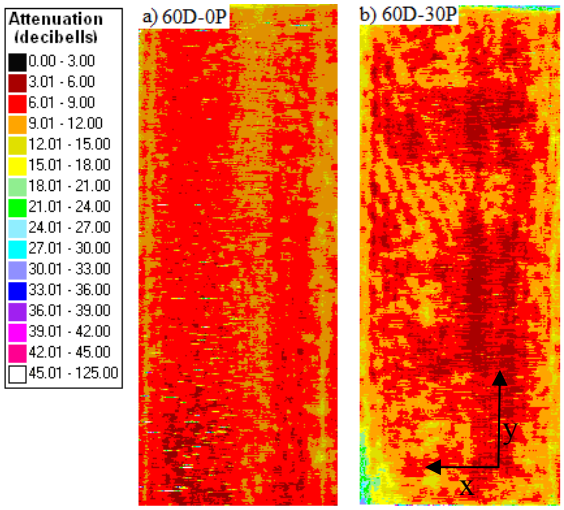

Figure B.14. C-Scan images of composite panels manufactured using (a) 60D-0P and (b) 60D-30P with a modified cure cycle including a vacuum-free dwell. Panel dimensions 80 mm (x) and 200 m (y).

The V_f values of the two panels cured with the modified cycles are shown in Figure B.15 along with those of the panels using the original cure cycle for contrast. Comparing the results from the two cure cycles leads to no obvious conclusions, with the fibre fractions remaining similar for both resins. The one notable result of the change in cure cycle is the standard deviation associated with the measurements, which for the modified cure cycle are much lower. This suggests (in accordance with the c-scan results) that the vacuum-free dwell resulted in a more uniform composite.

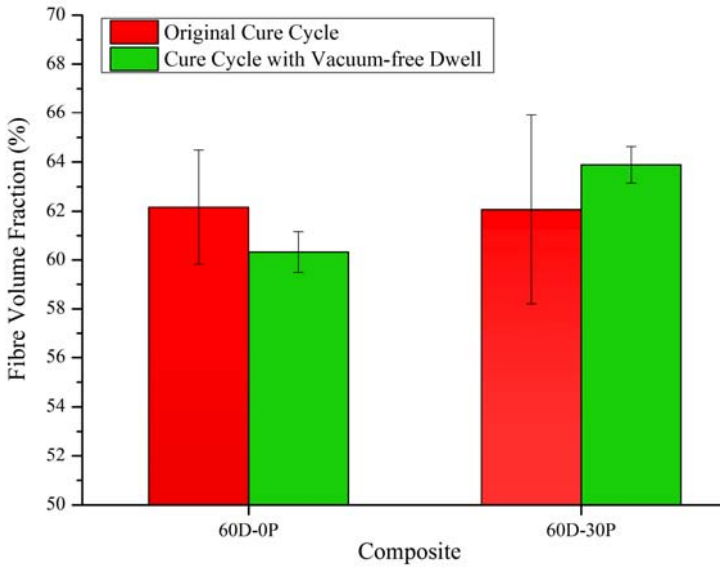

Figure B.15. Fibre volume fractions (%) for 60D-0P and 60D-30P: a comparison between the original values and those of the cure cycle containing a vacuum-free dwell.

Further confirmation of this is given in Figure B.16, which shows a comparison between the void content percentages for the original and modified cure cycles. The composites manufactured using the original cure cycle had void contents between 7.5-8%. With the use of the vacuum-free dwell, these percentages dropped to 3-3.5% for both the 60D-0P and 60D-30P panels. Therefore, the increase in initial viscosity prior to the application of the vacuum significantly improved the composite quality.

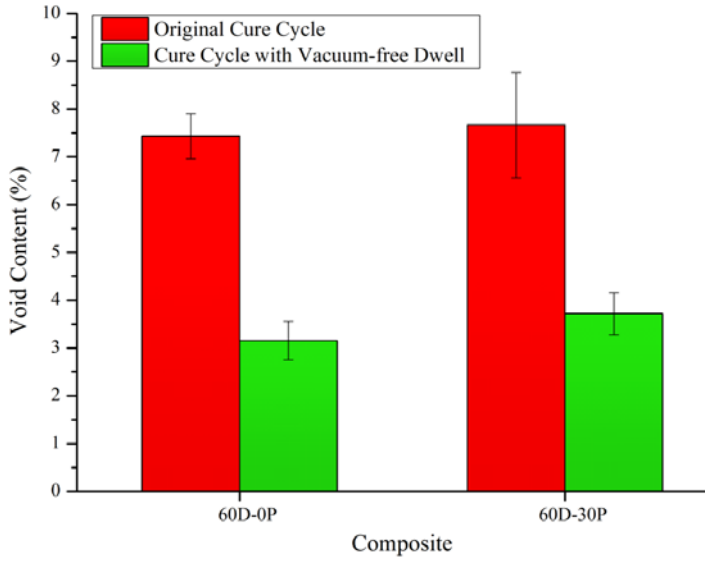

Figure B.16. Void contents (%) for 60D-0P and 60D-30P: a comparison between the original values and those of the cure cycle containing a vacuum-free dwell.

However, the void contents are still slightly higher than for all three 100T panels, suggesting that whilst the use of the vacuum-free dwell improved the composites quality the cure cycle was not completely optimised. Optimising the cure cycle would require a trial and error approach as to the length of time spent at the initial dwell. Additionally, the optimisation would be bespoke for each resin formulation, something that is beyond the scope of this work. Despite the lack of cure cycle optimisation the void contents for all six composites was below 4%. Using the work of Tang [249] as a guideline, all composites are of a satisfactory standard and any deviation in measured mechanical properties is due to the material properties.

B.4 Mechanical Properties

B.4.1 Mode I Double Cantilever Beam (DBC) Fracture Toughness

The mode I interlaminar fracture toughness was determined using a double cantilever beam (DCB) technique [239]. ASTM 5528-01 states the composite specimens should be manufactured using unidirectional fibre, as the use of non-unidirectional fibre may result in delamination from the midplane or significant data scatter resulting in 'unique' R curves. Attempts were made and recorded earlier in this chapter to use UD fibre to manufacture composites for mode I testing, however owing to processing constraints this was not possible. As such mode I samples were manufactured using a five harness satin weave carbon fibre.

Typical load versus crack opening displacement (COD) curves for the three 100T composites are shown in Figure B.17. The initial applied load increased linearly with crack opening displacement (COD) for all composites. After the initial crack, measurements were recorded whenever the crack propagated further. According to the standard, measurements should be taken at precise COD's, however owing to the use of woven fabric crack propagation often jumped; as such, measurements were recorded whenever possible. After the initial crack propagation the load versus COD plots showed a downward trend, whereby a greater COD resulted in a lower load required to propagate the crack further. 100T-0P did not show this trend as can be seen in Figure B.17. The load seemingly increases slightly with COD, however; a potential explanation for this is the nature of the crack tip. In all of the other composites tested crack propagation occurred via a single crack tip along the midplane. However, in 100T-0P the crack often jumped from the midplane onto neighbouring planes, resulting in multiple crack tips. The high crosslink density of the resin coupled with the lack of toughener seemingly leads to a low interlaminar fracture resistance, making accurate mode I G_{IC} measurements difficult to achieve. Whilst the measurements may not be a true reflection of G_{IC} for 100T-0P, they were recorded for comparison with the other composites.

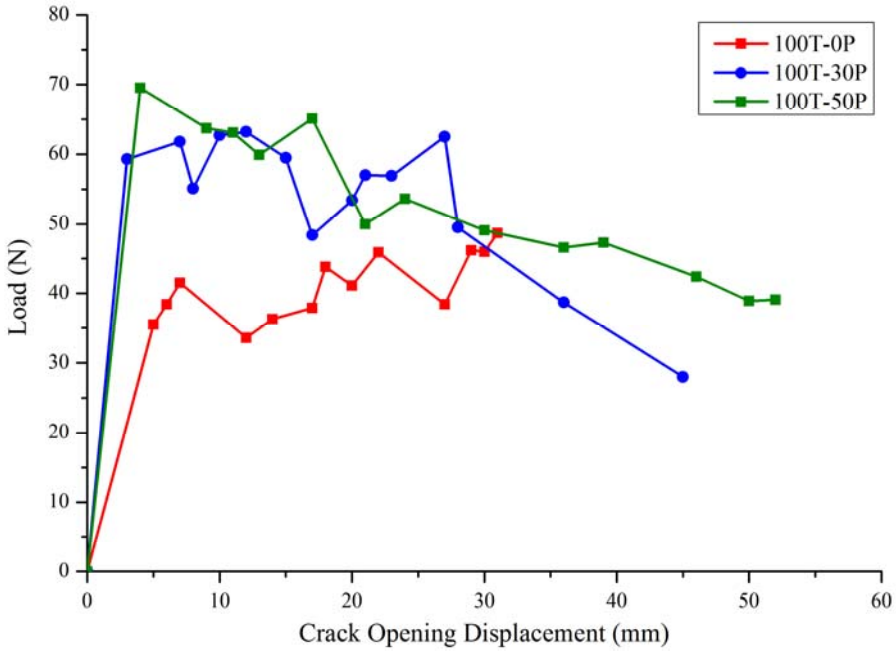

Figure B.17. Typical duel cantilever beam (DCB) load versus crack opening displacement for composites manufactured using 100T resins loaded with PES at 0%, 30% and 50%.

The initial mode I fracture toughness (G_{1C}^{INIT}) was determined from the load versus COD curves using the point of deviation from linearity on the initial rise in load. The results for G_{1C}^{INIT} are shown in Figure B.18. The trends for G_{IC} of the composites echo the results of the neat resins studied in chapter 6, whereby an increase in PES loading results in an increase in G_{1C}^{INIT}. The extent to which PES influences G_{1C}^{INIT} appears to vary between the 100T and 60D systems, with a greater effect observed for 100T. The G_{1C}^{INIT} values of the two untoughened composites are very similar at ~0.2 kJ m^{-2}. Upon addition of 30% PES G_{1C}^{INIT} of the 60D system increased by 52%, whereas the addition of 30% PES increases G_{1C}^{INIT} of 100T by 109%. This trend continues with 50% PES loading, as 60D has a G_{1C}^{INIT} improvement of 129% over the untoughened matrix, whereas the G_{1C}^{INIT} of 100T increases by 204%. The similarity between the untoughened composites suggests that the effect of any variation in crosslink density of the matrices is negligible towards G_{IC}, therefore the improved G_{1C}^{INIT} gained in the 100T systems are attributable to the phase separated morphology known to develop during the epoxy-amine network formation. The lack of phase separation in the 60D systems led to a homogeneous morphology that invariably resulted in poorer fracture resistance.

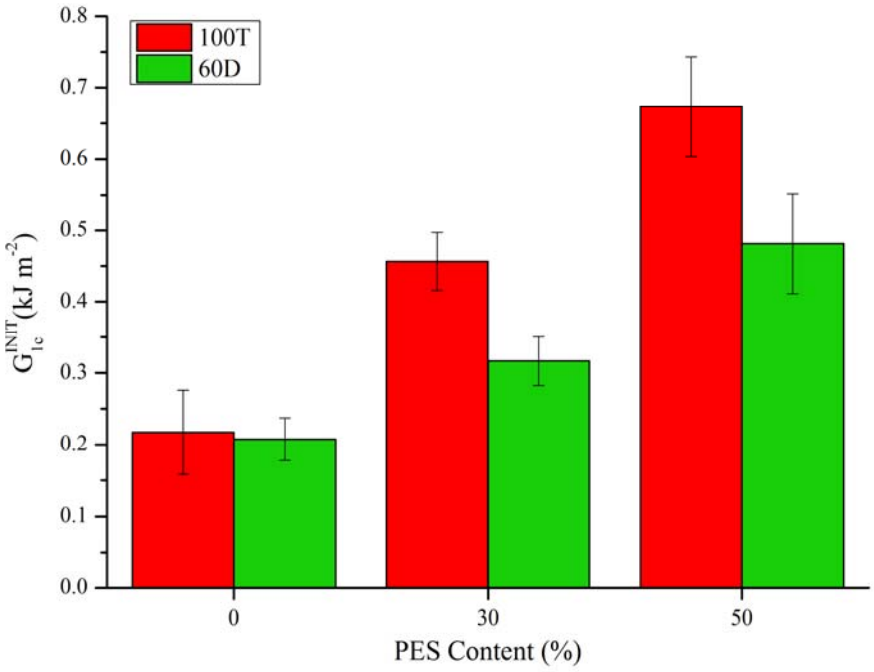

Figure B.18. The initial mode I interlaminar fracture toughness (G_{IC}^{INIT}) for composites manufactured using resin systems of 100T and 60D loaded at PES levels of 0%, 30% and 50%.

The effects of varying PES addition on composite G_{IC} appears to be somewhat of an unpublished topic. Whilst the effects of PES loading is a heavily studied topic for neat epoxy resins, no literature was found examining the effects of PES loading on TGPAP or DGEBF matrices when incorporated in a composite. Nor was any literature found on composites manufactured with DGEBA-PES, a frequently studied resin system. The only relevant study was that by Fernandez et al. [126], who studied the effects of varying PES loading in a TGDDM-DDM matrix reinforced with carbon fibre. They reported a phase-separated matrix via DMTA and SEM; however over the PES-loading range studied (≤15 wt%) there was little change in G_{IC} for the composites, with values remaining consistently between 0.30-0.40 kJ m^{-2} for all compositions. The lack of improvement in fracture resistance with PES addition may be due to the narrow range over which it was studied, as only up to 15 wt% PES could be added most likely due to the high initial viscosity of the TGDDM prepolymer.

Figure B.19 shows the mode I interlaminar fracture toughness (G_{Ic}^{PROP}) versus the crack length for 60D-50P and 100T-50P. For both composites G_{IC} increases with crack length although owing to the woven fabric used in these composites crack propagation is not steady, resulting in a jagged R-curve. Results by De Baere et al. [251] are in

agreement with those shown in Figure B.19. They studied the mode I fracture toughness of composites manufactured using a five harness satin weave fabric and reported the R-curves as 'saw tooth-like'. The R-curves shown in Figure B.19 are therefore typical of woven fabrics and indeed all the specimens tested in this study showed similar results.

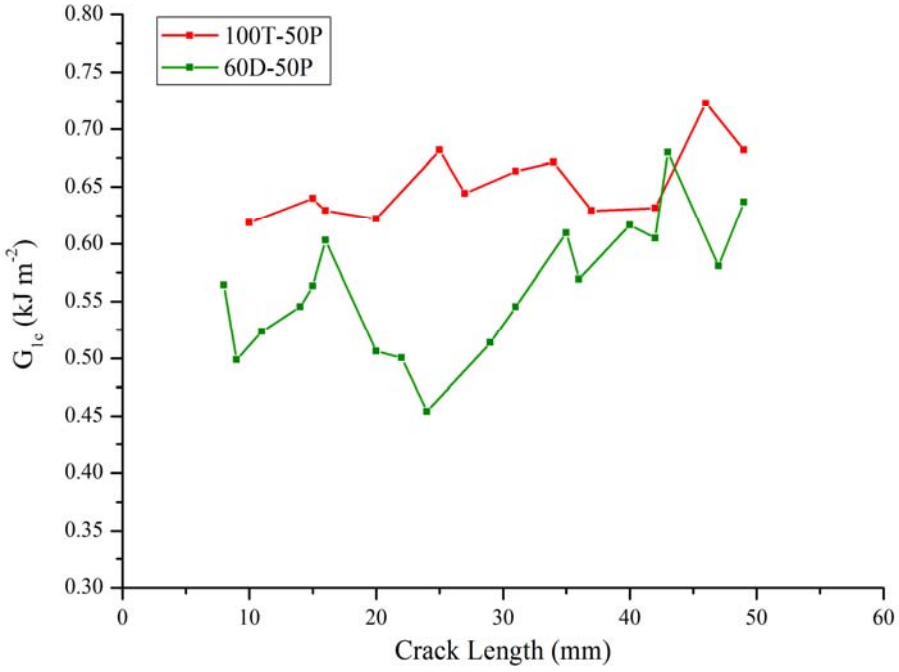

Figure B.19. Mode I interlaminar fracture toughness (G_{IC}) versus crack length (also known as R-curves) for 100T-50P and 60D-50P.

Composites manufactured from UD fabric used for mode I testing generate stable crack growth that allow measurements to be taken at precise COD's. This in turn allows average G_{IC} measurements to be made at each specified COD, which in turn can be used to generate standard deviations. The use of woven fabric meant measurements were taken whenever possible. Consequently, there is no consistency in precisely when the measurements were recorded, even between specimens of the same composite, making quantitative analysis difficult. As such, no error bars are provided for G_{1C}^{PROP} data. In an attempt to quantitatively analyse G_{1C}^{PROP}, the results from the five specimens tested for each composite were grouped as 'one sample' and plotted as a scatter graph (Figure B.20). From these plots, a line of best fit was taken through the scatter data and this was used as a means of comparison for the G_{1C}^{PROP} between composites manufactured with different resin systems.

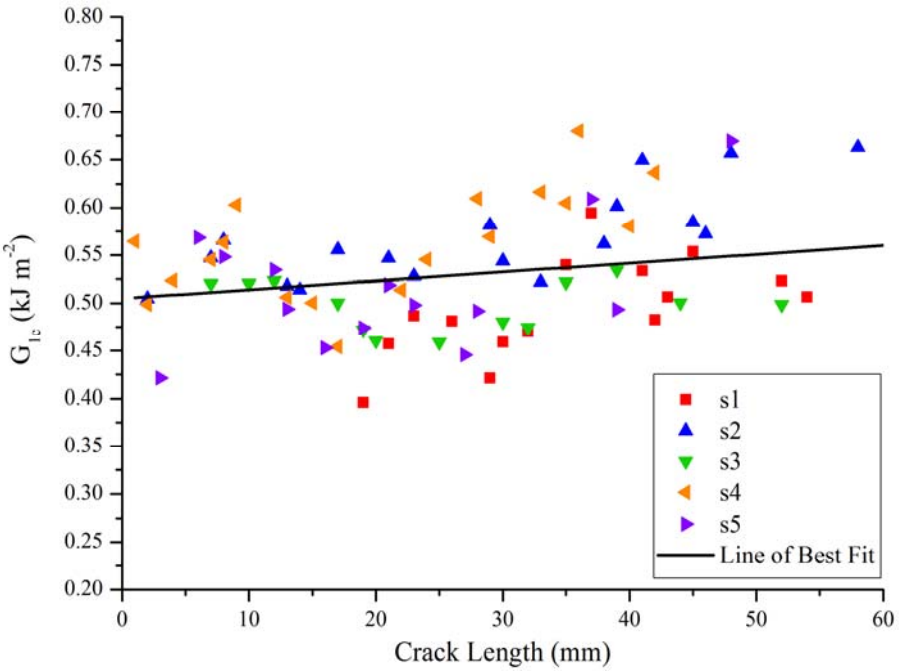

Figure B.20. A scatter plot of the mode I interlaminar fracture toughness (G_{IC}) versus crack length for five specimens of 60D-50P with a linear line of best fit.

Figure B.21 shows the linear lines of best fit for G_{1C}^{PROP} taken through the data points for the 100T composites. R^2 values for 100T-0P, 30P and 50P are 0.74, 0.35 and 0.05 respectively. These values indicate that as the level of toughener increase so does the scatter of the data. In other words, the inclusion of a second phase in the matrix increases the variation in the composites fracture data. It is worth noting that 100T-0P is only plotted to a 40 mm crack length. As stated previously, crack propagation in 100T-0P did not always occur along the midplane owing to the poor interlaminar fracture resistance. As the crack length increased, the crack increasingly deviated from the midplane. This ultimately led to failure of the specimens through interlaminar fracture before reaching the desired 60 mm crack length. This problem was not found for the toughened 100T composites, suggesting that PES improved interlaminar fracture toughness.

It is clear from Figure B.21 that the G_{1C}^{INIT} increases with PES content as was reported in Figure B.18. A second notable trend from the figure is the gradient of the three lines, whereby an increase in PES content reduces the gradient. This is potentially a result of micro-cracking within the polymer matrix.

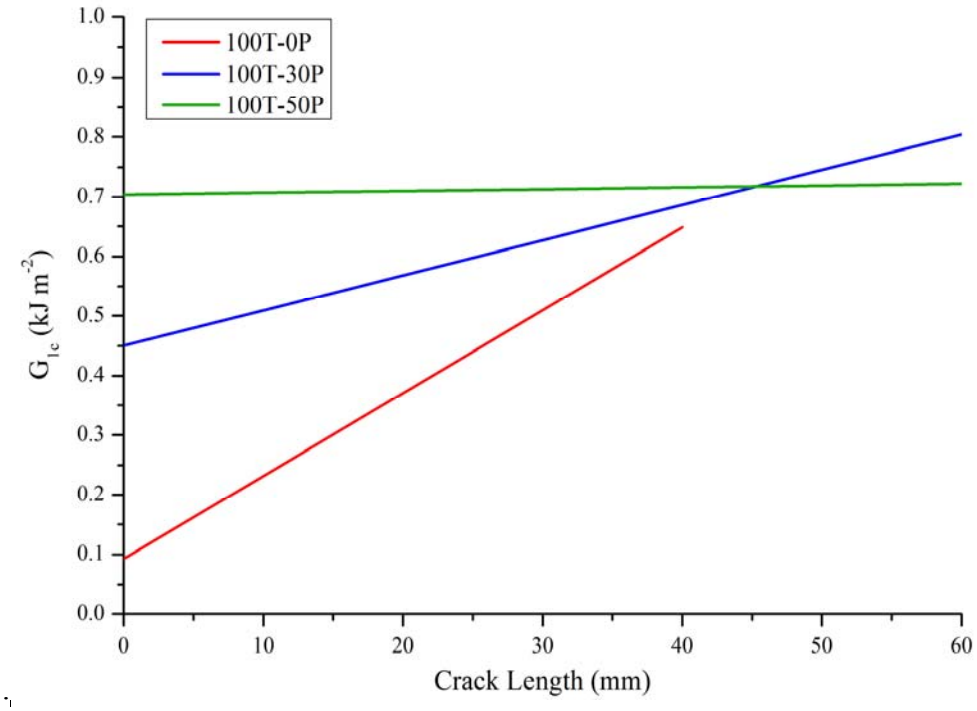

Figure B.21 A comparison between the linear lines of best fit taken from the mode I interlaminar fracture toughness (G_{IC}) versus crack length plots for 100T-0P, 100T-30P and 100T-50P.

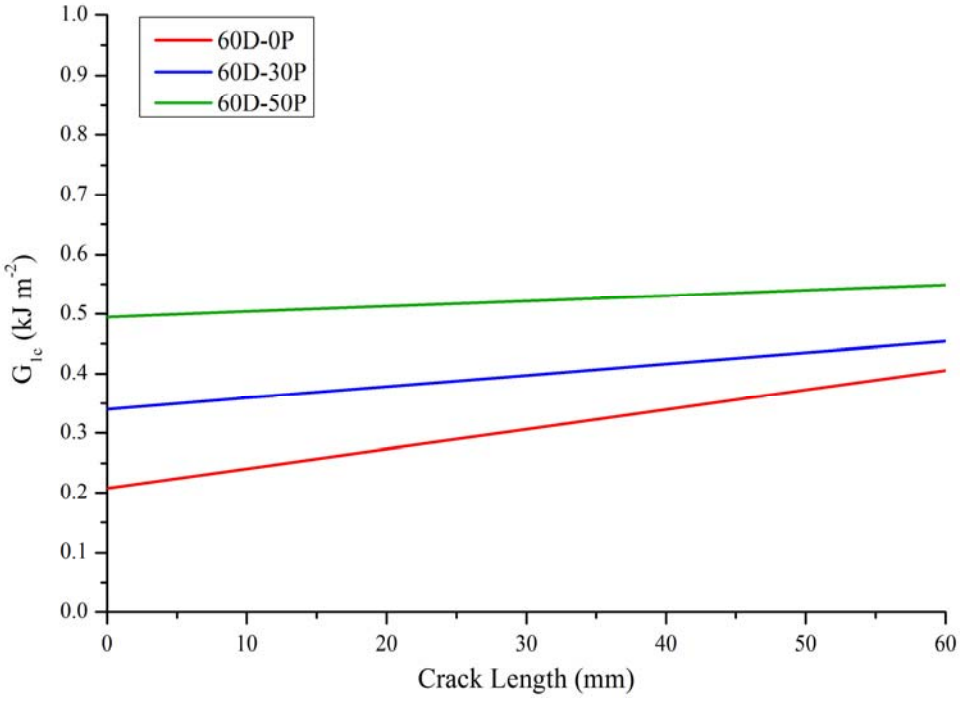

Figure B.22 A comparison between the linear lines of best fit taken from the mode I interlaminar fracture toughness (G_{IC}) versus crack length plots for 60D-0P, 60D-30P and 60D-50P.

Mimura et al. [110] showed that phase separated PES domains can lead to significant branching at the crack tip, as crack propagation is unfavourable through the PES 'rich' phase. G_{IC} is a measurement of the energy dissipated during fracture per unit of newly created fracture surface area. The fact that G_{IC} does not increase with crack length suggests that there is not a significant localised build-up of energy at the tip, most likely because micro-cracks in the phase-separated matrices dissipate the energy.

Figure B.22 shows the linear lines of best fit for G_{1C}^{INIT} taken through the data points for the 60D composites. R^2 values for 60D-0P, 30P and 50P are 0.43, 0.21 and 0.06 respectively. The trend between PES content and R^2 values corresponds with that found for the 100T composites, whereby increasing the PES content leads to an increase in data scatter. Similar to the G_{1C}^{PROP} results for 100T composites, an increase in PES increases G_{IC} for 60D composites, however the extent to which its inclusion affects G_{IC} is smaller. As discussed earlier for G_{1C}^{INIT} this is most likely due to the differing morphologies in the matrices, whereby the 60D toughened resins are homogenous and the 100T matrices show phase separation.

Comparison between the G_{1C}^{PROP} lines of best fit for the untoughened resins highlights the effects of crosslink density on resistance to crack propagation. In 60D-0P the crack propagated fully along the midplane until the desired 60 mm crack length, unlike 100T-0P. This suggests a higher interlaminar fracture resistance in 60D-0P. What is more, the gradient of the G_{IC} for 60D-0P is much shallower than 100T-0P. It is possible that the brittleness of the highly crosslinked 100T-0P matrix results in a sharper crack tip compared to 60D-0P; ultimately leading to a higher energy dissipation when the crack progresses.

B.4.2 Interlaminar Shear Strength (ILSS)

The interlaminar shear strength (ILSS) was measured using short beam 3-point bending in accordance with ASTM 2344/D [244]. ILSS is widely accepted as a means of measuring the failure of laminates in shear. It is well documented that the ILSS of a composite is largely dependent on the void content [147]–[149] as voids act as crack nucleation sites; thus higher void contents lead to a greater number of nucleation sites that can lead to premature failure. In all six composites, the void content was below

4% (see Figure B.11 and Figure B.12). Whilst there is research which suggests minimising the void content leads to an improvement in ILSS, Tang [249] reported that a void content up to 4% has little effect on the mechanical properties. Furthermore Hernandez et al. [160] attempted to relate ILSS to void content by fitting a model to experimental results they obtained using the least squared method. Whilst the author claimed a good fit between the experimental results and the model (i.e. that it showed a reduction in ILSS with void content) observation of their results shows them to be more in agreement with Tang [249] in that composites manufactured with 0.5% void content had a comparable ILSS to composites manufactured with a 3% void content. With this in mind, the results found for all composites in this study are of a satisfactory standard and that any deviation in ILSS is predominantly due to the material properties.

ILSS for the six composites are shown in Figure B.23. From the figure, the effects of PES on composites manufactured using 60D is minimal, with a slight increase in ILSS as PES content increases. Owing to the high number of specimens used for each composite, a student's T-test was used to determine whether the ILSS's measured were significantly different from one another, in particular the weak trend showing an increase in ILSS with PES content for the 60D composites. T-test results comparing the three 60D resins are shown in Table B.1. The table indicates that a significant difference exists between 60D-0P and 60D-30P, and 60D-30P and 60D-50P at the 95% confidence level. The difference between 60D-0P and 60D-50P is significant at the 99% confidence level, suggesting that whilst the improvement in ILSS for 60D with PES content is small over the range 0-50% PES, it is statistically significant.

Fernandez et al. [126] studied the ILSS of a woven carbon fibre composite with a TGDDM-DDM matrix, varying the addition of PES in the range 0-15 wt%. They reported no significant variation in ILSS with PES content and suggested the similarity in results was due to the lack of phase separation in the matrix. Whilst the results in this study are significant between 0% and 30% PES for the homogeneous matrices (60D), the ILSS only increases slightly; suggesting that at 15 wt% PES loading, similar results may be obtained to those of Fernandez.

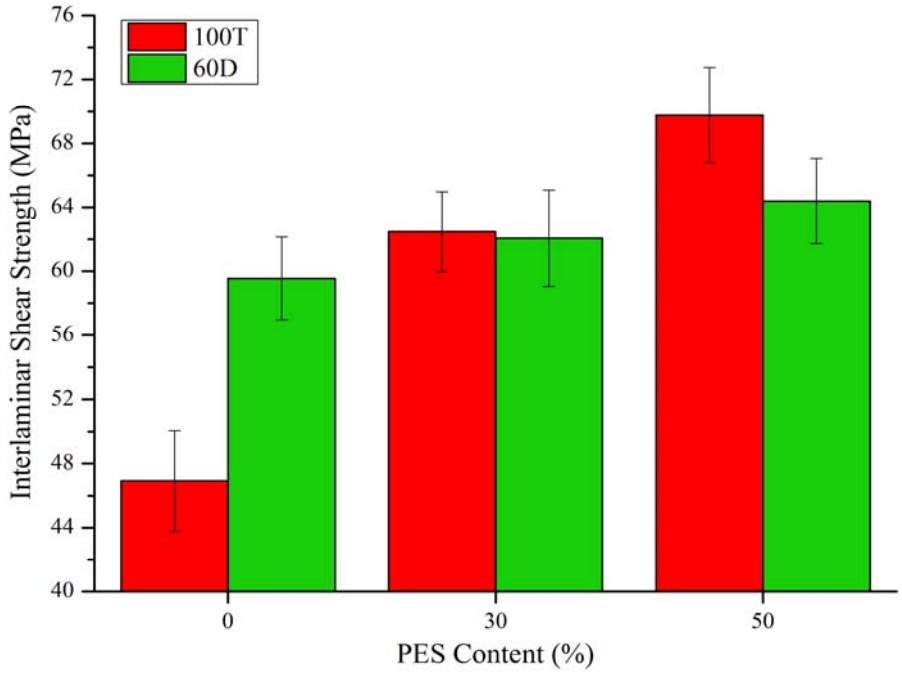

Figure B.23. Interlaminar shear strength (ILSS) of composites manufactured using 100T and 60D resins loaded with PES at 0%, 30% and 50%.

Table B.1. Results for the student T-test comparing ILSS results for composites manufactured from 60D at PES loading levels of 0%, 30% and 50%.

Comparison	Significance
60D-0P vs 60D-30P	97.6%
60D-30P vs 60D-50P	95.8%
60D-0P vs 60D-50P	99.9%
100T-50P vs 60D-50P	99.9%

The effect of PES on the ILSS of 100T composites is far greater, with a 49% increase in ILSS from 0% to 50% PES loading. This increase is attributable to the much lower ILSS of the 100T-0P composite compared to 60D-0P, with values of 46.9 ± 3.2 MPa and 59.5 ± 2.6 MPa respectively. The difference between these two values is due to material properties; namely the crosslink density of the epoxy matrix, whereby a higher crosslink density (found in 100T) leads to a reduction in the ILSS. This find is again supported by Fernandez [126] who reported the ILSS of composites with

matrices of TGDDM (a highly crosslinked epoxy resin similar to TGPAP) to be ~50MPa, similar to 47 MPa found for the untoughened TGPAP in this study.

It is interesting that 30% PES loading significantly improves the ILSS of 100T to the point where it is the same as 60D-30P. At 50% PES loading the ILSS of 100T is greater than 60D with values for 100T-50P and 60D-50P at 69.8 ± 3.0 MPa and 64.4 ± 2.7 MPa respectively. Whilst these values are similar, a student T-test comparing the two 50% PES-containing composites (Table B.1) reveals the difference in ILSS between the two composites is significant to the 99% confidence level. This suggests with a high degree of certainty that PES loading to 50% in a matrix that is known to phase separate provides the additional benefits of a higher ILSS than in a matrix that is known to remain homogenous.

B.4.3 Flexural Properties

Flexural properties were measured by three point bending in accordance with British Standard BS ISO 178:2010 [245]. The flexural strength is the stress at failure on the surface of the laminate and should be accompanied by breaking of the fibres rather than interlaminar shear [156].

The results for flexural strength (Figure B.24) follow a similar pattern to the results for interlaminar shear, whereby the flexural strength significantly increases with PES content for the 100T composites. The 60D-0P and 60D-30P composites have similar flexural strengths, however with the addition of 50% PES 60D shows a drop in flexural strength by 12% compared to 60D-30P. There is no clear explanation for this result as ILSS results suggest an improvement with the addition of PES. Furthermore, the void content and V_f results indicate similar composite quality for the three 60D composites signifying that any difference in mechanical properties is purely due to the materials present in the composite. One would expect the flexural strength to increase with PES content owing to the higher ductility of PES compared to the brittle epoxy resin, as was found for the 100T composites. The addition of 30% PES to the untoughened 100T composite increased the flexural strength by 30%, whereas the addition of 50% PES increased it by 45%.

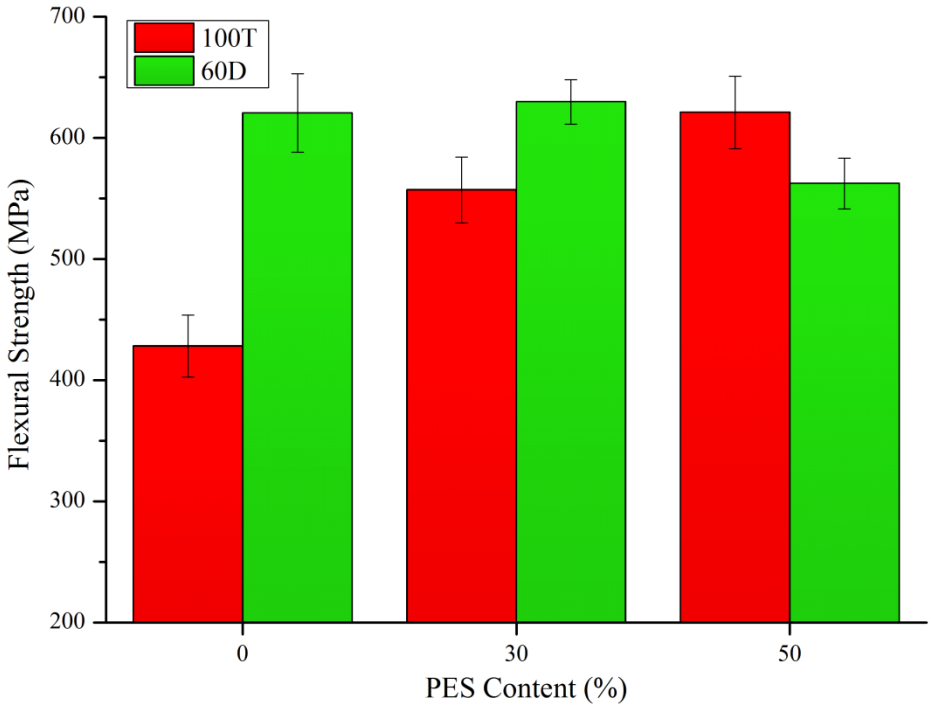

Figure B.24. Flexural strength of composites manufactured using 100T and 60D resins loaded with PES at 0%, 30% and 50%.

The same trend exists for the flexural failure strain of the 100T composites (Figure B.24). The untoughened 100T composite had a strain at failure of 0.93 ± 0.09% that increased to 1.24 ± 0.10% with 30% PES and to 1.51 ± 0.11% with 50% PES. PES is more ductile than epoxy resin thus its incorporation in a composite matrix should increase the deformation required for failure. This trend however appears to be dependent on phase separation, as the flexural strain showed no apparent trend with increasing PES loading for 60D, as the strain at failure remained consistently around 1.35%.

The lack of change in flexural strain with PES content for 60D is relatable to the DMTA results of neat resins in chapter 6, whereby there is no visible change in the tan δ peak heights or widths with PES content. The fact that only one peak exists for the materials suggest a homogeneous morphology and yet the lack of change in dimensions of the tan δ peak indicates the incorporation of PES has no effect on the crosslink density of the epoxy resin; a material property known to influence ductility [68] and therefore strain at failure.

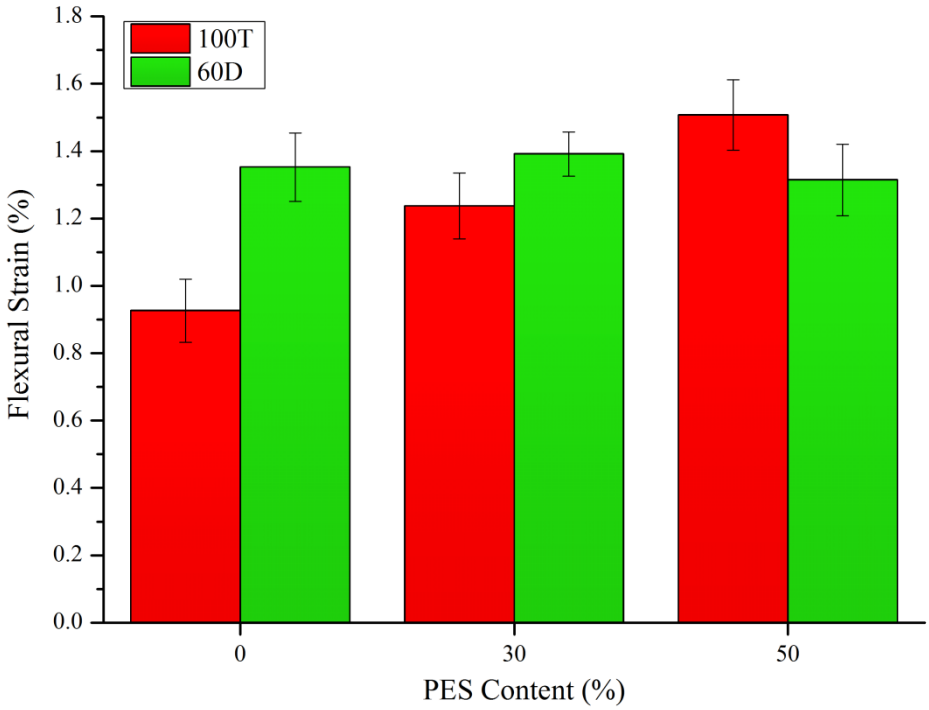

Figure B.25. Maximum flexural strain of composites manufactured using 100T and 60D resins loaded with PES at 0%, 30% and 50%.

Varying the PES content had little effect on the flexural modulus of composites tested in this study. Whilst the standard deviations associated with some of the composites were large, the averages are all between 43.0 GPa and 44.5 GPa. These results were to be expected, as modulus is a low-strain measurement and is therefore a fibre-dominated property.